THE MOTION AND BREAKUP OF FREELY FALLING DROPS IMMEDIATELY AFTER FORMATION

A thesis submitted for the degree of

Doctor of Philosophy

of

The University of Strathclyde

by

I E KALAFATOĞLU ChemEng

Department of Chemical and

Process Engineering

1975

TO S.B.

SUMMARY

The hydrodynamics and the breakup of single oscillating drops which are accelerating from rest through a continuous phase were studied. Specially purified chlorobenzene, 1,2-dichloroethane, and ethylbromide were used as the drop phase liquids and double distilled water was used as the continuous phase liquid.

The motion of the drops was recorded on cine-film using shadow and schlieren optical systems and these films were analysed frame by frame. Data is presented for the variation with time of the velocity of fall, the frequency of oscillation and the eccentricity of nonbreaking drops and the changes in the structure of the wake behind these drops is described.

A transition of the wake behind the accele - rating drops from class I to the wake class of the terminal region was observed. The first formation of a class III attached wake was followed by the onset of the terminal oscillations of the drop. A mechanism is proposed for the sustaining of these oscillations.

The mode of breakup of freely falling drops was investigated. Secondary drops were formed by a necking process of the liquid columns which were formed both at the rear and at the front of the primary drop. The occurrance and the sizes of the secondary drops are related to the size and the oscillations of the primary drop. Theoretical predictions are made of the onset of necking and of the rate of necking using respectively surface free energy considerations and a momentum balance on the liquid in the column.

ACKNOWLEDGEMENTS

The author would like to thank Professor G.S.G. Beveridge BSc, PhD, ARCST, CEng, FIChemE, FRSE for allowing him to use the facilities of the Department of Chemical and Process Engineering.

He would also like to thank Dr. R.M. Edge BSc, PhD, CEng, MIChemE who supervised the present research for his interest and invaluable assistance during the course of this work.

The final year students Mr. A.T. Flatman and Mr. D.V. Banks helped to take and analyse some of the films and this is gratefully acknowledged.

The apparatus used in this work was constructed in the laboratories of the Department of Chemical and Process Engineering and the author wishes to thank Mr. K.M. Campbell and his staff for their help.

The author wishes to acknowledge a scholarship received from the Ministry of Education of the Republic of Turkey for which he is grateful.

CONTENTS

SECTION 1

INTRODUCTION

Drops of one liquid dispersed in another liquid occur in many industrial operations and processes such as liquid-liquid extraction and direct contact heat transfer operations. There are considerable difficulties in investigating and predicting the behaviour of drops in commercial equipment in which there are present large numbers of drops. Therefore in order to advance the understanding of the physical laws which govern the behaviour of these drops many investigations have been made with single drops falling or rising through a continuous phase. Studies have been made of the heat and mass transfer occurring in such a system but the present work is concerned with the hydrodynamics of such drops.

For the investigation of the hydrodynamics of drops moving in another liquid it is convenient to define three periods during the motion; namely :

a) The formation and acceleration period,

b) The period of steady rise or fall which is often referred to as the terminal period,

c) The period of deceleration and coalescence. There has been considerable progress made towards the understanding of the hydrodynamics of single drops during the terminal period and of the coalescence of drops, but the acceleration period has been little studied and is not well understood. However, the initial motion is important, not only because it is relevant to the terminal hydrodynamics, but also because of its effects on the transfer rates in liquid-liquid extrac - tion and in heat transfer operations. The existence of high mass transfer rates during the initial motion has been reported by a number of authors whose results have been reviewed by JEFFREYS[74] and the importance of the initial motion in spray towers for direct contact heat transfer has been discussed by MARKOWITZ and BERGLES[114] and by LETAN and KEHAT[96]. The first object of the present work was therefore to investigate the initial hydrodynamics of drops falling through an aqueous continuous phase and the findings are presented in Sections 6 and 7 of the thesis. In this part of the work the range of drop sizes was chosen so that all the drops were oscillating in the terminal region because it was recommended by JEFFREYS[74] that in liquid-liquid extraction equipment oscillating drops should be used to obtain high mass transfer rates.

Nonbreaking drops which are oscillating occur over only a restricted range of drop sizes. It is found

that when the drop size is above a critical value the drops break up during the acceleration period[84] and therefore there is a distribution of drop sizes in the resulting dispersion. Although the breakup of drops both in steady sheared motion and when they are falling freely in air has been studied in some detail there has been no real study of the breakup of drops which is caused by oscillations during the acceleration period. The second part of the thesis is devoted to a study of this type of breakup and the findings are presented in Sections 8 and 9.

SECTION 2

LITERATURE SURVEY

2.1 INTRODUCTION

The present work deals mainly with the hydrodynamics of the acceleration period of drops which are in free fall. However, any investigation of the droplet hydrodynamics of the initial period of fall has to use the hydrodynamics of the terminal period for comparison. For that reason a survey of the literature on the hydrodynamics of the terminal period is presented below. A survey of the very limited literature on the acceleration period of fall of drops is presented under the heading "Initial Hydrodynamics". For convenience these surveys on drop hydrodynamics are divided into five sections. These sections deal with the velocity of fall or rise, the internal circulation, the drop shape, the drop oscillation, and the behaviour of the wake behind the drop. The surveys presented below also include relevant literature on the hydrodynamics of both single bubbles and solid spheres which are moving through a fluid. Literature which deals only with swarms of drops or only with the heat and mass transfer characteristics of drop systems is

not included.

The third part of the literature survey is devoted to the breakup of drops. Although there have been many investigations in this field, few of these are of importance to the present work. Therefore this survey is confined to those investigations which are of direct relevance and does not aim at surveying the complete field of drop breakup. In addition a section is included on the formation of drops from a breaking column of fluid as it has been found that this system has many similarities with the formation of secondary drops from a drop which is breaking during free fall.

The last chapter of the survey is devoted to the literature on the experimental technique which was used in the present work to make the wakes visible.

2.2 TERMINAL HYDRODYNAMICS

2.2.a) Terminal Velocity and Drag Coefficient

Before discussing the theoretical and experimental work on the terminal velocities and drag coefficients of drops which has been carried out by other workers, it is necessary to define these variables. In the case of small drops which do not oscillate and which fall in a vertical straight line the definitions are straightforward because the drop falls at a constant velocity U_∞ and the drag coefficient can be defined as the ratio of the drag force F_D to the product of the projected frontal area A and the dynamic head $\frac{1}{2}\rho_a U_\infty^2$:

$$(C_D)_\infty = \frac{F_D}{A \cdot \frac{1}{2}\rho_a U_\infty^2} \qquad (2.1)$$

When the drop falls freely at its terminal velocity U_∞, the gravity force will be balanced by the sum of the buoyancy force and the drag force :

$$V_1 \rho_d g = V_1 \rho_a g + (C_D)_\infty \cdot A \cdot \frac{1}{2}\rho_a U_\infty^2 \qquad (2.2)$$

where V_1 is the volume of the drop and ρ_d and ρ_a are the densities of the droplet and the continuous phases, respectively. Equation (2.2) can be rearranged to give for the drag coefficient :

$$(C_D)_\infty = 2 \frac{\rho_d - \rho_a}{\rho_a} \frac{V_1 g}{A U_\infty^2} \qquad (2.3)$$

At small sizes the drop has a spherical shape and equation (2.3) reduces to :

$$(C_D)_\infty = \frac{4}{3} \frac{\Delta\rho}{\rho_a} \frac{g D}{U_\infty^2} \qquad (2.4)$$

where D is the diameter of the drop. At somewhat larger sizes the drop still falls in a vertical straight line with a constant velocity, but deformation of the drop occurs and its shape approaches that of an oblate spheroid. If the horizontal axis is D_H and the vertical axis is D_V the drag coefficient can be calculated from equation (2.3) as :

$$(C_D)_\infty = \frac{4}{3} \frac{\Delta\rho}{\rho_a} \frac{g D_V}{U_\infty^2} \qquad (2.5)$$

For larger sizes of drops the definition of the terminal velocity and the drag coefficient becomes more obscure because the drops oscillate and move no longer in a vertical straight line. In this case it is usual to define the gross terminal velocity as a long vertical distance travelled by the drop divided by the corresponding elapsed time where the distance and the time interval are large enough to let the drop go through many oscillations. The definition of the drag coefficient also has to be modified because the projected frontal area is no longer constant. For convenience an equivalent spherical diameter $D_{E,1}$ is defined as equal to the diameter of a sphere having the same volume as the drop. This gives :

$$D_{E,I} = \left(\frac{6}{\pi} V_I \right)^{1/3} \qquad (2.6)$$

The drag coefficient is then calculated using the equivalent sherical diameter and the gross terminal velocity as if the drop was spherical and was falling at a constant velocity :

$$(C_D)_\infty = \frac{4}{3} \frac{\Delta\rho}{\rho_a} \frac{g D_{E,I}}{U_\infty^2} \qquad (2.7)$$

This is the form which is used throughout the present work.

Theoretical studies of the hydrodynamics of freely falling drops have been confined to spherical drops which are falling in a vertical straight line. These theoretical studies consist of solutions of the Navier-Stokes equations for a number of ranges of the Reynolds number.

The Navier-Stokes equations, which describe the motion in fluids, can be written in dimensionless form for incompressible flow as :

$$\frac{D\vec{U}^*}{Dt^*} = -\overrightarrow{\text{grad}}\, p^* + \frac{1}{Re} \nabla^{*2} \vec{U}^* + \frac{1}{Fr} \vec{g}^* \qquad (2.8)$$

These equations are solved with the appropriate boundary conditions in conjunction with the continuity equation :

$$\text{div}\, \vec{U}^* = 0 \qquad (2.9)$$

However, they can be solved only when certain simplifying assumptions are made. There have been two different approaches to the problem : At low Reynolds numbers a creeping flow solution has been made and at higher Reynolds numbers a boundary layer approach has been used.

The simplest theoretical work at low Reynolds numbers was carried out by STOKES[152][154]. He assumed that creeping flow conditions exist and that the velocity at the interface is zero. There is no internal circulation within such drops. Stokes showed that the drag force on such a drop is :

$$F_D = 3\pi \mu_a D U_\infty \qquad (2.10)$$

This, when combined with equation (2.2) gives for the terminal velocity of fall :

$$(U_\infty)_{St} = \frac{1}{18} \frac{\Delta\rho\, g\, D^2}{\mu_a} \qquad (2.11)$$

and when combined with equation (2.4) gives for the drag coefficient :

$$(C_D)_\infty = 24 \frac{\mu_a}{\rho_a D U_\infty} = \frac{24}{Re} \qquad (2.12)$$

The assumption of creeping flow in the analysis by Stokes limits the Reynolds number range to $Re \ll 1$. This range was extended by OSEEN[123], who took the inertia terms on the left-hand side of the Navier-Stokes equation (2.8) partly into account. The improved

expression for the drag coefficient becomes in this case :

$$(C_D)_\infty = \frac{24}{Re}\left(1 + \frac{3}{16} Re\right) \qquad (2.13)$$

This drag coefficient is valid again only for drops with no internal circulation.

The internal circulation within drops was considered both by HADAMARD[56][57] and RYBCZINSKI[137], independently. They considered drops for which there was a finite velocity at the interface and continuous velocity and stress distributions across the interface. Such drops exhibit internal circulation. If the nonlinear terms in the Navier-Stokes equation (2.8) are ignored, the terminal velocity of the drop is given by:

$$U_\infty = (U_\infty)_{St} \frac{3\mu_d + 3\mu_a}{3\mu_d + 2\mu_a} \qquad (2.14)$$

This equation predicts higher terminal velocities than the Stokes solution and only at very high values of the dispersed phase viscosity does the terminal velocity approach the Stokes solution. A solution for drops with a slower rate of circulation than the drops of Hadamard and Rybczinski has been attempted by BOUSSINESQ[16]-[21]. He assumed a thin layer of higher viscosity near the liquid interface which reduces the momentum transfer across the interface and he introduced the concept of a surface viscosity coefficient e. The terminal velocity of fall of such a drop is then given by :

$$U_\infty = (U_\infty)_{St} \frac{2e + D(3\mu_d + 3\mu_a)}{2e + D(3\mu_d + 2\mu_a)} \qquad (2.15)$$

This equation predicts a lower terminal velocity than the Hadamard-Rybczinski model, but still a higher one than the Stokes solution. The surface viscosity coefficient e can only be evaluated from experimental data and can be used to explain a drag curve intermediate between those of rigid and fully circulating fluid spheres. LEVICH[98], however, suggested that this surface viscosity was caused by the presence of surface-active agents at the interface. He was able to evaluate e theoretically. Further analysis of the surface viscosity is outwith the scope of the thesis and is discussed thoroughly by Levich. All the theories mentioned above assumed creeping flow conditions which limits their use to the Reynolds number range $Re \ll 1$.

Several authors have carried out experimental work on the velocity of fall of droplets at low Reynolds numbers and the results show good agreement with the above theories. GARNER and HAYCOCK[43] reported that their data on drag coefficients for Reynolds numbers less than unity agreed with the Stokes theory rather than with the Hadamard-Rybczinski theory. This is to be expected because there was no internal circulation in most of the drops. SATAPATHY and SMITH[139], however, showed that the velocity of fall of large drops at

Reynolds numbers less than 4 agreed more with the Hadamard-Rybczinski theory. Their drops had internal circulation because they used large drops. It has been shown that larger drops circulate more readily than smaller drops and this will be discussed in the next chapter. BOND[14] and BOND and NEWTON[15] also reported that the velocity of fall of small drops which were not circulating agreed with the Stokes theory, whereas the velocity of fall of larger drops with internal circulation agreed well with the Hadamard-Rybczinski theory. There are no reports in the literature of results for drops which agree with the Oseen theory although MÖLLER[118]'s results for solid spheres did agree with this theory for $Re < 0.6$. Thus it appears from the literature that the Stokes and the Hadamard-Rybczinski theories are sufficient to predict the terminal velocity at low Reynolds numbers for drops with and without a rigid interface, respectively.

At somewhat higher Reynolds numbers a boundary layer approach was used by LEVICH[97]. He considered bubbles rising in liquids and postulated that the tangential stresses vanished at the bubble-liquid interface and solved the Navier-Stokes equations for the velocity in the boundary layer. His analysis was

later shown by CHAO[27] to contain some error. Chao extended the analysis of Levich to liquid-liquid systems and considered equal tangential velocity components and equal shear stresses on the two sides of the interface, but he did not take the flow separation into conside - ration. Solving the Navier-Stokes equation he calculated the drag coefficient as

$$(C_D)_\infty = \frac{16}{Re}\left(1 + \frac{0.814}{Re^{1/2}}\right) b^* \qquad (2.16)$$

where b^* is a property parameter given by

$$b^* = \frac{2 + 3(\mu_d/\mu_c)}{1 + [(\rho_d/\rho_c)(\mu_d/\mu_c)]^{1/2}} \qquad (2.17)$$

Equation (2.16) differs from the original expression given by Chao. This is due to the ommision of curvature terms in the boundary condition in the development of the original expression. The correct expression given above was presented in a later study by WINNIKOW and CHAO[178]. They also considered the boundary layer separation to a limited extent. They calculated the total drag as the sum of the viscous drag and the pressure drag and both of these drags were expressed as functions of the Reynolds number, the angle of separation θ_s, and the property parameter b^* which is defined in equation (2.17). HARPER and MOORE[62] made a somewhat more detailed analysis of the contribution of flow separation at the rear of a spherical drop to the drag coefficient. WINNIKOW and CHAO[178]'s experimentally determined drag coefficients were 34 to

88 % higher than predicted by their theory for $138 < Re < 700$. This can be attributed to the failure of the theory to predict an accurate pressure distribution within the wake region and to the droplet deformation which was not considered. Their experimental results agree to a higher degree with Harper and Moore's theory and in the range $150 < Re < 500$ the experimental results were only from 6 to 25 % higher than the predicted values. This better agreement can be attributed to their more accurate prediction of the pressure distribution at the rear of the drop and it is probable that the neglection of droplet deformation is largely responsible for the disagreement which remains.

At higher Reynolds numbers the deformation of the drop is considerable and the motion is further complicated by the oscillations of the drop. No theoretical analysis has been attempted in this region and only empirical relationships exist between the gross terminal velocity, the drop diameter, and the physical properties of the systems. A large number of authors(36)(39)(48)(72)(77)(86)(88)(99)(139)(165)(178) have reported gross terminal velocities of drops falling or rising in liquid systems. Considerable differences exist between the reported values at intermediate drop sizes, although at higher or lower drop diameters there is fair agreement among the data. It has been shown by several authors(38)(39)(84)(100) that the presence of

surfactants in the system inhibits the internal circulation of drops and lowers the terminal velocity considerably and it is probable that the presence of trace quantities of surface active impurities accounts for the differences between the various experimental results.

The earlier investigations used technical grade liquids which were contaminated with surface active impurities. The generalized shape of the curve of the terminal velocity versus the equivalent spherical diameter which were obtained is shown in Fig.2.1. In region A of this curve, where the droplet diameter is relatively small, the velocity increases with increasing drop diameter and coincides with the curve for solid spheres. This is because the drops are stagnant and behave like rigid spheres. At higher diameters, in region B', the gross terminal velocity of a contaminated drop is less than that of a solid sphere of the same diameter. This is mainly because of droplet deformation. Some of the contaminated systems exhibit a maximum in the terminal velocity at higher diameters beyond which the terminal velocity decreases slightly and then remains constant. There have been several attempts to correlate the gross terminal velocities of drops in systems which were not specially purified. The earliest one is due to HU and KINTNER[72] who investigated drops of 10 technical-grade organic liquids of low viscosity

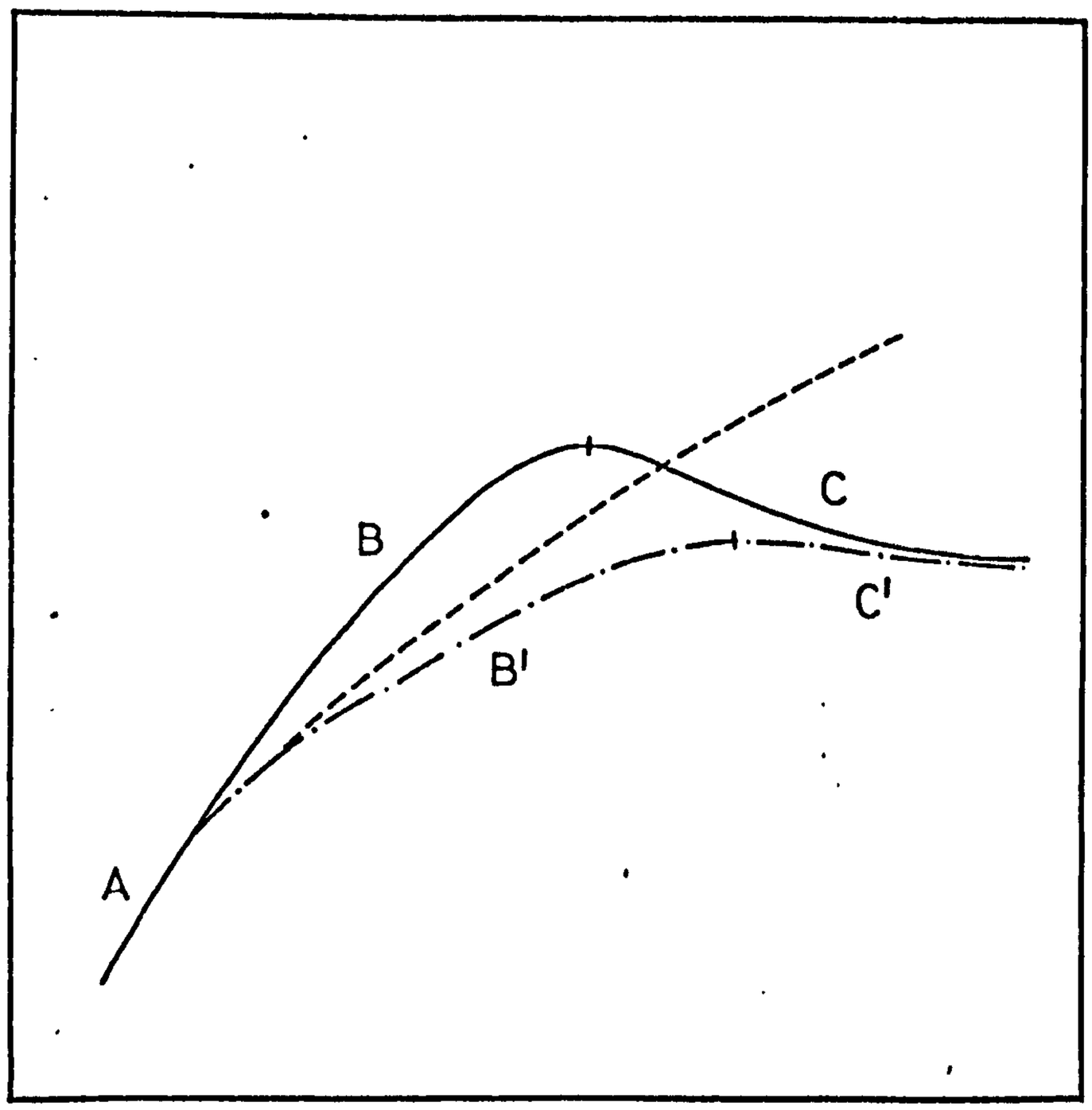

FIG. 2.1 GENERALIZED TERMINAL VELOCITY CURVE

and high interfacial tension, which were falling in water. They correlated the drag coefficients with the Reynolds number, the Weber number, and a dimensionless physical property group P, defined as :

$$P = \frac{\rho_w}{\Delta\rho} \frac{\rho_w \sigma^3}{g \mu_w^4} \qquad (2.18)$$

Their correlation is given by the two equations :

$$Y = \frac{4}{3} X^{1.275} \qquad \text{for} \quad 2 < Y \leqslant 70 \qquad (2.19)$$

and

$$Y = 0.045 X^{2.37} \qquad \text{for} \quad Y \geqslant 70 \qquad (2.20)$$

where

$$Y = (C_D)_\infty We\, P^{0.15} \qquad (2.21)$$

and

$$X = \left(Re / P^{0.15} \right) + 0.75 \qquad (2.22)$$

The break in the curve at Y = 70 corresponds to the peak terminal velocity. This correlation was shown by WARSHAY and coworkers[173] to be also valid for systems of low interfacial tension but to be insufficient for systems of high viscosity. JOHNSON and BRAIDA[77] modified the Hu-Kintner correlation in order to include the high viscosity systems, by applying an additional correction factor $\left(\mu_d / \mu_w\right)^{-0.14}$ to the right hand side of equation (2.21), where μ_w is the viscosity of water. A different correlation was presented by KLEE and

TREYBAL[86] who used 11 technical-grade systems which had a wide range of properties. They presented two correlations, one for each side of the peak velocity : For region B' in Fig.2.1

$$Re = 22.2\ (C_D)_\infty^{-5.18}\ We^{-0.169} \qquad (2.23)$$

or when solved for the velocity of fall

$$U_\infty = 38.3\ \rho_a^{-0.45}\ \Delta\rho^{0.58}\ \mu_a^{-0.11}\ D_{E,I}^{0.70} \qquad (2.24)$$

and for region C'

$$Re = 0.00418\ (C_D)_\infty^{2.61}\ We^{-1.81} \qquad (2.25)$$

or when solved for the velocity of fall

$$U_\infty = 17.6\ \rho_a^{-0.55}\ \Delta\rho^{0.28}\ \mu_a^{0.10}\ \sigma^{0.18} \qquad (2.26)$$

Equation (2.26) suggests that for large drops the gross terminal velocity does not depend on the drop diameter. This has been confirmed by other authors[72][83]. HARMATHY[61] who used the terminal velocities reported by various authors obtained a correlation similar to equation (2.26) in the form :

$$U_\infty = 1.53\ \left(\frac{g\,\Delta\rho\,\sigma}{\rho_a^2}\right)^{1/4} \qquad (2.27)$$

Subsequent investigators have worked with carefully purified systems to eliminate the effect of surfactants. The generalized shape of the terminal velocity versus diameter curve for purified systems is

given also in Fig.2.1. In region A, at small drop diameters it coincides with that of solid spheres and contaminated drops. At somewhat larger drop sizes, in region B, the terminal velocity still increases with increase in drop diameter, but is higher than the terminal velocity of solid spheres or contaminated drops of the same size. This increased velocity is mainly due to internal circulation. Further increase in the size of the drop increases the drop deformation and decreases the velocity. At a particular size there is a definite maximum in the terminal velocity. Around this peak the drop starts to oscillate. Beyond the peak the gross terminal velocity decreases with increasing diameter and approaches the value for contaminated drops.

THORSEN, STORDALEN, and TERJESEN[164] who worked with oscillating drops in region C of Fig.2.1, correlated their data for the gross terminal velocities of drops in carefully purified systems, which had low viscosities and high interfacial tension, by means of the equation

$$U_\infty = \frac{6.8}{1.65 - \Delta\rho/\rho_d}\left[\frac{\sigma}{(3\rho_d + 2\rho_a) D_{e,1}}\right]^{1/2} \qquad (2.28)$$

Recently EDGE and GRANT[33] also worked with oscillating drops in carefully purified systems and in a system in which the continuous phase was contaminated with known amounts of surfactants. They showed that when a

concentration of 10^{-2} g/l of sodiumlaurylsulphate was present in the continuous phase, further addition of surfactant caused no change in the terminal velocity. Systems with this amount of contamination were termed as grossly contaminated systems and they agreed well with the Hu-Kintner correlation whereas drops in purified systems had much higher terminal velocities. They correlated empirically the gross terminal velocity with the diameter, the frequency of oscillation and with the values of these two variables at the transition from nonoscillating to oscillating drops in purified systems. They also correlated the transition values of the diameter and of the frequency of oscillation with the densities and the interfacial tension of the systems. By combining these correlations the gross terminal velocity was given by :

$$U_\infty = \frac{K_1}{\sqrt{D_{E,1}}} - \frac{K_2}{D_{E,1}} \qquad (2.29)$$

where K_1 and K_2 are functions of the densities and the surface tension.

2.2.b) Internal Circulation

A finite viscosity and a mobile interface makes possible the transfer of shear stresses across the droplet interface. This induces an internal circulation of the liquid within the drop. The internal circulation of spherical drops with a noncontaminated interface was first described theoretically by HILL[65] and by HADAMARD[56][57] and RYBCZINSKI[137]. Hill investigated the motion of a spherical vortex in an ideal fluid in which viscous drag was absent. The second theory by Hadamard and Rybczinski examined the vortex induced by the presence of viscous drag in a fluid sphere which was falling slowly and steadily through another fluid. The main features of the two theories are as follows (Fig.2.2) :

a) In each investigation the velocity distribution was continuous across the interface.

b) In Hill's model the sign of the velocity gradient was different on either side of the interface whereas in Hadamard-Rybczinski's model the sign of the velocity gradient did not change across the interface.

The velocity distributions which were predicted by the two theories are shown in Fig.2.2. In both models the velocity distribution profile in the drop was quadratic

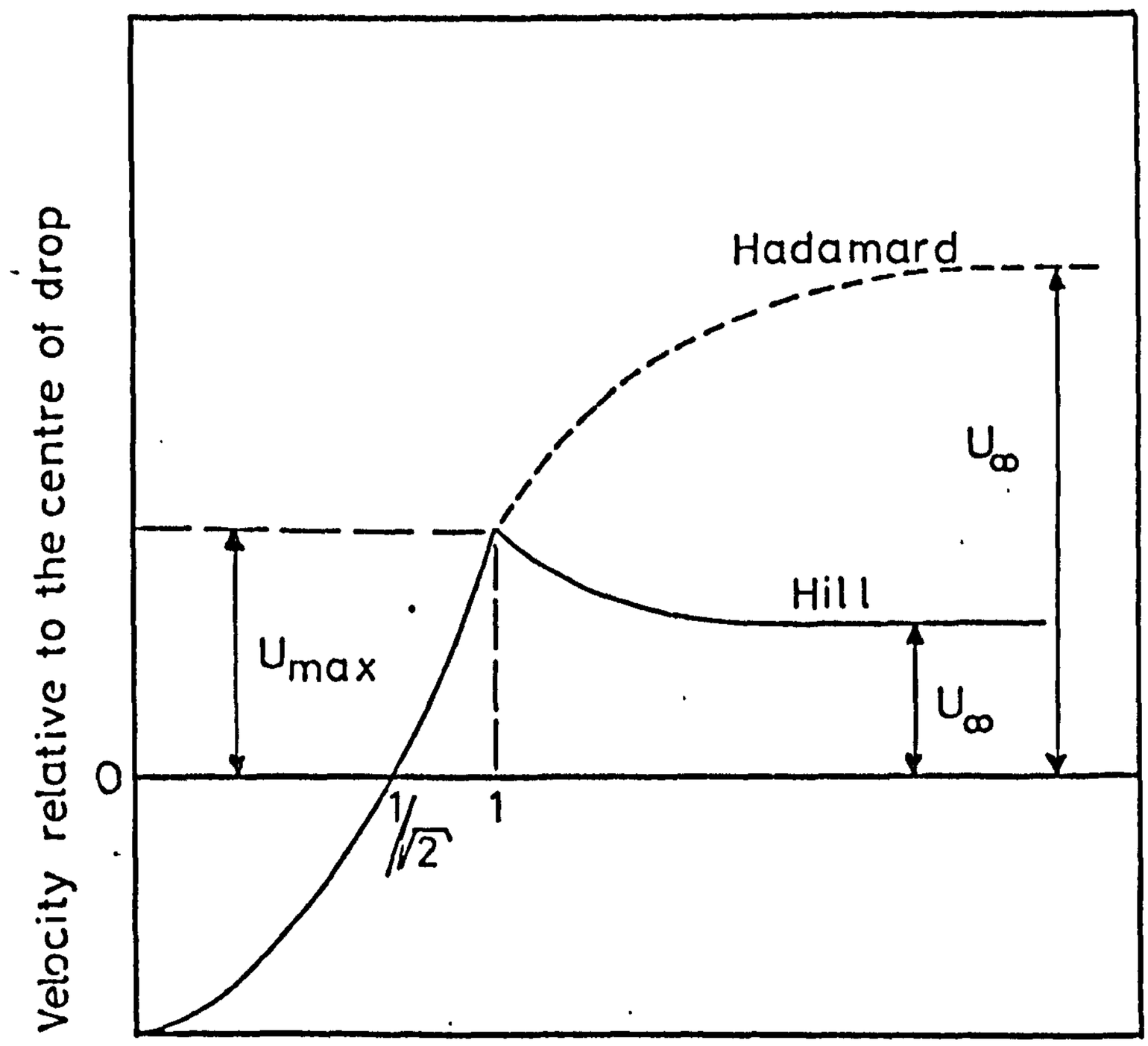

FIG. 2.2 VELOCITY DISTRIBUTIONS OF THE HILL AND HADAMARD MODELS

with respect to the distance from the center. On the equatorial plane of symmetry, at a distance of $R/\sqrt{2}$ from the center of the sphere, there was a ring of zero velocity which is called the stagnation ring. In Hill's model the maximum circulation velocity, which occurred in the largest closed streamline, was 1.5 times the velocity of travel through the medium whereas in the second model it was always less than half of the velocity of travel. It can be seen from Fig.2.2 that both the Hadamard-Rybczinski model and the Hill model predict similar velocity distributions within the drop, but the external flow pattern is different. However, for a given velocity of fall of the drop, the circulation velocities will be greater in Hill's case than in Hadamard-Rybczinski's case. HARPER and MOORE[62] studied theoretically the internal circulation of drops at somewhat higher Reynolds numbers. They assumed a spherical droplet shape and a boundary layer around the drop. The vortices inside the drop were shown to be similar to Hill's.

A number of authors have attempted to predict the onset of internal circulation. From surface energy considerations BOND[14] and BOND and NEWTON[15] postulated that the transition from noncirculating to circulating drops at low Reynolds numbers occurs over a narrow range of drop diameter and the transition drop diameter was found to be :

$$D_{trans} = 2\left(\frac{\sigma}{g\,\Delta\rho}\right)^{1/2} \qquad (2.30)$$

which corresponds to a transition Eötvös number of 4. Later HUGHES and GILLILAND[73] used a somewhat more refined force balance on the surface of the drop and gave the critical transition drop diameter at which the drops would be fully circulating as :

$$D_{trans} = 3\left(\frac{\sigma}{g\,\Delta\rho}\right)^{1/2} \qquad (2.31)$$

This corresponds to a transition Eötvös number of 9.

The oscillation of the drop is another cause of the internal motion of the droplet liquid. For the case of streamline motion the flow pattern with no internal vortices was calculated by LAMB[89]. He found that most of the motion occurs near the surface and the maximum velocity is at the 45° latitude on the surface. No authors have so far presented any experimental evidence of this type of internal motion.

Indirect evidence of the internal circulation of drops has been available for a long time, but the visualisation of the flow pattern within the drop and the calculation of circulation velocities has been achieved only within the last two decades. SPELLS[150] used the photoviscosity effect of high concentration glycerine solutions in water, SAVIC[141] and GARNER and HAYCOCK[43] added powdered aluminium to the dispersed

phase and GARNER[41] and GARNER and SKELLAND[46][47][48] used colour reactions or introduced small coal particles into the droplet liquid for the visualisation of the flow pattern within the drop. Both the Hadamard-Rybczinski and the Hill type of internal circulation were observed within the drops. BOND[14], BOND and NEWTON[15], KINTNER and coworkers[85], HORTON and coworkers[71], and GARNER and HAYCOCK[43] showed that the internal circulation within the drops at low Reynolds numbers agreed more with the Hadamard - Rybczinski theory, whereas the drops of Garner and Haycock at somewhat higher Reynolds numbers exhibited an internal circulation closer to Hill's theory. This is to be expected because at lower Reynolds numbers the viscous drag is appreciable and Hill did not consider the effect of the viscous drag on the internal circulation of the drop.

It was also found experimentally that as the drop diameter is increased there is not a sharply defined change from a noncirculating to a circulating drop and that over a range of drop sizes a drop will be partly circulating. GARNER and HAYCOCK[43] showed that the fraction of the volume of the drop which was circulating increased as the drop Reynolds number was increased. They showed that the internal circulation was more readily established when the interfacial tension was decreased or the continuous phase viscosity

was increased, but they also showed that the presence of impurities had an additional effect on the onset of internal circulation. It was found that, although the presence of surfactants reduces the interfacial tension and should therefore increase the extent of the internal circulation, the internal circulation was, in fact, reduced by their presence. Other authors[48][164] reported similar experimental findings. This can be explained as follows : As the surfactant molecules are adsorbed at the interface they are swept to the rear of the drop. Therefore the surfactant concentration will be higher at the rear of the drop and lower at the front. This concentration gradient of the surfactant molecules produces a surface tension gradient on the surface of the drop which resists the transfer of momentum across the interface. Thus the internal circulation is reduced in strength or stopped, depending on the concentration of the surfactant. Trace amounts of surfactants will stop the internal circulation of small drops, whereas higher concentra - tions are needed for larger drops.

Some authors [134][139] reported that regular internal circulation appeared to stop and random mixing set in when the drops were oscillating. However, GARNER and SKELLAND[48] reported one system which showed vigorous internal circulation although the drop was oscillating. The flow pattern in oscillating drops is still uncertain and needs to be clarified.

2.2.c) Drop Shapes

Whereas at low Reynolds numbers the drops have a spherical shape, at higher Reynolds numbers the shape is distorted approximately into that of an oblate ellipsoid. This occurs in the range where drops have higher velocities than those of solid spheres of the same volume (Fig.2.1). The distortion is usually described by the eccentricity E, defined as the ratio of the major axis of the ellipsoid to the minor. The eccentricity increases with drop size, and the drop looses its horizontal symmetry as the peak drop diameter in Fig.2.1 is approached. The definition of E then has to be modified to that of the ratio of the maximum horizontal diameter D_H to the maximum vertical diameter D_V :

$$E = \frac{D_H}{D_V} \tag{2.32}$$

Beyond the peak diameter the drops oscillate and a mean eccentricity has to be used.

Theoretical analyses of the shapes of drops have been made by SAITO[138] and by TAYLOR and ACRIVOS [162] who found an error in Saito's work. Both of these analyses dealt with drops moving at low Reynolds numbers and they are beyond the scope of this thesis. The only theoretical investigation of the shape of nonoscillating drops moving at higher Reynolds numbers is the

dimensional analysis which was made by HARMATHY[61]. He found that at high Reynolds numbers the shape of nonoscillating drops moving freely in liquid systems depended solely on the Eötvös number. A theoretical analysis of the eccentricities of oscillating drops has not been attempted.

Experimental measurements of drop eccentricities, however, have been reported by a number of authors[14][15][39][49][61][83][86][116][175][178]. BOND[14] and BOND and NEWTON[15] reported eccentricities at low Reynolds numbers. They found that when the Eötvös number was greater than unity the drop was distorted from its spherical shape and that circulating drops were more distorted than stagnant drops. DAVIES[31][32] gave 0.4, HARMATHY[61] 0.79, and WINNIKOW and CHAO[178] 0.2 for the critical Eötvös number for deformation to occur. This disagreement is probably due to the different amounts of surface active impurities which were present in the various systems used by these authors. Several authors have investigated the effect of surface active agents on drop distortion. GARNER and coworkers[41][48][49] found a reduction in the drop distortion when surfactants were present and they related this to the reduction in internal circulation. These authors suggested that if the interface is not contaminated with surfactants the internal circulation is greater and this causes an increased centrifugal

effect which leads to increased deformation of the drop. Several authors[38][39][178] also reported similar effects of surfactants. However, MELHUS and TERJESEN[116] reported increased deformation when surfactants were present. The difference in the results of Garner and coworkers and Melhus and Terjesen is probably caused by the differences in the degree of contamination which were present in their systems. In Garner's systems the degree of contamination was low and therefore this had little effect on the surface tension but had a large effect on the internal circulation. Thus their contaminated drops were less distorted than their pure drops. However, in Melhus and Terjesen's systems the concentration of the surface active agents was high, which lowered the surface tension considerably and allowed the drops to deform and this more than compensated for the decreased deformation resulting from the decreased internal circulation. Also EDGE and GRANT[37] showed that the presence of surfactants decreases the eccentricity of 1,2-dichloroethane drops falling in water. However, when a concentration of 10^{-2} g/l of sodiumlaurylsulphate was present in the continuous phase, further addition of surfactants caused no change in the eccentricity of the drops. The reduction in the interfacial tension at this concentration was about 2.9% which is small compared with those in the contaminated systems which were used by Melhus and Terjesen.

The dependence of the drop eccentricity on the Eötvös number, as predicted by HARMATHY[61], has been reported by various authors. Harmathy's semiempirical correlation between the eccentricity and the Eötvös number has the form :

$$E^{2/3} - \frac{0.6}{E^{1/3}} = 0.449\ (Eö)^{1/2} \qquad (2.33)$$

However, the agreement of this correlation with the published data on eccentricities is very poor. This is because to obtain equation (2.33), Harmathy used drag coefficients which were obtained for contaminated systems and for liquid-gas systems with very low or no internal circulation. He also included systems where the drops were oscillating and it is doubtful whether the mean eccentricities of oscillating drops can be correlated in the same way as the eccentricities of nonoscillating drops. A simpler correlation was obtained by WELLEK, AGRAWAL, and SKELLAND[175] as :

$$E = 1 + 0.129\ Eö \qquad (2.34)$$

These authors used the eccentricity data for nonoscil - lating drops in 45 systems. This correlation also cannot be applied to specially purified systems, because it was based on contaminated systems which had little or no internal circulation. This can be seen from the fact that equation (2.34) is similar to correlations obtained by other authors[40][45][132] who investigated the eccentricities of stagnant drops falling in air.

WINNIKOW and CHAO[178], however, worked with liquid-liquid systems which were specially purified and showed internal circulation. These authors also obtained linear relationships between the drop eccentricities and the Eötvös number for various systems but the linearity constant was much higher than the one given by Wellek, Agrawal and Skelland in equation (2.34) and it also increased with decreasing property parameter b^*, which is defined in equation (2.17). Winnikow and Chao associated small values of b^* with more vigorous internal circulation. This again suggests that increased internal circulation increases droplet distortion, as suggested by Garner and coworkers.

There is very little data on the mean eccentricities of oscillating drops. KEITH and HIXSON[83], KLEE and TREYBAL[86], and ELZINGA and BANCHERO[39] found that the eccentricity of oscillating drops in systems which were not specially purified was propor - tional to the equivalent spherical diameter. Their calculations of the mean eccentricity of oscillating drops was very dubious because they were based on rough averages of maximum and minimum distortions obtained from a number of still photographs of different drops of the same size. The scatter of data was also very large. EDGE and GRANT[38], however, calculated a mean eccentricity equal to the ratio of the average D_H to the average D_V over 5 complete oscillation cycles.

They also obtained a large scatter for the eccentricity, but the eccentricity seemed to be independent of the equivalent spherical diameter. It can be concluded that there is poor agreement in the literature on how the mean eccentricity of oscillating drops changes with the equivalent spherical diameter. This is mainly because of the difficulty in measuring the mean eccentricity.

2.2.d) Drop Oscillations

In a given system as the size of the drop is increased, a size is reached at which the drop is deformed and assumes generally an oblate ellipsoidal shape. Such a shape is unstable in low viscosity fields, and the drop will oscillate. For small drop sizes these oscillations are axially symmetric periodic changes between a more oblate form and a less oblate form although they are commonly referred to as oblate-prolate oscillations. Larger drops, however, fall through the continuous phase in an erratic oscillatory motion. This type of oscillations is described as random wobbling.

There have been no theoretical studies of the frequency or of the amplitude of oscillation of a drop moving in a fluid. However, there have been several studies of the small amplitude oscillations of drops at rest. The surface-tension oscillations were first considered by RAYLEIGH[130]. He ommitted the effect of the continuous phase and obtained for the frequency of oscillation :

$$\omega_n^2 = \frac{1}{4\pi^2} n(n-1)(n+2) \frac{8\sigma}{\rho_d D^3} \qquad (2.35)$$

This analysis was later extended by LAMB[89]. He took the density of the continuous phase into consideration and obtained for the frequency of oscillation :

$$\omega_n^2 = \frac{1}{4\pi^2} \frac{n(n-1)(n+1)(n+2)}{n\rho_a + (n+1)\rho_d} \frac{8\sigma}{D^3} \qquad (2.36)$$

which reduces to Rayleigh's result if $\rho_a = 0$. The first mode of oscillation which can be observed experimentally is for n=2. This is the case of ellipsoidal deformation and the frequency is given by :

$$\omega^{*2} = \frac{1}{4\pi^2} \frac{192}{2\rho_a + 3\rho_d} \frac{\sigma}{D^3} \qquad (2.37)$$

The frequency of oscillation calculated from equation (2.37) will be subsequently referred to as "Lamb's frequency of oscillation".

The most extensive analysis of small amplitude oscillations of a drop at rest in another fluid has been carried out by MILLER and SCRIVEN[117] who took the viscosities of both phases into consideration. They obtained an equation for the frequency of oscillation which could only be solved numerically except for a number of special cases. For the limiting case of low viscosity they obtained for the primary mode of oscillation :

$$\omega = \omega^* - \omega_v \qquad (2.38)$$

where

$$\omega_v = \omega^{*1/2} \frac{17.7}{(2\rho_a + 3\rho_d)D} \frac{(\mu_d \mu_a \rho_d \rho_a)^{1/2}}{(\mu_d \rho_d)^{1/2} + (\mu_a \rho_a)^{1/2}} \qquad (2.39)$$

For the case of two inviscid liquids ($\mu_d = \mu_a = 0$) equation (2.38) reduces to Lamb's solution.

At the larger amplitude of oscillations which occur with the larger sizes of drops it has been found that the frequency of oscillation decreases as the amplitude is increased. SCHROEDER and KINTNER[146] attempted to describe this effect by considering an amplitude factor b_A, defined as :

$$b_A = 1 - \frac{D_{v,max} - D_{v,min}}{2 D_{v,avg}} \qquad (2.40)$$

Using a procedure which was similar to Lamb's they obtained for the frequency of oscillation :

$$\omega = b_A^{1/2} \omega^* \qquad (2.41)$$

For small amplitude oscillations b_A tends to unity and equation (2.41) reduces to Lamb's solution. The authors were not able to determine the amplitude factor b_A theoretically. There have been no other attempts at a theoretical analysis for large amplitude oscillations of drops.

Several authors[25][36][37][38][39][43][48][72][73][77][86][99][134][139][146][164][178] reported the existence of steady-state nondamping oscillations for drops moving in a liquid continuous phase. The onset of these oscillations has been found to occur near the peak terminal velocity in Fig.2.1 and at a critical transition Weber number. HU and KINTNER[72] gave a value of 3.58, and WINNIKOW and CHAO[178] 4.08 for this transition Weber number. EDGE and GRANT[36],

however, showed that the transition occurred at a break in the plot of the Weber number against the Ohnesorge number. They found that the transition Ohnesorge number is predicted satisfactorily when the transition equivalent sherical diameter is given by the equation :

$$D_{E,I_{trans}} = \frac{0.162}{(\Delta\rho/\rho_d)^{1/2}} \qquad (2.42)$$

There are few authors who reported detailed measurements of the frequency and the amplitude of oscillations. SCHROEDER and KINTNER[146] correlated the amplitude coefficient b_A given in equation (2.40) with the equivalent spherical diameter as :

$$b_A = 0.805\ D_{E,I}^{0.225} \qquad (2.43)$$

The amplitude data was scattered considerably, but they obtained consistent measurements for the frequency of oscillations which agreed with equation (2.41) with an average error of $\pm$ 9.01 %. The systems which were investigated by Schroeder and Kintner were not specially purified before use and were probably contaminated.

Specially purified systems were investigated by THORSEN, STORDALEN, and TERJESEN[164]. They correlated the drop Strouhal number with the physical constants of the systems. The Strouhal number appeared to be a constant and was a function of the densities only :

$$Sr = 0.535 - 0.324\,\frac{\Delta\rho}{\rho_d} \qquad (2.44)$$

Constant Strouhal numbers were also obtained by EDGE and GRANT[36][37][38]. They presented measurements of the frequency of oscillations for five carefully purified systems and for one system contaminated with a surfactant to various degrees. They were able to correlate their data for the frequency of oscillation in purified systems as :

$$\omega = \omega^* - \frac{0.695}{(\Delta\rho/\rho_d)^{0.2} D_{E,1}^2} \qquad (2.45)$$

The frequency of oscillation was higher for grossly contaminated systems and agreed with the Schroeder-Kintner correlation.

Mechanism of Oscillations

There has been much speculation both about the onset of the oscillations of drops and on the maintenance of these oscillations. In the literature there is no agreement on the stage at which a drop, which is falling from rest, starts to oscillate. HUGHES and GILLILAND[73] reported that the oscillations were started by the elongation of the drop at the forming tip. SCHROEDER and KINTNER[146], however, observed that tip-induced oscillations tended to die out. WINNIKOW and CHAO[178] observed that the natural oscillations of drops didn't start immediately after detachment from the tip but at some distance from it and this distance was shorter for larger drops.

Several authors related the initiation and the maintenance of oscillations to the shedding of vortices in the wake behind the drop. SCHROEDER and KINTNER[146] and THORSEN, STORDALEN, and TERJESEN[164] considered that a vortex trail must be present if there is to be a driving mechanism for the oscillations. SCHROEDER and KINTNER considered by analogy an undamped spring which was perturbed by a continuing outside force and oscillated at or near its natural frequency as long as the sustaining mechanism was present. They suggested that a drop with a vortex trail had a sustaining mechanism and would oscillate at or near its natural frequency. However, they gave no details of the sustaining mechanism. Thorsen and coworkers claimed that the shedding of the wake into the outer stream created a pulsating pressure distribution over the surface of the drop which was considered to be the driving mechanism for the oscillations of the drop. Once the oscillation had started there was an interaction between the interfacial tension force trying to conserve the spherical form of the drop, and the pulsating pressure distribution over the surface. DAVIES[33] suggested that when the frequency of wake shedding was equal or close to the natural frequency of drop oscillations this would create a resonance and would lead to a periodic building up and damping out of the drop oscillations. EDGE and GRANT[37], however, found that the frequency of drop oscillations both determined

and was equal to the frequency of wake shedding.

2.2.e) Drop Wakes

When a drop moves through a continuous phase disturbances occur in the continuous phase behind the drop. These disturbances are usually referred to as the wake. Also immediately adjacent to the rear surface of the drop there may be a region which contains a quantity of the continuous phase and which moves with the drop. This region is usually referred to as the attached wake.

The theoretical determination of the flow patterns around fluid objects is usually difficult. The nonlinear Navier-Stokes equations (2.8) need to be solved with the appropriate boundary conditions. A general solution is not possible and only approximate solutions can be obtained when simplifying assumptions are made.

The symmetrical flow pattern around spherical drops at low Reynolds numbers was calculated by STOKES (152)(154). He ignored the inertia terms in the Navier-Stokes equations. Later OSEEN(123) considered the inertia terms to a limited extent and obtained a nonsymmetrical flow pattern. Oseen's solution of linearized Navier-Stokes equations has been improved by

GOLDSTEIN[51], TOMOTIKA and AOI[170], and PEARCEY and McHUGH[125]. These solutions were limited by the linearizing approximations to Reynolds numbers below 2. It was also assumed that there was zero velocity at the interface. HADAMARD[56] and RYBCZINSKI[137], however, calculated the flow pattern around spherical drops which were moving at low Reynolds numbers in a continuous phase and for which there was a finite velocity at the interface. Under the creeping flow condition,which was assumed by all the above mentioned authors, the flow does not separate from the interface so that there is no attached wake at the rear of the drop.

At higher Reynolds numbers the inertia terms in the Navier-Stokes equations become more important and a solution has not been obtained for drops. However, the flow pattern has been calculated for the flow around rigid spheres at moderate Reynolds numbers and these flow patterns have provided a useful starting point for examining the wakes found experimentally behind drops.

In solving the Navier-Stokes equations for the solid sphere important simplifications are possible, although at moderate or high Reynolds numbers approximate methods are still necessary. A discussion of the methods which have been used to solve the

Navier-Stokes equations for the flow of fluids around a rigid sphere at moderate and high Reynolds numbers is outwith the scope of this thesis and the reader is referred to papers by KAWAGUTI[80][81][82], THOM[163], ALLEN and SOUTHWELL[3], LISTER[101], JENSON[75], HAMIELEC, HOFFMAN and ROSS[58], SPALDING and PATANKAR[149], and RIMON and CHENG[133].

Wakes behind solid spheres :

The flow around solid spheres has been well established experimentally. At low Reynolds numbers the flow is symmetrical as predicted by Stokes. As the Reynolds number is increased the upstream-downstream symmetry is lost as predicted by Oseen. At a critical Reynolds number the flow separates from the interface forming an attached wake at the rear of the sphere. This critical Reynolds number was found experimentally to be 1 by BOND[13], between 8.15 and 23.5 by NISI and PORTER[121], 14 by GARNER, JENSON, and KEEY[44], 21 by GARNER and SKELLAND[48], 24 by TANEDA[156][157][158], and above 720 by WILLIAMS[177]. As the Reynolds number is further increased the attached wake increases in size and the circulation within the wake gains in strength. There is no change in the general flow pattern except for the advance of the separation ring towards the equator of the sphere. At a certain Reynolds number the attached wake becomes unstable and starts

to oscillate about the axis of the motion. Part of the attached wake is also shed periodically and the wake has some similarity with the Karman vortex street behind a cylinder. The critical Reynolds number for this transition was found to be 130 by TANEDA[157], 150 by JOHNSTONE and WILLIAMS[78], 200 by NEMENYI[120], 270 by GOLDBURG and FLORSHEIM[50], between 480 and 520 by GARNER and GRAFTON[42], 450 by MÖLLER[118], 500 by SCHMIEDEL[144].

The periodicity of the vortex shedding has been measured by several authors and usually has been presented in the form of Strouhal number. Strouhal numbers for solid spheres have been reported by MÖLLER[118], SCHMIEDEL[144], GOLDBURG and FLORSHEIM[50] and WINNY[179]. The shedding of vortices was described in detail by Möller. Up to a Reynolds number of 1000 the vortices which were shed were linked together to form a vortex chain. At Reynolds numbers greater than 1500 only discrete vortices were observed which formed a vortex street. These vortices were unstable, and they joined together to form periodic balls of vorticity. Möller was able to give Strouhal numbers for this periodicity as well. SCHMIEDEL[144] found that the periodic discharge of vortices from the attached wake occurred in the range $500 < Re < 1000$. However, GARNER and GRAFTON[42] observed the shedding well above a Reynolds number of 1000. GOLDBURG and

FLORSHEIM[50] observed irregularities in the shedding of the wakes at and above a Reynolds number of 650. Above this Reynolds number the wake was asymmetric.

There is obviously a large discrepancy between these reported values of the critical Reynolds numbers for the attached wake formation and for the wake shedding. These authors used different designs of apparatus and different experimental methods in making the wakes visible. Also different methods were used to move the spheres in the fluid and only some of these allowed side to side motion of the sphere to occur and each method had a different effect on the flow profile. The turbulence in the continuous phase and the walls of the container also could effect the flow pattern. Also the Reynolds number based on the diameter of the sphere as the characteristic length is probably not an adequate criteria for dynamical similarity in the wide range of systems considered above. These could explain the discrepancies mentioned above.

Wakes Behind Liquid Drops :

The flow and wake patterns at low Reynolds numbers have been observed by GARNER and coworkers[41][43][48][49], and by SATAPATHY and SMITH[139]. GARNER and HAYCOCK[43] and Satapathy and Smith observed that for Reynolds numbers less than 1 the flow pattern

agreed well with the Stokes theory. Nonsymmetrical flow patterns were observed between Reynolds numbers 1 and 4 by Satapathy and Smith. The first attached wake formation was reported to occur at various critical Reynolds numbers : 4 by Satapathy and Smith, below 10 by MAGARVEY and BISHOP[106], at 20 by GARNER[41], between 19 and 23 by GARNER and SKELLAND[48]. As the Reynolds number was further increased the size of the wake increased. Contamination of the interface decreased the internal circulation which resulted in a movement of the separation ring towards the equator of the drop and also in an increase in the size of the attached wake. This has been observed by GARNER and TAYLBAN[49] and by ELZINGA and BANCHERO[39].

Satapathy and Smith observed that above a Reynolds number of 40, the wake lost its stability and started to oscillate from side to side, and at a Reynolds number of 45 it started to break up on alternating sides of the drop. There is some disagreement in the frequencies of the wake shedding. WINNIKOW and CHAO[178] found that the wake shedding frequency was up to 70% higher than the droplet frequency of oscillation the difference being greater for smaller drops. EDGE and GRANT[37], however, were not able to find any difference between the two frequencies and in trying to explain Winnikow and Chao's findings they pointed out that the latter

investigators obtained their results from single still shadowgraphs and not from cine-films and were therefore probably in error.

As in the case of solid spheres there is disagreement in the reported values of the critical Reynolds numbers for the onset of the separation of the flow. It is in fact difficult to decide visually when an attached wake is formed at the rear of a drop and it is a matter of personal opinion. The use of dyes for the visualisation of the wakes and also the extraneous impurities which are present in the systems also effect the internal circulation and this in turn effects the wake formation. Two more sources of disagreement need to be taken into consideration when comparing various results. The critical Reynolds number is defined as

$$Re_{crit} = \left[\frac{U_\infty D \rho_a}{\mu_a}\right]_{crit} \qquad (2.46)$$

where ρ_a and μ_a are the density and viscosity of the continuous phase, respectively, and $[U_\infty]_{crit}$ the critical velocity of the drop relative to the ambient fluid. GARNER and coworkers[41][43][48][49] and WINNIKOW and CHAO[178] defined $[D]_{crit}$ as the equivalent spherical diameter of the drop at the onset of separation. SATAPATHY and SMITH[139] and MAGARVEY and BISHOP[106] defined it as the maximum diameter D_H of the drop in a horizontal plane. Secondly the use of a critical Reynolds number as defined in equation(2.46)

does not take into account the differing physical properties of the drop phase liquids which were used by the various authors.

Wake Classification :

It is convenient to classify wakes according to the nature of the motions set up in the continuous phase far behind the drop. Although the motion within the attached wake at the rear surface of the drop determines the trail far behind, these motions are much more difficult to observe.

MAGARVEY and coworkers[105][106][107][109], who used unpurified systems, described in detail and classified the droplet wakes at some distance behind the drop. They recognized six distinct and reproducible trail configurations for the range of stable drop sizes. The classes and the range of Reynolds numbers corresponding to each class are indicated in Table 2.1. The line of demarkation was not sharp between any two classes. The trail left by the moving drop was a single thread regardless of separation, provided the Reynolds number was less than 210. The double thread configuration, characterized by the Reynolds numbers between 210 and 270, was accompanied by an asymmetry of the attached wake. In the Reynolds number range of 270 to 290 the wake appeared as double thread

Wake Class	range of Reynolds number	Nature of the wake
I	0 - 210	Single thread
II	210 - 270	Double thread
III	270 - 290	Double thread with waves
IV	290 - 410	Procession of vortex loops
V	290 - 700	Double row of vortex rings
VI	700 - 2500	Asymmetrical wake

Table 2.1 Wake classification of MAGARVEY and BISHOP[106]

characterized by equally spaced wavy disturbances. This range was considered as a transition to the next class. Above a Reynolds number of 290 two distinct wake patterns were observed. These were classified as either class IV or class V wakes and whichever pattern occurred seemed to be a matter of chance and the authors suspected that the initial conditions determined which class of wake was formed. Class IV wakes were observed up to a Reynolds number of 410 and were characterized by a series of vortex loops connected by an intricate system of vortex filaments. Class V wakes were observed up to a Reynolds number of 700 and consisted of a double row of vortex rings. These rings all moved at the same acute forward angle with the line of fall of the drop and there was a perfect symmetry. Above a Reynolds number of 700 the symmetry was lost and the discharge of one element did not initiate conditions which led to a discharge from the diametrically opposite side of the wake axis as was the case with the class V wakes. This classification has been adopted by several authors although the Reynolds number ranges marking the classes were disputed. DIMIAN and RUCKENSTEIN[35] and MUNTEAN, DIMIAN, and HRISTESCU[119] obtained different Reynolds number ranges to mark the wake classes, higher or lower ones depending on the method used to make the wakes visible. The disagreement in the Reynolds number ranges is probably because of interfacial contamination and therefore these results

are only of qualitative importance.

WINNIKOW and CHAO[178] investigated the wakes behind drops in purified systems. They observed threadlike wakes at Re = 805 and class III wakes at Re = 660. This shows that the Reynolds number alone is not sufficient to determine the wake classes for purified systems. The change in the wake class was found to depend on the Reynolds number as well as on the property parameter b^* which is defined in equation (2.17). This property parameter was considered as a measure of the internal circulation.

EDGE and GRANT[37] who also used specially purified systems considered only 5 wake classes. These wake classes are listed in Table 2.2 and illustrated in Fig.2.3. The transition from one wake type to the other was not sharply defined and at certain drop sizes the wake resembled a mixture of two wake classes. Transition of the wake structure from a thread-like wake to a vortex street was related to a transition Ohnesorge number.

Class	Description
I	Nonoscillating drop. Single thread wake.
II	Drop oscillating with small amplitude. Single thread wake with pulses.
III	Drop oscillating vigorously. Chain of vortices formed along the axis of fall.
IV	Drop oscillating vigorously and falling in a zig-zag path. Vortices shed on alternate sides of the vertical axis.
V	Random wobble of the drop. Irregular detachment of vortices.

Table 2.2 Wake classification by EDGE and GRANT[37]

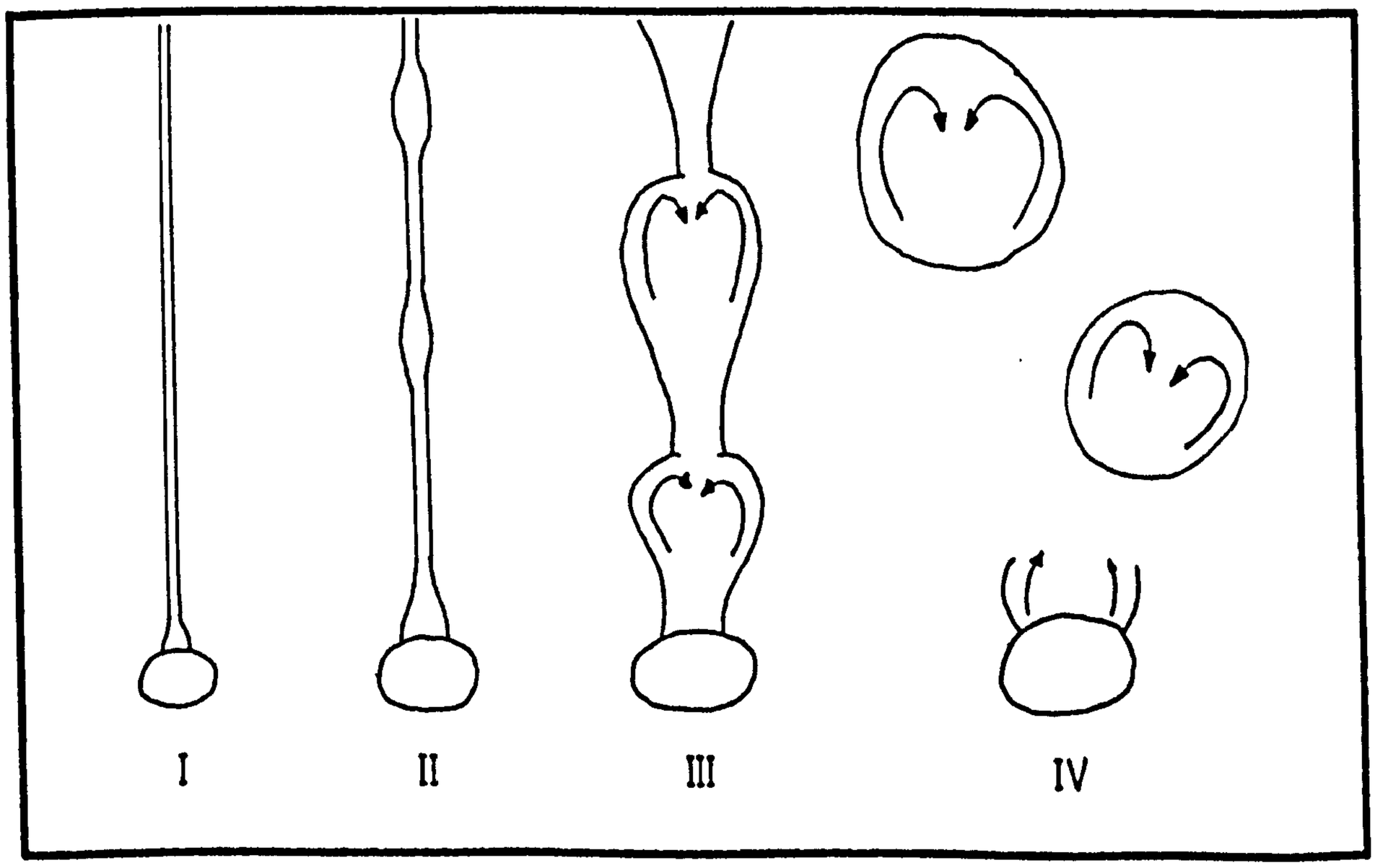

Fig.2.3 Illustration of the wake classes

2.3 INITIAL HYDRODYNAMICS

There hasbeen little investigation of the hydrodynamics of accelerating drops. The main studies which have been made are on the velocity of fall and there are also some observations on the wakes behind accelerating drops. There does not appear to be any research on the shapes or on the frequency of oscillations of accelerating drops.

2.3.a) Velocity of Fall

There have been a number of theoretical studies on the velocity of fall of accelerating drops. For the accelerational motion of a drop falling through a stagnant continuous phase of infinite extent a force balance gives :

$$V_1 \rho_d \frac{dU}{dt} = V_1(\rho_d - \rho_a) g - C_D \; A \frac{\rho_a}{2} U^2 \qquad (2.47)$$

This equation has been solved by LAPPLE and SHEPHERD[91] for the velocity of fall of spherical drops at low Reynolds numbers. The solution can be given in the form

$$U = (U_\infty)_{St}\left[1 - \exp\left(-\frac{18\,\mu_a}{\rho_d D^2} t\right)\right] \qquad (2.48)$$

where $(U_\infty)_{St}$ is the Stokes velocity given in equation (2.11). To obtain the equation (2.48) they assumed the drag coefficient C_D in equation (2.47) to be given by the equation (2.12). For higher Reynolds numbers they

assumed the drag coefficient to be constant throughout the accelerational period and to be equal to that in the terminal period of fall. The solution is then given by :

$$U = U_\infty \tanh \sqrt{\frac{3}{4} \frac{\Delta\rho}{\rho_d} \frac{\rho_a}{\rho_d} \frac{g(C_D)_\infty}{D_{E,1}}}\, t \qquad (2.49)$$

The assumption, that the drag coefficient is constant and equal to that in the terminal period is not based on any theoretical reason and it is very doubtful.

In the acceleration period there is a resultant force on the drop which varies with time, and the momentum produced by this force is distributed between the drop and the surrounding medium. This will give rise to an effect which is equivalent in a nonviscous medium to an increase in the effective mass of the drop. STOKES[151][153] and later LAMB[89] showed that for a spherical drop the increase in the effective mass is equal to half of the mass of the medium displaced by the drop. If this is taken into consideration equation (2.47) is transformed into :

$$V_1\left(\rho_d + \frac{\rho_a}{2}\right)\frac{dU}{dt} = V_1\left(\rho_d - \rho_a\right) - C_D\, A\, \frac{\rho_a}{2}\, U^2 \qquad (2.50)$$

This equation has been solved by HU and KINTNER[72] who assumed that the drag coefficient in this equation is constant and equal to that in the terminal period. They found that thevelocity of fall is given by :

$$U = U_\infty \tanh \sqrt{\frac{3}{4} \frac{\Delta\rho}{\rho_d + \frac{\rho_a}{2}} \frac{\rho_a}{\rho_d + \frac{\rho_a}{2}} \frac{g(C_D)_\infty}{D_{E,1}}}\, t \qquad (2.51)$$

This equation takes into consideration the effect of the acceleration on the velocity of fall only to a limited degree. Improved analyses on the accelerational velocity of fall were made by BASSET[6][7][8], PICCIATI[126] and BOGGIO[11] for noncirculating drops and by PEARCEY and HILL[124] for circulating drops. These analyses are tedious to use and are limited to nonoscillating drops. The hydrodynamics of accelerating drops which are oscillating is complex and no author has attempted to analyse theoretically the motion of these drops.

Experimental investigation of accelerating particles has been made mainly in the fields of solid spheres falling both in air and in water and water drops falling in air. Reported accelerational drag coefficients were much higher than the corresponding terminal drag coefficients[1][2][30][103][104][145]. SCHMIDT[145] fitted his velocity versus time data to a curve which is given by the equation :

$$U = U_\infty (1 - C^t) \qquad (2.52)$$

where C is a constant.

The accelerational drag coefficient is calculated from equation (2.52) as :

$$C_D = (C_D)_\infty \frac{U_\infty^2}{U^2}\left[1 + \frac{\rho_d}{\Delta\rho}\frac{\ln C}{g}(U_\infty - U)\right] \qquad (2.53)$$

LUNNON[103][104] gave for the accelerational drag coefficient :

$$C_D = (C_D)_\infty + \frac{4}{3}\frac{\rho_d}{\rho_a}\frac{b}{m}\frac{D}{U^2}\frac{dU}{dt} \qquad (2.54)$$

where m is the mass of the sphere and b the "carried mass" which is a measure of the increase in the effective mass mentioned earlier. In Lunnon's experiments b varied between one half and twice the displaced mass. The equations (2.53) and (2.54) show that the accelerational drag coefficients are higher than the terminal drag coefficients and vary with time. Thus the assumption of constant drag coefficients during acceleration which was made to obtain equation (2.49) is not valid.

Two authors using widely different systems observed an oscillation in the velocity against time curves. This occurred before the terminal velocity was reached. SCHMIDT[145] observed this phenomenon with wax spheres falling through water and with rubber balloons rising in air, and LAWS[92][93] recorded it with water droplets falling through air. In Schmidt's case there was a maximum in the velocity which was followed by a minimum before the terminal velocity was reached. The maximum was less than the terminal velocity in most of the cases. To investigate this he looked at the wake pattern behind the spheres by wetting them with a coloured dye solution. He observed that at a time corresponding to the above minimum in the velocity versus time curve the first shedding of the wake

occurred. Schmidt concluded that the increase in the volume of the wake before shedding was reducing the kinetic energy of the sphere and correspondingly its velocity. In Laws' case, above a certain drop size the velocity overshot the terminal velocity and then decreased to the terminal value thus exhibiting a maximum. Laws suggested that the drop distortion was lower at this maximum than in the terminal region and that this accounted for the lower air resistance. However, he had no experimental evidence to substantiate this view.

2.3.b) Wakes

There does not appear to be any theoretical analysis of the formation of the wake behind accelerating drops and only the simpler cases of solid spheres or circular and elliptical cylinders have been analyzed. These deal mainly with the growth of a wake behind the body after impulsive start of motion or during a motion with constant acceleration. The point at which separation first occurs was found to coincide with the downstream stagnation point by BOLTZE[12] for a sphere after impulsive start of motion, by BLASIUS[10] for a circular cylinder both after impulsive start of motion and for a motion with constant acceleration. However, for elliptic cylinders in impulsive flow GÖRTLER[53] showed that the attached wake was formed forward of the rear stagnation point when $E > 2/\sqrt{3}$.

Experimental investigations have been concerned mainly with the wakes behind solid spheres and circular cylinders. For spheres falling in water SCHMIDT[145] observed that the first boundary layer separation occurred at some point forward of the rear stagnation point. However, the boundary layer separation was shown by SCHWABE[147][148], GOLDSTEIN[52] and SCHLICHTING[143] to occur first at the rear stagnation point for cylinders during constant acceleration, as suggested by BLASIUS[10].

The evolution of a wake behind an accelerating liquid sphere was observed by MAGARVEY and BLACKFORD[108]. Firstly a threadlike wake was formed which separated somewhere near the rear stagnation point the exact position of which could not be determined. Secondly a wake with vortex loops was formed which separated forward of the rear stagnation point and then the separation point moved towards the rear of the drop during the growth of the wake. They observed that the transition wake patterns which were found with accelerating drops were different to the wake types which were found in the terminal region. However, they did not give details of their results or of their experimental technique.

2.4 BREAKUP OF DROPS

The breakup of drops has been observed in widely varying systems. Similarities between these systems, however, do exist, and three basic types of breakup have been classified by HINZE[68]. These are the breakup of drops in a viscous liquid flow, the breakup of drops in a gaseous flow, and the breakup of drops which occurs during emulsification in turbulent flow. Theoretical studies of the mechanism of droplet breakup have been made mainly in two of these fields : drops in a steady viscous sheared motion and drops falling in air. The first of these has been analysed using a procedure based on Rayleigh's theory for the breakup of a liquid column and is for that reason of some relevance to the present work. The second type of breakup is also of some relevance as it has been observed that liquid-liquid systems which have low interfacial tension often break up in a manner similar to the breaking of liquid drops falling through air. There does not appear to be any theoretical analysis of the mechanism of the breakup of drops falling freely through another phase, although there have been several experimental studies of these systems.

2.4.a) Breakup of Drops Falling in Air

During its free fall in air a breaking drop flattens and it then forms into a rim with a thinner section that extends behind like a bag. Then the bag bursts into a fine spray of very small droplets leaving a ring behind which then disintegrates into a circle of several droplets. This bursting process is often described by the term "bag breakup" and was first observed by LENARD[94][95] and HOCHSCHWENDER[69] and subsequently by LANE[90] and MAGARVEY and TAYLOR[110]. KLÜSENER[87] explained this bag-type deformation of the drop from pressure-distribution considerations. He proposed that if the balance between the surface tension pressure and the dynamic air pressure is disturbed so that the latter is much higher the drop will disintegrate. This explanation was also supported by TRIEBNIGG[172] and LITTAYE[102] and it suggests that breakup occurs when the Weber number exceeds a critical value. HINZE[66][67] showed that this critical Weber number depended both on the variation with time of the dynamic forces and on the viscosity of the droplet liquid. He found that for the case of freely falling water drops in still air the critical Weber number was approximately 10. This is somewhat higher than the value of 2.3 which was suggested by LEVICH[16] from theoretical considerations of the breakup of drops in an air flow.

Although this is the only type of breakup which has been reported in any detail for drops falling in air it must be borne in mind that it occurs over a limited range of Weber numbers. This was observed by LANE[90] who found that when the Weber number was appreciably higher than the critical value, breakup occurred in a chaotic way.

2.4.b) Breakup of Drops in Viscous Sheared Flow

The first work on this mode of breakup is due to TAYLOR[159][160][161] who examined the deformation and breakup of a drop in another liquid in plane - hyperbolic or couette-flow conditions. He observed that the originally spherical drop was pulled out into a long narrow shape so that ultimately a long cylindrical column was formed which finally broke up into droplets. This observation of the cylindrical threads which form during the breakup led TOMOTIKA[168][169] to apply the theory of liquid jet stability to the breakup of these threads. The theory which was developed by Tomotika was in good agreement with Taylor's observations. Taylor's theory on the deformation of drops in viscous sheared flow was later modified by various authors[4][5][26][135][136][171]. Basing on these modifications KARAM and BELLINGER[79] suggested that $E < 1/3$ for breakup to occur. His experimental results supported this suggestion.

2.4.c) Free Fall Breakup in Liquid-Liquid Systems

Several types of breakup have been reported in the literature for drops falling freely through another liquid. KINTNER[84] and SCHROEDER and KINTNER[146] reported that under extreme conditions, nozzle-induced oscillations can be of sufficient violence to cause drop breakup. They also concluded that drop breakup is not caused by the terminal oscillations of the drop which are not nozzle-induced and do not decay with time. HU and KINTNER[72] and ELZINGA and BANCHERO[39] also observed breakup which was caused by oscillations of large amplitude, but they did not report at what stage of the fall this occurred. Hu and Kintner, using both dimensional analysis and force balances, suggested that this breakup occurs at a constant Eötvös number. From their experimental data they obtained for this critical Eötvös number for droplet breakup :

$$E\ddot{o}_{crit} = 14.2 \tag{2.55}$$

or for the critical drop diameter :

$$D_{E\ddot{o}crit} = 0.1204\left(\frac{\sigma}{\Delta\rho}\right)^{0.5} \tag{2.56}$$

In this work they used technical-grade liquids. EDGE and GRANT[38], however, showed that both the frequency and the amplitude of oscillation are effected by the presence of surfactants in the system. This suggests that equation (2.56) cannot be valid for specially

purified systems. The approach of Elzinga and Banchero was different. They noted GUNN's[54] proposition that an oscillating drop falling in air exhibits a sideways drift from the vertical path when the wake shedding frequency is equal to the natural frequency of oscillation and they suggested that this resonance could also increase the amplitude of oscillation thereby causing the drop to rupture. They used the Lamb's frequency as the natural frequency of oscillation and Hu and Kintner's data for the frequency of wake shedding. They obtained for the critical diameter for breakup :

$$D_{E,lcrit} = 777 \left(\frac{\sigma}{3\rho_d + 2\rho_a}\right)^{0.22} \frac{\mu_c^{0.78}}{\rho_d^{0.78} U_\infty^{1.22}} \qquad (2.57)$$

This analysis disregards the fact that the natural frequency of oscillation of drops is much lower than the Lamb's frequency especially at high Reynolds numbers when the oscillations have large amplitudes. Also EDGE and GRANT[37] have shown that the frequency of natural oscillations and the frequency of wake shedding are identical even for nonbreaking drops.

The bag-type breakup, which was observed for liquid drops falling through air, has also been observed by STUKE[155] and O'BRIEN[122] with liquid drops falling through another liquid. Droplet velocities in liquid-liquid systems are much lower than in liquid-gas systems and this type of breakup

is only possible when the interfacial tension is very low, and it has not been observed in the types of systems which are commonly in use in liquid-liquid extraction.

2.5 BREAKUP OF A LIQUID COLUMN

The earliest investigations on the behaviour of liquid jets were carried out by BIDONE[9], MAGNUS[111] and SAVART[140]. However, little of their work was related to the stability of cylindrical jets of liquid and the first investigation of consequence on the subject is by PLATEAU[127][128]. He studied both theoretically and experimentally the stability of cylindrical columns of liquid and found that a fluid cylinder is unstable and will break up when its length exceeds its circumference. However, the classical work in this field was carried out by RAYLEIGH[129][130][131].

Rayleigh's Analysis of the Stability of a Liquid Column:

Rayleigh clarified and extended Plateau's theory. He considered a cylinder of inviscid fluid and of infinite length. The surface of the cylinder was subjected to a spectrum of infinitesimal disturbances at one end and he determined the conditions under which these disturbances will grow. The disturbed surface was represented in cylindrical coordinates by :

$$r = \bar{r} + f(\theta, z) \qquad (2.58)$$

where $f(\theta, z)$ is small compared with $\bar{r}$. The volume of the disturbed cylinder was assumed to be equal to the volume of the undisturbed cylinder. If $f(\theta, z)$ is

expanded in a Fourier series

$$r = \bar{r} + \sum_{j}\sum_{n} \alpha_n \cos n\theta \cos k_j z \qquad \begin{matrix} n=0,1,\ldots \\ k_j>0 \\ j=1,2,\ldots \end{matrix} \qquad (2.59)$$

where α_n is the amplitude of a disturbance and

$$k_j = \frac{2\pi}{\lambda_j} \qquad (2.60)$$

where λ_j is the wavelength of the disturbance. The criterion for the growth of the disturbance which Rayleigh used was that if the surface area of the disturbed surface is smaller than that of the original cylinder, then the disturbance will grow. This is because the surface free energy of the disturbed surface will then be less than the surface free energy of the undisturbed surface. The resulting change in the surface free energy per length of the column, $\Delta\varepsilon$, was calculated to be for a column of radius R_c

$$\Delta\varepsilon = \frac{\pi\sigma}{4R_c}\left[(k_j R_c)^2 + n^2 - 1\right]\alpha_n^2 \qquad (2.61)$$

For $n \geq 1$, $\Delta\varepsilon$ is always positive and therefore the system is stable when nonsymmetrical disturbances are present. Only when n=0, which corresponds to the case of symmetrical disturbances and when

$$k_j R_c < 1 \qquad (2.62)$$

will $\Delta\varepsilon$ be negative. If equation (2.62) is combined

with equation (2.60)

$$\lambda_j > 2\pi R_c \tag{2.63}$$

Hence the jet is unstable to an axisymmetrical disturbance when the wavelength of the disturbance is longer than the perimeter of the cylinder. Thus a critical wavelength can be defined as

$$\lambda_{crit} = 2\pi R_c \tag{2.64}$$

All disturbance waves with a wavelength longer than the critical wavelength will amplify with time. Rayleigh assumed that all the initial disturbances were of the same magnitude and therefore that the wave with the largest growth rate was the dominant wave on the surface of the column and ultimately led to the breakup of the column into drops. He evaluated the growth rate of the dominant wave from energy considerations. If there is no net flow of fluid into the column the sum of the kinetic energy and the surface free energy of the column will be constant. Differentiation of this energy balance with respect to time leads to

$$\frac{d^2\alpha_n}{dt^2} + \frac{\sigma}{\rho_c R_c^3} \frac{ik_j R_c I_n'(ik_j R_c)}{I_n(ik_j R_c)} \left[(k_j R_c)^2 + n^2 - 1\right]\alpha_n^2 = 0 \tag{2.65}$$

For axisymmetrical disturbances, n=0, the solution of this equation is of the form :

$$\alpha_0 = \delta_0 e^{qt} \tag{2.66}$$

where q is the growth rate of the disturbance given by:

$$q^2 = \frac{\sigma}{\rho_c R_c^3} \frac{i k_j R_c J_n'(i k_j R_c)}{J_n(i k_j R_c)} (1 - k_j^2 R_c^2) \qquad (2.67)$$

From this equation the maximum growth rate is obtained as

$$q_{max} = 0.343 \sqrt{\frac{\sigma}{\rho_c R_c^3}} \qquad (2.68)$$

The wavelength of this optimum disturbance is then given by

$$\lambda_{opt} = 1.434 (2\pi R_c) \qquad (2.69)$$

The case of a viscous liquid jet in a vacuum was later considered by RAYLEIGH[131]. His solution was complex but for the limiting case of a fluid with a high viscosity the maximum growth rate was given by

$$q_{max} = \frac{\sigma}{6 \mu_c R_c} \qquad (2.70)$$

which occurs at $k_j R_c = 0$ or $\lambda_{opt} \to \infty$. This suggests that when the viscosity is high the liquid cylinder does not tend to disintegrate into equispaced drops, but breaks at a few widely spaced positions. The effect of viscosity was also investigated by WEBER[174]. He gave the maximum growth rate as :

$$q_{max} = \left[\frac{6 \mu_c R_c}{\sigma} + \sqrt{\frac{8 \rho_c R_c^3}{\sigma}} \right]^{-1} \qquad (2.71)$$

and the optimum wavelength as :

$$\lambda_{opt} = 2\pi R_c \sqrt{2\left(1 + \sqrt{\frac{9}{2}\frac{\mu_c^2}{\sigma \rho_c R_c}}\right)} \qquad (2.72)$$

For the case of zero viscosity the equations (2.71) and (2.72) do not reduce exactly to the equations (2.68) and (2.69), respectively. This is due to the simplifications which were made during the derivation of the equations (2.71) and (2.72). The case of viscous jets which are flowing in viscous liquids has been investigated theoretivally by TOMOTIKA[168]. However, this investigation is only of value for systems which have a higher viscosity than those used in the present work. The effect of mass transfer on jet stability was investigated by various authors[23][24][115]. However, in the present system only slight mass transfer was occurring. Thus the effect of mass transfer on jet stability is not discussed.

Secondary Droplet Formation During Coalescence

When a drop of liquid coalesces at a plane interface multi-staged coalescence often occurs and the primary drop is succeeded by a secondary drop of smaller size or a succession of secondary drops of decreasing size. The phenomenon was first observed by

MAHAJAN[112][113] and as many as eight successive stages have been observed by researchers[29]. Details of this phenomenon were first published by WESTWATER[176]. Later CHARLES and MASON[28] who used high speed cine photography in their investigations found that after the rupture of the film which separated the resting primary drop from the interface the drop drained into the lower phase. During this process a column of liquid was formed and it was suggested that the Rayleigh theory could be used to predict the breakup mechanism. They applied the Rayleigh theory making the following assumptions :

a) The coalescing drop drains to form a cylindrical column the height of which is equal to the diameter of the primary drop:

$$H = D_{E,I} \qquad (2.73)$$

b) The liquid column drains as a cylinder with constant height H until the radius of the column has reduced to a value R_c. A disturbance can then grow on the surface of the column. This disturbance is the optimum disturbance which was discussed by Rayleigh and the wavelength of the disturbance is related to the dimensions of the column by the equation

$$\lambda_{opt} = H = Z_o (2\pi R_c) \qquad (2.74)$$

where Z_o=1.434. This is the value predicted by Rayleigh for the ratio of the wavelength of the optimum disturbance to the diameter of the column when the column is of infinite length (equation 2.69).

c) There is no further drainage during the growth of the disturbance so that the volume of the secondary drop is equal to the volume of the column at the start of the growth of the disturbance.

The authors did not measure the height or the diameter of the columns neither prior tonor during necking and had no experimental evidence of the validity of the above assumptions. Their assumptions predicted that the ratio of the diameter of the secondary drop to the diameter of the primary drop was given by :

$$\frac{D_{E,2}}{D_{E,1}} = \left(\frac{3}{2\pi^2 Z_o^2}\right)^{1/3} = 0.42 \qquad (2.75)$$

This value falls within the range 0.13-0.57 which Charles and Mason obtained from their experiments, but the average value for the first stage was 0.29, which is much lower than 0.42. Also measurements of the dimensions of the liquid column from the pictures which were published by the authors indicate that Z_o has a value of approximately 0.5 and not 1.434. There seems to be no valid reason why the disturbance which breaks the column should have the same wavelength as the disturbance which breaks a column of infinite length.

2.6 METHOD OF WAKE VISUALISATION

To observe the vortex pattern behind drops which are moving in a liquid phase several investigators[110][139][155][180] added dyes to the droplet liquid and observed the transfer of the dye into the wakes behind the drops. However, it is obvious that the introduction of foreign material into the system changes the flow characteristics and therefore cannot be used in the investigation of the wake patterns in purified systems.

There are methods, however, which make use of the disturbances, which are already present in the system, to visualize the flow pattern. These are the interferometer, the schlieren, and the direct shadow methods. All of these methods require that the refractive index varies in the region which is to be visualized and this is produced by heat and mass transfer. The methods are complementary rather than alternative. Each one shows features of the flow which may not be clearly observed by the others. Briefly, the interferometer method makes use of the change in the velocity of light which is caused by a change in the refractive index, the schlieren method makes use of the refractive index gradient, and the direct shadow method is dependent on the second derivative of the refractive index. The schlieren method has been used

in the present work to visualize the wake patterns and will be examined further.

The Schlieren Method

When a light beam passes through a medium in which there is a refractive index gradient normal to the beam, then the beam is deflected from its path. It was shown[142] that the curvature at any point on the path taken by the deflected ray is proportional to the refractive-index gradient at that point in the direction normal to the ray. Two methods are available to detect the deflection of the light beam : the Toepler method[70][142][166] and the graded filter method[70]. Fig.2.4 shows the arrangement of a typical schlieren apparatus using the Toepler method with a Z layout. A rectangular light source is placed at the focal plane of the first concave mirror M_1 and an image of this light source is formed at the focal plane of the second concave mirror M_2. A knife edge is positioned at K so that it covers part of this image. The position of the knife edge measured along the axis of the light beam is critical and this position is adjusted so that when there is no optical disturbance present in the working section there is a uniform illumination on the screen Q. When an optical disturbance is present in the working section the image of the source is displaced so that the illumination of the screen in the

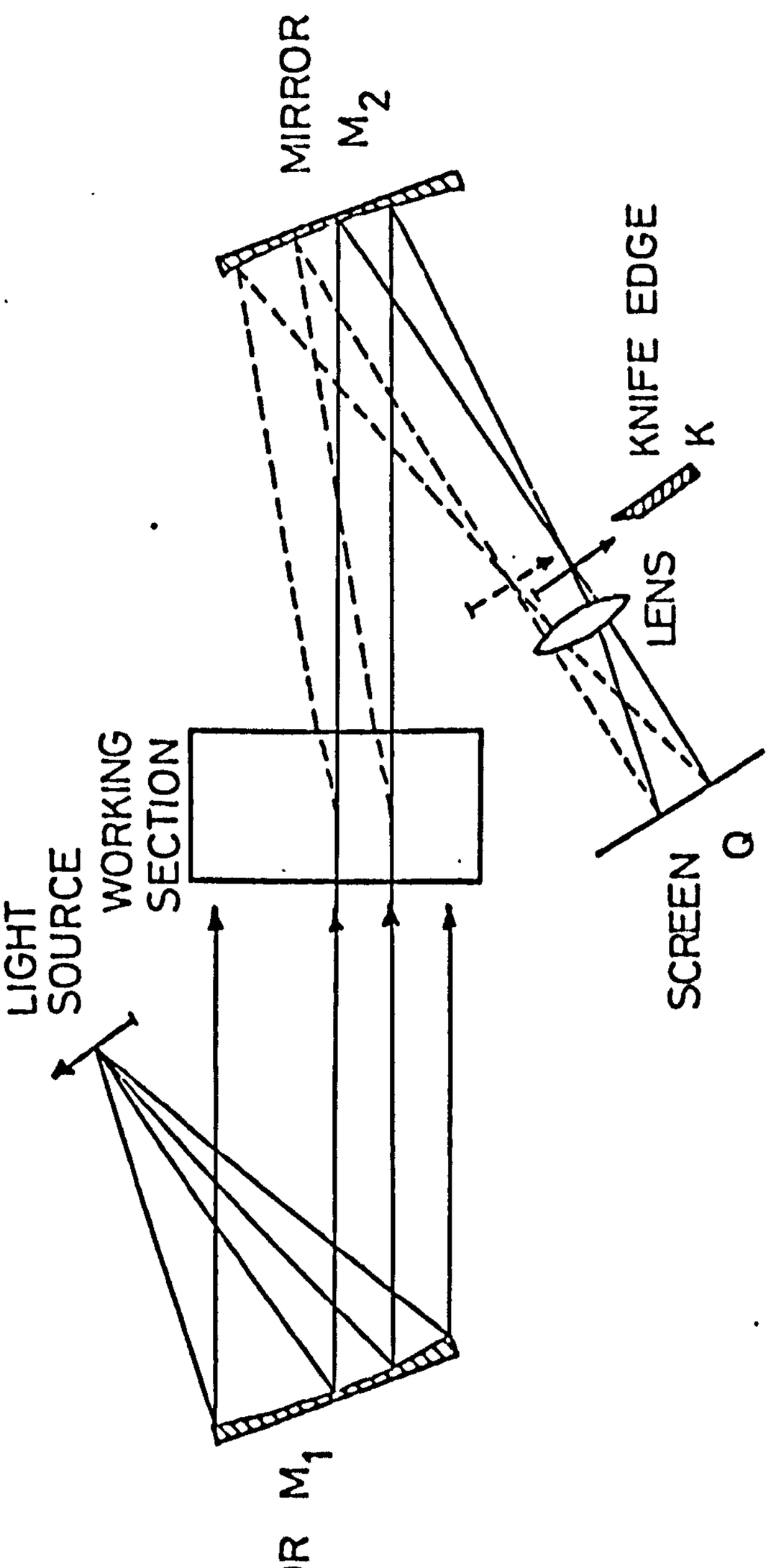

FIG.2.4 ARRANGEMENT OF A TYPICAL SCHLIEREN APPARATUS

region which contains the image of the disturbance is either decreased or increased depending on which way the beam is deflected by the disturbance. Only deflections of the beam at right angles to the knife edge have any effect on the illumination of the image; deflections parallel to the knife edge have no effect.

In the second schlieren method a graded filter is used in the focal plane of the second concave mirror instead of a knife-edge. The proportion of the light that is transmitted changes with the displacement of the image of the source. The advantage of this method is that some indication of the magnitude of the refractive-index gradients which exist in the working section can be obtained from measurements of the illumination which is present at various points on the screen.

SECTION 3

APPARATUS AND EXPERIMENTAL METHODS

3.1 INTRODUCTION

In order to visualise the wakes behind the drops a schlieren system was used and liquid-liquid systems were chosen for the experiments so that slight mass transfer took place between the drops and the continuous phase. This method of flow visualisation was the most suitable one for use with purified liquids because with the other methods which were considered the hydrodynamics of the drops were changed to a higher degree by the visualisation method.

The schlieren system which was used was of the conventional type using a Z layout except that the knife edge was modified. This system is described below in detail.

3.2 THE ARRANGEMENT OF THE OPTICAL SYSTEM

The general layout of the optical system is shown in Fig.3.1. The working section where the drops were observed was the horizontal part of a Q.V.F. crosspiece. The ends of this section were closed with two glass windows W_1 and W_2 which were of schlieren quality. These windows were 6 inch in diameter and 1 inch thick.

A mercury vapour discharge lamp was used as the lightsource. 70 volts D.C. was supplied continuously to the lamp. A condenser lens C was used to focuse the light beam to obtain a sharp image of the arc of the lamp at the slit S. A heat filter was positioned between the lamp and the lens, and a monochromatic filter between the lens and the slit. Arrangement was also made to accommodate neutral density filters between the lens and the slit. A screen was fitted around the filter holder to prevent unfiltered light reaching the slit. The light was reflected by two mirrors M_1 and M_2 before it passed through the working section. The mirror M_1 was a plane one which merely folded the diverging light beam from the slit on to the mirror M_2. The mirror M_2 was concave and it was positioned at a distance from the slit equal to its focal length. Thus it transformed the diverging light beam into a parallel one. The parallel light beam passed through

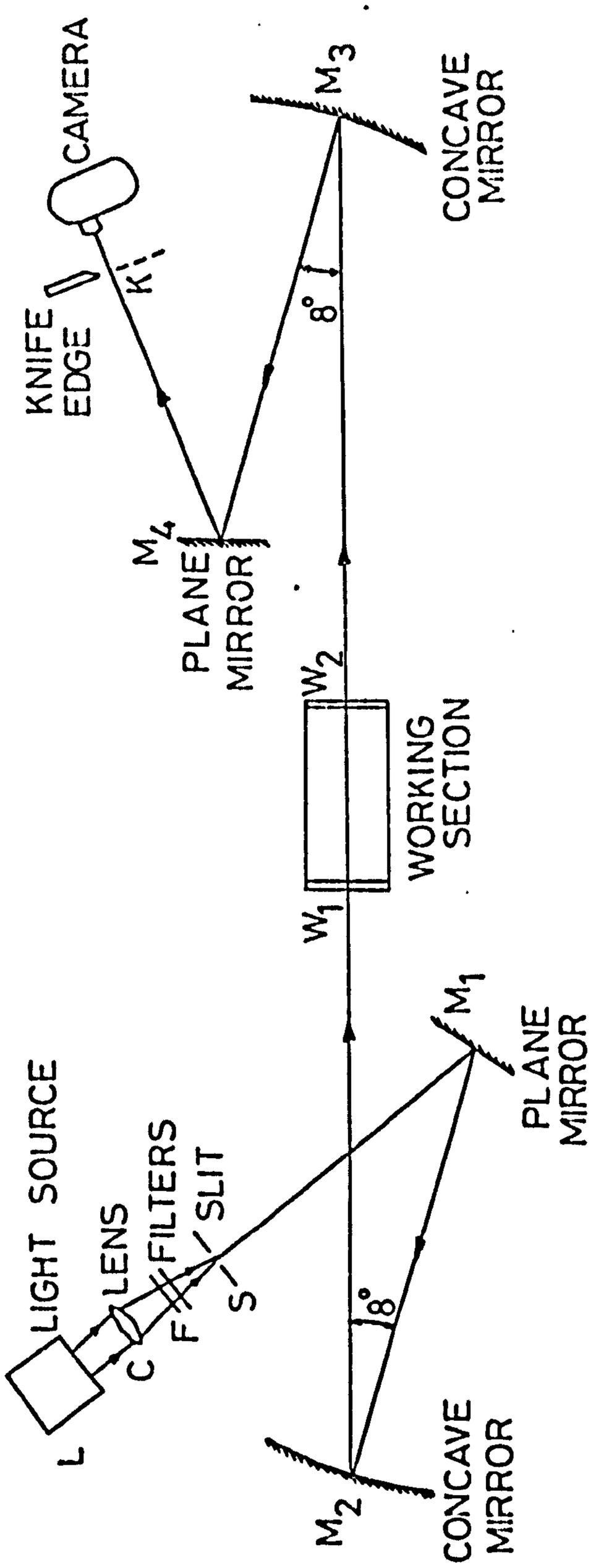

FIG.3.1 LAYOUT OF THE SCHLIEREN OPTICAL SYSTEM

the working section on to the concave mirror M_3. This mirror was identical to M_2 and condensed the parallel light beam. The light beam was then folded at a second plane mirror M_4 before it converged to the focal point of M_3. The knife edge K was positioned at this focal point and the camera was set up behind the knife edge at a position where the diameter of the diverging light beam was less than the diameter of the camera lens. The distance between the mirror M_3 and the test section was made approximately equal to the focal length of the mirror. This allowed the camera to be focussed at approximately infinity and thus a large depth of field was obtained. The light source and the mirrors M_1 and M_2 are shown in Fig.3.2 and the mirrors M_3 and M_4 are shown in Fig.3.3.

The mirrors were of schlieren quality and they were always kept covered when not in use to prevent any dust settlement on their surfaces. The plane mirrors M_1 and M_4 were 4 inch in diameter, and the spherical ones M_2 and M_3 were 8 inch in diameter with a focal length of 6 foot. The angles of reflection at the two concave mirrors were approximately 8^o and were in opposite directions. This arrangement minimized the aberration caused by the mirrors. The axis of the light beam was set up at a height of 160 cm above floor level for convenient viewing. All of the mirrors, the optical benches which supported the light source and

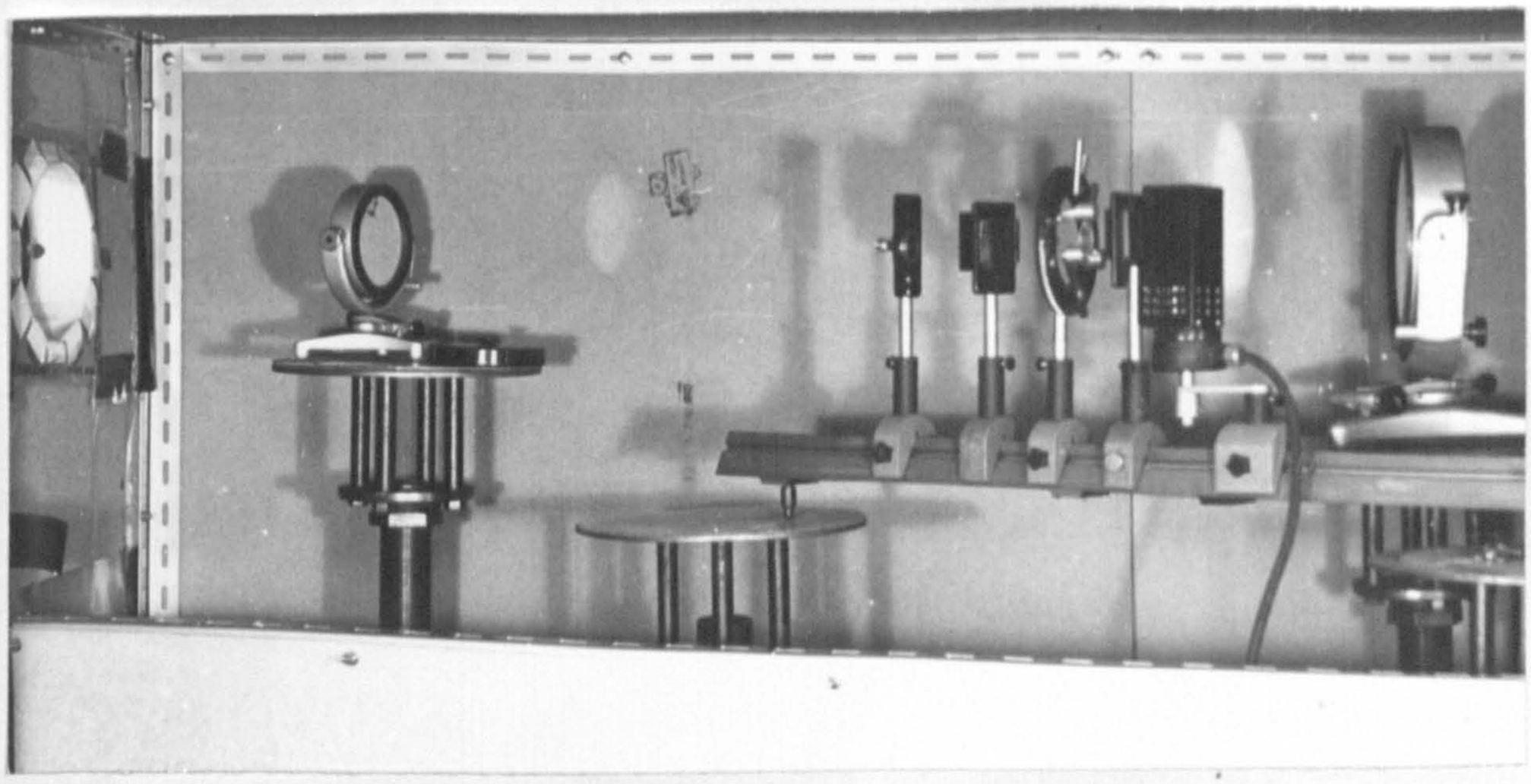

FIG.3.2 THE LIGHT SOURCE AND THE MIRRORS M_1 AND M_2

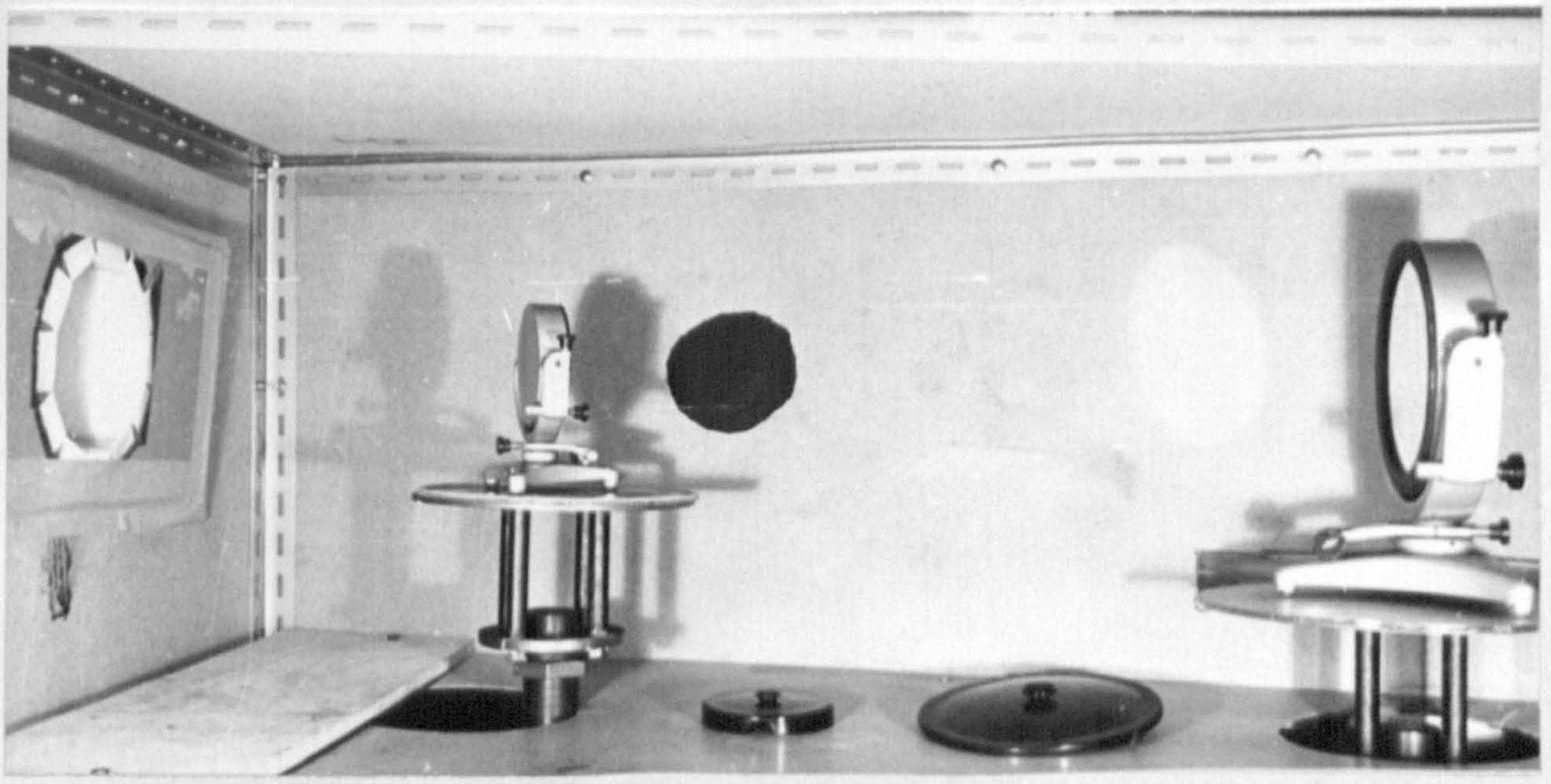

FIG.3.3 THE MIRRORS M_3 AND M_4

the filters, and the knife edge were positioned on pillars the heights of which were adjustable. These pillars, which are shown in Fig.3.4, were mounted in sand filled cylinders to damp vibrations and to minimize accidental movement of the pillars. Two large hardboard boxes on each side of the working section totally enclosed the optical system. This protected the system from dust and accidental damage, and also diminished the atmospheric thermal convection currents between the mirrors. These currents lead to random schlieren images and are therefore undesirable.

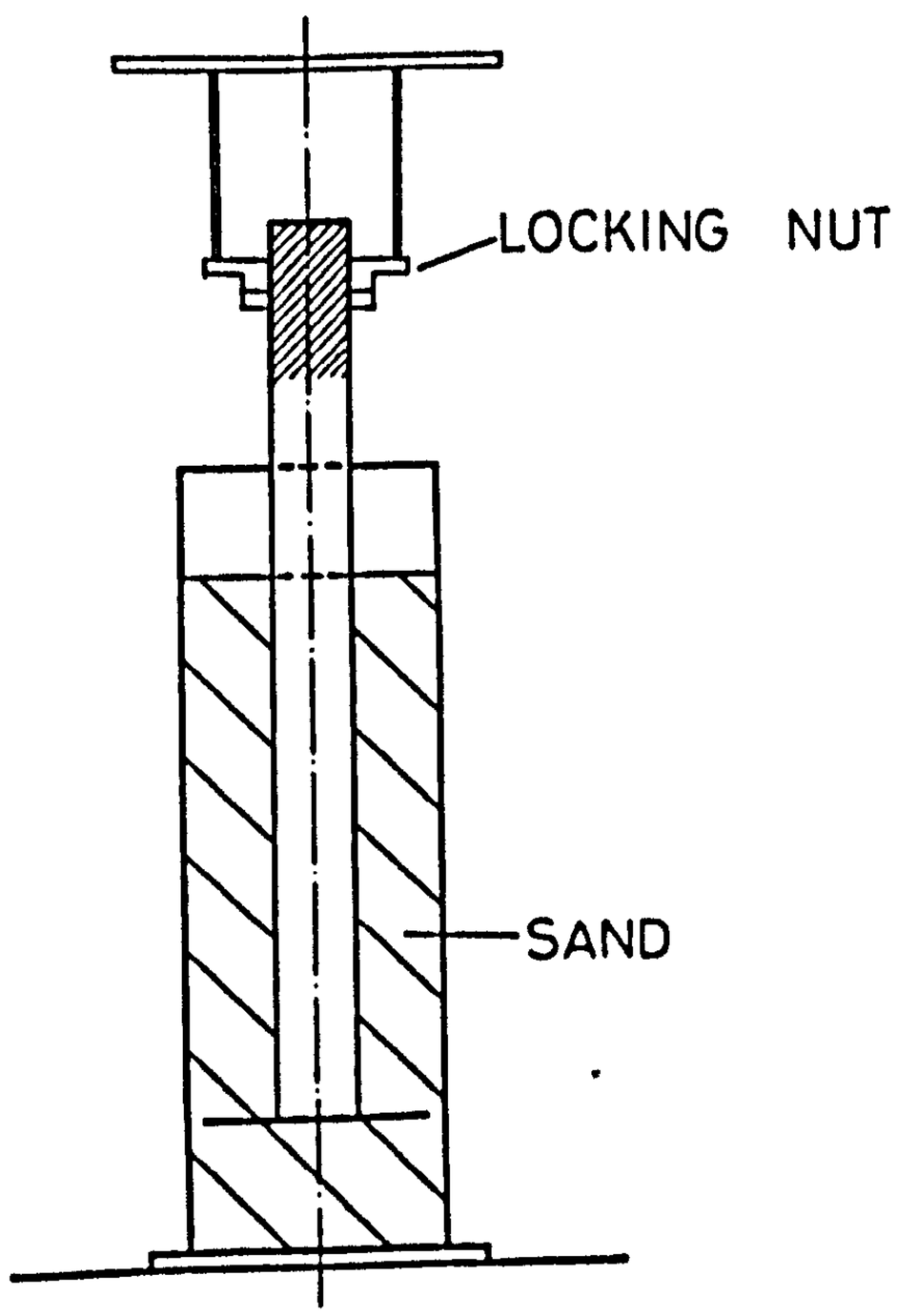

FIG.3.4 CROSS SECTION OF A PILLAR

3.3 METHOD OF SETTING UP THE OPTICAL SYSTEM

The plane mirror M_1 and the concave mirror M_2 were placed approximately in the required positions. The lens, the lamp, and the slit were assembled on the optical bench so that the image of the arc of the lamp was focussed on the back of the slit. The optical bench was then placed so that the slit was close to the focal point of the concave mirror M_2. M_1 and M_2 were arranged so that the light beam passed through the working section. This light beam was reflected back by a plane mirror which was positioned in the parallel light beam from M_2. Thus an image of the slit was formed near the slit. The position of the optical bench was changed until this image of the slit coincided with the slit. The light beam from the concave mirror M_2 was then parallel. Then the concave mirror M_3 was placed at its working position and was aligned with the parallel light beam from M_2. The plane mirror M_4 was then positioned so as to fold the beam and produce an image of the slit at K in a convenient position. The working section was then viewed through the camera. The schlieren system was considered to be satisfactory when a sharp image of the slit was obtained at the plane of the knife edge and when the moving of the knife edge into the light beam darkened uniformly the field of view in the camera.

3.4 THE KNIFE EDGE

The knife edge which was used during the present work is shown in Fig.3.5. A square glass slide was covered on one side only with two razor blades leaving a thin gap between the blades. The glass exposed by the gap was then vacuum coated with aluminium. When the razor blades were removed an opaque strip was left in the centre of the slide. The width of the strip was chosen so that the schlieren system operated almost in the dark ground mode. This type of knife edge was used in preferance to the conventional type because it gave a clearer indication of the boundary of the attached wake. The glass slide was then fitted into the slide holder with the strip vertical. A fine screw adjustment moved the strip horizontally in a plane normal to the axis of the light beam. This slide holder was fitted to an optical bench so that the opaque strip could be positioned with great accuracy at any point in the optical system.

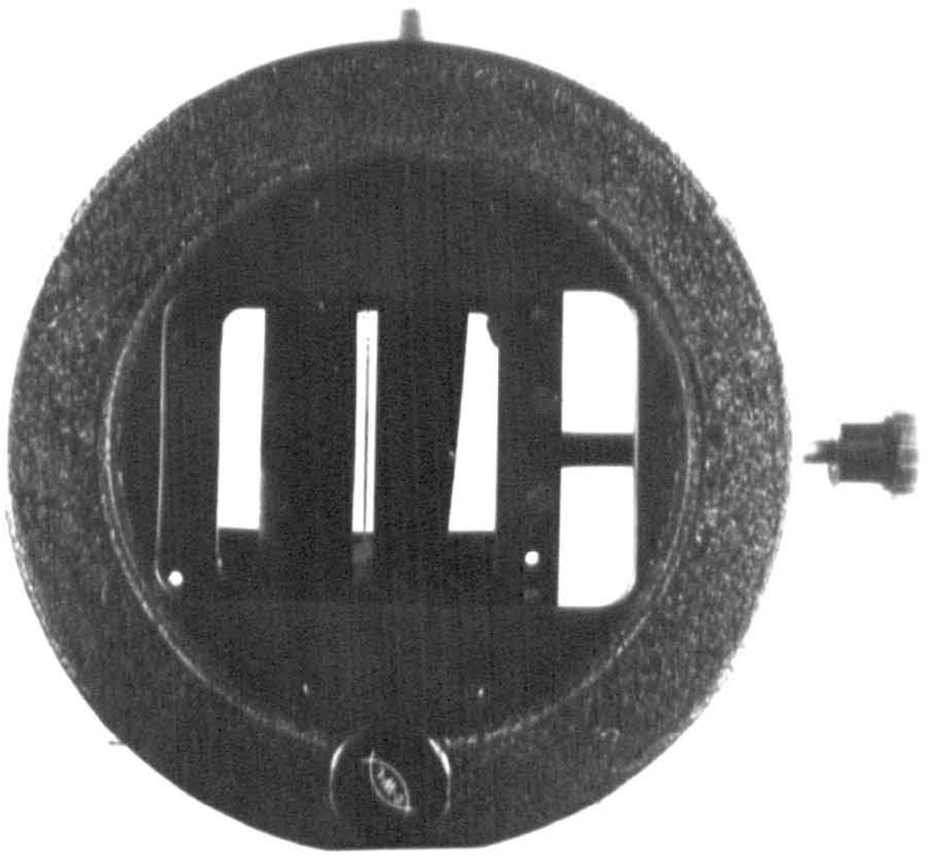

FIG.3.5 THE KNIFE EDGE

3.5 THE SCHLIEREN AND SHADOW IMAGES

In the present work slight mass transfer from the drop to the continuous phase made possible the application of the schlieren method to the visualisation of the wakes behind drops. The boundary layer separating from the surface of the drop had a higher density than the rest of the continuous phase and was visible in the schlieren image as it flowed around the attached wake and then either entered the attached wake or passed into the bulk fluid. In this way the wake was observed. Best results were obtained for the wake region in the immediate neighbourhood of the drop where the density gradient was high and therefore the corresponding refractive index gradient was high. Further downstream, the dissolved droplet liquid was more uniformly distributed in the continuous phase and the refractive index gradient was less than in the regions nearer to the drop. The schlieren image in these regions was less well defined.

A typical schlieren image of the wake is shown in Fig.3.6. This schlieren image is two dimensional whereas the flow around the drop is three dimensional. However, when the drop is falling in a vertical straight line the flow pattern is approximately symmetrical about an axis through the centre of the drop which is parallel to the direction

of motion and therefore it can be assumed that the schlieren image is of a cross-section of the flow at the median plane. The symmetry is lost when the drop moves away from the straight line, but as the drops do not zig-zag in the same vertical plane, the behaviour of the wake can be determined from an examination of the schlieren cine-films of the wakes behind a number of drops.

The schlieren system was converted to a focussed direct shadow system by removal of the knife edge from the light beam. The direct shadow system was less sensitive in detecting the wakes behind drops. However, a sharper outline of the drop was obtained with this system and all measurements were taken from direct shadow images.

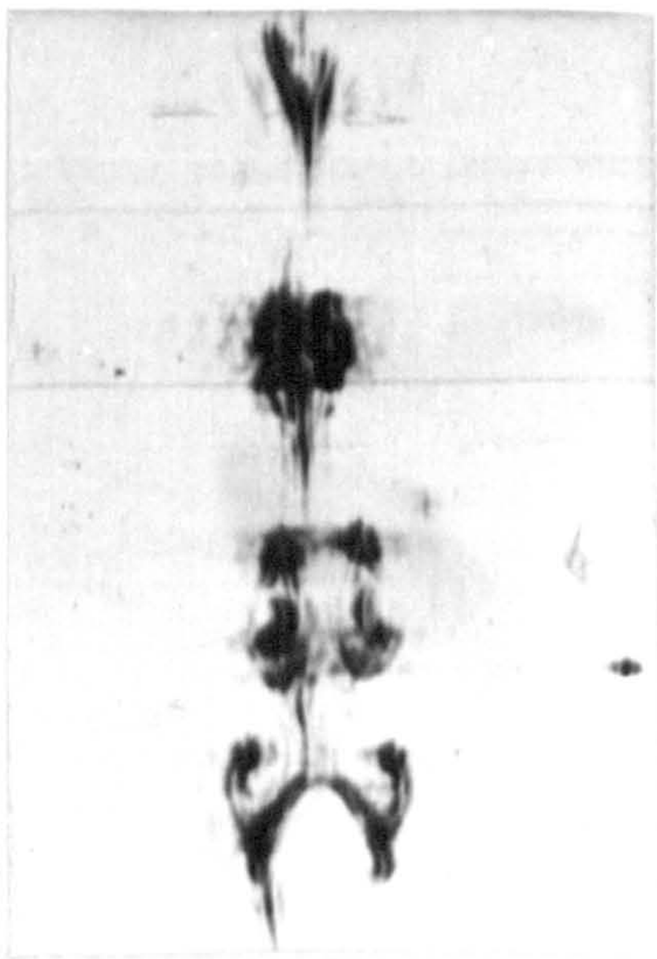

FIG.3.6 A TYPICAL SCHLIEREN IMAGE

3.6 GLASS COLUMN AND SURROUNDINGS

The continuous phase was contained in the glass column shown in Fig.3.7 and Fig.3.8. The glass column was a Q.V.F. standard cross-piece. The horizontal arms of the cross-piece were of 6 inch in diameter and the vertical arms were 4 inch in diameter. The 6 inch diameter branches were closed with schlieren quality glass windows. The cross-piece could be extended upwards by clamping additional Q.V.F. tubes on to the upper 4 inch diameter arm. The lower 4 inch diameter arm was reduced in diameter using standard Q.V.F. parts and then closed at the bottom by a stopcock with a glass barrel and P.T.F.E. plug.

The glass column and the auxiliary drop forming equipment were enclosed in a constant temperature air-bath. This air-bath was made of hardboard sheets bolted together and sealed with tape. The temperature in the air bath was controlled by a reverse acting relay, operating with a contact thermometer and three 100 watt light bulbs. The air in the box was circulated by three small fans and their most efficient position was found by trial and error. Doors were provided in the air bath to give access to the apparatus. To allow the schlieren beam to pass through the column two schlieren windows of 6 inch in diameter were mounted in Q.V.F. flanges and these were

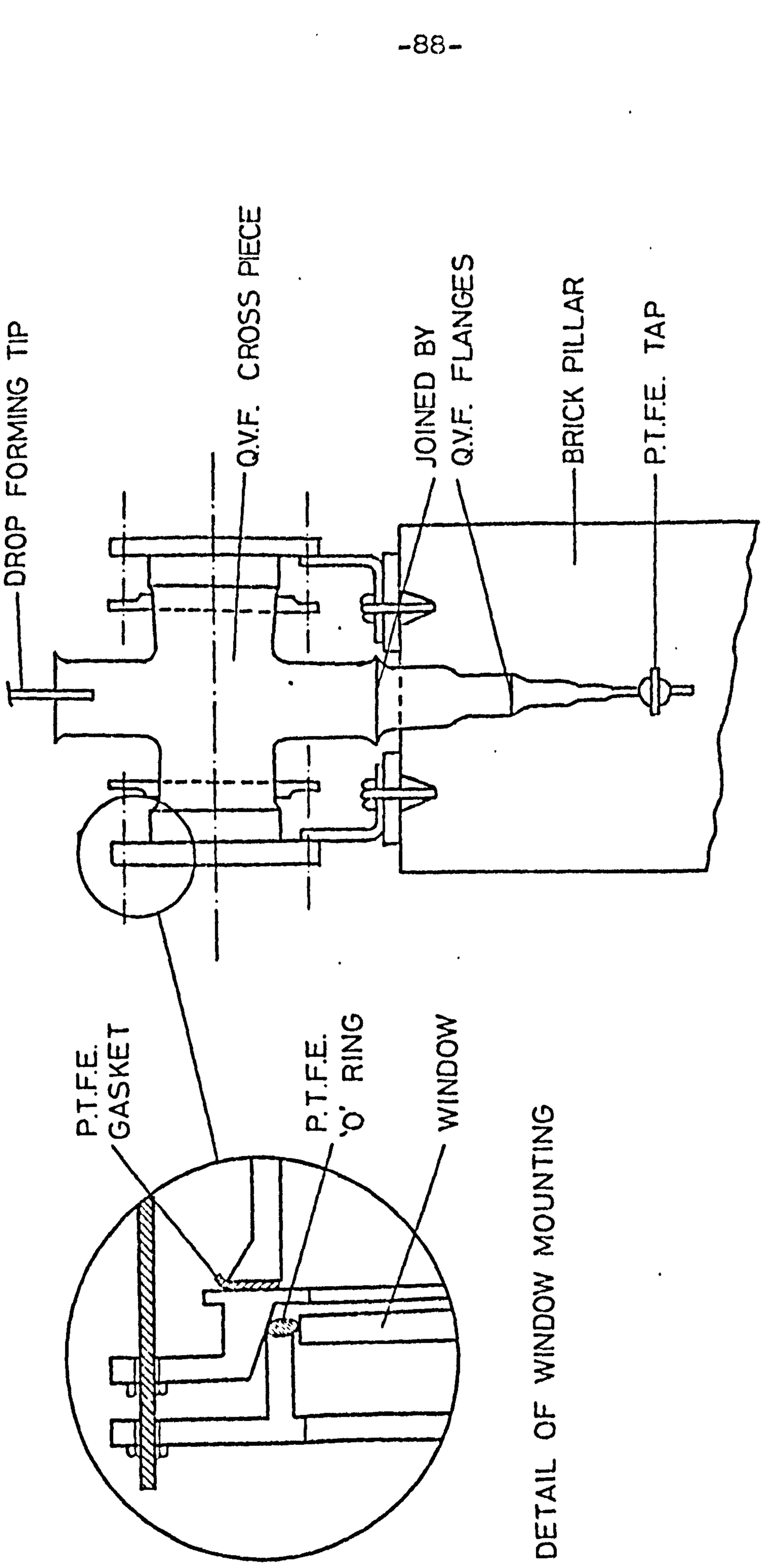

FIG.3.7 THE COLUMN AND SUPPORTS

DETAIL OF WINDOW MOUNTING

ON-OFF TAP

D

E FINE TAP

DROP FORMING TIP

COLUMN

bolted on to the walls of the air bath in line with the schlieren beam. The ambient temperature of the laboratory was maintained close to 24.5°C by electrical fan heaters which were controlled from a contact thermometer.

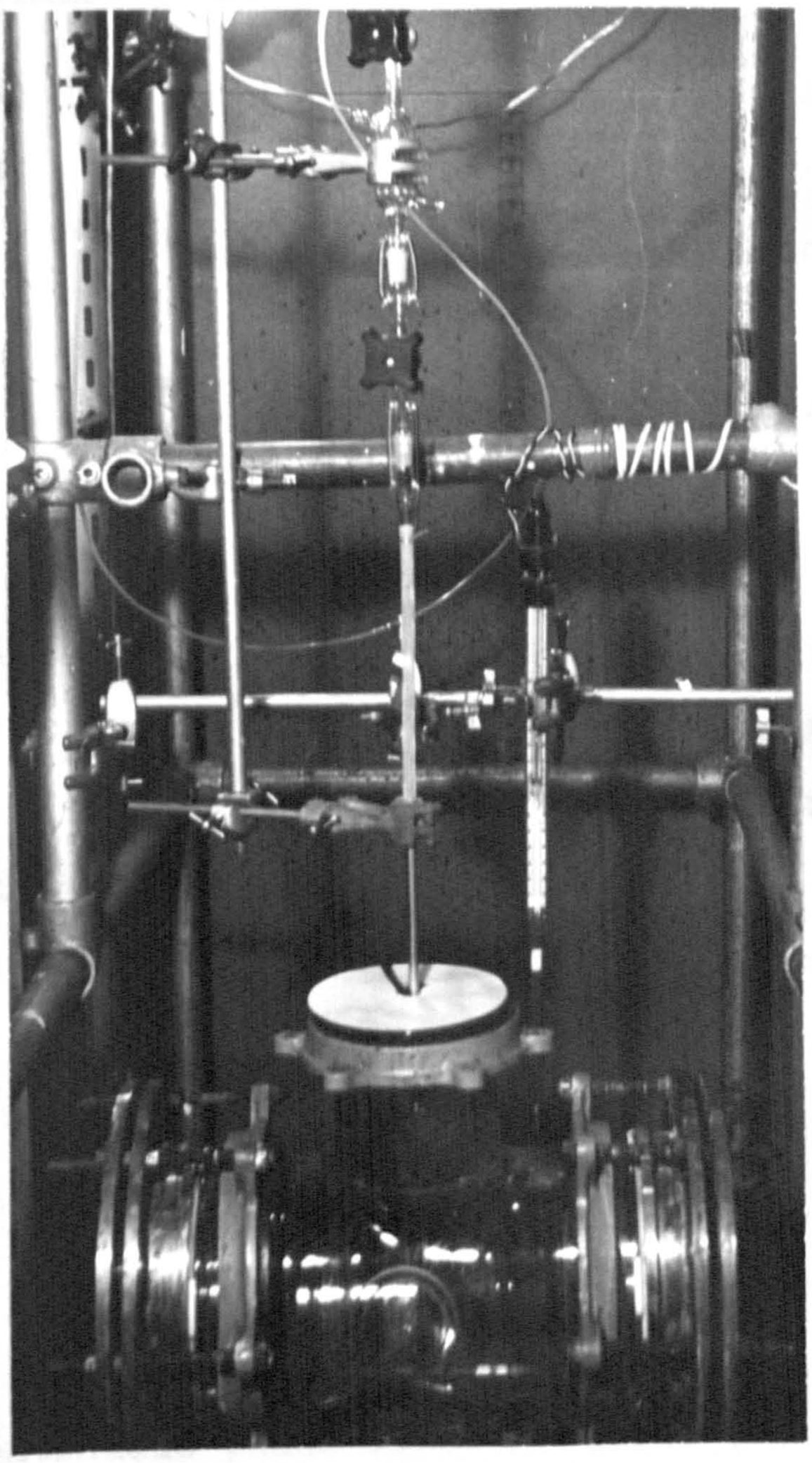

FIG.3.8 GLASS COLUMN WITH THE DROP FORMING TIP

bolted on to the walls of the air bath in line with the schlieren beam. The ambient temperature of the laboratory was maintained close to 24.5°C by electrical fan heaters which were controlled from a contact thermometer.

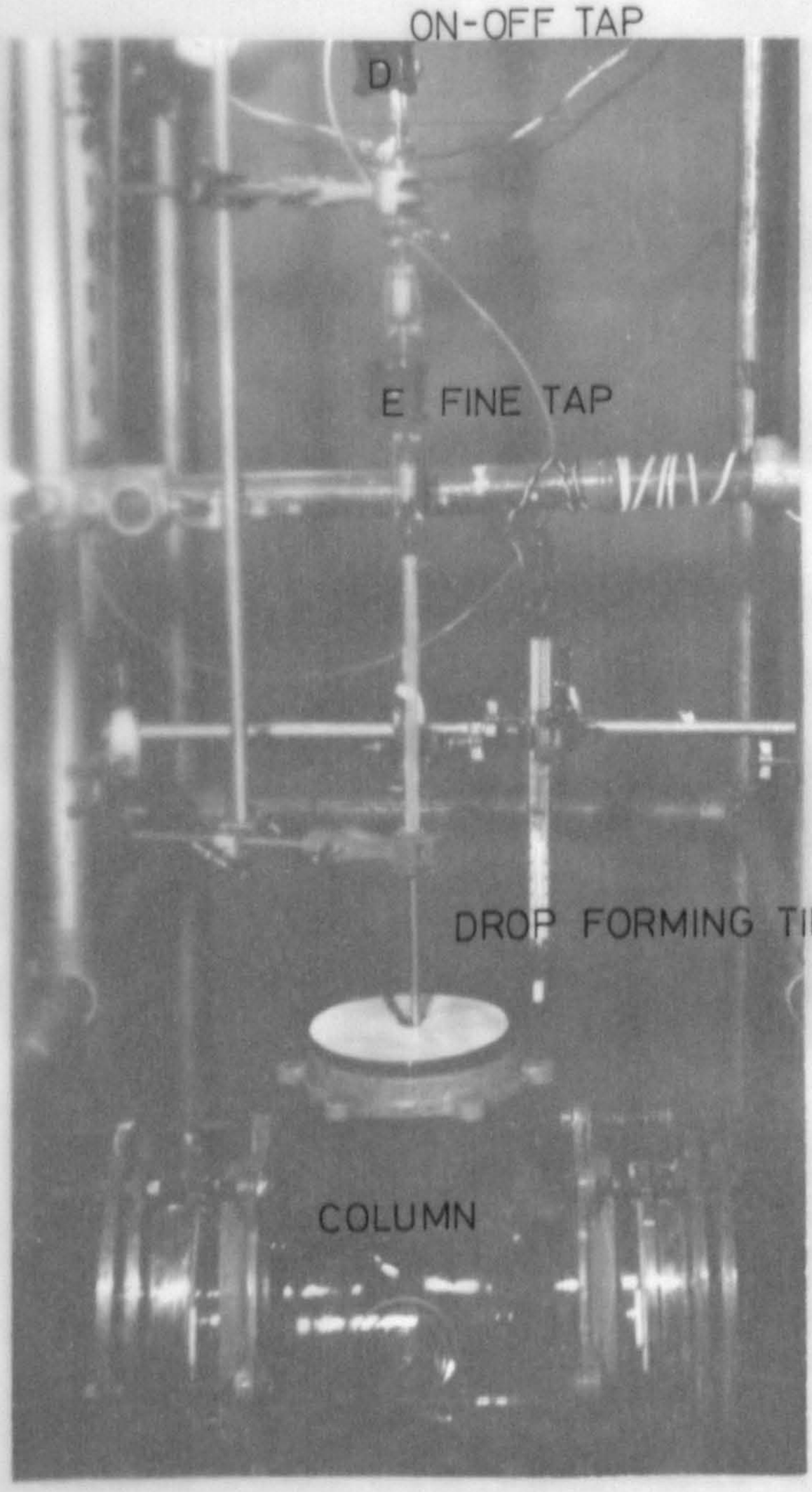

FIG.3.8 GLASS COLUMN WITH THE DROP FORMING TIP

3.7 EQUIPMENT FOR DROP FORMATION

An all glass reservoir, shown in Fig.3.9, contained the droplet phase liquid. It was made of a glass flask which was 2 litre in volume and was pressurized from a nitrogen container. The pressure inside the flask was regulated accurately with a bleed valve and was measured with a mercury manometer. The flask was filled from a side branch A, was emptied from branch B, and was depressurized from branch C.

The flow of the dispersed phase liquid was controlled by the P.T.F.E. plug-taps D and E which are shown in Fig.3.8. Tap D was used as an on and off tap. Tap E had a groove on each side of the plug. These grooves were deeper at the hole of the plug and were cut circumferencially from the hole. This arrangement allowed the flow rate to be set accurately. The final adjustment to the flow rate was made by varying the pressure inside the reservoir. The connections from the taps to the reservoir and to the drop forming tip were in P.T.F.E. tubing.

The drops were formed just below the surface of the continuous phase from the stainless steel tips which are shown in Fig.3.10. The tips had sharp

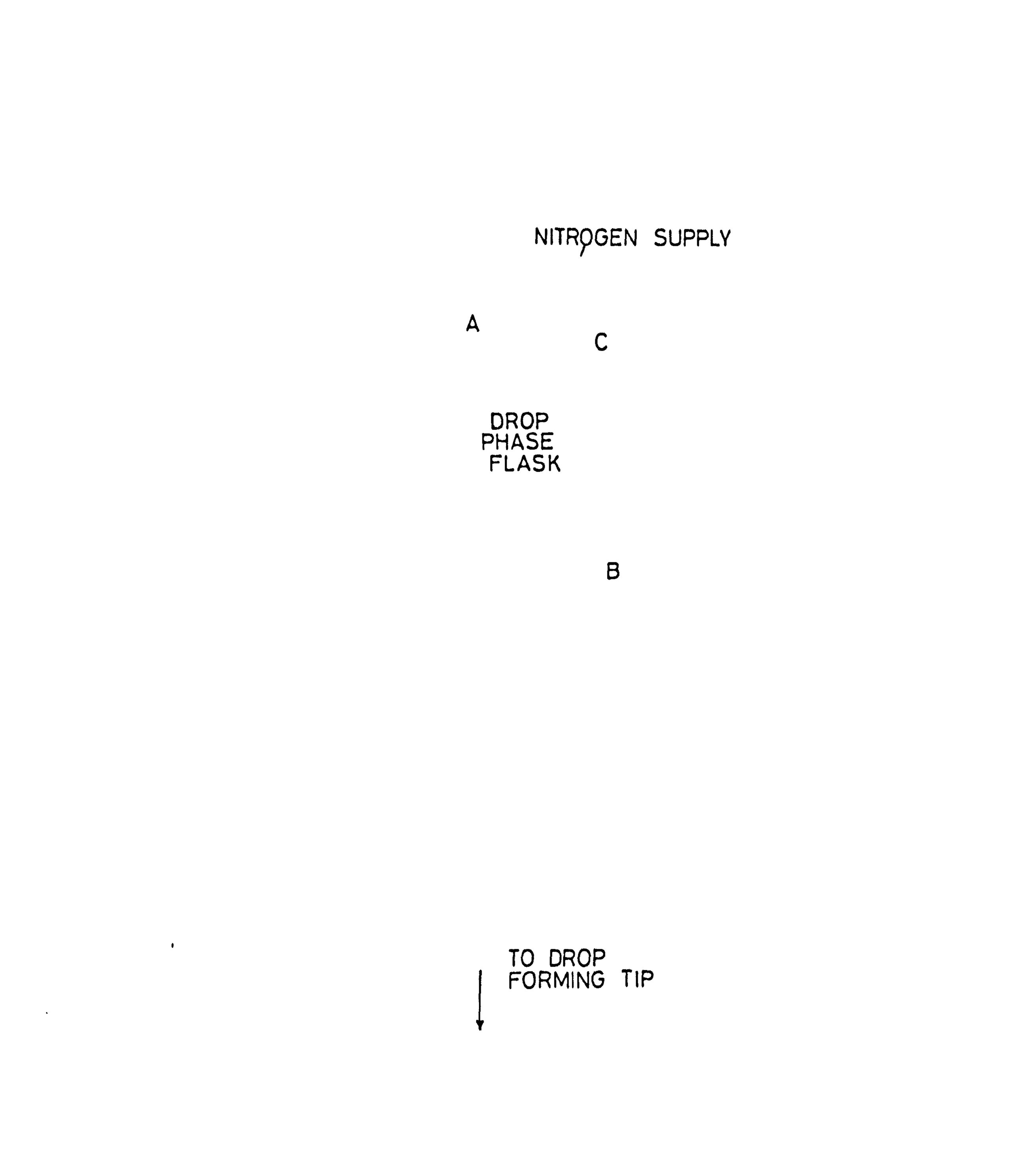
NITROGEN SUPPLY
A
C
DROP
PHASE
FLASK
B
TO DROP
FORMING TIP

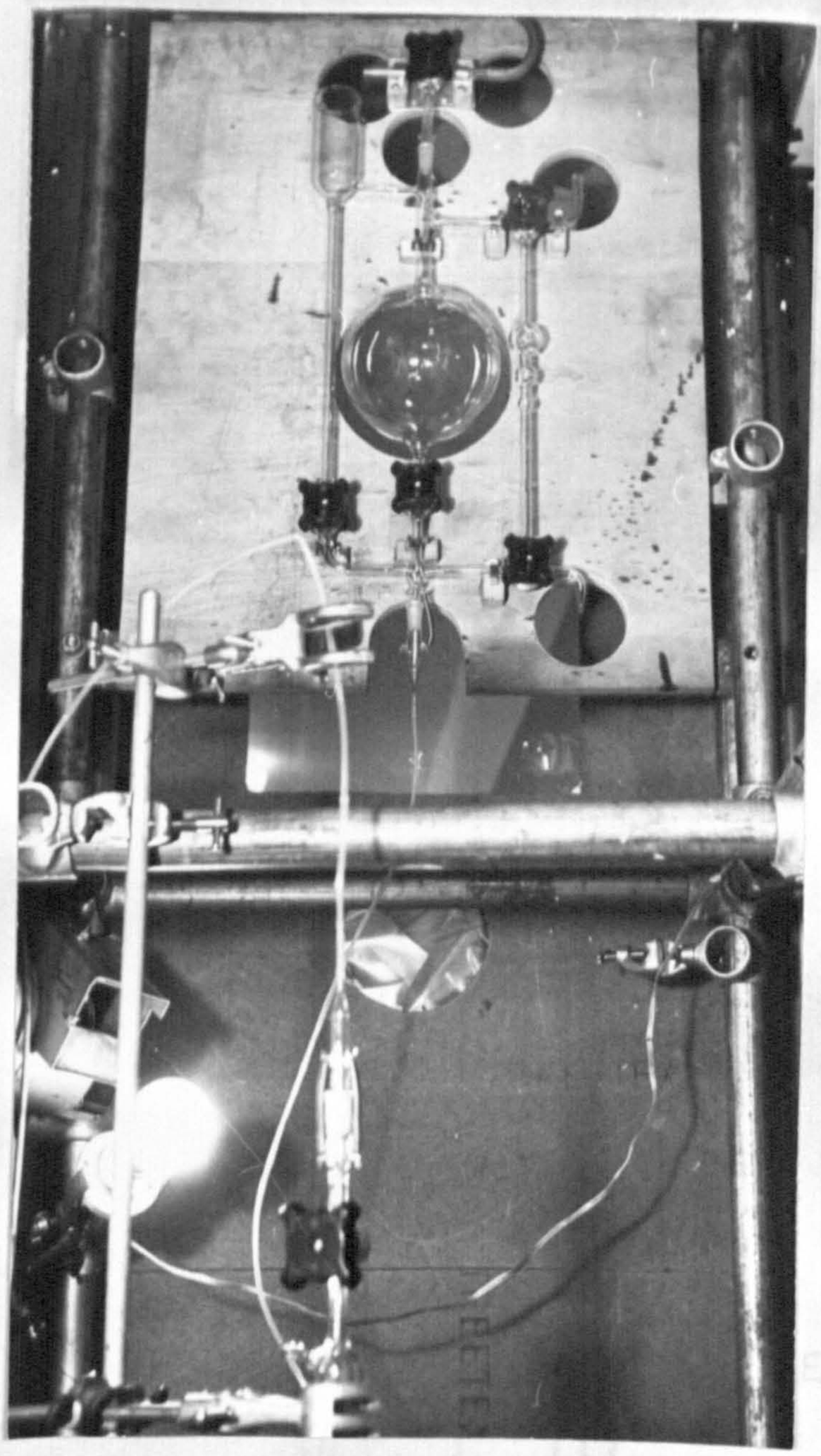

FIG.3.9 DROP LIQUID RESERVOIR

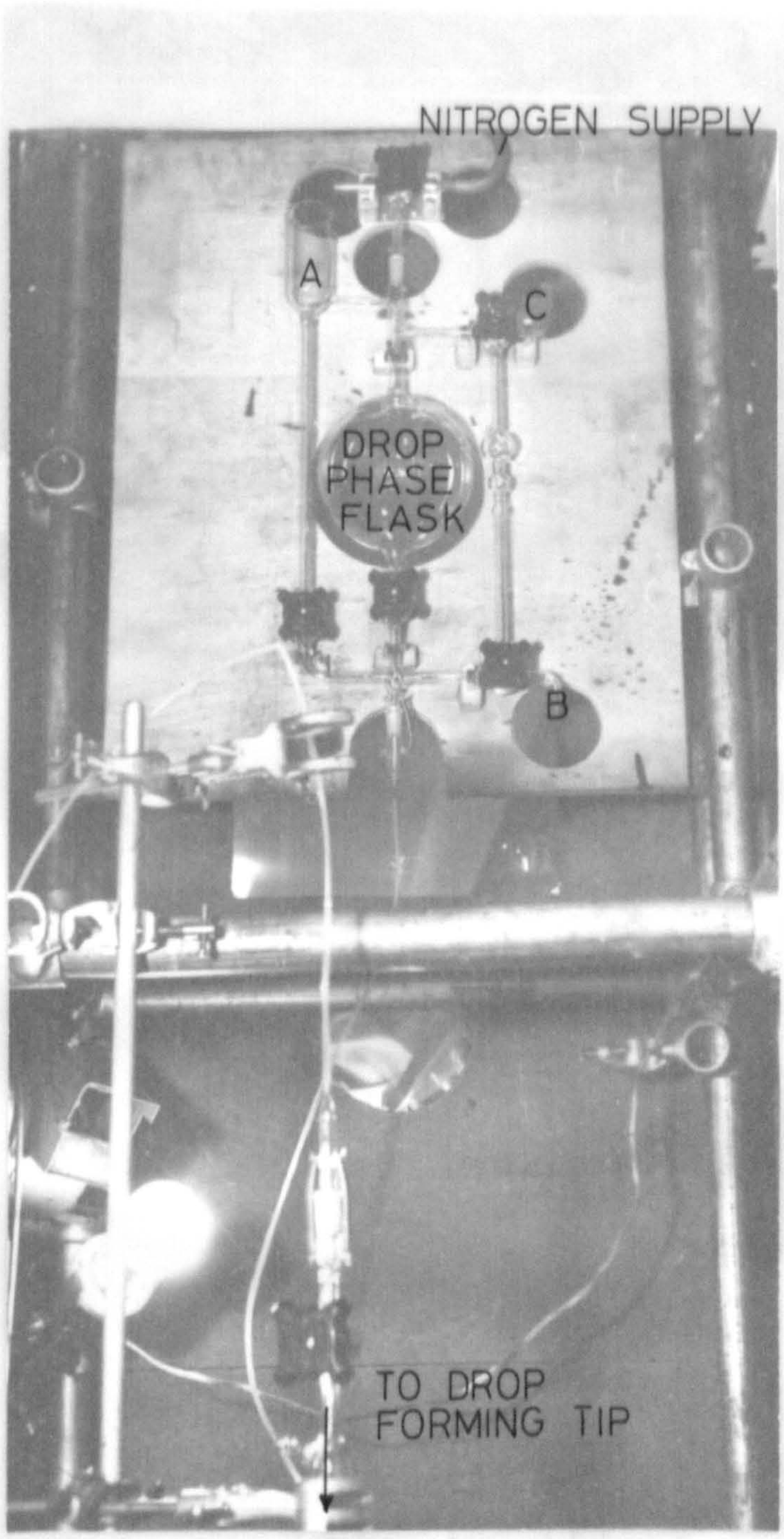

FIG.3.9 DROP LIQUID RESERVOIR

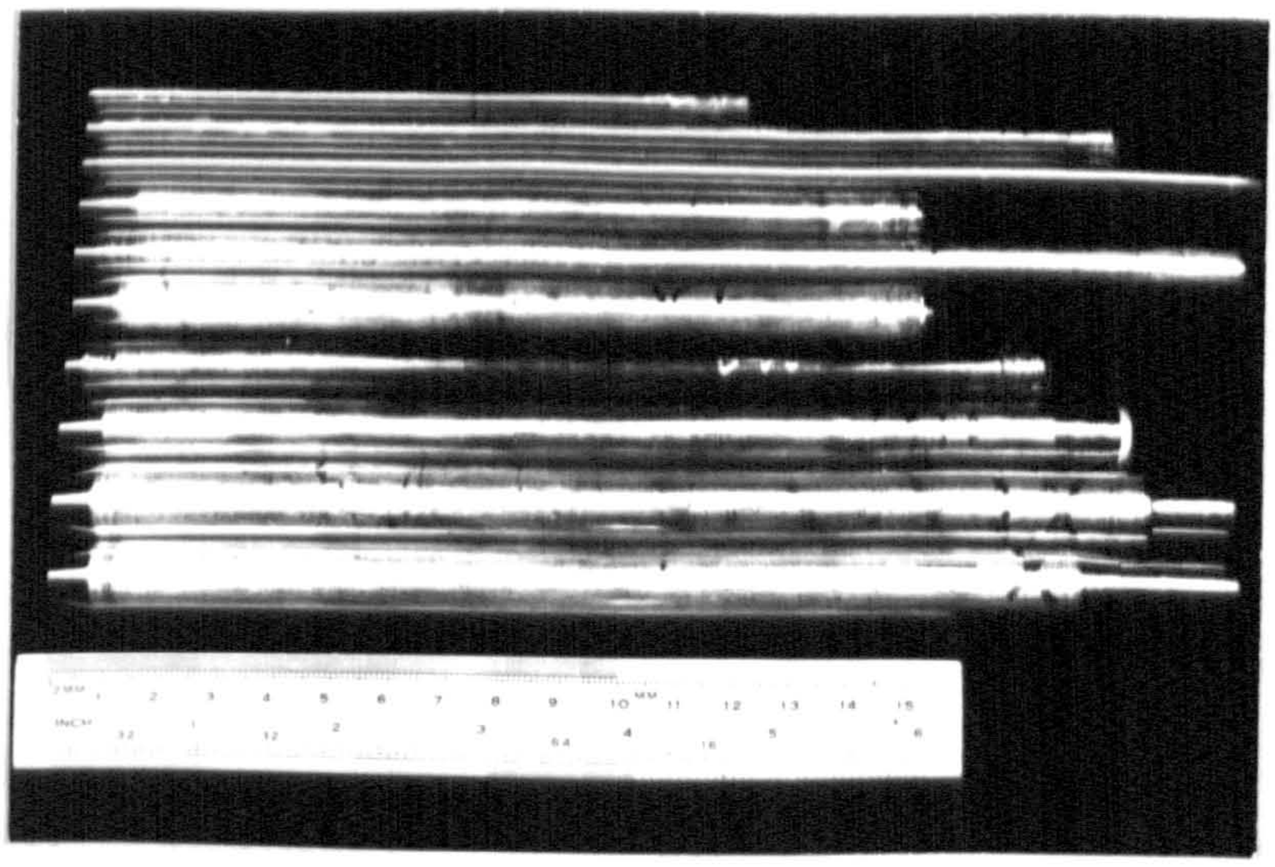

FIG.3.10 DROP FORMING TIPS

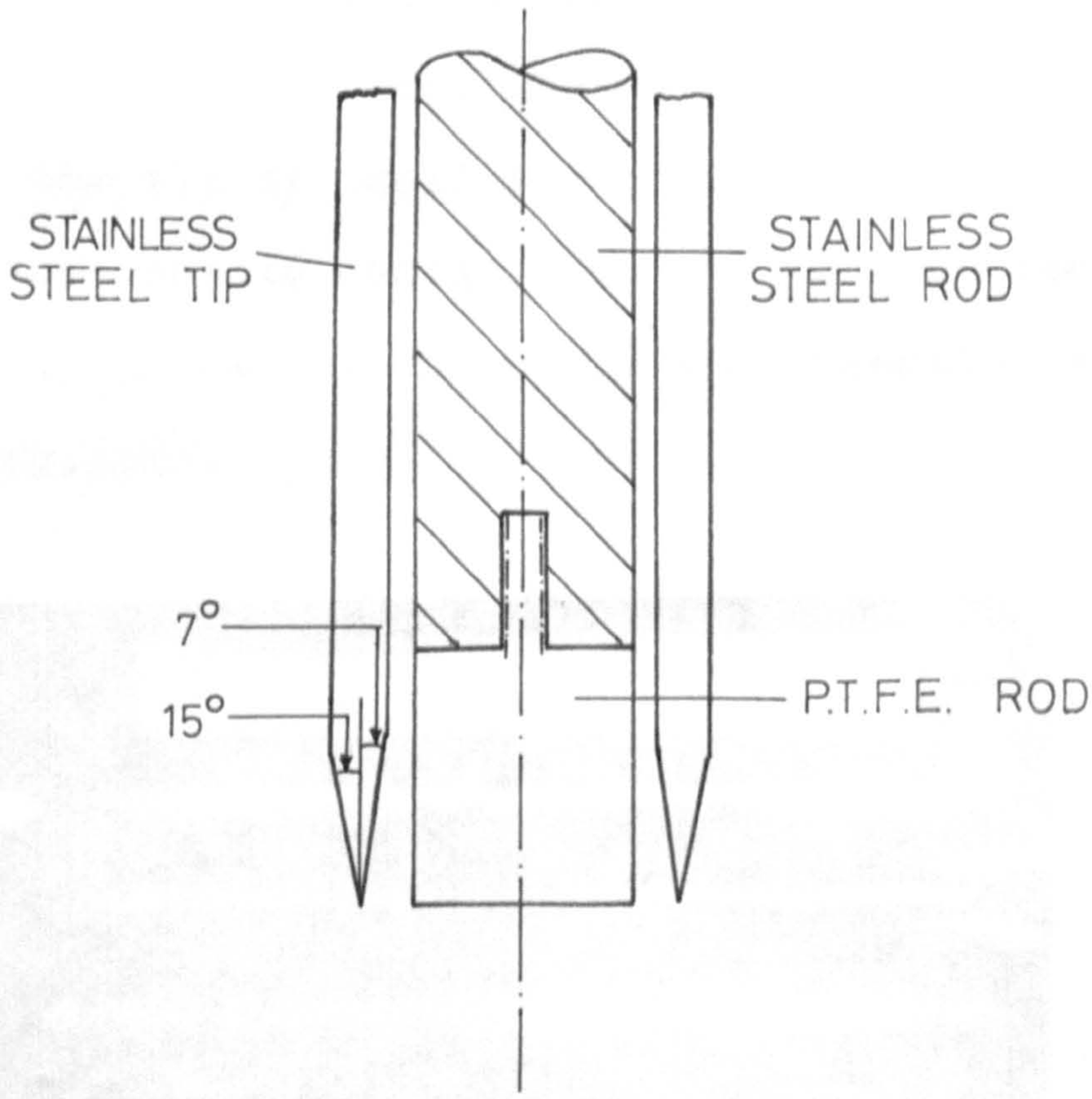

FIG.3.11 DETAIL OF A DROP FORMING TIP

circular edges on which the drops were formed. The internal diameters of the tips lay between 0.2 cm and 1.2 cm. Details of a drop forming tip are shown in Fig.3.11. The end of a piece of stainless steel tubing was cut at a 7^{o} angle inside and a 15^{o} angle outside to give a sharp edge.

Drop formation from the larger tips was difficult because the continuous phase tended to flow up the tip. This was prevented by inserting a stainless steel rod into the tip as shown in Fig.3.11. For better wetting of the front surface of the rod by the drop phase a piece of P.T.F.E. rod was screwed into the end of the stainless steel rod. The whole rod was held tightly in the tip by small pieces of P.T.F.E. Great care was taken not to contaminate the rod and the tubing during assembly. The whole tip assembly is shown in Fig.3.12.

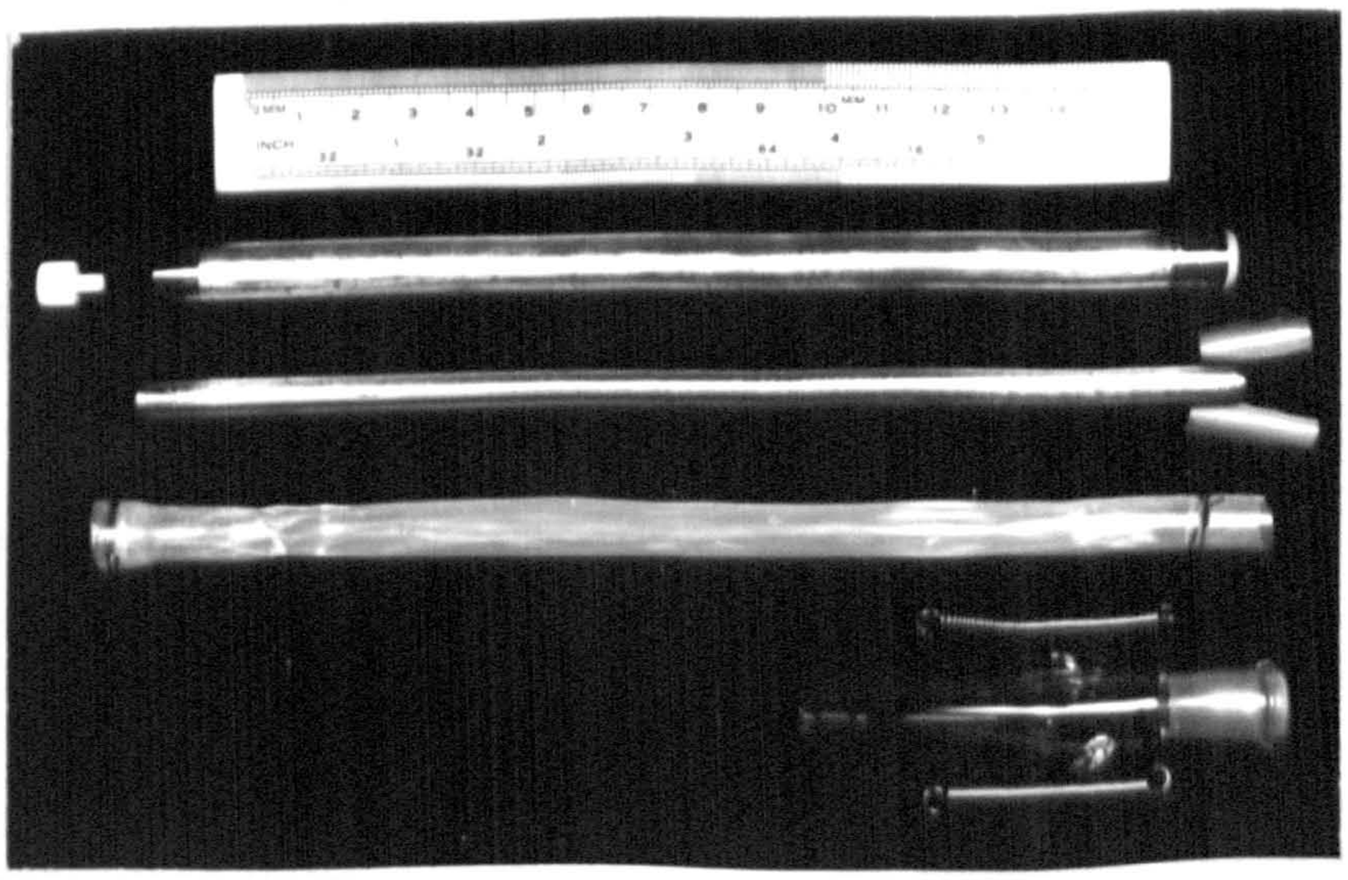

FIG.3.12 TIP ASSEMBLY

3.8 CLEANING OF THE APPARATUS

Great care was taken to keep clean all the surfaces that would be in contact with either the droplet phase or the continuous phase. The surfaces were cleaned with chromic acid at least once each month and whenever the droplet liquid was changed. The column was flushed with distilled water at least once a week.

The following procedure was used for cleaning the apparatus: The glass column and the droplet phase reservoir were washed with acetone to remove any organic liquid and left for drying. Then they were filled with chromic acid solution and left for at least 48 hours. The acid was then drained and the apparatus was washed repeatedly with single distilled water and finally with double distilled water. The smaller pieces of the apparatus were also washed with acetone, dried, and then immersed into the chromic acid tank for at least 48 hours. They were then washed with distilled water before the final drying. Great care was taken during the handling of the chromic acid and special boots, apron, face mask, and long gloves were worn. The chromic acid was prepared in the manner described in Appendix IV.

3.9 PHOTOGRAPHY OF THE DROPS

Two types of cine-cameras were used during the experiments. A Bolex 16 mm reflex cine-camera was used for the investigation of the drop hydrodynamics during the acceleration period of fall. It was also used for the measurements of the secondary droplet sizes. The breakup of drops was investigated with a high-speed Wollensak Fastax cine-camera.

The Bolex camera was operated at a nominal speed of 64 frames per second and at maximum aperture. It was firmly mounted on two sand filled columns to damp vibrations. The camera was held horizontally, as shown in Fig.3.13, so that the longer side of the rectangular frame of the film was vertical. Using this arrangement a vertical distance of fall of 14 cm was observed in the field of view.

The speed of the film was measured with the help of a synchronous electric motor. The motor turned a lightweight wheel and four equally spaced pointers were attached onto the wheel. A fixed marker was also fitted just clear of the revolving pointers. The whole arrangement was positioned at the side of the schlieren beam so that the revolving pointers and the fixed marker were just visible on the edge of each frame of the film. The speed of the motor was checked

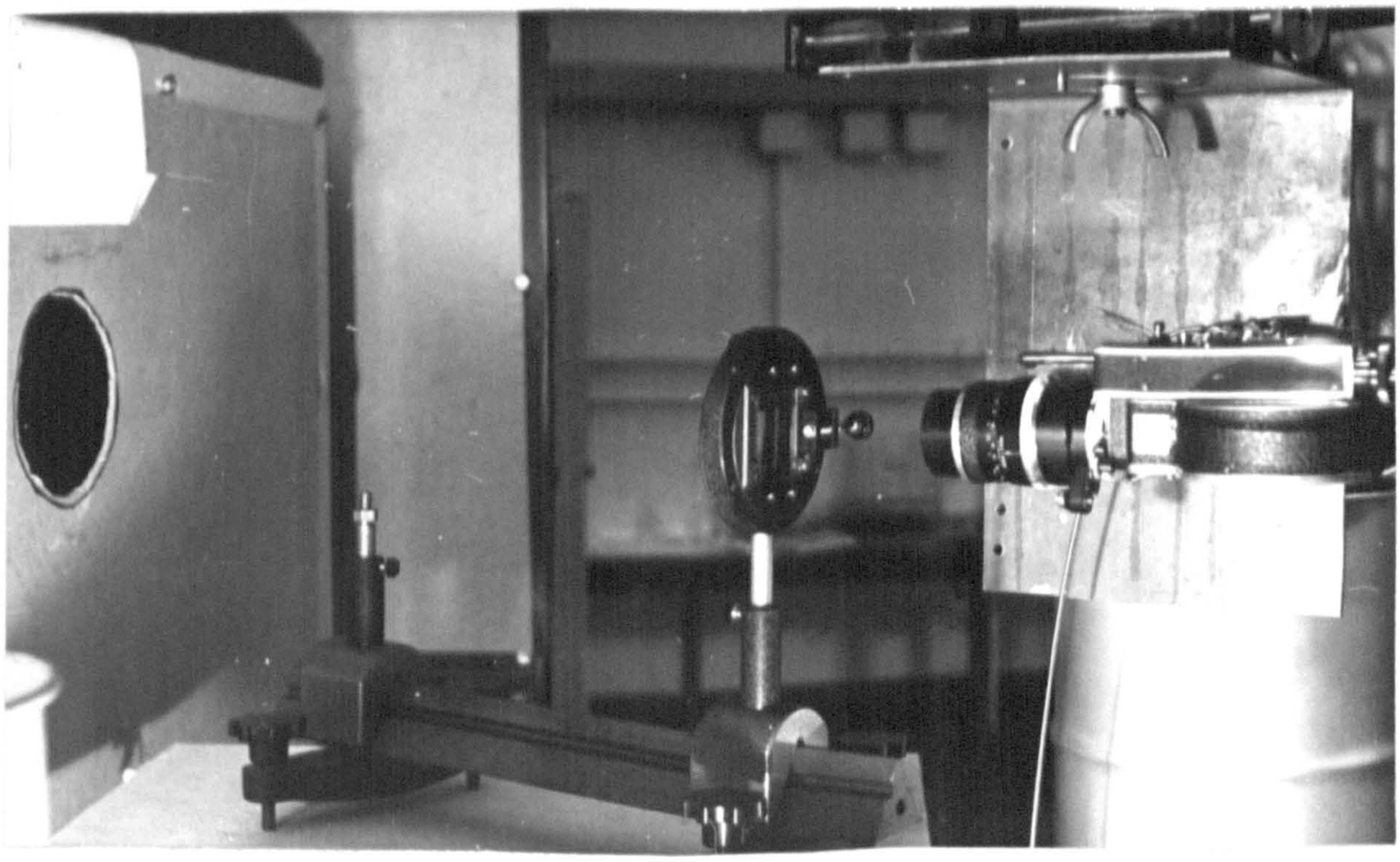

FIG.3.13 THE BOLEX CAMERA

FIG.3.14 THE FASTAX CAMERA

periodically. From the speed of the motor and the number of frames which were exposed during a certain number of revolutions of the wheel the film speed was calculated.

The Fastax camera was firmly mounted on its special stand and the arrangement is shown in Fig.3.14. The camera was again held horizontally instead of vertically to allow a longer vertical distance of fall to be observed. In this case a vertical distance of fall of 12 cm was observed. The film speed during each run was not constant, but increased with time and reached the highest value at the end of the film. To measure the film speed at any time a spark timer was used which was fitted into the camera. The spark timer left marks on the film and the time interval between successive marks was 1 millisecond. The number of the frames and the number of the timing marks were counted for a short length of film and the film speed was calculated from these. The maximum speed was between 1000 and 1400 frames per second for all experiments.

The optimum exposure was found by taking trial films. In order to obtain the most satisfactory schlieren image the slit breadth in the optical system was adjusted to the smallest possible size consistent with a satisfactory film exposure. The breadth of the slit was not changed for the shadow photography, but

the strength of the light was reduced with the help of neutral density filters which were fitted between the lens and the slit.

The drops were formed at a constant rate during the runs so that it was possible to start the Bolex camera about 1 second before the drop was due to appear at the top of the light beam. The Fastax camera was started about 1.5 second before the drop appeared in the field of view or before it detached from the tip. This ensured that when the drop appeared at the top of the field of view or when it detached from the tip the film speed was close to the maximum speed and was increasing slowly.

Kodak TRI-X and Ilford PAN-F films of 100 foot or 50 foot length were used. These were processed to the negative and were used in this form for all measurements.

3.10 ANALYSIS OF THE FILMS

The films were analyzed with the help of a "Specto" projector. The film was advanced manually frame by frame or was projected continuously at either 2 or 16 frames per second. The film was projected on to a large plane mirror mounted at 45^{o} to the horizontal level on a table. The mirror reflected the image onto a horizontal large white surface. The magnification of the image was obtained from the image of a stainless steel scale which was positioned in the field of view and inside the glass column. The magnification factor was 5.8 for the Bolex films and 6.5 for the Fastax films.

3.11 DETERMINATION OF DROP SIZES

The sizes of the primary drops were found by direct weighing of a known number of drops. The drops were formed in a beaker containing double distilled water. The rate of formation was the same as that used during the experiments. To ensure a constant temperature of 25°C the formation of the drops were carried out in the air bath. Correction was made for the loss of water by evaporation.

The diameters of the secondary drops were calculated from the projected images. The axially symmetric images of the secondary drops were traced on to tracing paper and the volume of the drop was calculated with the help of the formula

$$V = \frac{\pi}{12} h \sum_i \left(d_i^2 + d_i \cdot d_{i+1} + d_{i+1}^2 \right) \qquad (3.1)$$

where h and d_i are the distances shown in Fig.3.15.

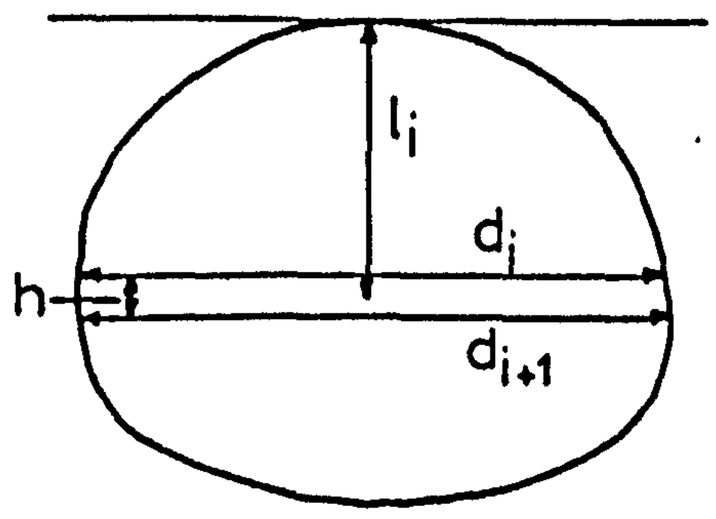

FIG.3.15 CALCULATION OF DROP VOLUME

3.12 PROCEDURE FOR AN EXPERIMENT

The liquid phases were freshly distilled before the experiment. The two phases were left in the air bath for a minimum time of 24 hours to allow the temperature to reach equilibrium. Thus it was ensured that the temperature of the two phases was within the range 25.0 $\pm$ 0.1^{o}C.

During the experiment the reservoir was filled with the drop phase liquid and it was ensured that there were no air bubbles in the tubing which connected the reservoir to the drop forming tip. The rate of formation was set to that required by adjusting both the fine tap and the pressure inside the drop phase reservoir and was determined by measuring with a stop-watch the time taken for the formation of a number of drops. A period was allowed before the filming in which no drops passed down the column in order to allow the disturbances in the column to die out. Then a succession of drops was formed and the fall of these drops through the continuous phase was filmed. The number of drops which were allowed to pass down the column during the experiments in which schlieren films were taken was reduced to a minimum in order to minimize the extraneous density gradients in the continuous phase.

SECTION 4

SYSTEMS USED

4.1 SELECTION OF THE SYSTEMS

About ten litres of the continuous phase were needed to fill the glass column and the column had to be refilled frequently. For reasons of safety and cost only water was considered for the continuous phase. The drop-phase liquids which were used by EDGE and GRANT[36][37][38] for their studies of the drop hydrodynamics of the terminal region were also used in the present work. The original choice of these systems took into account several factors which were also important in the present work. These were the density, the solubility, the toxicity, the flammability of the liquid and its ease of purification. The experimental technique which was used in the present work required that the density of the drop phase organic liquid should be greater than that of water and that the solubility of the organic liquid in water should be small but enough to give a satisfactory schlieren image of the wakes behind the drops.

The liquids which were chosen had low

viscosities and high interfacial tensions. The densities ranged between 1.099 and 1.451 g/cm^3 which allowed the density difference between the drop phase and the continuous phase to be varied by a factor of 4.5 approximately. The physical properties of the liquids at 25^{o}C are given in Table 4.1. The viscosities of the systems were obtained from the literature. The densities and the interfacial tensions were determined using specific gravity bottles and the drop volume method by HARKINS and BROWN[60], respectively. This latter method is discussed in detail below.

Liquid	Density g/cm^3	Viscosity (36) cP	Interfacial Tension dynes/cm
Water	0.997		
Chlorobenzene	1.099	0.756	36.5
1,2-Dichloroethane	1.240	0.778	27.8
Ethylbromide	1.451	0.371	32.4

Table 4.1 Physical Properties at 25°C of the Liquids Used

4.2 PURIFICATION OF THE SYSTEMS

Great care was taken for the purification of the liquids which were used for the droplet phase. "Analar" or "G.P.R." quality reagents were purified by fractionation at a high reflux ratio in a 30 plate all glass Oldershaw column. The first and the last 10% portions of the distillate were discarded. The water, which was used as the continuous phase, was double distilled using conventional types of water stills.

The droplet phase and the continuous phase were not mutually saturated before the experiments in order to make the wakes visible in the schlieren system.

4.3 THE DETERMINATION OF THE INTERFACIAL TENSION

The interfacial tension between the drop phase and the continuous phase was determined by the drop volume method of HARKINS and BROWN[60]. It was carried out inside the air bath with the two liquids unsaturated and at 25°C. The drops were formed from stainless steel tips with sharp and well defined ends. The diameters of the tips were measured with a travelling microscope. The formation of the drops was controlled with an "Agla" micrometer syringe.

The tips, P.T.F.E. tubing, and the syringe were cleaned in the usual way with chromic acid. The drops were formed into a small beaker filled with double distilled water. The drops were formed to a size, which was near to the detaching size, in about 1 minute. A short time was allowed for the movement of the drop liquid to settle down and then the volume of of the drop was increased by 0.0001 cm^3 at intervals of about 10 seconds until it detached from the tip.

Harkins and Brown gave for the interfacial tension

$$\sigma = \frac{V \Delta\rho g \varphi}{2\pi r} \qquad (4.1)$$

where r is the radius of the tip and φ is a correction factor which has been determined as a function of

$(r/V^{1/3})$ by Harkins and Brown. In the present work $(r/V^{1/3})$ ranged between 0.29 and 0.59. Harkins and Brown did not give the values of φ for $(r/V^{1/3})$ less than 0.3. However, their values can be extrapolated for this region, as was shown by DAVIES and RIDEAL[34].

SECTION 5

INTRODUCTION TO THE EXPERIMENTAL RESULTS

5.1 SCOPE OF THE EXPERIMENTS

In the present work the initial period of fall of oscillating drops has been investigated. This period was completed in all cases in the first 14 cm of fall after the release of the drop from the tip. An analysis of the eccentricities of drops falling at their terminal velocity was also made. This was necessary because there was no eccentricity data available for the terminal period with which to compare the drop eccentricities of the initial period. The measurements for the terminal region were taken when the drop was at a distance from the tip of between 24 and 38 cm. The velocity of fall and the frequency of oscillation in the terminal period were investigated in a previous work by EDGE and GRANT[36]. These authors used drop sizes which were similar to those used in the present work and their results for the terminal region are presented in Table 11 of Appendix III.

The experiments can be divided into two main sections. In the first section the initial

hydrodynamics of the drops which were not breaking up were investigated. In the second section the breakup of drops during the initial period of fall was investigated. These latter drops were of larger diameter than those which were dealt with in the first section. The results of the experiments and the conclusions are presented separately for the two sections of the investigation.

5.2 EXPERIMENTS ON THE INITIAL PERIOD OF FALL

These experiments investigated the variation with time of the following variables :

a) the class of the attached wake,

b) the shape and eccentricity of the drop,

c) the frequency of the drop oscillations,

d) the velocity of fall of the drops.

Measurements were made of D_H and D_V, the longest horizontal and vertical dimensions of the drop, and the distance between the tip and the drop as it fell through the continuous phase. These measurements required a frame by frame analysis of the films. For a single drop about 60 frames were analysed and this was very time consuming. Therefore the number of systems and the number of drop sizes which were studied were of necessity limited.

5.3 EXPERIMENTS ON THE BREAKUP OF DROPS

These experiments investigated the breakup of drops and the sizes of the secondary drops which were formed during the breakup. For each drop 80 frames of the high-speed film were analysed and this was very time consuming. Therefore the analyses were restricted to 3 drops of each size and to 3 systems.

5.4 ACCURACY OF THE MEASUREMENTS

To estimate the accuracy of the measurements which were taken from the projected film a number of trial films were taken with solid spheres of known diameters. These diameters were similar to the diameters of the primary drops which were investigated in the present work. The diameters of the spheres which were measured from the projected images were within an error of $\pm$ 2% of the true diameters. This corresponded to an accuracy of $\pm$0.2 mm for the measurements from the projected images. For the smallest secondary drops the accuracy of the measurements is therefore about $\pm$ 5%. The percentage standard deviation, which is abbreviated as % S.D. in the tables or elsewhere, was used as a measure of variation between the results which were obtained for various drops of the same size. It is the standard deviation of the results given as a percentage of the arithmetic mean.

SECTION 6

INITIAL HYDRODYNAMICS

EXPERIMENTAL RESULTS

6.1 DROP SIZES

Drops were formed from 5 tips both with the chlorobenzene system and with the 1,2-dichloroethane system. For each tip three separate measurements were made of the sizes of the drops. The results are presented together with the rate of formation of the drops in Tables 1 and 2 of Appendix III. The agreement between the three separate measurements of the drop size for each tip was good and the percentage standard deviation was less than 1.0% in most cases.

6.2 DROP WAKES

The transition of the wake type behind accelerating drops was investigated for both the chlorobenzene and the 1,2-dichloroethane systems. A typical transition of the wake from class I to class IV is shown by a 1,2-dichloroethane drop with an equivalent spherical diameter of 0.578 cm and this transition is illustrated in Fig.6.1. The wake classification proposed by EDGE and GRANT[37] is used throughout the work and the class of the wake which exists behind a drop under given conditions is indicated on various graphs throughout the thesis.

6.3 THE SHAPES OF DROPS DURING ACCELERATION

For the investigation of the shapes of drops D_H and D_V, the longest horizontal and the longest vertical dimensions of the drop respectively, were measured and the drop eccentricity was calculated as their ratio on each frame for 60 frames of the cine-film. This analysis was carried out both for chlorobenzene and 1,2-dichloroethane drops and for one drop of each size. The variation with time of D_H, D_V, and E are presented in Figures 1-10 of Appendix II. The equivalent spherical diameter and the terminal mean eccentricity are also shown on these graphs.

6.4 THE SHAPES OF DROPS AT THE TERMINAL PERIOD

Curves of D_H, D_V, and E versus time were obtained in the manner described in section 6.3 for chlorobenzene and 1,2-dichloroethane drops falling at their terminal velocities and a mean eccentricity for the oscillating drops was obtained as follows : From the eccentricity versus time curves the average of the maximum values and the average of the minimum values were calculated separately. The average value of these two gave a mean eccentricity for the drop. Two drops of each size were analysed and the results are presented in Tables 12 and 13 of Appendix III. An overall mean of the drop eccentricity for the range of drop sizes studied was also calculated for each system. The percentage standard deviation of the individual mean eccentricities about the overall mean eccentricity was 3.50% for chlorobenzene drops and 2.88% for 1,2-dichloroethane drops.

6.5 THE FREQUENCY OF OSCILLATION

The change with time of the frequency of oscillation of drops during the initial period of fall was obtained from the D_H versus time curves which are presented in Figures 1-10 of Appendix II. The D_H curves were chosen rather than the D_V curves because the oscillations were better defined in these curves. The frequency of oscillation at a particular time was calculated as follows : The number of the D_H-peak starting from the tip was plotted against the time and a curve was drawn through the points. The slope of this curve was the frequency of oscillation at a particular time. A single drop of each size was analysed in this way with both the chlorobenzene and the 1,2-dichloro - ethane systems. The results are presented in Fig.6.2 and Fig.6.3. The terminal frequencies of oscillation are also shown in these figures.

The smallest drop of 1,2-dichloroethane ($D_{E,1}$= 0.360 cm) had a frequency of oscillation which was too high shortly after detachment to be measured accurately from the Bolex films. Thus these drops are not included in Figure 6.3. With the smallest size of the chlorobenzene drops ($D_{E,1}$= 0.560 cm) the initial oscillations died out after some time had elapsed but started again later. Thus there is a break in the curve of frequency of

oscillation against time which occurs between 0.3 sec and 0.6 sec. From Figures 6.2 and 6.3 the time at which the frequency of oscillation was equal to the Lamb's frequency was found for each size of drop and for each system and using Figures 1-10 of Appendix II, the drop eccentricity at that particular time was estimated. The results are presented in Table 12 of Appendix III.

6.6 THE VELOCITY OF FALL

The variation of the velocity of fall of an accelerating drop was obtained from a frame by frame analysis of the movement of the centre of gravity of the drop. The velocity of the centre of gravity of the drop was calculated as the ratio of the displacement of the centre of gravity between two successive frames of the cine-film to the corresponding elapsed time. The calculation was carried out as follows : The image of a drop was traced onto tracing paper and the distance of the rear surface of the drop from the drop forming tip was noted. Then the position of the centre of gravity was calculated from :

$$z = \frac{\sum_i l_i \left(d_i^2 + d_i \cdot d_{i+1} + d_{i+1}^2\right)}{\sum_i \left(d_i^2 + d_i \cdot d_{i+1} + d_{i+1}^2\right)} \qquad (6.1)$$

where z is the distance between the centre of gravity and the rear surface of the drop and l_i and d_i are the distances shown in Fig.3.15. The time interval between two frames was calculated from the film speed. Because of the labour involved in the frame by frame analysis of the films and in calculating the centre of gravity, only the chlorobenzene system and two drops of each size were investigated. The variation of the velocity with time for one drop of each size is presented along with the gross terminal velocity of fall in Figures 20-24 of Appendix II. The time when the first class III wake was formed is also shown on these graphs.

ANALYSIS AND DISCUSSION OF THE RESULTS

6.7 WAKE TRANSITION BEHIND ACCELERATING DROPS

Immediately after the detachment of the drop from the tip the boundary layer streamed from the rear of the drop in a manner similar to the class I wake. All drops then showed a transition through the various wake classes until the wake class of the terminal region was established. This transition through the wake classes was rapid for the larger drops but was more gradual for the smaller drops. The various wake classes were easily distinguishable for the larger drops. For the smaller drops, however, the wake classes tended to merge and some of the attached wakes resembled a mixture of two classes.

All the drops with a wake pattern similar to the classes II, III, and IV of the terminal region carried an attached wake. Part of the attached wake was shed during each oscillation cycle and a new wake was formed when D_H of the drop was near to a maximum value. The formation of the first attached wake and of each subsequent new wake did not occur at the rear stagnation point but at some point forward and then moved towards the rear of the drop. This is in contrast with the formation of an attached wake behind a solid sphere[12] where the separation of the boundary layer

occurs at the rear stagnation point and moves forward as the size of the wake increases. This can be attributed to the high eccentricity of the drop. A similar phenomenon which was found with solid elliptic cylinders in impulsive flow has been investigated by GÖRTLER[53], SCHLICHTING[143], and TOLLMIEN[167]. They found that only when $E < 2/\sqrt{3}$, the boundary layer separates at the rear stagnation point and then the point of separation moves forward over the surface of the cylinder as the attached wake grows in size. However, when $E > 2/\sqrt{3}$, the attached wake is formed by a sudden separation forward of the rear stagnation point.

Wake Transition for a Class IV Drop

To illustrate the transition of the wake from class I to class IV and the corresponding changes in the shape of the drop, the wake pattern of a 1,2-dichloroethane drop with an equivalent spherical diameter of 0.578 cm is shown in Fig.6.1.

Immediately after release from the tip the boundary layer streamed from the drop and the wake was similar to a class I wake. Immediately after the first D_H peak the boundary layer separated forward of the rear stagnation point to form a small attached wake (frame 6). This wake elongated and pinched near the drop as the next D_H peak was approached and it shed

FIG.6.1 DROP SHAPE AND STRUCTURE OF THE WAKE DURING ACCELERATION FROM REST

1,2-Dichloroethane drop in water. $D_{E,1}$= 0.578 cm
Numbers refer to frame numbers on the cine-film at 61.1 f.p.s. where frame 1 is the first frame after detachment of the drop from the tip. ⚑ indicates the frame at which there occurs a new separation of the boundary layer.

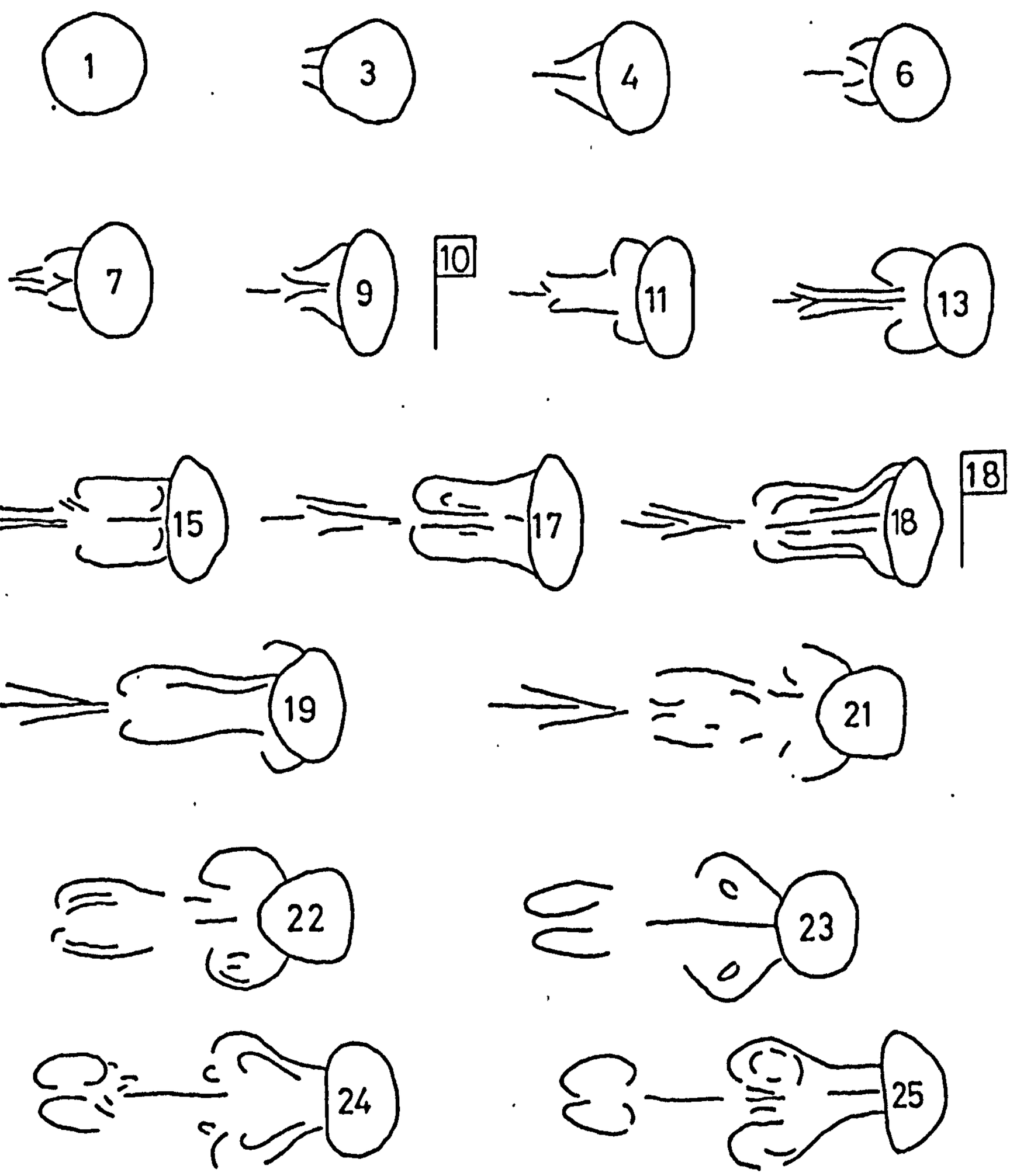

FIG.6.1 Continued.

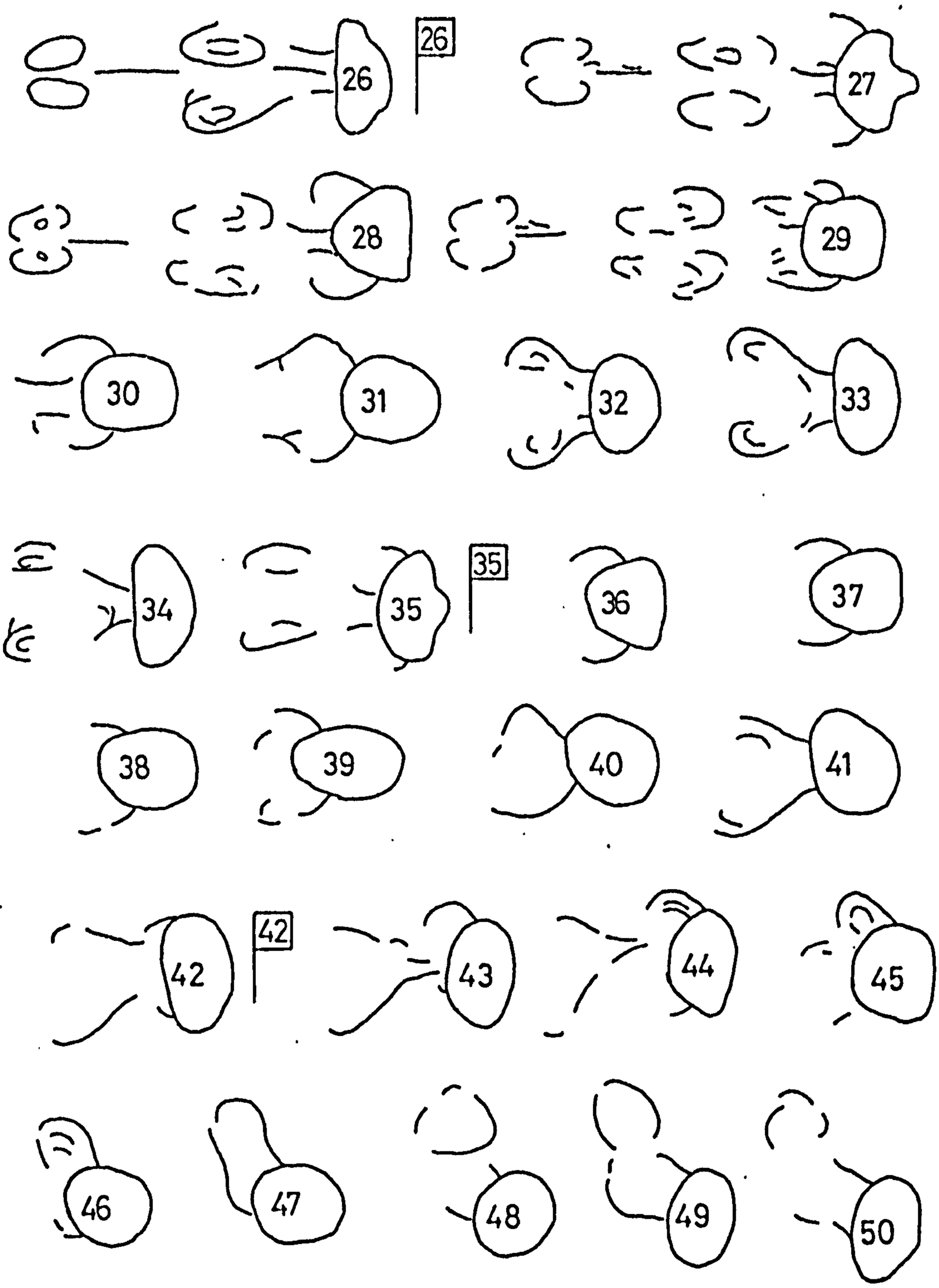

like a class II wake(frames 7-11). Immediately after the next D_H peak a new separation of the boundary layer occurred and a new attached wake was formed. The process was then repeated. Each successive separation of the boundary layer was further forward on the drop surface than the previous separation and each successive wake was larger than the previous wake. This can be attributed to the increasing eccentricity of the drop during acceleration.

The wake type formed at each shedding remained similar to a class II wake until the drop caved at its leading surface during a peak in a D_H oscillation cycle (frames 11-13). The drop illustrated in Fig.6.1 shed only one class II attached wake but smaller drops shed several before caving. The new wake was then formed by the boundary layer separating much further forward on the drop surface than previously. This resulted in a much larger attached wake which shed at the next D_H peak, like a class III wake (frames 17-19). The next wake was likewise much larger than the previous wake. The drop then underwent a large D_V oscillation cycle during which it deformed into the wake region (frames 21-22).

Each class III attached wake after shedding moved initially in a vertical straight line but subsequently curved away from this line; alternate

wakes moving in opposite directions away from the vertical. Each successive wake moved in the vertical line for a shorter period. It is probable that the movement of the attached wake was influenced by residual vorticity in the continuous phase which resulted from the passage of the previous drops.

The drop continued to move in a vertical straight line but prior to the next D_H peak its minor axis was tilted from the vertical (frame 34). The next wake detached unsymmetrically and the drop lost its symmetry about its minor axis (frame 40). The following wake was formed noticeably to one side of the drop (frame 43) and detached from the drop by following a path different to the path of the drop. The drop now followed the well known zig-zag course with the wakes being formed and shed on alternate sides of the rear surface of the drop.

Wake Transitions for Class III Drops

Class III drops showed more gradual wake transitions than did the class IV drops. Thus a class III drop had a class II wake for a much longer period than did a class IV drop. Also a class III drop showed a less distinct change from a class II wake to a class III wake than did a class IV drop. A further difference between the class III and

class IV drops is that when class III attached wakes are shed from a class III drop, they travel in a vertical straight line.

6.8 THE TERMINAL ECCENTRICITY OF OSCILLATING DROPS

Previous authors found that the eccentricity of nonoscillating drops was a linear function of the Eötvös number or equivalently a function of the second power of the equivalent spherical diameter for a particular system. The eccentricity data of oscillating drops in not specially purified systems, however, was scattered and there was no agreement. There was also no agreement when the systems were specially purified. The main difficulty was in defining and measuring the mean eccentricity.

In the present work the mean eccentricity was defined as the mean of the average maximum and minimum eccentricities. The results presented in Table 11 of Appendix III show that the mean eccentricity was approximately constant in the range of drop sizes under investigation. The amplitude of the eccentricity oscillations, ΔE, which was defined as the difference between the mean maximum eccentricity and the mean minimum eccentricity, varied with the drop size and was larger for larger drops. The scatter of the amplitude data was large and a correlation with the drop diameter was not possible. SCHROEDER and KINTNER[146] and EDGE and GRANT[38] also reported scatter in their amplitude data.

6.9 THE SHAPES OF OSCILLATING DROPS DURING ACCELERATION

Tip induced oscillations resulted from the deformation of the drop at the tip prior to detachment. These oscillations decayed and, in the case of the smaller sizes of drops which were investigated, they died out (Figures 1 and 6 of Appendix II). The D_H oscillations were more persistent than the D_V oscillations.

The drops did not show undamped oscillations until their eccentricity was above the terminal mean eccentricity. The onset of the undamped oscillations coincided with the shedding of the first attached class III wake behind the drop. The first of these oscillations was of larger amplitude than the oscillations which were observed in the terminal region.

6.10 THE FREQUENCY OF OSCILLATION OF ACCELERATING DROPS

It can be seen from Figures 6.2 and 6.3 that during acceleration there is a considerable change in the frequency of oscillation. The change in the frequency of oscillation can be related to the change in the eccentricity of the drop as it accelerates through the continuous phase. Shortly after detachment the frequency was larger than the terminal value and was close to the theoretical Lamb's frequency of oscillation given by equation (2.37). Lamb's frequency was derived for small amplitude oscillations about a spherical shape. From Table 12 of Appendix III it is seen that drops with the eccentricity near to 1 have a frequency of oscillation which is close to Lamb's frequency of oscillation.

As the eccentricity of the drop increased with time the frequency of oscillation decreased. When the drop eccentricity was near the terminal mean eccentricity the frequency of oscillation was close to the terminal frequency of oscillation. As the drop eccentricity increased beyond the terminal mean eccentricity the frequency of oscillation decreased below the terminal value and reached a minimum. With the onset the regular terminal oscillations, however, the frequency of oscillation increased and reached the terminal value.

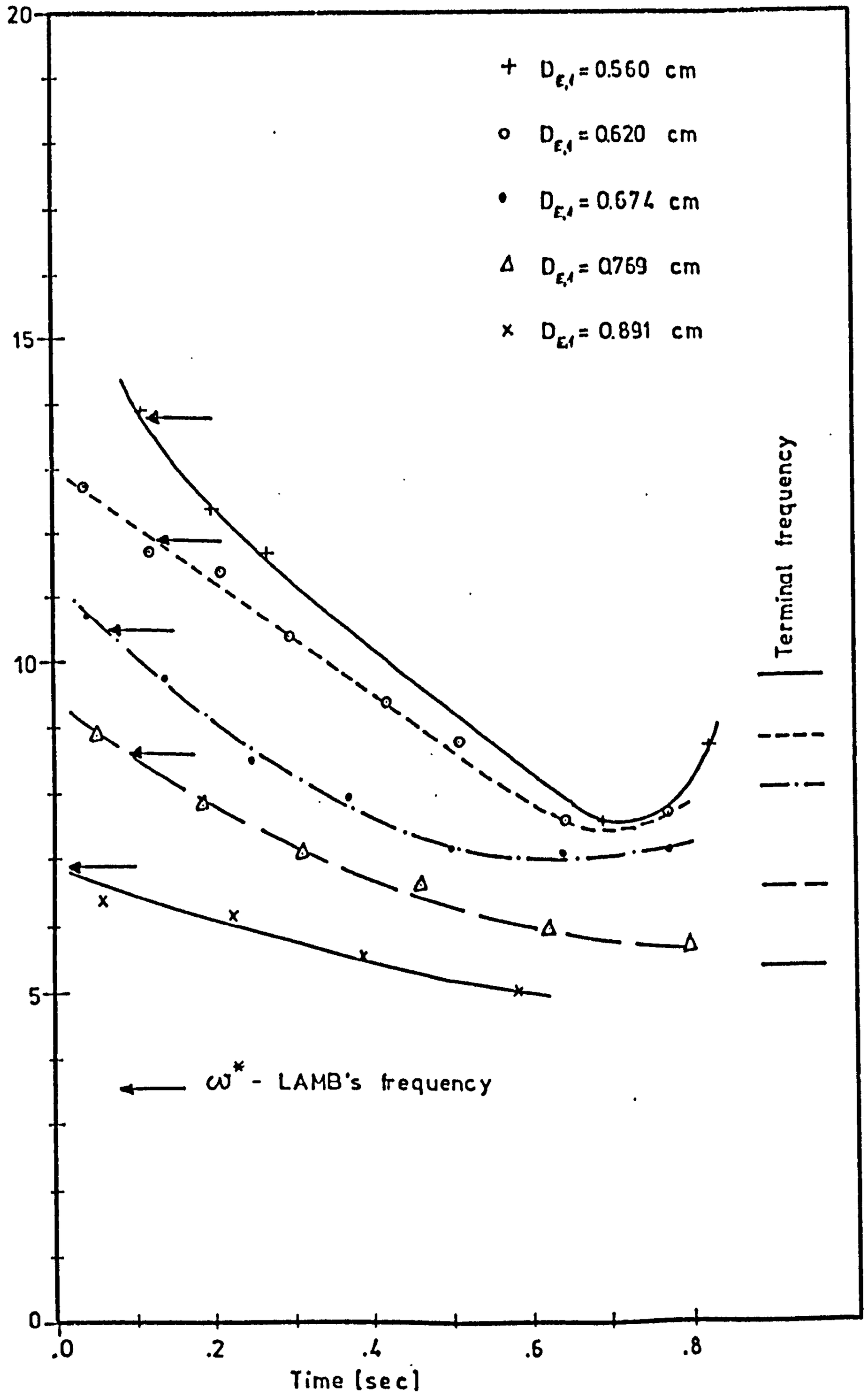

Fig.6.2 Variation with time of the frequency of oscillation for chlorobenzene drops falling from rest

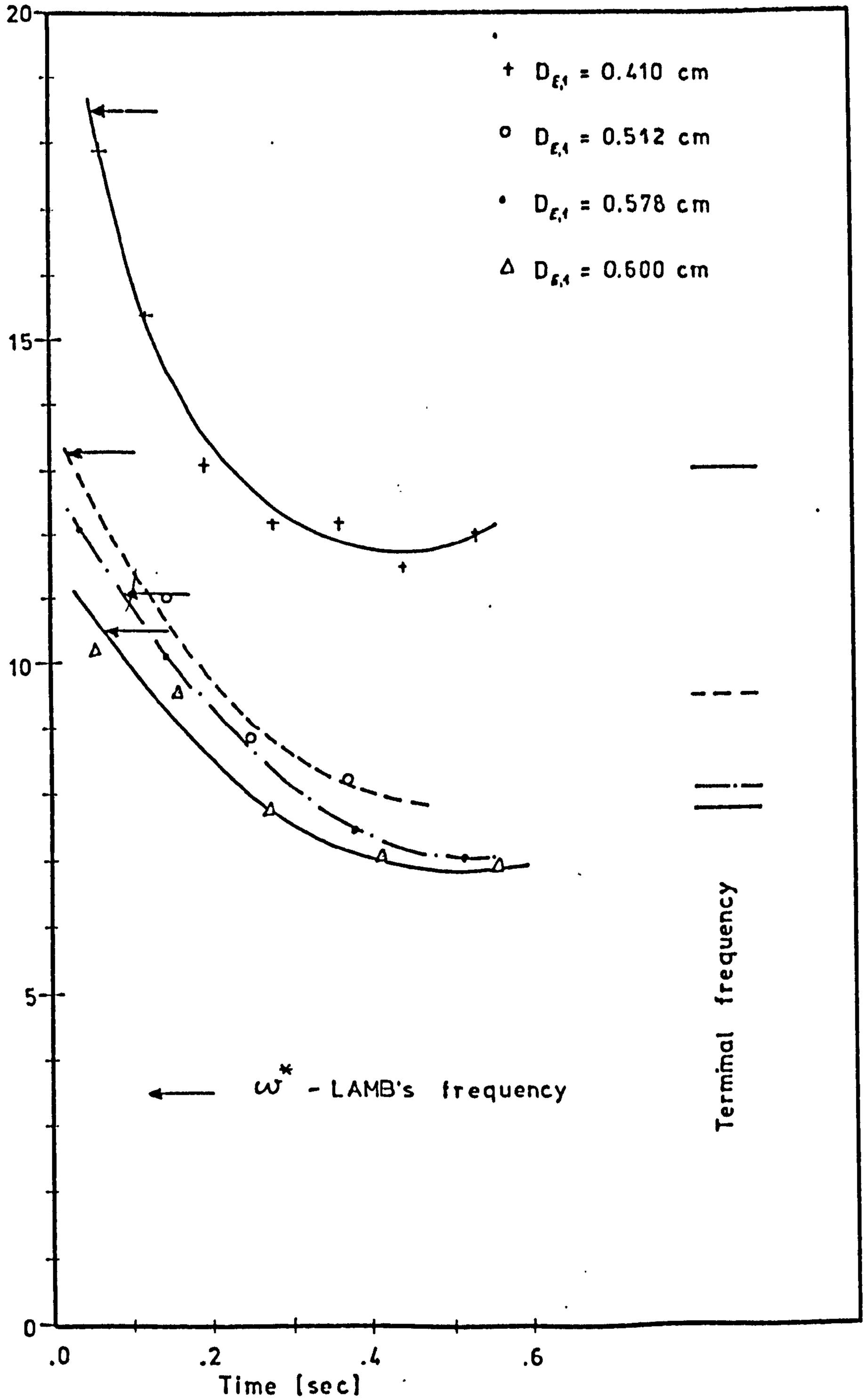

Fig.6.3 Variation with time of the frequency of oscillation for 1,2-dichloroethane drops falling from rest

6.11 VELOCITY OF FALL DURING ACCELERATION

The experimental results for the variation of the velocity of fall with time in the initial period of fall was found to fit the equations of the form :

$$U = U_\infty \tanh \tau t \qquad (6.2)$$

This agreement is shown in Figures 20-24 of Appendix II. Equations of this form were proposed by HU and KINTNER[72] (equation 2.51) and the theoretical derivation is discussed in Appendix I-A. In these equations

$$\tau = \frac{\Delta\rho/\rho_d}{1 + k\rho_a/\rho_d} \frac{g}{U_\infty} \qquad (6.3)$$

where k is a factor which is determined experimentally and can be regarded as a measure of the increase in the effective mass of the drop during acceleration. The values of τ, k, and $t_{0.9}$, which is the time required by the drop to reach 90% of the gross terminal velocity U_∞, for the various drop sizes are presented in Table 13 of Appendix III.

The results show that the value of k is of the order of 0.5, the value given by STOKES[151][153] for rigid spheres accelerating at low Reynolds numbers. These results also show that the value of k decreases with increase in drop size. Therefore the ratio of the effective mass to the true mass for large drops is less

than that for small drops and therefore they attain the terminal velocity sooner. The reason for this is probably the high eccentricity of the larger drops and the faster transition of the attached wake class behind these drops.

It was also found that all drops, except those which had class IV wakes in the terminal period, reached the terminal velocity before they had a class III wake and therefore before the large amplitude oscillations of the terminal region commenced. In the case of larger class IV drops the large amplitude oscillations commenced before a constant velocity was reached. During the high amplitude oscillations which accompanied the transition from a class II to a class III wake, cyclic variations of the velocity commenced and the mean velocity of the drop rose initially above the terminal value by up to 10%. A similar phenomenon was also observed by LAWS[92][93]. This high velocity may be caused by the streamlined shape of the drop which occurs during the large amplitude peak in D_V. Once the terminal wake was established and the drop oscillations became regular the velocity fell to the terminal value. The cyclic variations of the velocity still continued and it was found that the velocity reached a maximum when D_H was a minimum and vice versa.

6.12 SUGGESTED MECHANISM OF DROP OSCILLATION AND WAKE SHEDDING

There has been much speculation whether the oscillations of the drop cause the shedding of the wake or vice versa. However, there has been no convincing mechanism proposed for the process. During the present work it was found that the frequency of oscillation of the drop and the frequency of wake shedding were identical and no evidence was found to substantiate the resonance theory by DAVIES[12]

The work of SCHWABE[147][148] who investigated the pressure distribution around a solid cylinder during its acceleration from rest, is a useful guide to the mechanism of droplet oscillation and wake shedding. He found that as the size of the wake increased the pressure over the rear part of the cylinder fell. A similar fall in the pressure will occur over the rear surface of a drop as the wake behind it grows in volume. Frames 18-27 of Fig.6.1 will be used to illustrate a suggested mechanism of drop oscillation and wake shedding which is based on this variation of pressure at the rear of the drop.

Because of the high eccentricity of the drop in frames 17-18 a large wake grows behind the drop. This leads to a fall in pressure over the rear surface

of the drop and the drop deforms into the wake region (frames 21-22). The drop has now assumed a more streamlined shape and the position of the separation of the boundary layer moves towards the rear of the drop (frame 23) causing the attached wake to shed. The pressure over the rear surface of the drop rises and the drop returns to the more oblate form, causing a new separation of the boundary layer and a new attached wake to be formed (frame 26). This process then repeats. The suggested mechanism of oscillation and wake shedding can be summarised as follows : The variation in drop shape leads to the formation and detachment of a succession of attached wakes and the growing and shedding of these wakes lead to cyclic variation in pressure over the rear surface of the drop which sustains the oscillations of the drop.

In the case of class IV drops in the terminal region, the zig-zagging of the drop modifies the formation and shedding of the wake but the basic sustaining mechanism for drop oscillation will still be present.

SECTION 7

CONCLUSIONS

1. The wake behind a drop which is falling from a tip shows a transition through the various wake classes until the wake class of the terminal region is finally established.

2. A class III wake does not form behind a drop until the eccentricity of the drop has exceeded the mean eccentricity of the terminal region, and the drop has caved at its front surface.

3. The formation of the first class III attached wake behind a drop is followed by a sudden rise in the amplitude of oscillation of the drop. This is the first of the terminal region oscillations.

4. The frequency of oscillation of a drop shortly after detachment from a tip is close to the theoretical value predicted by Lamb (equation 2.37). The drop is then oscillating

about a shape which is roughly spherical. The subsequent reduction in the frequency of oscillation may be attributed to the increase in the eccentricity of the drop as it falls.

5. The velocity of fall of a drop during acceleration is given by an equation of the form

$$U = U_\infty \tanh \tau t$$

The value of τ and the rate of acceleration are larger for larger drops.

SECTION 8

BREAKUP OF DROPS

EXPERIMENTAL RESULTS

8.1 PRIMARY DROP SIZES

The size of the drops was determined by weighing 15-60 drops which were formed from each tip into a weighing bottle which was partly filled with double distilled water. The determination was repeated three times and all measurements were made at a drop formation rate of 10 seconds per drop. 10 tips were examined for the chlorobenzene system, 8 tips for the 1,2-dichloroethane system, and 11 tips for the ethylbromide system. The agreement between the three determinations made for each tip size and each system was good and the percentage standard deviation was less than 1.0 % in all cases. The results are presented in Tables 2, 4, and 5 of Appendix III. A number of measurements were also made at other rates of formation. These measurements were restricted to 6 tips and to the chlorobenzene system. The results are presented in Table 3 of Appendix III. The agreement between the three measurements made for each tip size was good and

the percentage standard deviation was less than 1.0 % in all cases.

8.2 SECONDARY DROP SIZES

The sizes of the secondary drops were calculated from the images of the drops on the projected film. The results are presented in Tables 6-9 of Appendix III. The average standard deviation for all the drops which were investigated was 4.6%. The results are also presented in Figures 8.3 - 8.5 in which the equivalent spherical diameter of the secondary drop $D_{E,2}$ is plotted against the equivalent spherical diameter of the primary drop $D_{E,1}$.

8.3 ECCENTRICITY AND SHAPES OF BREAKING DROPS

As in the case of the nonbreaking drops, D_H and D_V were measured by a frame by frame analysis and the drop eccentricity was calculated as the ratio of the two. This analysis was carried out both for chlorobenzene and 1,2-dichloroethane drops. The variation with time of D_H, D_V and E are presented for 5 drops of chlorobenzene and 4 drops of 1,2-dichloroethane in Figures 11-19 of Appendix II.

Photographs which were taken during the critical oscillation of a chlorobenzene drop with an equivalent spherical diameter of 1.088 cm are presented in Fig.8.2.

8.4 DROP DIMENSIONS DURING BREAKUP

During breakup the drop deformed into the shape which is shown in Fig.8.1. Measurements were made of the dimensions which are indicated in Fig.8.1 for drops both of chlorobenzene and 1,2-dichloroethane which were breaking to give a rear formed secondary drop. 6 drop sizes were studied for the chlorobenzene system and 5 drop sizes for the 1,2-dichloroethane system and for each drop size three drops were studied. The results which were obtained for the three drops at any particular size were found to be similar. The variation with time of the drop dimensions are presented in Figures 25-35 of Appendix II for one drop of each size. Breakup occurred by necking of the column which was present at the rear of the drop. Measurements were made of the column dimensions immediately prior to the necking and the results are presented in Table 18 of Appendix III.

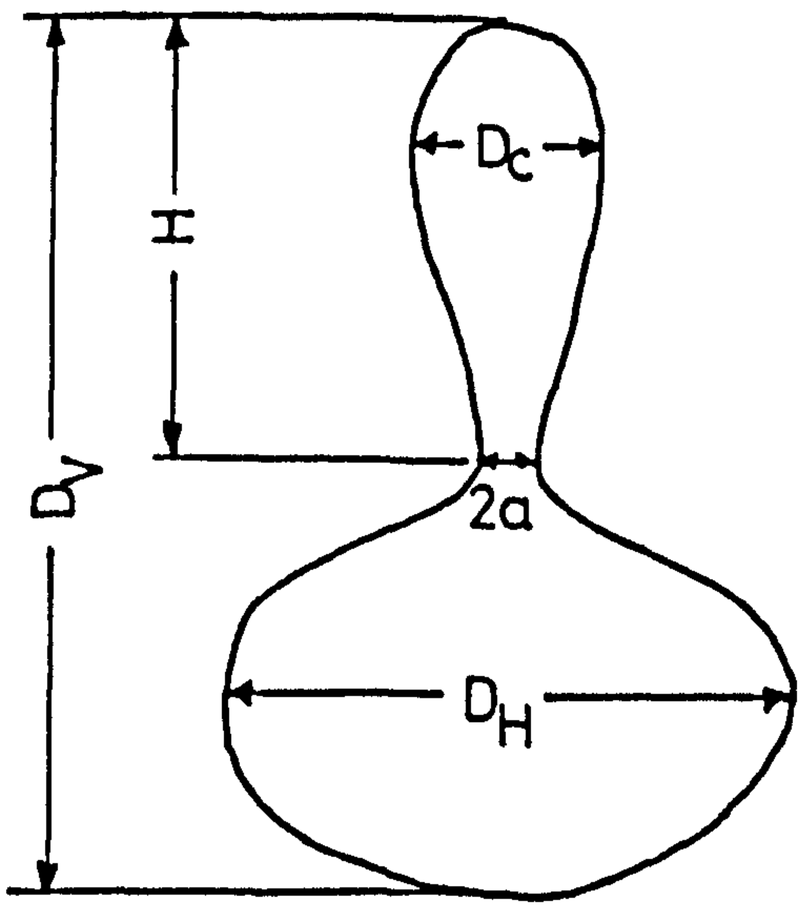

FIG.8.1 DROP DIMENSIONS DURING BREAKUP

8.5 DRAINAGE OF THE REAR COLUMN

The variation with time of the volume of the liquid column which forms behind a breaking primary drop was studied. The volume of the column was calculated in the manner described in Section 3.10. This type of calculation was very time consuming and only one drop of chlorobenzene with an equivalent spherical diameter of 1.088 cm was examined. The results are presented in Fig.8.9. Also shown in this figure are the corresponding drop dimensions.

ANALYSIS AND DISCUSSION

8.6 THE CRITICAL OSCILLATION AND THE FORMATION OF SECONDARY DROPS

It is shown in Section 6.9 that the formation of the first attached class III wake initiates the terminal oscillations of the drops. The first of these oscillations occurs immediately after the shedding of the first class III wake and is of a high amplitude whereas the subsequent oscillations are of smaller amplitude. This oscillation will be referred to as the critical oscillation.

The critical oscillation does not occur at a fixed distance below the forming tip, as reported by SCHROEDER and KINTNER[146]. It can be seen from Figures 1-19 of Appendix II and Tables 14-16 of Appendix III that as the diameter of the primary drop is increased there is a decrease in the number of oscillations which occur before the critical oscillation.

The changes in the shape of the drop during the critical oscillation which leads to the breakup of the drop is shown in Fig.8.2. During this critical oscillation the eccentricity of the drop decreases to a value of 0.66 approximately (photograph 1) and the drop necks (photograph 2). This value is about twice

FIG.8.2 THE SHAPE OF A DROP OF CHLOROBENZENE DURING THE CRITICAL OSCILLATION. $D_{E,1}$= 1.088 cm

1: 0 (msec) 2: 7 (msec) 3: 19 (msec)

4: 32 (msec) 5: 69 (msec) 6: 82 (msec)

7: 90 (msec) 8: 99 (msec) 9: 109 (msec)

FIG.8.2 Continued.

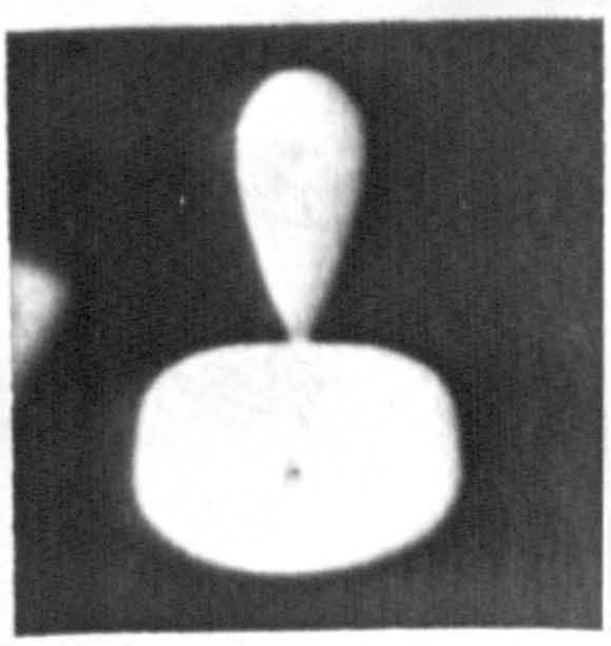

10: 113 (msec)

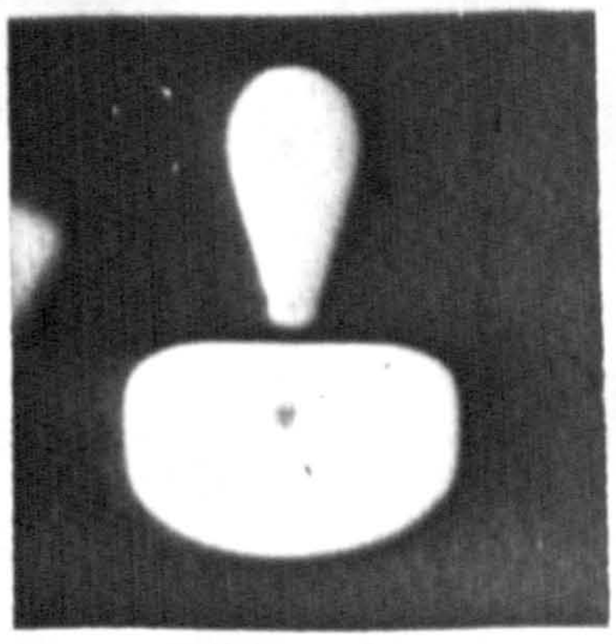

11: 121 (msec)

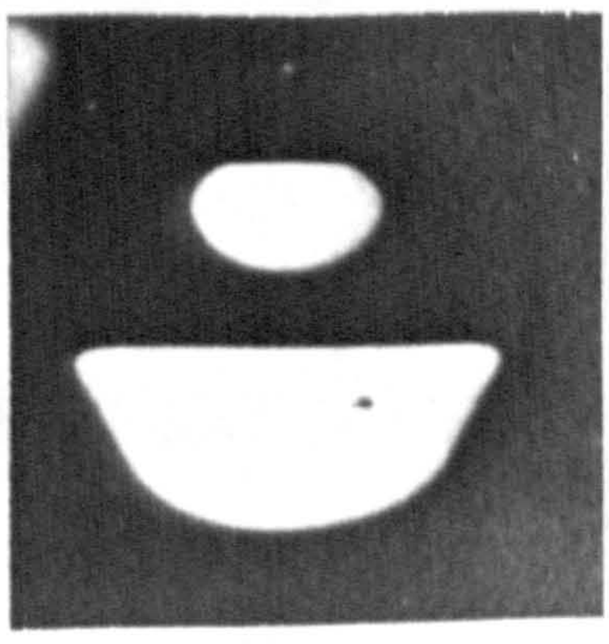

12: 160 (msec)

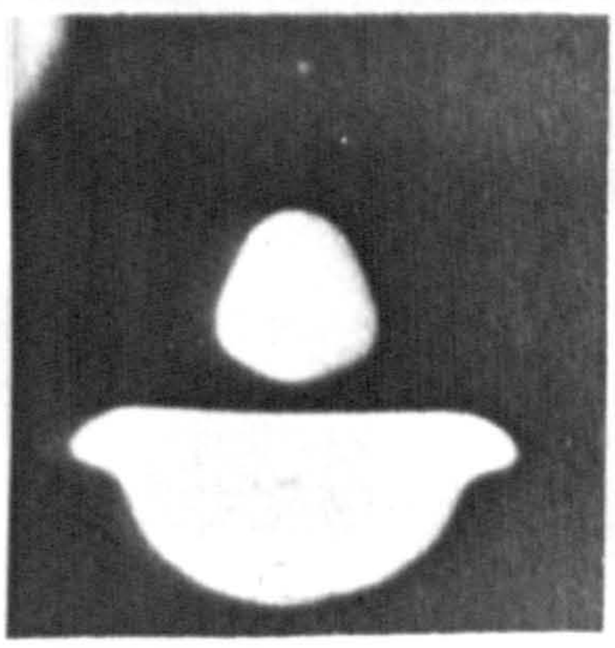

13: 180 (msec)

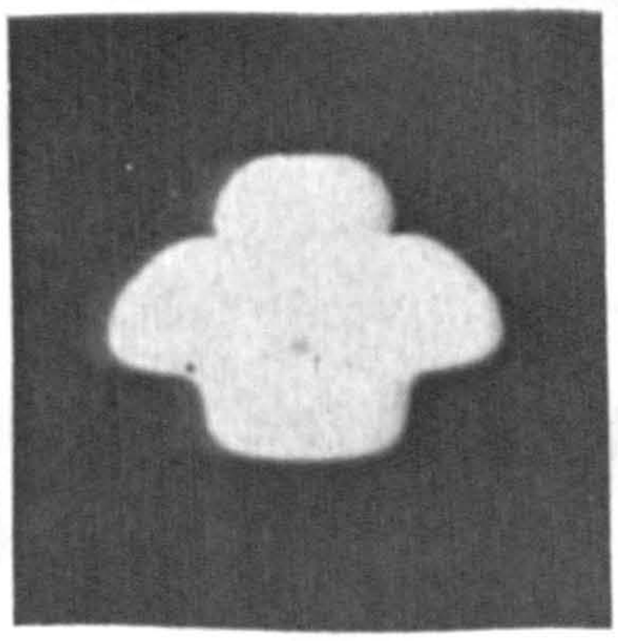

14: 212 (msec)

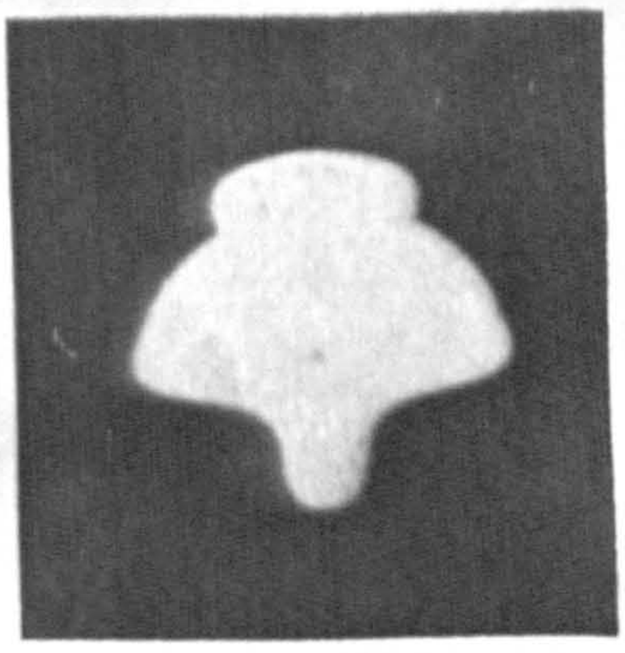

15: 234 (msec)

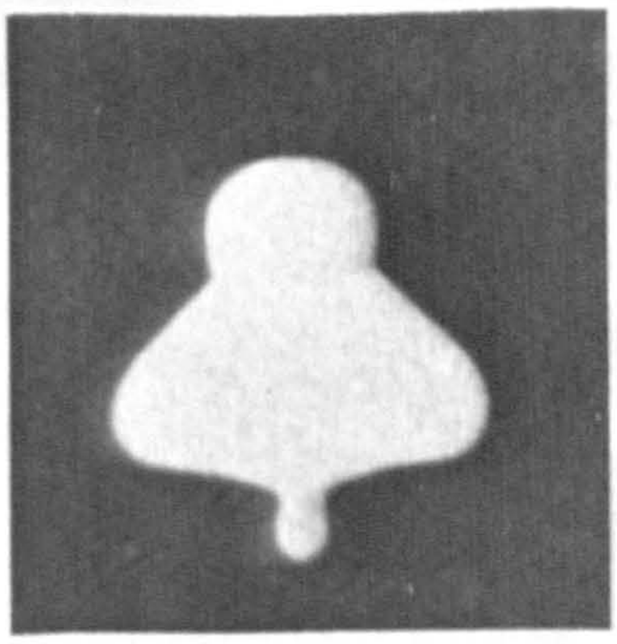

16: 251 (msec)

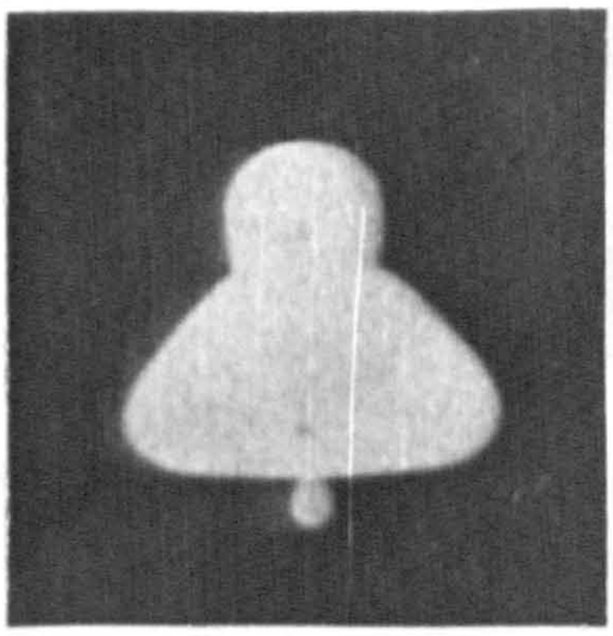

17: 257 (msec)

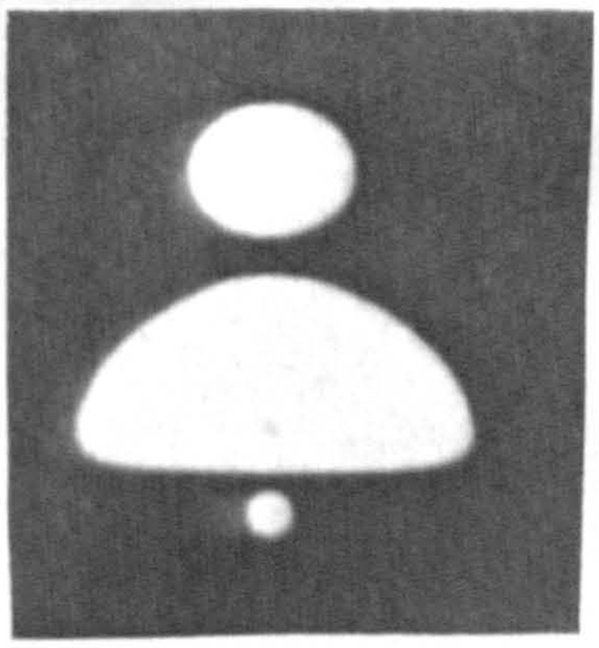

18: 288 (msec)

the value given by KARAM and BELLINGER[79] for the breakup of drops in sheared viscous flow. However, the flow conditions in the present system are very much different than those discussed by Karam and Bellinger and no theoretical investigations exist for the present system. In the present system the necking of the drop is followed by the draining of the rear part of the drop into the front part (photographs 3 to 5) and a column of liquid is formed at the rear of the drop (photograph 6) which subsequently breaks up by a necking process (photographs 7 to 11). Later a column of liquid forms at the front of the drop (photograph 15) which subsequently produces a front formed secondary drop (photograph 18). As an illustration of the formation of secondary drops, the breakup of chlorobenzene drops will be discussed. This system was investigated in more detail than the other two systems.

Breakup of Chlorobenzene Drops

With chlorobenzene drops no breakup occurs until the critical oscillation corresponds with the fourth D_V peak. Drops with equivalent spherical diameters between 0.896 cm and 0.923 cm broke up at the fourth D_V peak. Each drop produced a secondary drop from a column of liquid which formed behind the primary drop and the size of this drop is shown in Fig.8.3. It can be seen that there is a rapid rise of $D_{E,2}$ with

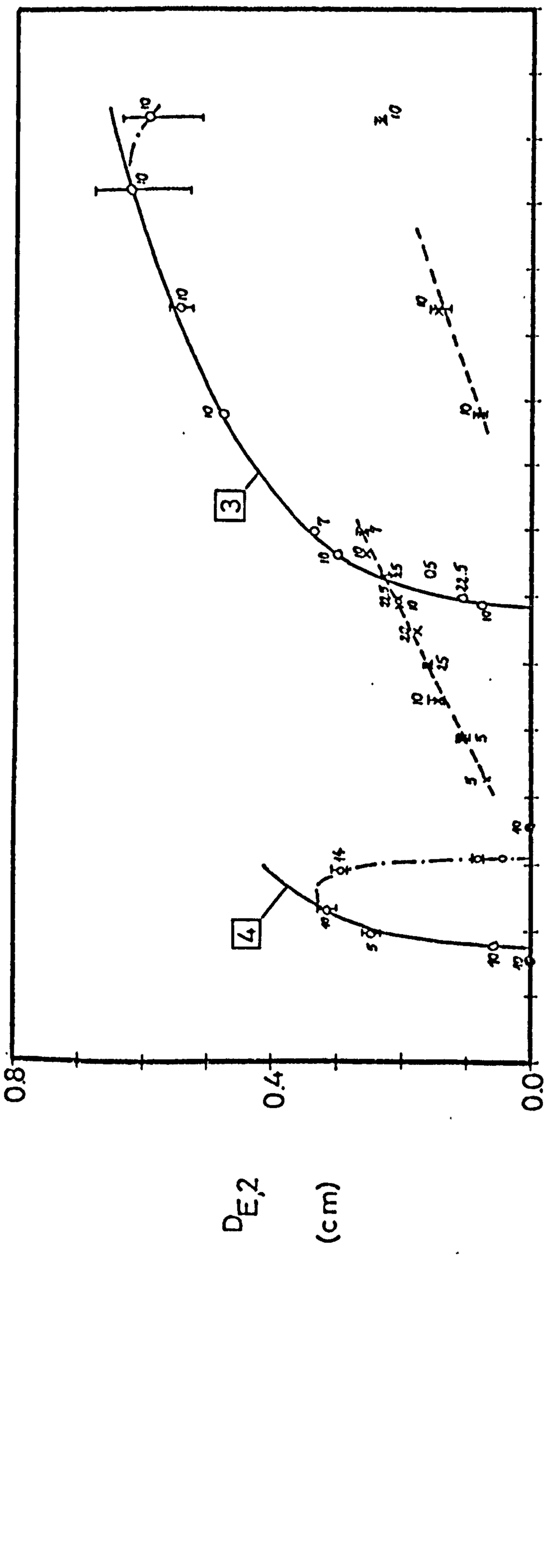

Fig.8.3 The equivalent spherical diameter of the secondary drop for the chlorobenzene/water system
• no secondary drop, —o— rear formed, —+— front formed, [ ] limits of scatter; numbers refer to the intervals (sec) between the primary drops, —— Equation 8.1
□ number of D_V-peak at which rear breakup occurs

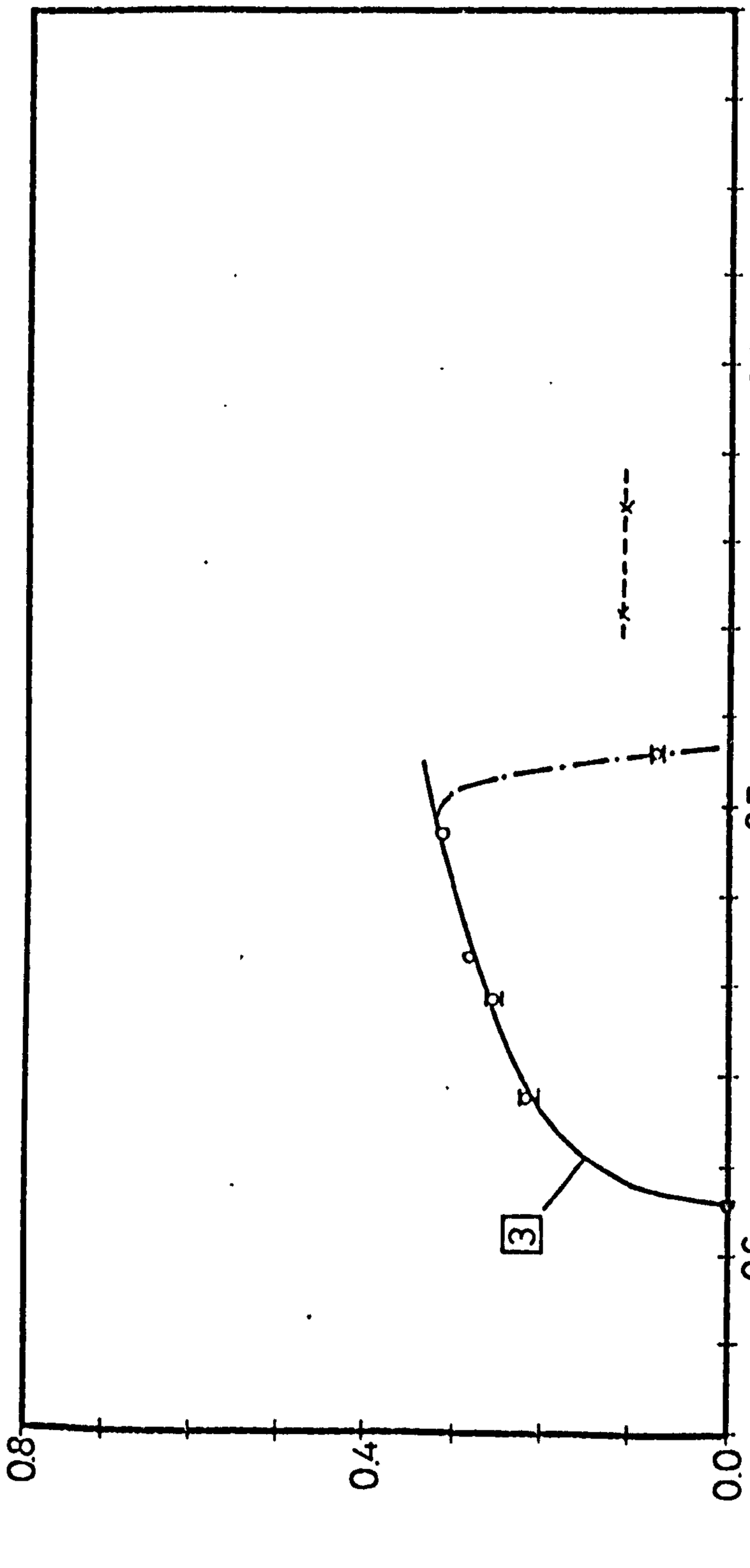

Fig.8.4 The equivalent spherical diameter of the secondary drop for the 1,2-dichloroethane/water system
• no secondary drop formed,-•-rear formed,-×-front formed, I limits of scatter; primary drops were formed at 10 sec intervals,—Eqn.8.1 □number of D_V-peak at which rear breakup occurs

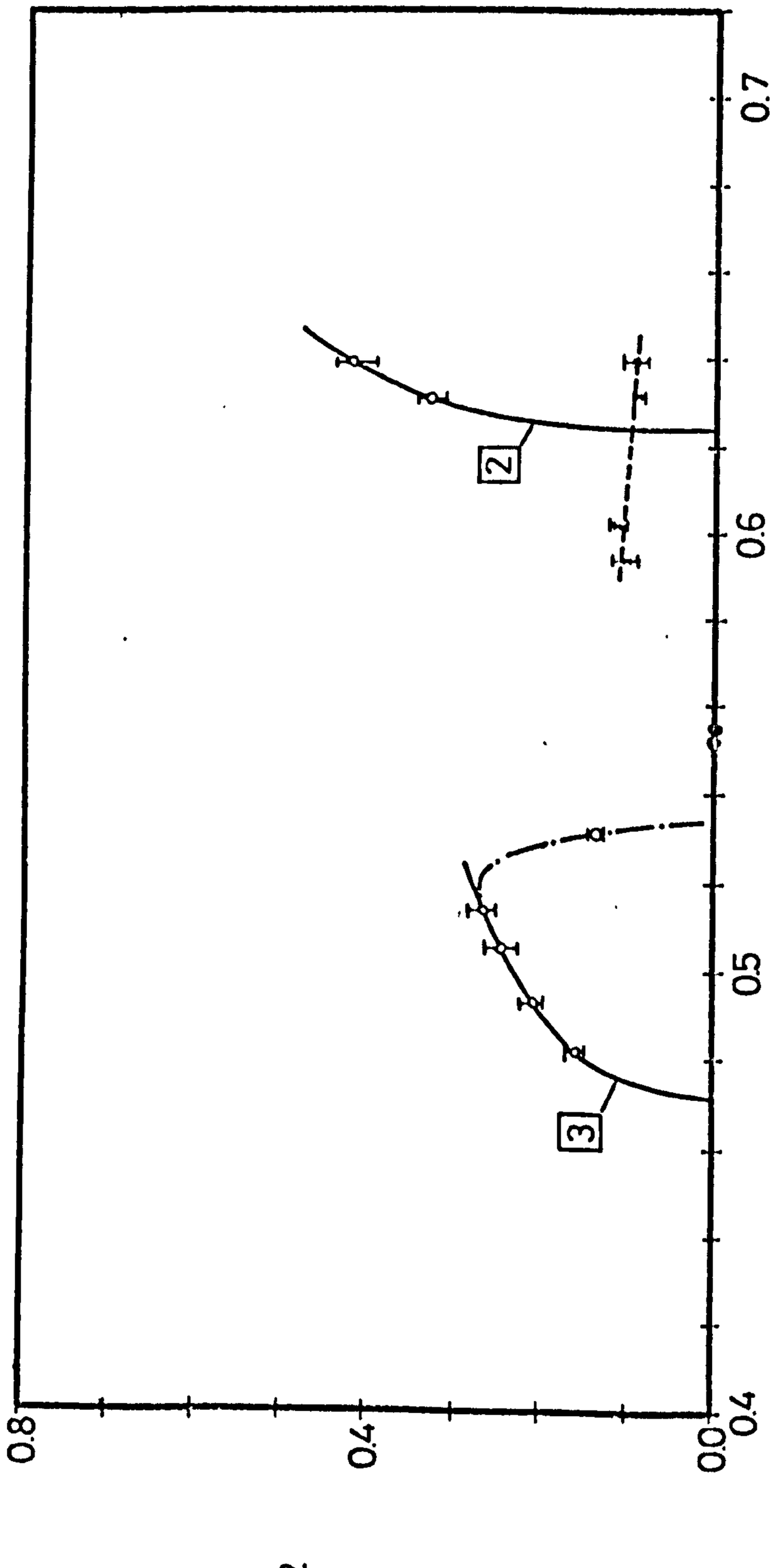

Fig.85 The equivalent spherical diameter of the secondary drop for the ethylbromide/water system
• no secondary drop formed,·-·-front formed,·--·-rear formed, I limits of
were formed at 10 sec intervals,——Eqn. 8.1 □number of D_V-peak at w

increase in $D_{E,1}$ which occurs when $D_{E,1}$ is increased above the critical drop diameter. Just above a drop size of $D_{E,1}$=0.906 cm there occurs a maximum in $D_{E,2}$. Beyond this maximum there is a sharp decrease in $D_{E,2}$ and a range of drop sizes is found at which no secondary drops are formed. For example drops with an equivalent spherical diameter of 0.932 cm do not breakup at all. This can be attributed to the transition of the critical oscillation from the fourth to the third D_V peak. To illustrate this transition Fig.8.6 shows the variation of the maximum D_V, the previous minimum D_V and the amplitude A_V with the primary drop diameter where A_V is defined as the difference between $D_{V,max}$ and $D_{V,min}$. It can be seen that in the transition region the amplitude of the fourth oscillation is decreasing with $D_{E,1}$ whereas the amplitude of the third oscillation is increasing. In this region neither the third nor the fourth D_V peak is of sufficient amplitude to cause breakup of the rear formed column. However, some secondary drops are formed in this transition region by breakup from a front formed column which occurs after the third but before the fourth D_V peak. The size of this front formed secondary drop is small and increases with the size of the primary drop. When the size of the primary drop is increased beyond a second critical size, the amplitude of the third D_V peak becomes large enough to produce a rear formed secondary drop. The size of the

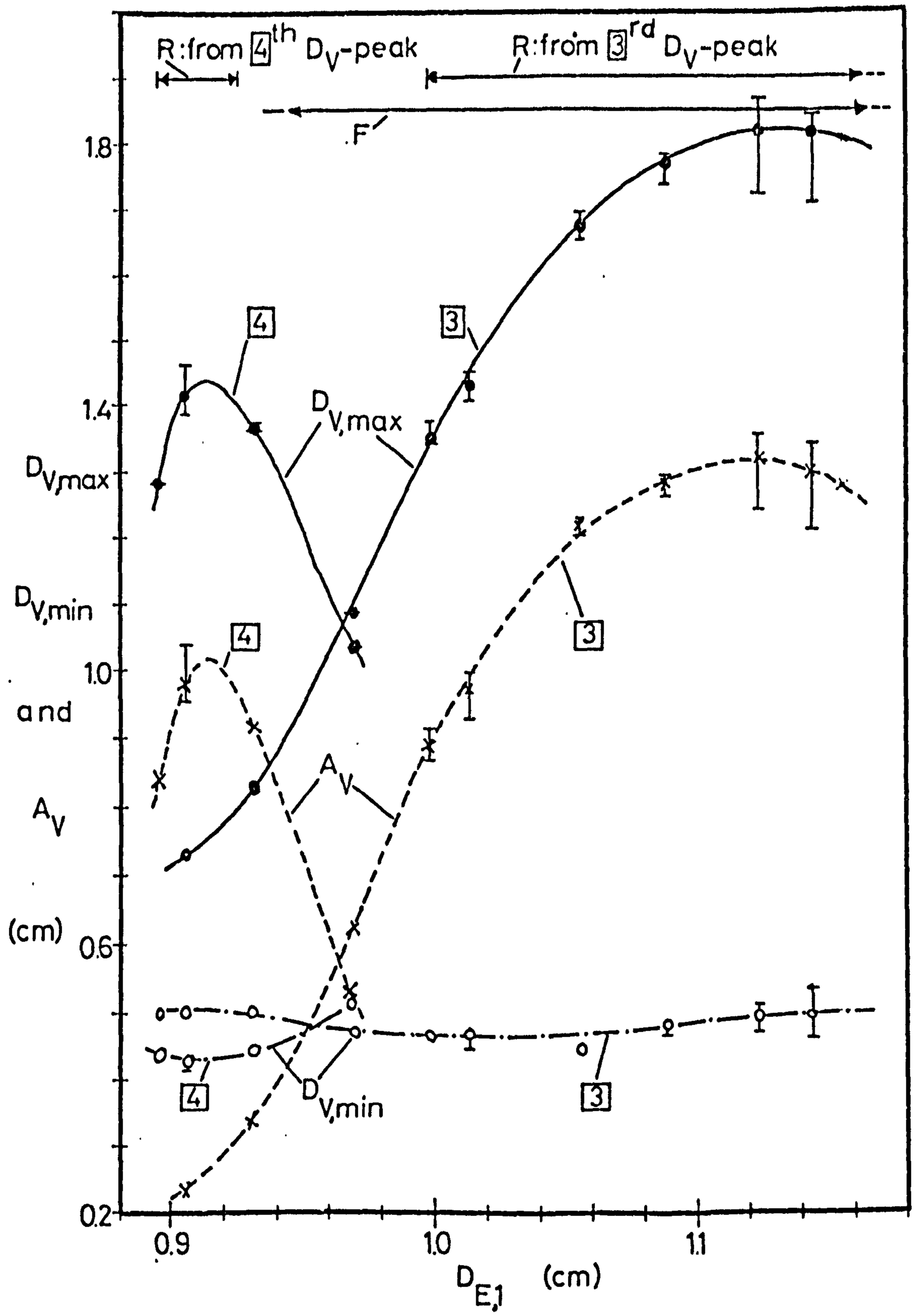

Fig.8.6 Change of $D_{V,max}$, $D_{V,min}$, and $A_V[=D_{V,max} - D_{V,min}]$ for chlorobenzene drops falling freely in water,

⟷ breakup range for R(rear) and F(front) breakup

□ D_V-oscillation number, I limits of scatter

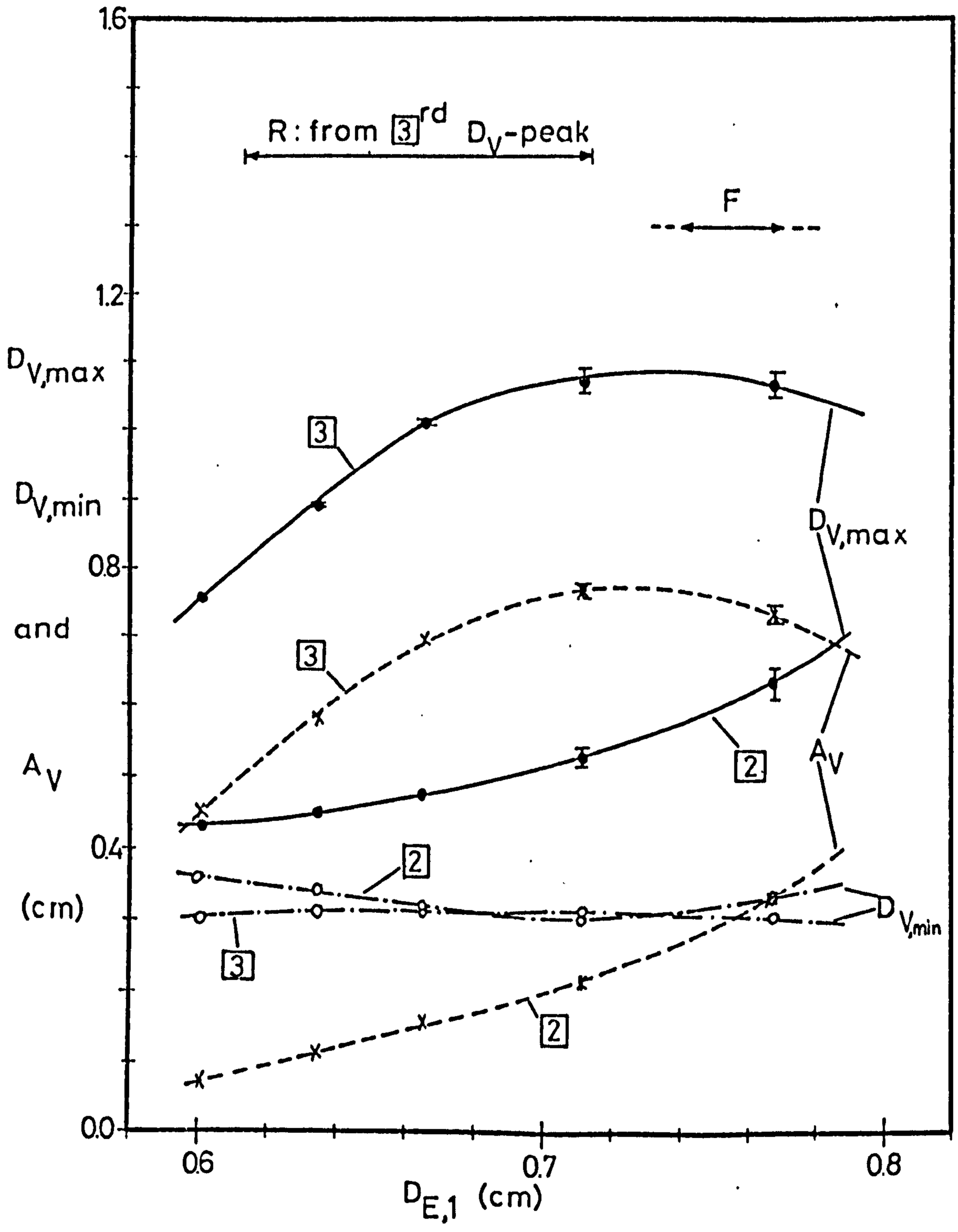

Fig.8.7 Change of $D_{V,max}$, $D_{V,min}$, and $A_V[=D_{V,max}-D_{V,min}]$ for 1,2-dichloroethane drops falling freely in water,

⟷ breakup range for R(rear) and F(front) breakup

□ D_V-oscillation number, I limits of scatter

secondary drop produced at the third oscillation increases with the size of the primary drop in a manner similar to that found for the fourth oscillation. The results for the larger primary drops suggest that as the primary drop size is increased the secondary drop size passes through a further maximum and then decreases and that this is related to a transition of the critical oscillation from the third D_V peak to the second D_V peak. However, sufficient data is presently not available to confirm this transition.

The drops which have a rear breakup at the third oscillation also have subsequently a front breakup. For these drops there is a discontinuity in the relationship between the size of the front formed secondary drops and the size of the primary drops (Fig.8.3). The onset of the formation of secondary drops from a rear column may cause the discontinuity in this relationship. However, it is thought that this is only part of the explanation because if it was the sole cause of the discontinuity , the discontinuity should occur closer to the critical size for rear breakup on the third D_V peak than is shown in Fig.8.3. An investigation of the formation of a front column and its breakup has not been attempted in this work because of the difficulties involved in measuring the front column dimensions. These difficulties are caused by the cavity which forms at the front of the drop and

obscures much of the front formed column (photograph 17 of Fig.8.2). The results for the two largest sizes of drops in the chlorobenzene system showed an anomaly. The larger drop which had a size of $D_{E,1}$=1.146 cm produced a front formed secondary drop of approximately expected size. However, the smaller drop which had a size of $D_{E,1}$=1.124 cm did not produce a front formed secondary drop. The reason for this is not known, but it was noticed that with these two sizes of drop the measurements of the drop dimensions during the necking process were much less reproducible than with the other drops studied.

The Effect of the Rate of Formation on Breakup

The results which are given in Table 3 of Appendix III show that the size of the primary drop which is formed from a particular tip increased with increase in the rate of formation. This in agreement with the findings of other workers(63)(64). Therefore, the size of the secondary drop, which depends on the size of the primary drop,varies with the rate of formation. However, the dependence of the size of the secondary drops on the size of the primary drops which were formed at rates other than 10 seconds per drop, was similar to the one which was obtained for drops formed at 10 seconds intervals (Fig.8.3). Thus the formation time of the primary drop has no effect

on the breakup other than changing the size of the primary drop.

Secondary Drop Formation in Other Systems

Breaking drops of 1,2-dichloroethane and ethylbromide showed a transition of the critical oscillation which was similar to that observed with chlorobenzene drops. The smallest 1,2-dichloroethane drops broke up from a rear column at the third D_V peak and also showed a maximum value of $D_{E,2}$ in their relationship between $D_{E,2}$ and $D_{E,1}$ (Fig.8.4). Beyond a critical primary drop size of $D_{E,1}$=0.714 cm the amplitude of the third oscillation was not sufficient to give a rear formed secondary drop. However, front formed secondary drops were produced at drop sizes above $D_{E,1}$=0.743 cm. These changes in the mechanism of the secondary drop formation are caused by the transition of the critical oscillation from the third to the second D_V peak. This is shown in Fig.8.7 in which the amplitude of the third D_V peak is decreasing and the amplitude of the second D_V peak is increasing with increase in $D_{E,1}$ in this region. Although for the range of drop sizes investigated there was no breakup at the second peak it is expected that this will be observed with larger sizes of primary drop.

A transition of the critical oscillation from the third D_V peak to the second D_V peak was also observed for ethylbromide drops (Fig.8.5). Also in the transition region front formed breakup occurred. With this system rear formed secondary drops were produced at the second D_V peak with the two largest sizes of drops which were studied. These drops also produced a front formed secondary drop between the second and the third D_V peaks.

Size of the Rear Formed Secondary Drop

From Figures 8.3 to 8.5 it can be seen that there is no single relationship between $D_{E,2}$ and $D_{E,1}$. However, for drops breaking at a particular D_V peak and for the region where $D_{E,2}$ is increasing with $D_{E,1}$ a simple empirical relationship was found to give a good correlation for the rear formed secondary drops :

$$V_2 = V_o (D_{E,1} - D^*_{E,1}) \qquad (8.1)$$

where V_2 is the volume of the secondary drop and V_o and $D^*_{E,1}$ are empirical constants which have different values for the various D_V peaks and systems. $D^*_{E,1}$ can be regarded as the critical diameter for breakup on the corresponding D_V peak. Equation (8.1) predicts the sizes of the rear formed secondary drops with an average error of 2.2%. Values of V_o and $D^*_{E,1}$ for various D_V peaks and systems are presented in Table 17

of Appendix III.

It was found that for the three systems which were investigated the following equation predicted the critical diameter for breakup to occur to within 1.9% :

$$D_{E,crit} = \frac{0.269}{(\Delta\rho/\rho_d)^{0.3}} \qquad (8.2)$$

However, this equation is tentative because a limited number of systems were investigated. Also the effect of the interfacial tension on the secondary drop formation was not sufficiently studied and was ommitted from equation (8.2). This equation has some similarities with the HU and KINTNER[72] correlation (equation 2.56). However, the Hu and Kintner correlation gives values of $D_{E,1,crit}$ which are much higher than those which were found in the present work. This is probably because equation (2.56) was derived from results which were obtained for impure systems.

8.7 THE STABILITY OF THE REAR COLUMN

Measurements of the dimensions of the column which is formed behind the primary drop immediately prior to necking are given in Table 18 of Appendix III. It was found that the ratio $H/2\pi R_c$ was approximately 0.40. This is not in agreement with the theory which was developed by Charles and Mason[28] for the breakup of a column of liquid which forms during the coalescence of a drop at a plane liquid-liquid interface. This theory assumed that the wavelength of the disturbance which was breaking the column was equal to the height of the column and predicted $H/2\pi R_c$ to be 1.434. When assessing the value of the Charles and Mason model in the present work, the original criterion used by Rayleigh for stability (Section 2.5) must be kept in mind and it should be noted that the change in surface area which occurs during necking is not great. This means that unless the model describes accurately the surface area of the system its use will not be valid. As an illustration of the invalidity in the present work of the pictorial model used by Charles and Mason (Model A, Fig.8.8) the breakup of a drop with an equivalent spherical diameter of 1.088 cm will be used. Immediately prior to necking the column has the dimensions D_c=0.530 cm and H=0.747 cm (Fig.8.9). This gives a secondary drop which has a surface area of 0.93 cm^2. The model A gives before necking an area

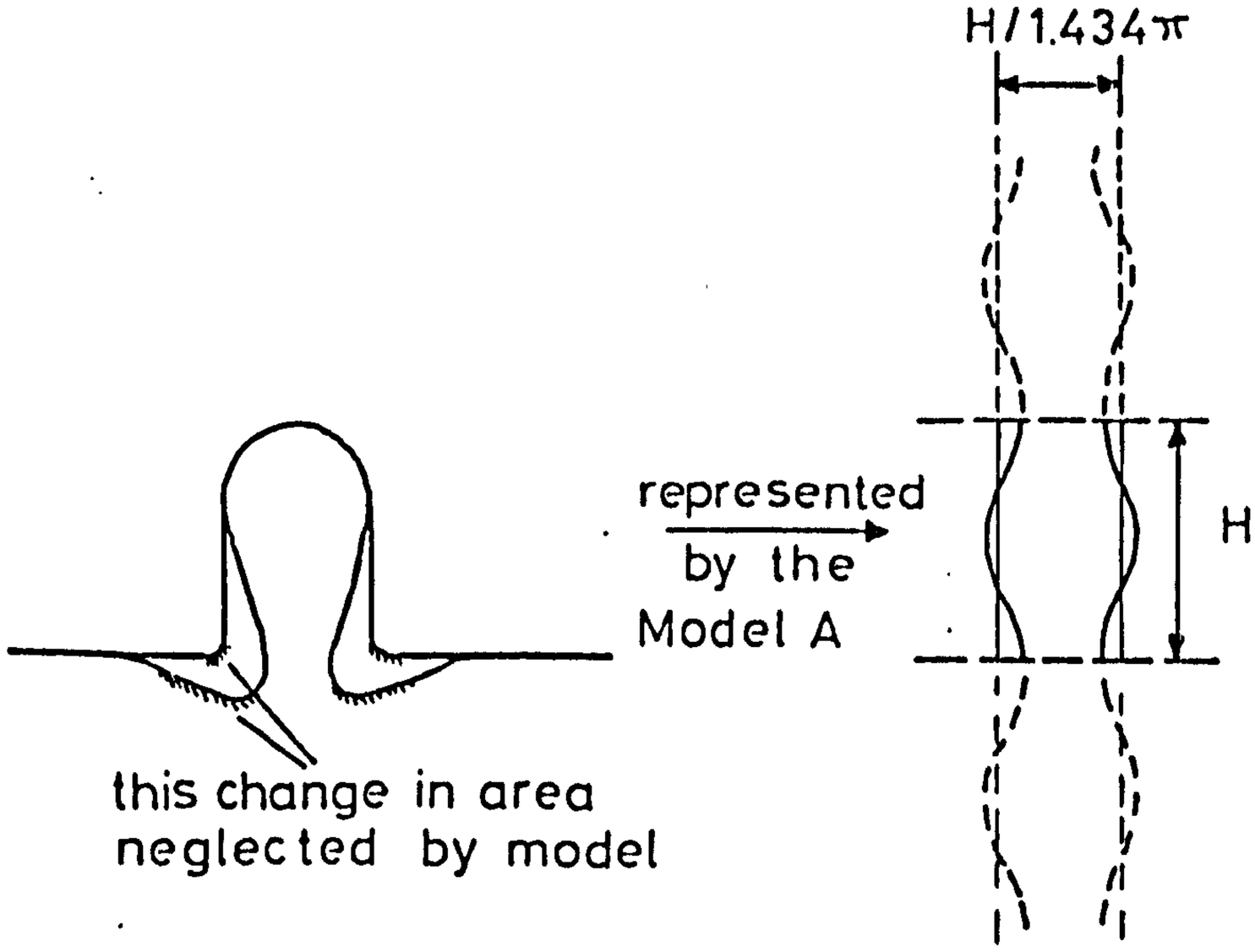

Fig.8.8 Model A used by CHARLES and MASON[28] to examine secondary drop formation during coalescence

of 1.24 cm^2 and a secondary drop with a surface area of 1.42 cm^2. Therefore the difference in the surface area between the experimental and predicted secondary drops is greater than the change in the surface area predicted by the model. The model also neglects the changes in area of the surfaces attached to the liquid column which occur during the necking process. This is illustrated in Fig.8.8. In the present work these are of a similar magnitude to the changes which occur in the surface area of the column and need to be taken into consideration. The dangers in applying carelessly a theory, such as the Rayleigh theory, to a system for which it was not developed is well illustrated by the following argument which was developed using the results of the present work.

Visual observations of the shape of the column during necking suggested that the surface is well represented by a section of a wave, which has a length h, joined to a section of the surface $r' = R_c$ where the wavelength of the wave is 4h and $h=H-R_c$ (Models B1 and B2, Appendix I-B). The changes in the surface area of these models which occur during necking are investigated in Appendix I-B with surface waves represented by either

$$r = (R_c-\alpha) + \alpha \cos\frac{2\pi z}{4h} \qquad (8.3)$$

for Model B1 or by

$$r = R_c - \alpha \sin \frac{2\pi z}{4h} \tag{8.4}$$

for Model B2 where

$$0 < z < h \qquad \text{and} \qquad \alpha \ll R_c \tag{8.5}$$

In Model B no drainage is assumed during necking and no account is taken of the changes in the area of the surfaces attached to the liquid column. If Rayleigh's result (equation) is used to predict the stability of thu surface wave in this model :

$$\lambda_{crit} = 2\pi R_c \tag{8.6}$$

the critical ratio of the height of the column to the circumference is found to be

$$\left(\frac{H}{2\pi R_c}\right)_{crit} = \frac{1}{4} + \frac{1}{2\pi} = 0.41 \tag{8.7}$$

This predicts that when the liquid column has shrunk to a radius R_c such that $H/2\pi R_c = 0.41$ a disturbance wave can grow on its surface. This is in fair agreement with the experimental results as is shown in Table 18 of Appendix III. However, a close examination of this procedure shows that it is unjustified. For both of the B models it is shown in Appendix I-B that for the surface area of the column to decrease during necking

$$H < R_c \tag{8.8}$$

However, it can be seen from Table 18 of Appendix III that for all the drop sizes and systems $H > R_c$.

Therefore both of the B models give an increase in the surface area during necking and will not lead to secondary drop formation.

The case of a draining column is represented by models C1, C2, and C3 which are discussed in Appendix I-C. Model C1 represents the shrinking of a draining column and models C2 and C3 represent the necking of a draining column where the surface of the column is represented by equations (8.3) and (8.4), respectively. Using, as the criterion for stability, that the surface area of the system must decrease if the drainage is to proceed by the process described in the model, critical values of R_c at the onset of necking were estimated for the various models (Appendix I-C) and the results are given in Table 19 of Appendix III. Provided R_c is less than the critical value given for the particular drainage model, drainage can occur by that drainage model. The results show that drainage of the column can occur by either shrinking or necking and that drainage by shrinking can occur at higher values of R_c than can drainage by necking. This is in agreement with the experimental results. The theoretical values of the critical R_c for drainage by both shrinking or necking are low. However, this was expected because of the dificulty in describing the surface of a breaking drop. Because the changes in surface area of the column during draining are small reliable

theoretical values of the critical R_c can only be obtained when the model describes very accurately the surface of the drop.

8.8 DRAINAGE OF THE REAR COLUMN

Examination of Fig.8.9 shows that the rear column drains for a short time (40 - 43 msec) as a shrinking cylinder and then drains by a necking process (43 - 76 msec). The decrease in the volume of the rear column during necking is about 56% of the final volume. This shows another major shortcoming of the theory by Charles and Mason who assumed that there is no drainage during necking.

BROWN and HANSON[22][59] developed a theory to calculate the rate of drainage of a shrinking cylinder of liquid. They obtained for the volumetric rate of draining

$$\frac{dV}{dt} = -\frac{\pi}{4}\frac{\sigma}{\mu_c}\frac{R_c^3}{2H-R_c} \qquad (8.9)$$

The volumetric rate of draining predicted by the above equation is compared with the experimental results presented in Fig.8.9. Using Fig.8.9 the rate of drainage is calculated to be - 6.28 cm^3/sec. Equation (8.9), however, predicts a value of - 77.3 cm^3/sec. The most important shortcoming of the Brown and Hanson theory is that they considered only the pressure drop due to frictional drag forces and neglected the change in the hydrostatic pressure along the liquid column. These pressure changes are of similar order in the present system.

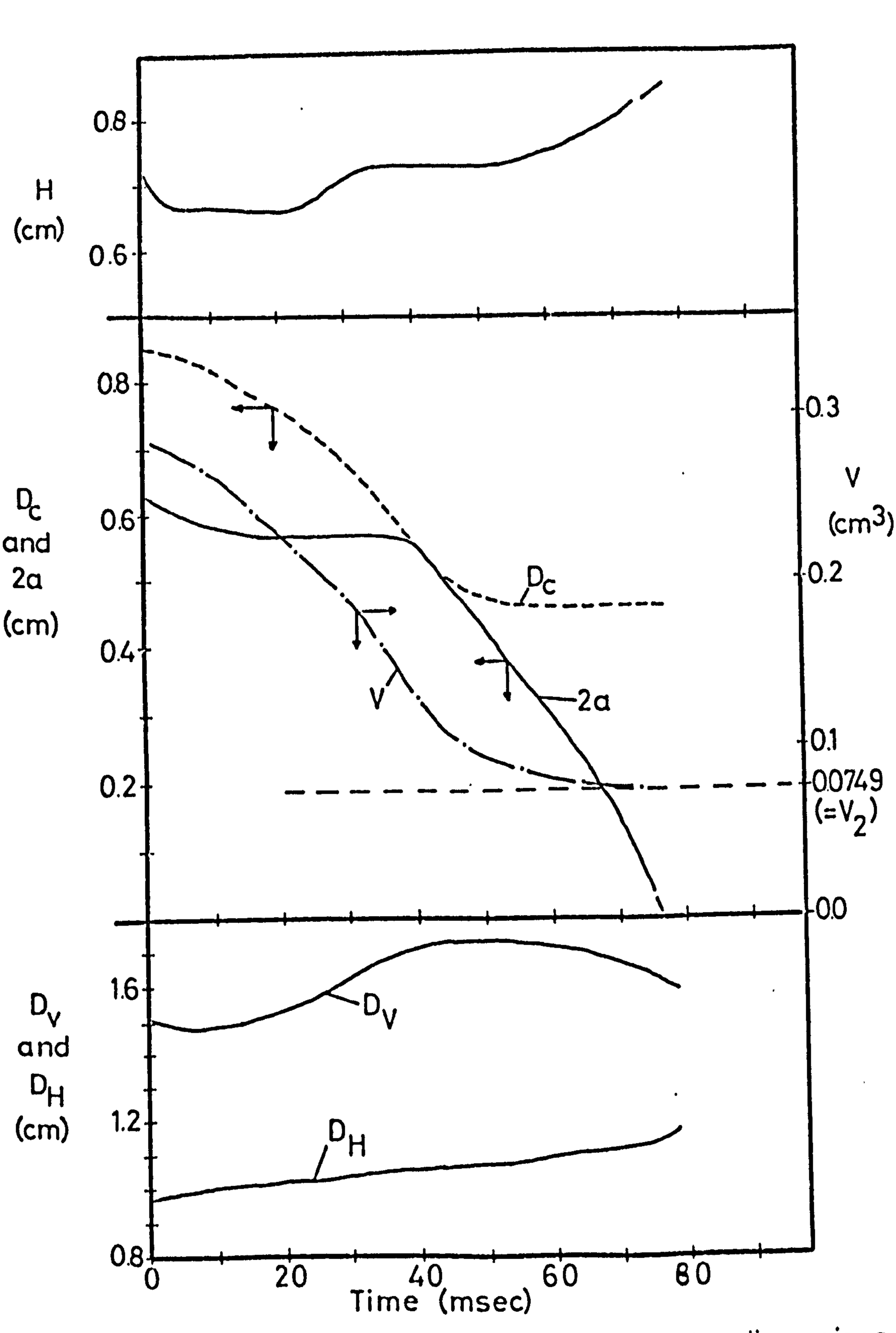

Fig.8.9 The volume of the rear column and the dimensions of the drop during breakup; chlorobenzene/water system $D_{E,1}=1.088$ cm, $D_{E,2}=0.523$ cm, $V_2=0.0749\ cm^3$

8.9 ESTIMATION OF THE RATE OF NECKING AT THE ONSET OF NECKING

Estimation of the rate of necking (da/dt) at the onset of necking was obtained from a momentum balance :

$$\frac{7}{6}\rho_d \frac{(H-R_c)^2}{R_c^2}\left(\frac{da}{dt}\right)^2 = -1.12\,\frac{\rho_a}{2}\,U_\infty^2 + \Delta\rho\, g\, D_V + 2\sigma\left(\frac{1}{C_A} - \frac{1}{C_B}\right) \qquad (8.10)$$

The derivation of this equation is given in Appendix I-D. The calculated values of (da/dt) are compared with the experimental results in Table 20 of Appendix III. No results are presented for drops which formed rear columns which were not cylindrical ($D_{E,1}$=1.124 cm and $D_{E,1}$=1.146 cm for chlorobenzene and $D_{E,1}$=0.694 cm and $D_{E,1}$=0.712 cm for 1,2-dichloroethane) and for drops where the columns did not neck at constant R_c ($D_{E,1}$=0.998 cm for chlorobenzene). In spite of the many simplifying assumptions which were made in the derivation of equation (8.10) the agreement is good.

SECTION 9

CONCLUSIONS

1. Secondary drops are produced by the breakup of liquid columns which are formed both at the rear and front of freely falling drops when these drops are above a critical size. The breakup from the rear column occurs during a critical oscillation of high amplitude which follows the first shedding of a class III attached wake. The breakup occurs at an earlier peak in the relationship of D_V against time as the drop size is increased.

2. The critical drop diameter for the onset of breakup can be predicted by the equation

$$D_{E_1,crit} = \frac{0.269}{(\Delta\rho/\rho_d)^{0.5}}$$

3. Secondary drops are formed from the liquid columns by a necking process. The volumes of the secondary drops which are formed from

the rear column at a particular D_V peak and for a particular system can be predicted by an equation of the form

$$V_2 = V_o (D_{E,1} - D^*_{E,1})$$

This equation only applies to the region where the secondary drop size is increasing with increase in primary drop size.

4. The rate of formation of the primary drop does not effect the relationship between the size of the secondary drop and the size of the primary drop from which it was produced.

5. The rate of necking of the rear column at the onset of necking may be predicted from a momentum balance on the fluid in the column.

6. Considerations of the surface free energy of a drop during breakup predict that drainage of the rear formed column can occur either by shrinking or by necking. They also predict that the rear column will drain initially by shrinking and finally by necking.

APPENDIX I

THEORETICAL CONSIDERATIONS

I-A THE VELOCITY OF FALL AND THE DRAG COEFFICIENT DURING ACCELERATION

A force balance on an accelerating drop can be written as

$$V_1 \rho_d \frac{dU}{dt} = V_1 \Delta\rho g - C_D \frac{\rho_a}{2} A U^2 \qquad \text{(I-A.1)}$$

The drag coefficient C_D is not constant during acceleration and its value is higher than the terminal value $(C_D)_\infty$ because of the accelerational drag. As a first approximation the drag can be split into two parts :

$$C_D \frac{\rho_a}{2} A U^2 = (C_D)_\infty \frac{\rho_a}{2} A U^2 + b \frac{dU}{dt} \qquad \text{(I-A.2)}$$

where b is a factor which takes into consideration the effect of the acceleration. Equation (I-A.2) can be substituted into equation (I-A.1) to give

$$(V_1 \rho_d + b)\frac{dU}{dt} = V_1 \Delta\rho g - (C_D)_\infty \frac{\rho_a}{2} A U^2 \qquad \text{(I-A.3)}$$

If b is assumed to be of the form

$$b = k\, V_1 \rho_a \qquad \text{(I-A.4)}$$

equation (I-A.3) becomes

$$V_1 (\rho_d + k\rho_a)\frac{dU}{dt} = V_1 \Delta\rho g - (C_D)_\infty \frac{\rho_a}{2} A U^2 \qquad \text{(I-A.5)}$$

If k=0.5, which is the theoretical value given by STOKES[151][153], then equation (I-A.5) reduces to equation (2.50) and a solution of this latter equation

was given by HU and KINTNER[72]. Equation (I-A.5) can be rearranged to give

$$\frac{dU}{dt} + (C_0)_\infty \frac{\rho_a}{\rho_d + k\rho_a} \frac{A}{2V_1} U^2 = \frac{\Delta\rho}{\rho_d + k\rho_a} g \qquad \text{(I-A.6)}$$

The solution of this differential equation is of the form

$$U = U_\infty \tanh \tau t \qquad \text{(I-A.7)}$$

where

$$U_\infty = \sqrt{2 \frac{\Delta\rho}{\rho_a} \frac{V_1 g}{A(C_0)_\infty}} \qquad \text{(I-A.8)}$$

and

$$\tau = \frac{\Delta\rho}{\rho_d + k\rho_a} \frac{g}{U_\infty} \qquad \text{(I-A.9)}$$

If equation (I-A.2) is combined with equations (I-A.8) and (I-A.9) the drag coefficient C_D becomes

$$C_D = (C_D)_\infty + (C_D)_\infty \left(\frac{g}{\tau U_\infty} - \frac{\rho_d}{\Delta\rho} \right) \frac{U_\infty^2}{g} \frac{1}{U^2} \frac{dU}{dt} \qquad \text{(I-A.10)}$$

or rearranging

$$\frac{C_D}{(C_D)_\infty} = 1 + \left(\frac{g}{\tau U_\infty} - \frac{\rho_d}{\Delta\rho} \right) \frac{U_\infty^2}{g} \frac{1}{U^2} \frac{dU}{dt} \qquad \text{(I-A.11)}$$

Substitution of equation (I-A.7) into equation (I-A.11) gives finally for the drag coefficient

$$\frac{C_D}{(C_D)_\infty} = 1 + \left(1 - \frac{\tau U_\infty}{g} \frac{\rho_d}{\Delta\rho} \right) \operatorname{csch}^2 \tau t \qquad \text{(I-A.12)}$$

I-B STABILITY OF A NONDRAINING COLUMN

In models B1 and B2 the surface of the column prior to necking is represented by a cylindrical column of radius R_c and of height $h = (H - R_c)$ and a hemispherical cap of radius R_c. The stability of this column to a small disturbance is examined for the case of a nondraining column. The criterion for stability is that if the surface area of the column decreases during necking then the disturbance will grow. In these models no account is taken of the changes in surface area of the main drop to which the column is attached.

Model B1

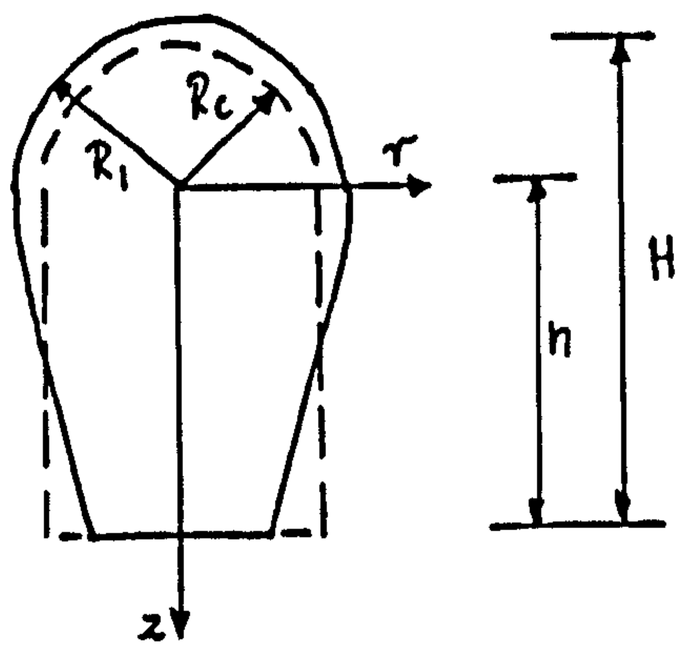

The surface of the disturbed column is represented by the equations

$$r = (R_1 - \alpha) + \alpha \cos\frac{\pi z}{2h} \qquad \text{for } 0 \leq z \leq h \quad \text{(I-B.1)}$$

$$r' = R_1 \qquad \text{for } -R_1 \leq z \leq 0 \quad \text{(I-B.2)}$$

where

$$R_1 = R_c + \beta \qquad \text{(I-B.3)}$$

and a disturbance of small amplitude is considered so

that

$$\alpha^2 \ll R_c^2 \qquad \beta^2 \ll R_c^2 \tag{I-B.4}$$

For a nondraining column the volume of the undisturbed column equals the volume of the disturbed column

$$\frac{2}{3}\pi R_c^3 + \pi R_c^2 (H-R_c) = \frac{2}{3}\pi R_1^3 + \pi R_1^2 (H-R_1) - 2\pi\alpha R_1 (H-R_1) + \pi\alpha^2 (H-R_1) \tag{I-B.5}$$

which gives when combined with equation (I-B.3) :

$$\beta = \alpha \frac{\pi-2}{\pi} \frac{H-R_c}{H} \tag{I-B.6}$$

The surface area of the undisturbed column is :

$$A_c = 2\pi R_c^2 + 2\pi R_c (H-R_c) \tag{I-B.7}$$

The surface area of the disturbed column is :

$$A_1 = 2\pi H R_c + 2(\pi-2) R_c \alpha \frac{H-R_c}{2H} \tag{I-B.8}$$

Therefore for the disturbance to grow

$$A_1 < A_c \tag{I-B.9}$$

or from equations (I-B.7) and (I-B.8)

$$(\pi-2) R_c \alpha \frac{H-R_c}{H} < 0 \tag{I-B.10}$$

This condition is satisfied only when

$$H < R_c \tag{I-B.11}$$

Model B2

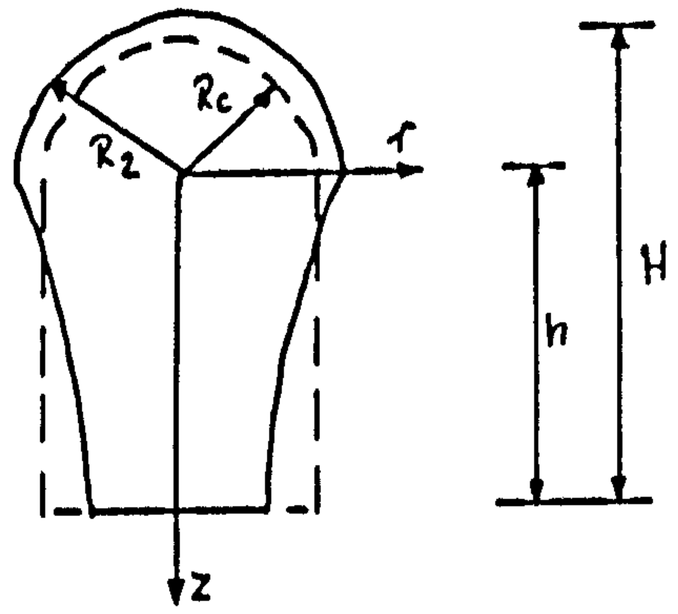

The surface of the disturbed column is represented by the equations

$$r = R_2 - \alpha \sin \frac{\pi z}{2h} \qquad \text{for } 0 \leq z \leq h \qquad \text{(I-B.12)}$$

$$r' = R_2 \qquad \text{for } -R_2 \leq z \leq 0 \qquad \text{(I-B.13)}$$

where

$$R_2 = R_c + \beta \qquad \text{(I-B.14)}$$

and a disturbance of small amplitude is considered so that

$$\alpha^2 \ll R_c^2 \qquad \beta^2 \ll R_c^2 \qquad \text{(I-B.15)}$$

For a nondraining column the volume of the undisturbed column equals the volume of the disturbed column :

$$\frac{2}{3}\pi R_c^3 + \pi R_c^2 (H - R_c) = \pi H R_2^2 - \frac{\pi}{3} R_2^3 - 4 R_2 (H - R_2)\alpha \qquad \text{(I-B.16)}$$

which gives when combined with equation (I-B.14)

$$\beta = \alpha \frac{4}{\pi} \frac{H - R_c}{2H} \qquad \text{(I-B.17)}$$

The surface area of the undisturbed column is :

$$A_c = 2\pi R_c^2 + 2\pi R_c (H - R_c) \qquad \text{(I-B.18)}$$

The surface area of the disturbed column is :

$$A_2 = 2\pi H R_c + 2R_c \frac{H - R_c}{H} \alpha \qquad \text{(I-B.19)}$$

Therefore for the disturbance to grow

$$A_2 < A_c \qquad \text{(I-B.20)}$$

or from equations (I-B.18) and (I-B.19)

$$2 R_c \alpha \frac{H - R_c}{H} < 0 \qquad \text{(I-B.21)}$$

This condition is satisfied only when

$$H < R_c \qquad \text{(I-B.22)}$$

I-C STABILITY OF A DRAINING COLUMN

In models C1 to C3 the surface of the column is described by equations which are similar to those used for models B1 and B2. However, the analysis of the necking process for the C models differs from that for the B models in that account is taken of changes in the area of the main part of the drop to which the column is attached. The procedure used to examine whether drainage of the column can occur by the process described in a particular C model is similar to that used in Appendix I-B: Only if the area decreases during the drainage process can the model describe a possible mode of drainage.

Model C1

In this model drainage occurs by shrinking and the surface of the column is represented by a cylindrical column, which has a radius R_c and a height $h = (H - R_c)$, and a hemispherical cap of radius R_c where H is a constant and R_c is a function of time. Fig.8.9 suggests that when the column is draining by shrinkage and its shape is cylindrical then dR_c/dt=const and this will be assumed in the analysis.

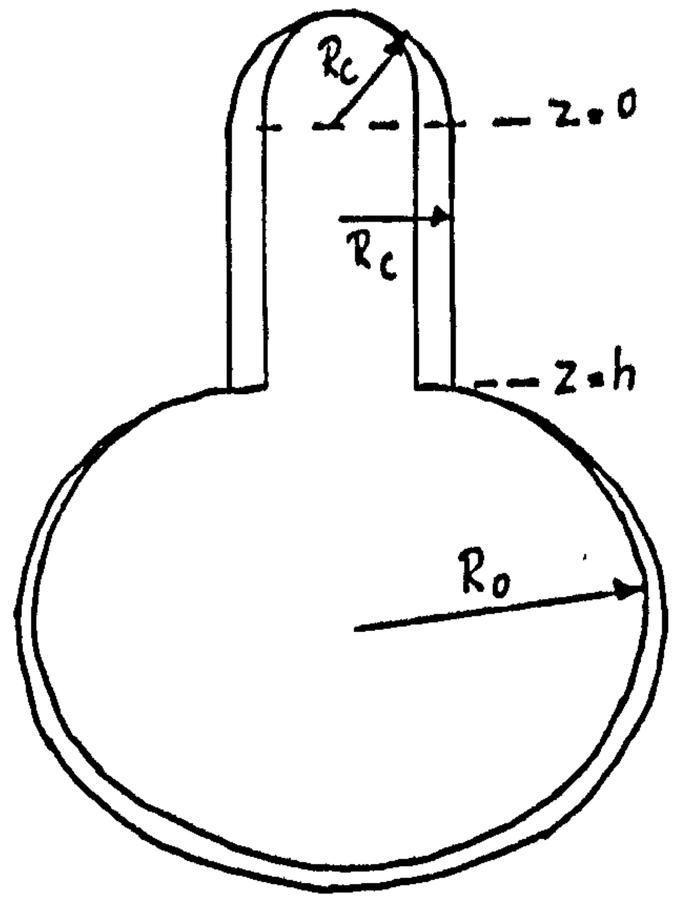

The total volume of the drop is constant and is given by

$$V_1 = \pi H R_c^2 - \frac{\pi}{3} R_c^3 + \frac{4}{3}\pi R_o^3 - \frac{\pi}{4}\frac{R_c^4}{R_o} \qquad \text{(I-C.1)}$$

Differentiation with respect to R_c leads to

$$\frac{dV_1}{dR_c} = 0 = 2\pi H R_c - \pi R_c^2 + 4\pi R_o^2 \frac{dR_o}{dR_c} - \pi \frac{R_c^3}{R_o} + \frac{\pi}{4}\frac{R_c^4}{R_o^2}\frac{dR_o}{dR_c} \qquad \text{(I-C.2)}$$

The total surface area of the drop is given by

$$A_1 = 2\pi H R_c + 4\pi R_o^2 - 2\pi R_o\left(R_o - \sqrt{R_o^2 - R_c^2}\right) \qquad \text{(I-C.3)}$$

and therefore differentiation with respect to R_c and for the case

$$R_c^2 \ll R_o^2 \qquad \text{(I-C.4)}$$

gives

$$\frac{dA}{dR_c} = 2\pi H + 8\pi R_o \frac{dR_o}{dR_c} - 2\pi R_c \qquad \text{(I-C.5)}$$

This can be combined with equations (I-C.2) and (I-C.4)

to give

$$\frac{dA_1}{dR_c} = 2\pi H - 2\pi R_c + 2\pi \frac{R_c^2}{R_o} - 4\pi H \frac{R_c}{R_o} \qquad \text{(I-C.6)}$$

For drainage by shrinkage to be possible dA_1/dR_c must be positive and therefore

$$R_c^2 - 2\left(H + \frac{R_o}{2}\right) R_c + HR_o > 0 \qquad \text{(I-C.7)}$$

The only solution of this equation which is acceptable is given by

$$R_c < \left(H + \frac{R_o}{2}\right) - \sqrt{\left(H + \frac{R_o}{2}\right)^2 - HR_o} \quad = R_{c,crit} \qquad \text{(I-C.8)}$$

As a first approximation it is assumed that

$$R_o = \frac{1}{2} D_{E,1} \qquad \text{(I-C.9)}$$

and the calculated values of the critical R_c are presented in Table 19 of Appendix III.

Model C2

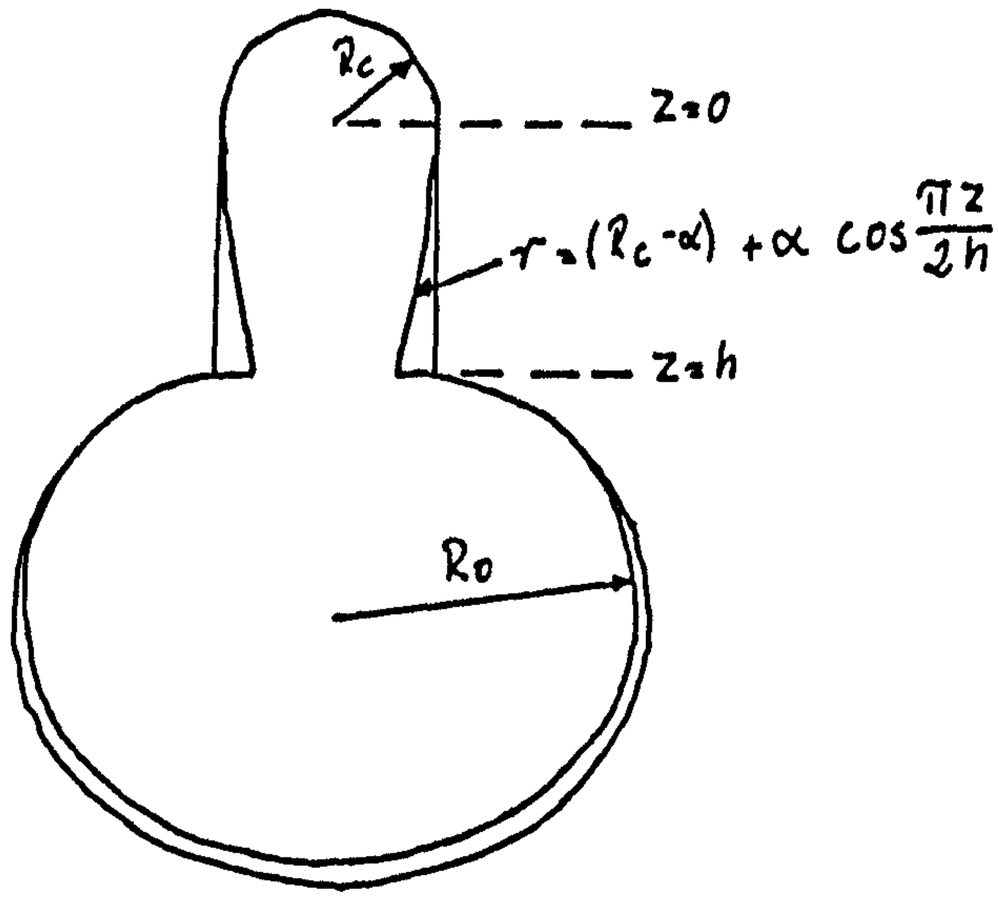

In this model drainage occurs by necking. Prior to necking the surface of the column is represented by a cylindrical column, which has a radius R_c and a height $h = (H - R_c)$, and a hemispherical cap of radius R_c where H is a constant. During necking the surface of the column is represented by the equations :

$$r = (R_c - \alpha) + \alpha\cos\frac{\pi z}{2h} \qquad \text{for } 0 \leq z \leq h \qquad \text{(I-C.10)}$$

$$r' = R_c \qquad \text{for } -R_c \leq z \leq 0 \qquad \text{(I-C.11)}$$

The total volume of the drop is constant and is given by

$$V_2 = \pi H R_c^2 - \frac{\pi}{3} R_c^3 - 2(\pi-2)R_c(H-R_c)\alpha + \frac{4}{3}\pi R_o^3 - \frac{\pi}{4}\frac{(R_c-\alpha)^4}{R_o} \qquad \text{(I-C.12)}$$

Differentiation with respect to α leads to

$$0 = \frac{dV_2}{d\alpha} = -2(\pi-2)R_c(H-R_c) + 4\pi R_o^2\frac{dR_o}{d\alpha} + \pi\frac{(R_c-\alpha)^3}{R_o} + \frac{\pi}{4}\frac{(R_c-\alpha)^4}{R_o^2}\frac{dR_o}{d\alpha} \qquad \text{(I-C.13)}$$

The total surface area of the drop is given by

$$A_2 = 2\pi H R_c - 2(\pi-2)(H-R_c)\alpha + 4\pi R_o^2 - 2\pi R_o\left(R_o - \sqrt{R_o^2 - (R_c-\alpha)^2}\right) \quad \text{(I-C.14)}$$

and therefore differentiation with respect to α and for the case

$$R_c^2 \ll R_o^2 \quad \text{(I-C.15)}$$

gives

$$\frac{dA_2}{d\alpha} = -2(\pi-2)(H-R_c) + 8\pi R_o \frac{dR_o}{d\alpha} + 2\pi(R_c-\alpha) \quad \text{(I-C.16)}$$

This can be combined with equations (I-C.13) and (I-C.15) and with the condition that at the onset of necking $\alpha = 0$ to give

$$\frac{dA_2}{d\alpha} = -2(\pi-2)(H-R_c) + 2\pi R_c + 4(\pi-2)(H-R_c)\frac{R_c}{R_o} \quad \text{(I-C.17)}$$

For draining by necking to be possible $dA_2/d\alpha$ must be negative and therefore

$$R_c^2 - \left(H + \frac{\pi-1}{\pi-2}R_o\right)R_c + \frac{1}{2}HR_o > 0 \quad \text{(I-C.18)}$$

The only solution of this equation which is acceptable is given by

$$R_c < \frac{1}{2}\left(H + \frac{\pi-1}{\pi-2}R_o\right) - \sqrt{\frac{1}{4}\left(H+\frac{\pi-1}{\pi-2}R_o\right)^2 - \frac{1}{2}HR_o} = R_{c,crit} \quad \text{(I-C.19)}$$

As a first approximation it is assumed that

$$R_o = \frac{1}{2}D_{\varepsilon_{11}} \quad \text{(I-C.20)}$$

and the calculated values of the critical R_c are presented in Table 19 of Appendix III.

Model C3

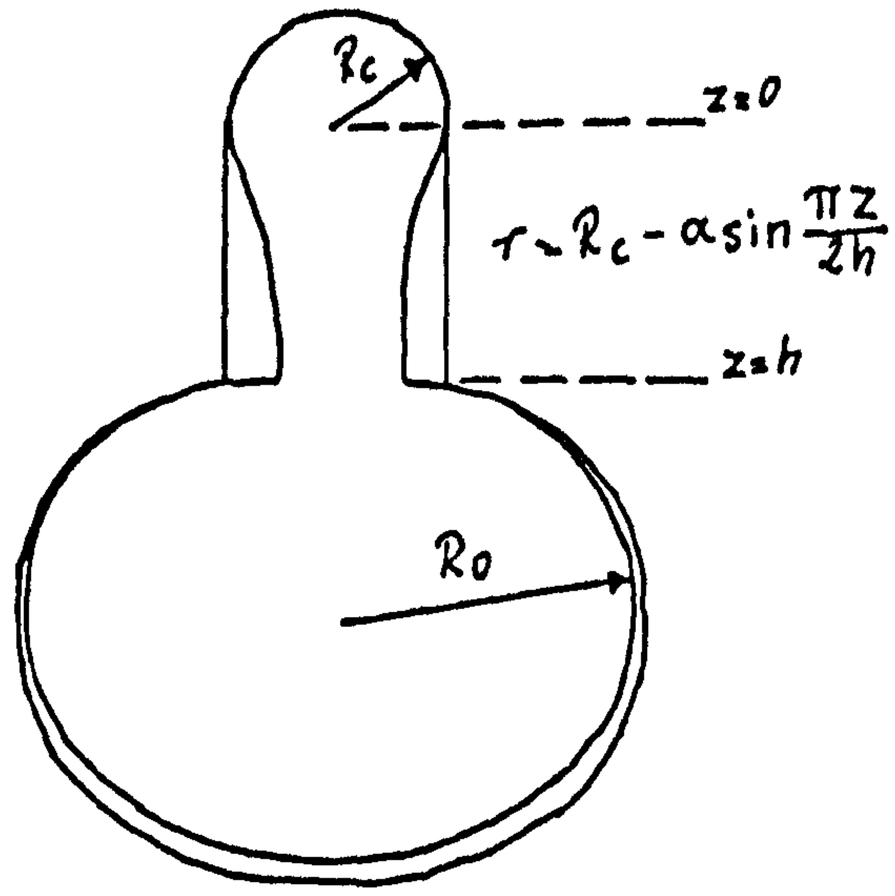

In this model drainage occurs by necking. Prior to necking the surface of the column is represented by a cylindrical column, which has a radius R_c and a height $h = (H - R_c)$, and a hemispherical cap of radius R_c where H is a constant. During necking the surface of the column is represented by the equations :

$$r = R_c - \alpha \sin \frac{\pi z}{2h} \qquad \text{for } 0 < z < h \qquad \text{(I-C.21)}$$

$$r' = R_c \qquad \text{for } -R_c < z < 0 \qquad \text{(I-C.22)}$$

The total volume of the drop is constant and is given by

$$V_3 = \pi H R_c^2 - \frac{\pi}{3} R_c^3 - 4 R_c (H - R_c) \alpha + \frac{4}{3} \pi R_0^3 - \frac{\pi}{4} \frac{(R_c - \alpha)^4}{R_0} \qquad \text{(I-C.23)}$$

Differentiation with respect to α leads to

$$\frac{dV_3}{d\alpha} = 0 = -4 R_c (H - R_c) + 4\pi R_0^2 \frac{dR_0}{d\alpha} + \pi \frac{(R_c - \alpha)^3}{R_0} + \frac{\pi}{4} \frac{(R_c - \alpha)^4}{R_0^2} \frac{dR_0}{d\alpha} \qquad \text{(I-C.24)}$$

The total surface area of the drop is given by

$$A_3 = 2\pi H R_c - 4(H-R_c)\alpha + 4\pi R_o^2 - 2\pi R_o\left(R_o - \sqrt{R_o^2 - (R_c-\alpha)^2}\right) \qquad \text{(I-C.25)}$$

and therefore differentiation with respect to α and for the case

$$R_c^2 \ll R_o^2 \qquad \text{(I-C.26)}$$

gives

$$\frac{dA_3}{d\alpha} = -4(H-R_c) + 8\pi R_o \frac{dR_o}{d\alpha} + 2\pi(R_c-\alpha) \qquad \text{(I-C.27)}$$

This can be combined with equations (I-C.24) and (I-C.26) and with the condition that at the onset of necking $\alpha = 0$ to give

$$\frac{dA_3}{d\alpha} = -4(H-R_c) + 2\pi R_c + 8(H-R_c)\frac{R_c}{R_o} \qquad \text{(I-C.28)}$$

For draining by necking to be possible $dA_3/d\alpha$ must be negative and therefore

$$R_c^2 - \left(H + \frac{\pi+2}{4}R_o\right)R_c + \tfrac{1}{2}HR_o > 0 \qquad \text{(I-C.29)}$$

The only solution of this equation which is acceptable is given by

$$R_c < \tfrac{1}{2}\left(H + \frac{\pi+2}{4}R_o\right) - \sqrt{\tfrac{1}{4}\left(H+\frac{\pi+2}{4}R_o\right)^2 - \tfrac{1}{2}HR_o} = R_{c,crit} \qquad \text{(I-C.30)}$$

As a first approximation it is assumed that

$$R_o = \tfrac{1}{2} D_{Ell} \qquad \text{(I-C.31)}$$

and the calculated values of the critical R_c are given in Table 19 of Appendix III.

I-D ESTIMATION OF THE RATE OF NECKING AT THE ONSET OF NECKING

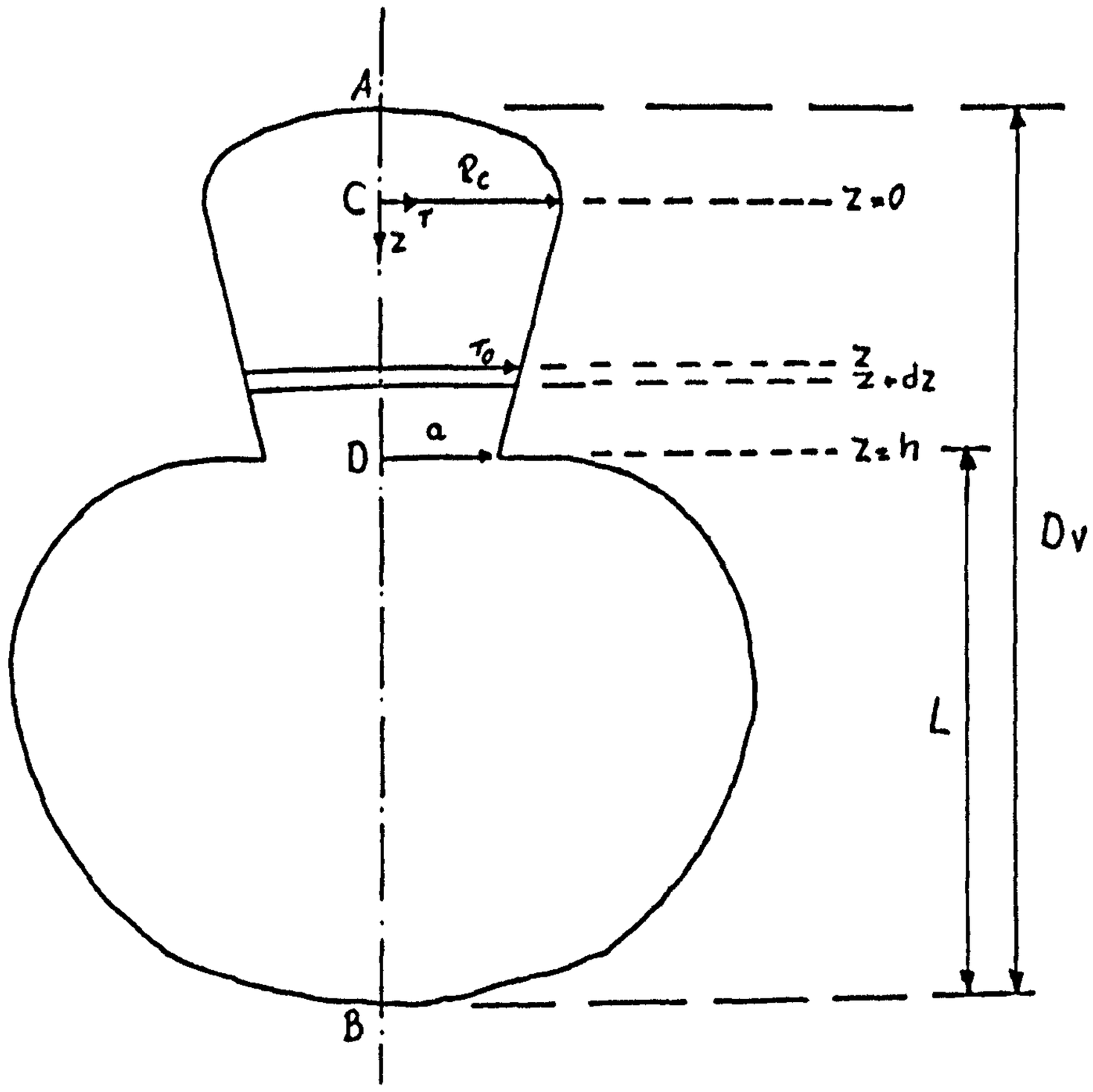

An estimate of the rate of necking at the onset of necking is obtained from a momentum balance. The column was approximated to a frustum of a cone plus a nondraining hemispheroidal cap. da/dt, the rate of necking was assumed to be constant. The volume of the frustum between Z=O and z is given by :

$$V_z = \pi R_c^2 z - \pi \frac{z^2}{h} R_c (R_c - a) + \frac{\pi}{3} \frac{z^3}{h^2} (R_c - a)^2 \qquad \text{(I-D.1)}$$

The change in the volume V_z during necking is then

$$\frac{dV_z}{dt} = \pi \frac{z^2}{h} \left[R_c - \frac{2}{3} \frac{z}{h} (R_c - a) \right] \left(\frac{da}{dt} \right) \qquad \text{(I-D.2)}$$

A parabolic velocity profile is assumed at position z

$$V_z = V_{0z}\left(1 - \frac{r^2}{r_0^2}\right) \qquad \text{(I-D.3)}$$

where r_o is the radius at z and

$$r_0 = R_c - \frac{z}{h}(R_c - a) \qquad \text{(I-D.4)}$$

The net flow of liquid out of the frustum is given by

$$\frac{dV_z}{dt} = -\int_0^{r_0} V_z\, 2\pi r\, dr \qquad \text{(I-D.5)}$$

which when combined with equation (I-D.3) gives

$$\frac{dV_z}{dt} = -\frac{\pi}{2} V_{0z} r_0^2 \qquad \text{(I-D.6)}$$

From equations (I-D.2) and (I-D.6)

$$V_{0z} = -2\frac{z^2}{r_0^2 h}\left[R_c - \frac{2}{3}\frac{z}{h}(R_c - a)\right]\left(\frac{da}{dt}\right) \qquad \text{(I-D.7)}$$

A momentum balance for an element in the fluid is considered

$$\begin{pmatrix}\text{Rate of change of}\\ \text{momentum in the element}\end{pmatrix} = \begin{array}{l}\text{rate of momentum into the element}\\ - \text{ rate of momentum out of the element}\\ + \text{ net pressure force}\\ + \text{ net body force}\end{array} \qquad \text{(I-D.8)}$$

The momentum of the fluid in the element is given by

$$M = \int_0^{r_0} \rho_d V_z\, dz \cdot 2\pi r\, dr \qquad \text{(I-D.9)}$$

which when combined with equation (I-D.7) gives

$$M = -\pi \rho_d \frac{z^2}{h}\left[R_c - \frac{2}{3}\frac{z}{h}(R_c - a)\right]\left(\frac{da}{dt}\right) dz \qquad \text{(I-D.10)}$$

Differentiation with respect to time gives for the

rate of change of momentum of the fluid in the element

$$\frac{dM}{dt} = -\pi \rho_d \frac{z^2}{h}\left\{\left[R_c - \frac{2}{3}\frac{z}{h}(R_c - a)\right]\frac{d^2a}{dt^2} + \frac{2}{3}\frac{z}{h}\left(\frac{da}{dt}\right)^2\right\} dz \quad \text{(I-D.11)}$$

Constant rate of necking is assumed so that

$$\frac{d^2a}{dt^2} = 0 \quad \text{(I-D.12)}$$

Thus equation (I-D.11) becomes

$$\frac{dM}{dt} = -\frac{2}{3}\pi \rho_d \frac{z^3}{h^2}\left(\frac{da}{dt}\right)^2 dz \quad \text{(I-D.13)}$$

The rate of net flow of momentum into the element is given by

$$\phi = \int_0^{r_0} \rho_d V_z^2 \, 2\pi r \, dr$$

$$\phi = \frac{4}{3}\pi \rho_d \frac{z^4}{h^2} \frac{\left[R_c - \frac{2}{3}\frac{z}{h}(R_c - a)\right]^2}{\left[R_c - \frac{z}{h}(R_c - a)\right]}\left(\frac{da}{dt}\right)^2 \quad \text{(I-D.14)}$$

The net pressure force acting on the z faces of the element is given by

$$F_{p_{z,1}} = -\frac{\partial}{\partial z}\left\{P\,\pi\left[R_c - \frac{z}{h}(R_c - a)\right]^2\right\} dz \quad \text{(I-D.15)}$$

and the net pressure force acting in the z direction on the angled faces of the element is

$$F_{p_{z,2}} = -\left(P + \frac{\partial P}{\partial z}\frac{dz}{2}\right)\cdot 2\pi\left[R_c - \frac{z}{h}(R_c - a)\right]\frac{R_c - a}{\sqrt{h^2 + (R_c - a)^2}}\, dz \quad \text{(I-D.16)}$$

The body force on the element is

$$F_g = \rho_d g \pi\left[R_c - \frac{z}{h}(R_c - a)\right]^2 dz \quad \text{(I-D.17)}$$

The momentum balance of equation (I-D.8) becomes then

$$-\frac{2}{3}\pi\rho_d\frac{z^3}{h^2}\left(\frac{da}{dt}\right)^2dz = -\frac{\partial\phi}{\partial z}dz - \frac{\partial}{\partial z}\left\{P\pi\left[R_c-\frac{z}{h}(R_c-a)^2\right\}dz\right.$$

$$-\left(P+\frac{\partial P}{\partial z}\frac{dz}{2}\right)2\pi\left[R_c-\frac{z}{h}(R_c-a)\right]\frac{R_c-a}{\sqrt{h^2+(R_c-a)^2}} \quad \text{(I-D.18)}$$

$$+\rho_d g\pi\left[R_c-\frac{z}{h}(R_c-a)\right]^2dz$$

At the onset of necking $a=R_c$ and the momentum balance becomes

$$-\frac{2}{3}\pi\rho_d\frac{z^3}{h^2}\left(\frac{da}{dt}\right)^2dz = -\frac{\partial\phi}{\partial z}dz - \pi R_c^2\frac{\partial P}{\partial z}dz + \pi\rho_d g R_c^2 dz \quad \text{(I-D.19)}$$

If this equation is integrated with respect to z between the limits z=0 and z=h

$$-\frac{\pi}{6}\rho_d h^2\left(\frac{da}{dt}\right)^2 = -\left|\phi\right|_{z=0}^{z=h} - \pi R_c^2\Delta P + \pi\rho_d g h R_c^2 \quad \text{(I-D.20)}$$

From equation (I-D.14)

$$\left|\phi\right|_{z=0}^{z=h} = \frac{4}{3}\pi\rho_d h^2\left(\frac{da}{dt}\right)^2 \quad \text{(I-D.21)}$$

Thus equation (I-D.20) becomes

$$-\frac{\pi}{6}\rho_d h^2\left(\frac{da}{dt}\right)^2 = -\frac{4}{3}\pi\rho_d h^2\left(\frac{da}{dt}\right)^2 - \pi R_c^2\Delta P + \pi\rho_d g h R_c^2 \quad \text{(I-D.22)}$$

or when solved for ΔP

$$\Delta P = -\frac{7}{6}\rho_d\frac{h^2}{R_c^2}\left(\frac{da}{dt}\right)^2 + \rho_d g h \quad \text{(I-D.23)}$$

ΔP can be calculated from a consideration of the pressure distribution around the surface of the drop. The only data available for the pressure difference in the outer fluid between the front and rear stagnation points is that given by JENSON, HORTON, and WEARING[76]

for the flow past a sphere. From their results it appears that the ratio of the pressure drop between the front and rear stagnation points to the dynamic head is constant and equal to - 1.12 for the Reynolds number range under investigation. This is used for the present system as a first approximation. Thus the pressure difference between the points A and B (Figure) is :

$$\Delta P_{AB} = +1.12 \frac{\rho_a}{2} U_\infty^2 + \rho_a g D_V \qquad \text{(I-D.24)}$$

Therefore the pressure difference between the points C and D is given by

$$-\Delta P_{CD} = -\Delta P_{AB} + 2\frac{\sigma}{C_A} - 2\frac{\sigma}{C_B} + \rho_d g R_c + \rho_d g L \qquad \text{(I-D.25)}$$

where C_A and C_B are the radii of curvature at points A and B. If this combined with equation (I-D.24)

$$\Delta P_{CD} = -1.12 \frac{\rho_a}{2} U_\infty^2 + 2\sigma\left(\frac{1}{C_A} - \frac{1}{C_B}\right) + \rho_d g h + \Delta\rho g D_V \qquad \text{(I-D.26)}$$

If equation (I-D.23) is substituted in equation (I-D.26)

$$\frac{7}{6}\rho_d \frac{(H-R_c)^2}{R_c^2}\left(\frac{da}{dt}\right)^2 = -1.12 \frac{\rho_a}{2} U_\infty^2 + \Delta\rho g D_V + 2\sigma\left(\frac{1}{C_A} - \frac{1}{C_B}\right) \qquad \text{(I-D.27)}$$

It is assumed that $C_A = 2R_c$. U_∞ can be calculated from correlations given by EDGE and GRANT[36][38] for chlorobenzene

$$U_\infty = \frac{15.8}{\sqrt{D_{a_{11}}}} - \frac{3.07}{D_{\varepsilon_{11}}} \qquad \text{(I-D.28)}$$

and for 1,2-dichloroethane

$$U_\infty = \frac{15.1}{\sqrt{D_{E,1}}} - \frac{2.95}{D_{E,1}} \qquad \text{(I-D.29)}$$

Measurements of H, R_c and C_B which were taken from cine-films were used in equation (I-D.27) to calculate da/dt. The results are presented in Table 20 of Appendix III.

APPENDIX II

GRAPHS OF RESULTS

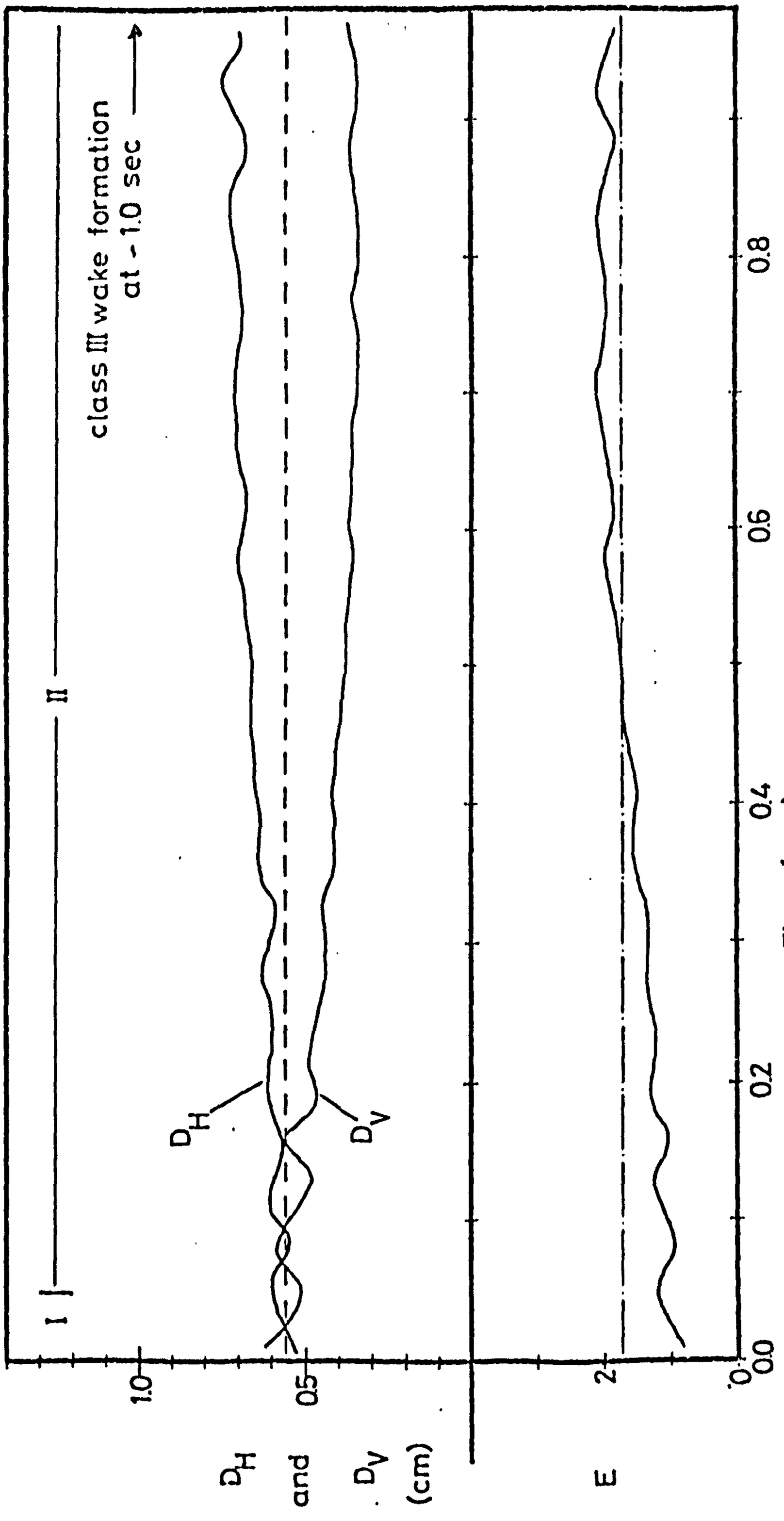

Fig.1 Variation of D_H, D_V, and E with time for nonbreaking chlorobenzene drop falling from rest in water. —— $D_{E,I}$ =0.560 cm, —·—terminal E_{mean}, roman numbers refer to wake classes

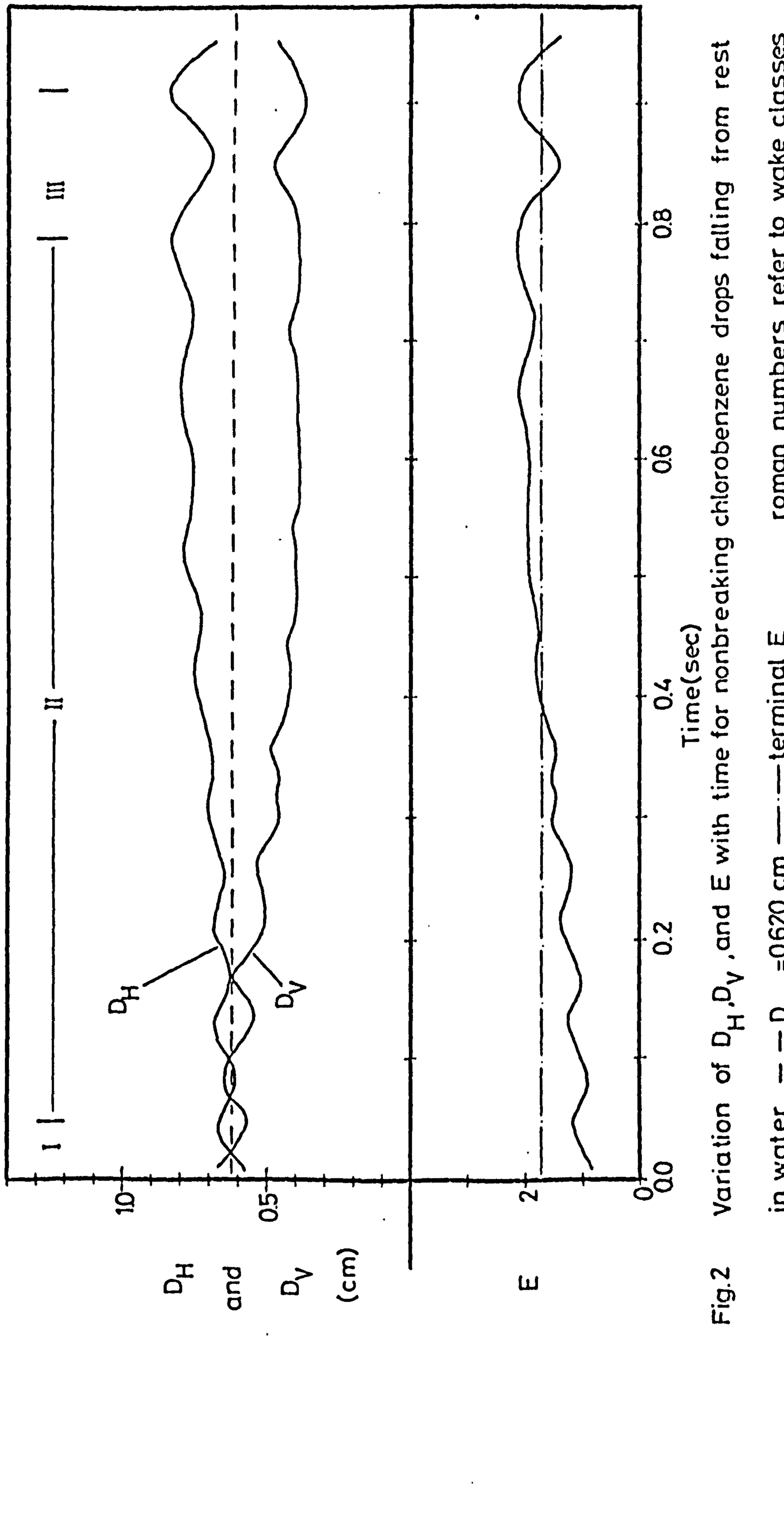

Fig.2 Variation of D_H, D_V, and E with time for nonbreaking chlorobenzene drops falling from rest in water. — — terminal E_{mean}, roman numbers refer to wake classes — — — $D_{E,1}$ =0.620 cm, ——— to

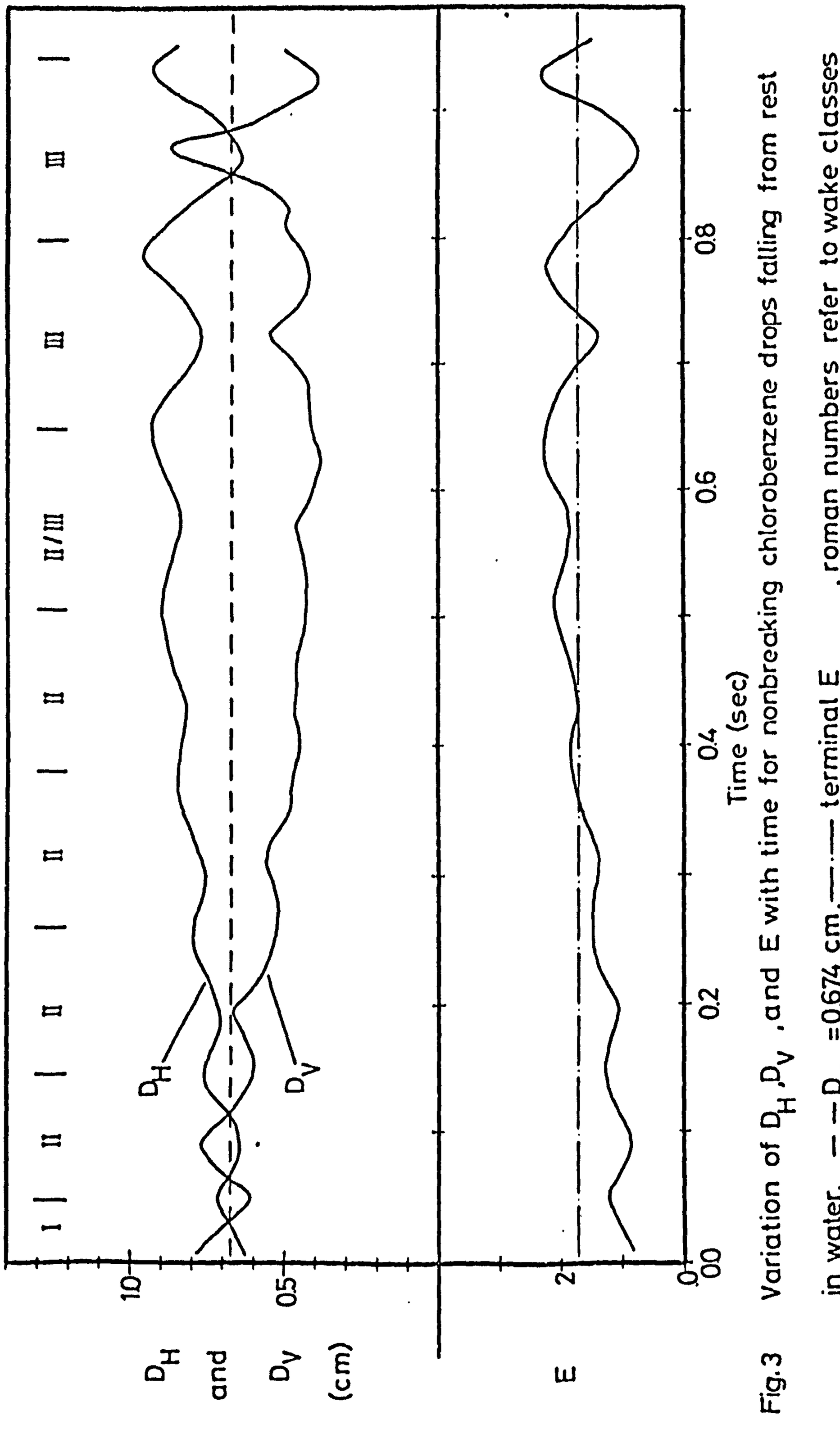

Fig.3 Variation of D_H, D_V, and E with time for nonbreaking chlorobenzene drops falling from rest in water. — — $D_{E,1}$ =0.674 cm, —·— terminal E_{mean}, roman numbers refer to wake classes

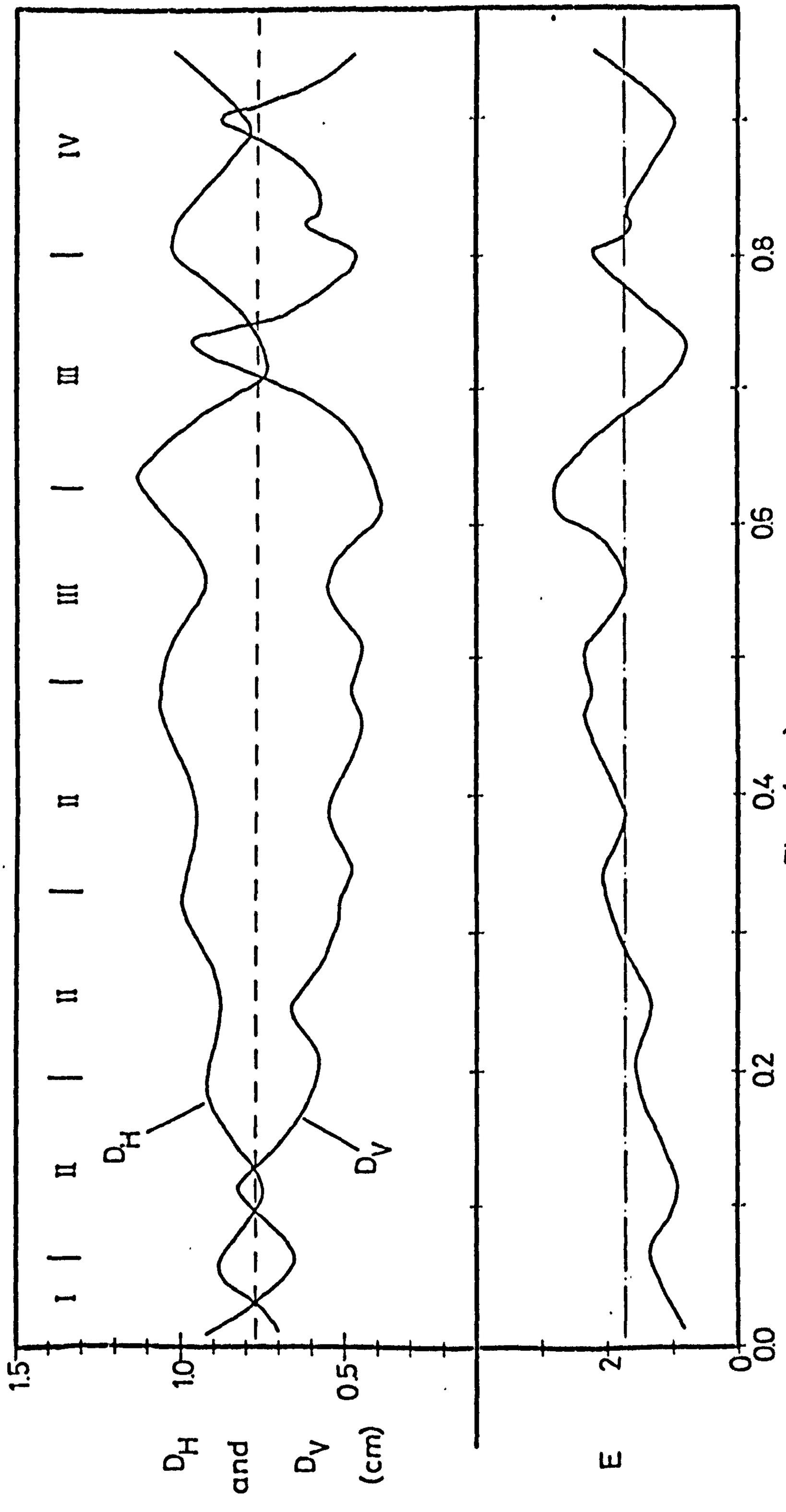

Fig.4 Variation of D_H, D_V, and E with time for nonbreaking chlorobenzene drops falling from rest in water. —— D_{E1} =0.769 cm, ——— terminal E_{mean}, roman numbers refer to wake classes

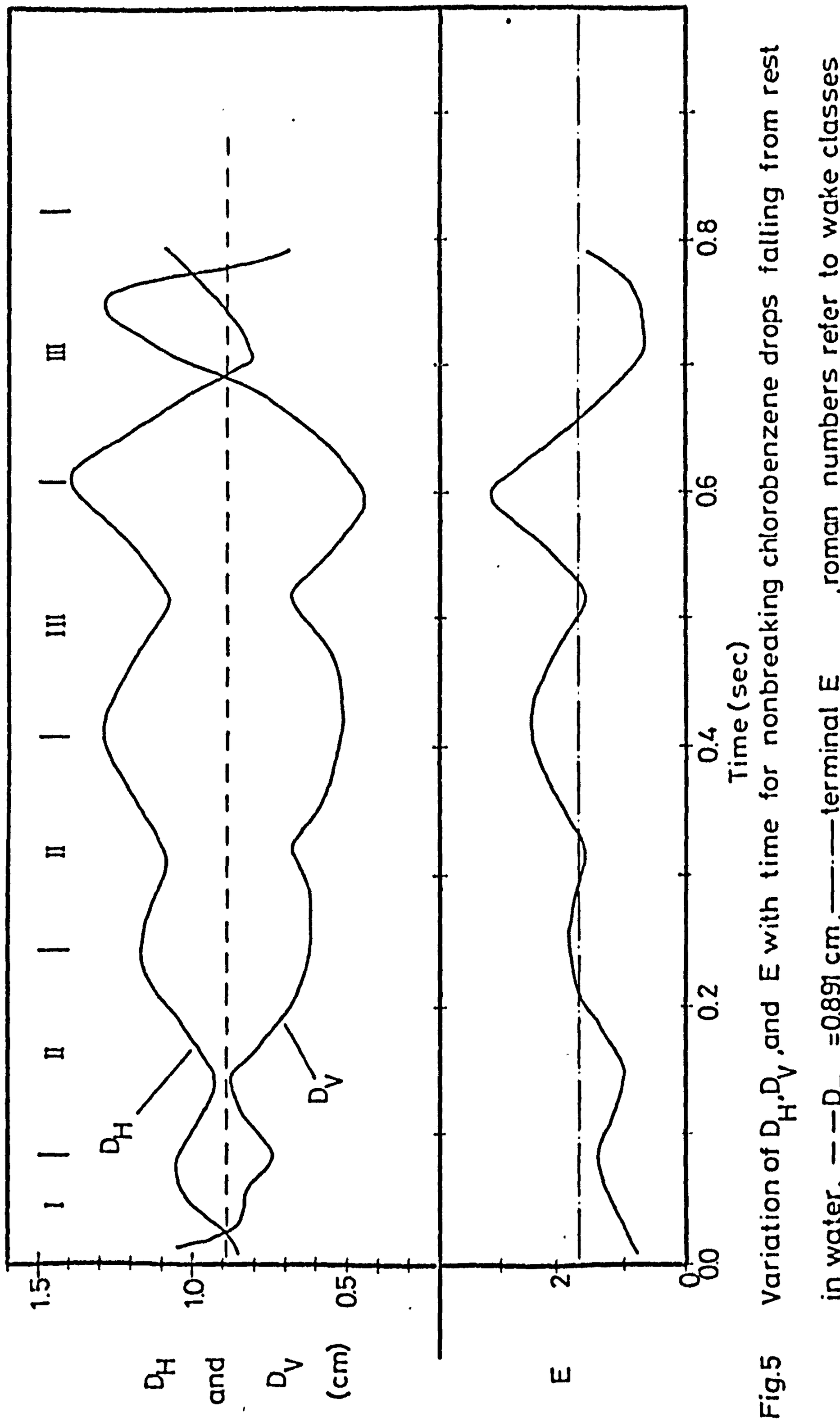

Fig.5 Variation of D_H, D_V, and E with time for nonbreaking chlorobenzene drops falling from rest in water. —— terminal E_{mean}, roman numbers refer to wake classes ——— $D_{E,1}$ =0.891 cm,

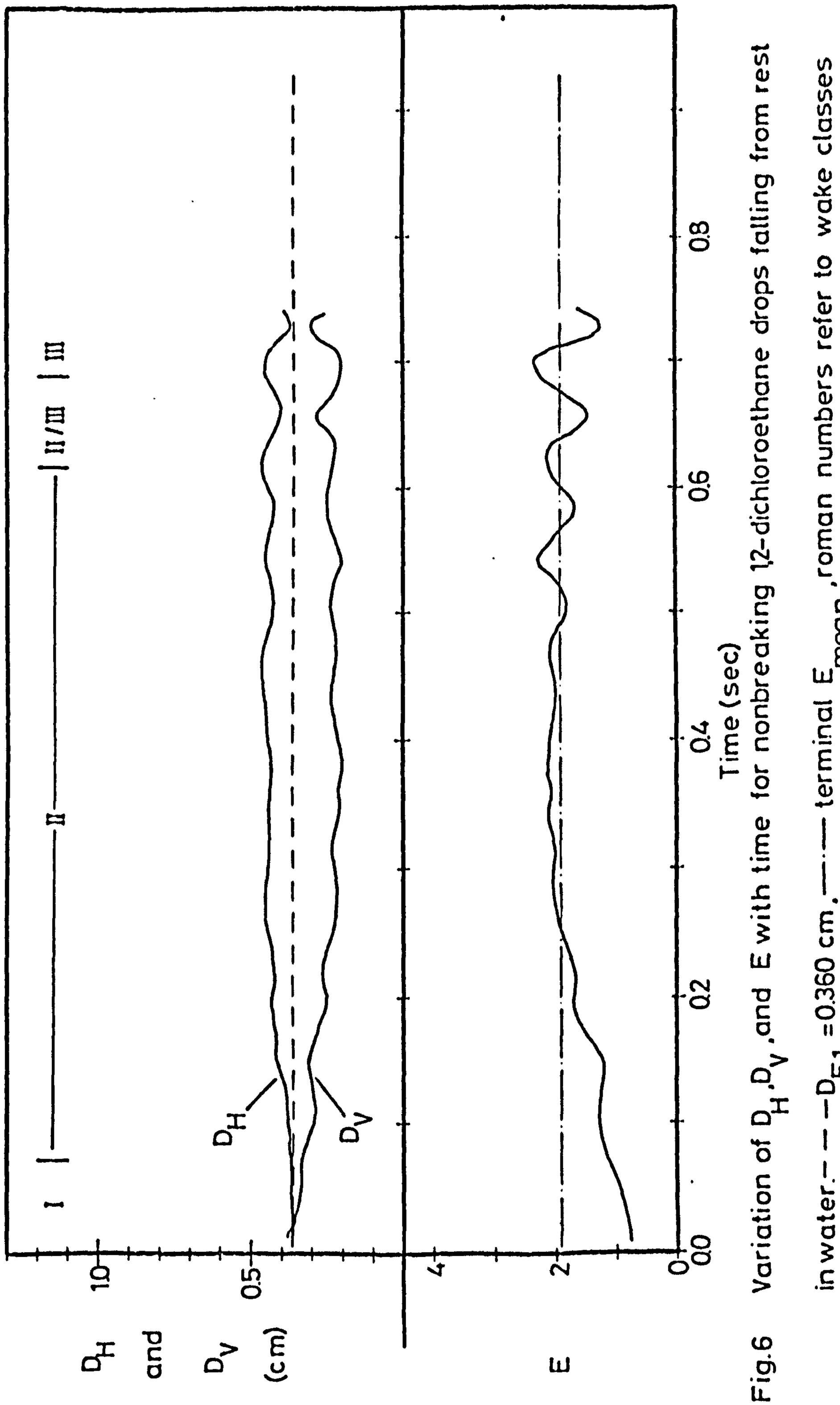

Fig.6 Variation of D_H, D_V, and E with time for nonbreaking 1,2-dichloroethane drops falling from rest in water.- - - $D_{E,1}$ =0.360 cm, —·— terminal E_{mean}, roman numbers refer to wake classes

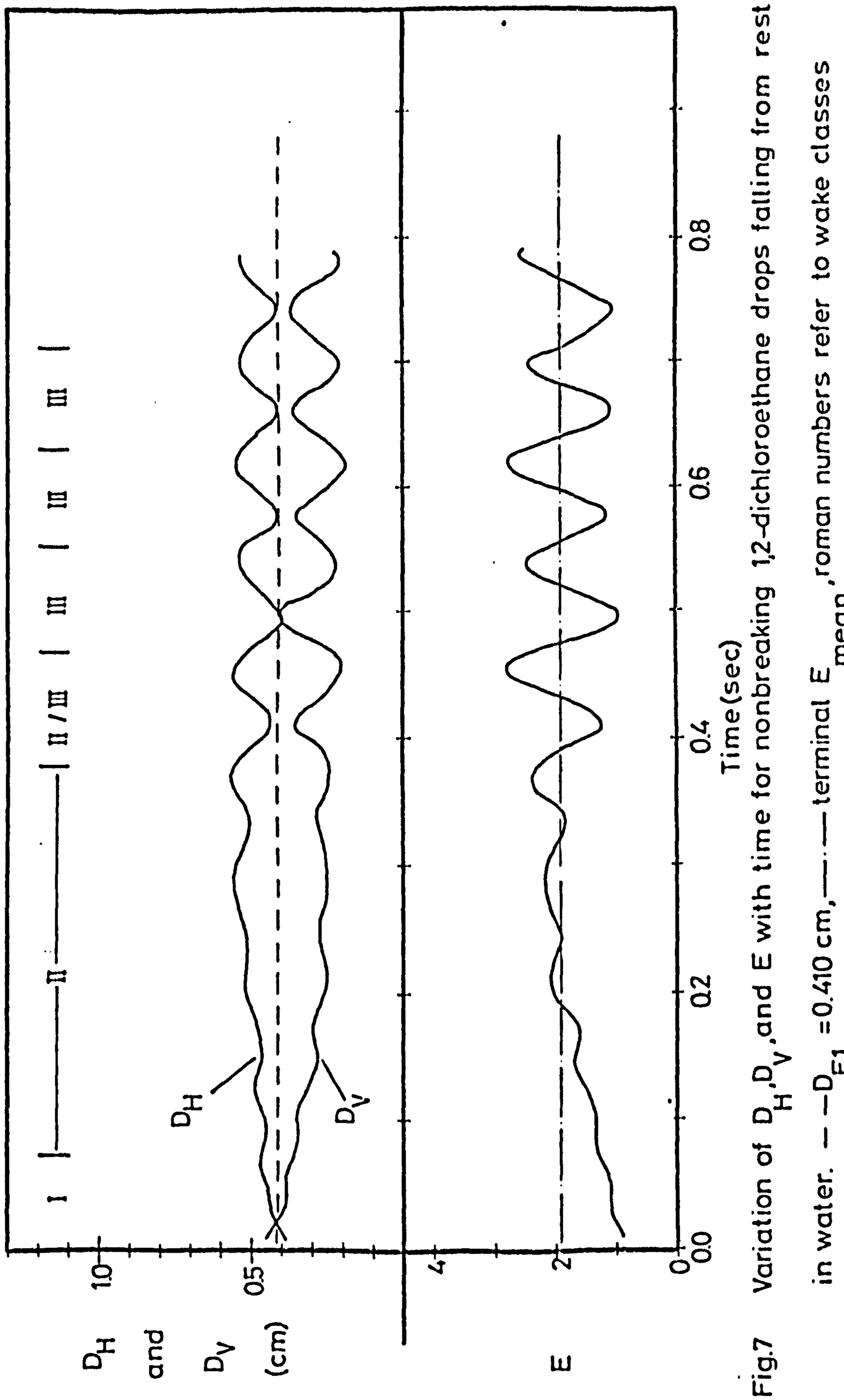

Fig.7 Variation of D_H, D_V, and E with time for nonbreaking 1,2-dichloroethane drops falling from rest in water. — — $D_{E,1}$ =0.410 cm, —·— terminal E_{mean}, roman numbers refer to wake classes

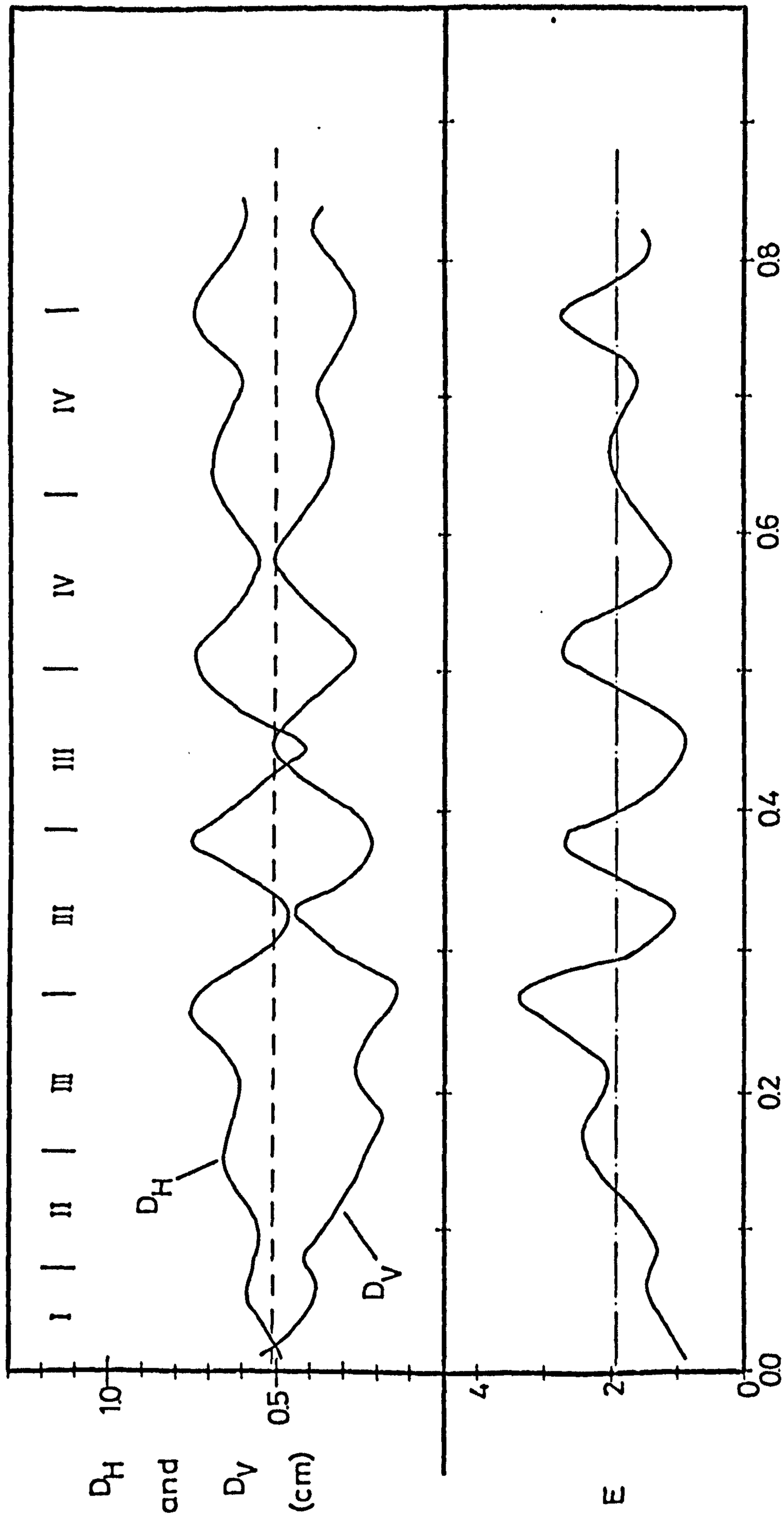

Fig.8 Variation of D_H, D_V, and E with time for nonbreaking 1,2-dichloroethane drops falling from rest in water. —— terminal E, ——— E_{mean}, roman numbers refer to wake classes —— $D_{E,1}$ =0.512 cm,

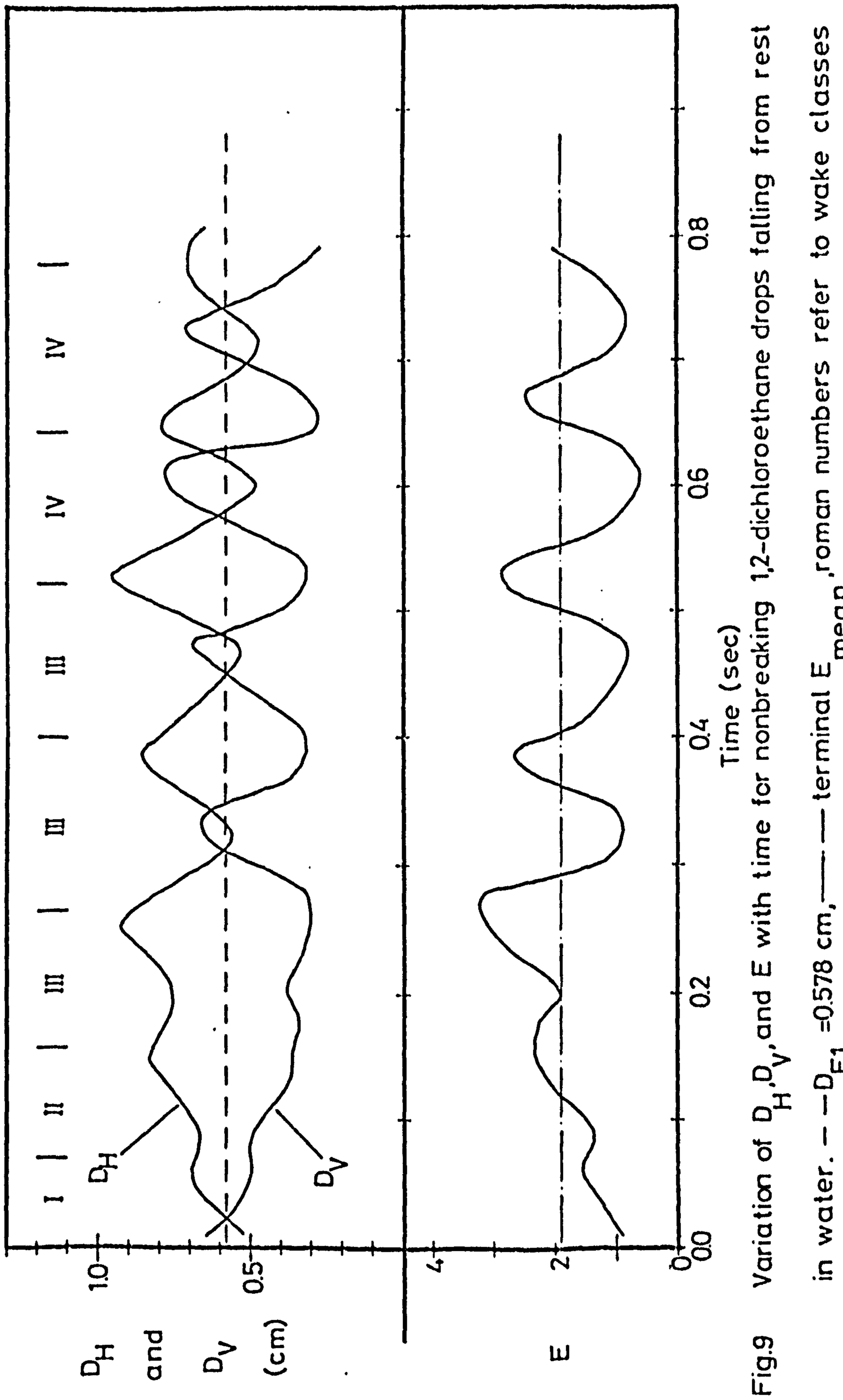

Fig.9 Variation of D_H, D_V, and E with time for nonbreaking 1,2-dichloroethane drops falling from rest in water. — — $D_{E,1}$ =0.578 cm, —— — terminal E_{mean}, roman numbers refer to wake classes

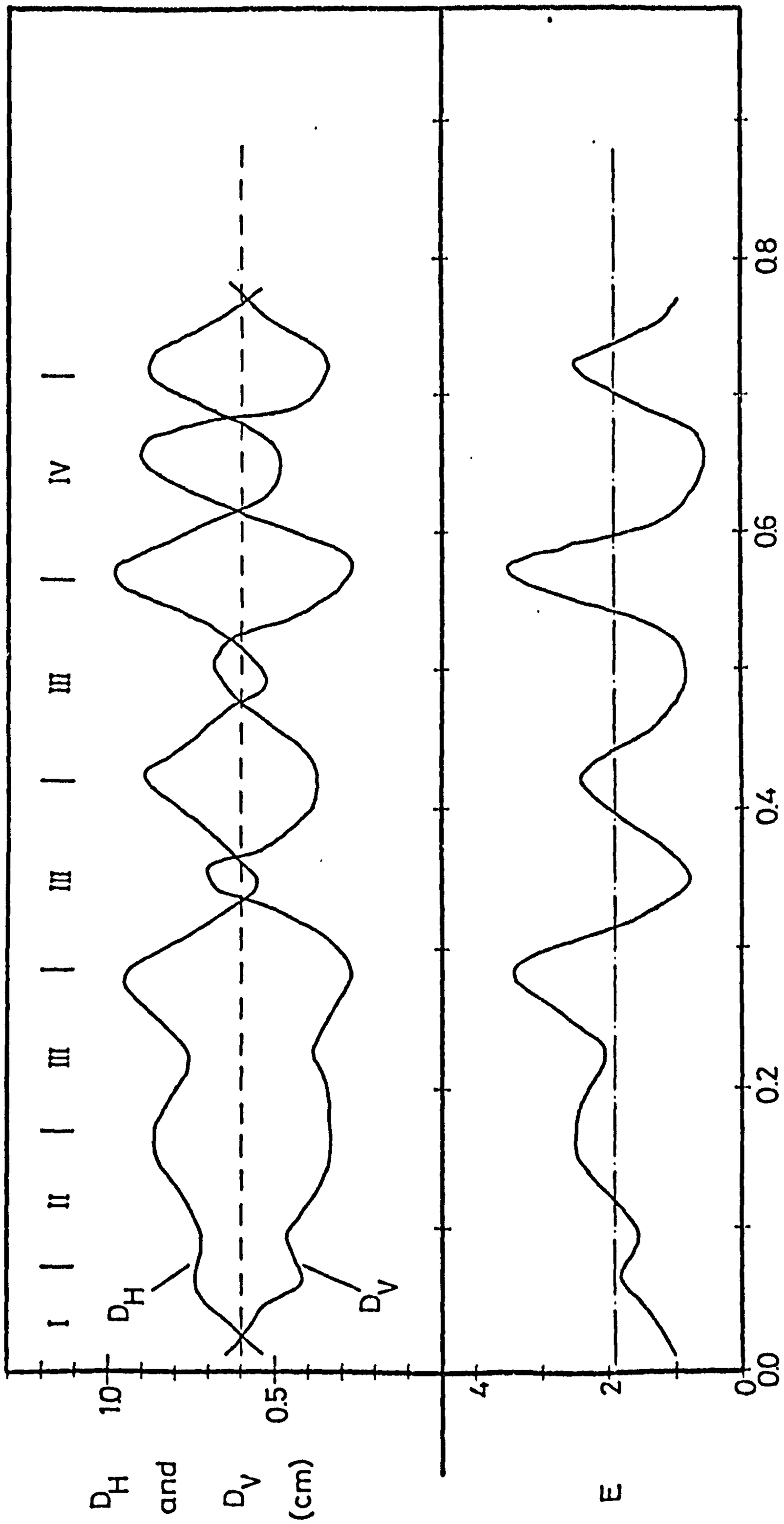

Fig.10 Variation of D_H, D_V, and E with time for nonbreaking 1,2-dichloroethane drops falling from rest in water. —— $D_{E,1}$ =0.600 cm, ——·—— terminal E_{mean}, roman numbers refer to wake classes

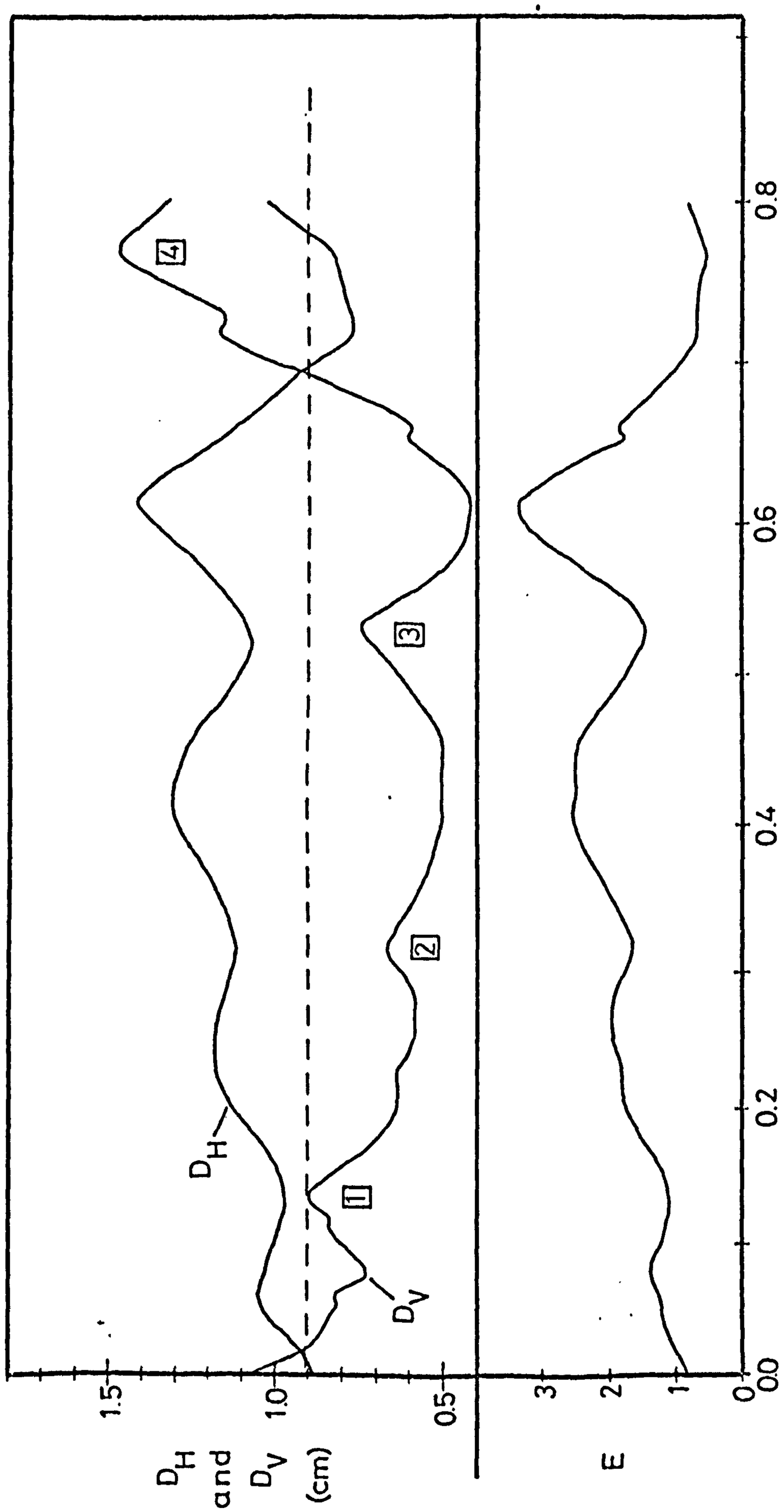

Fig.11 Variation of D_H, D_V, and E with time for the breaking chlorobenzene drops falling from rest in water. ——— D_{EJ}= 0.906 cm, □ D_V-oscillation number

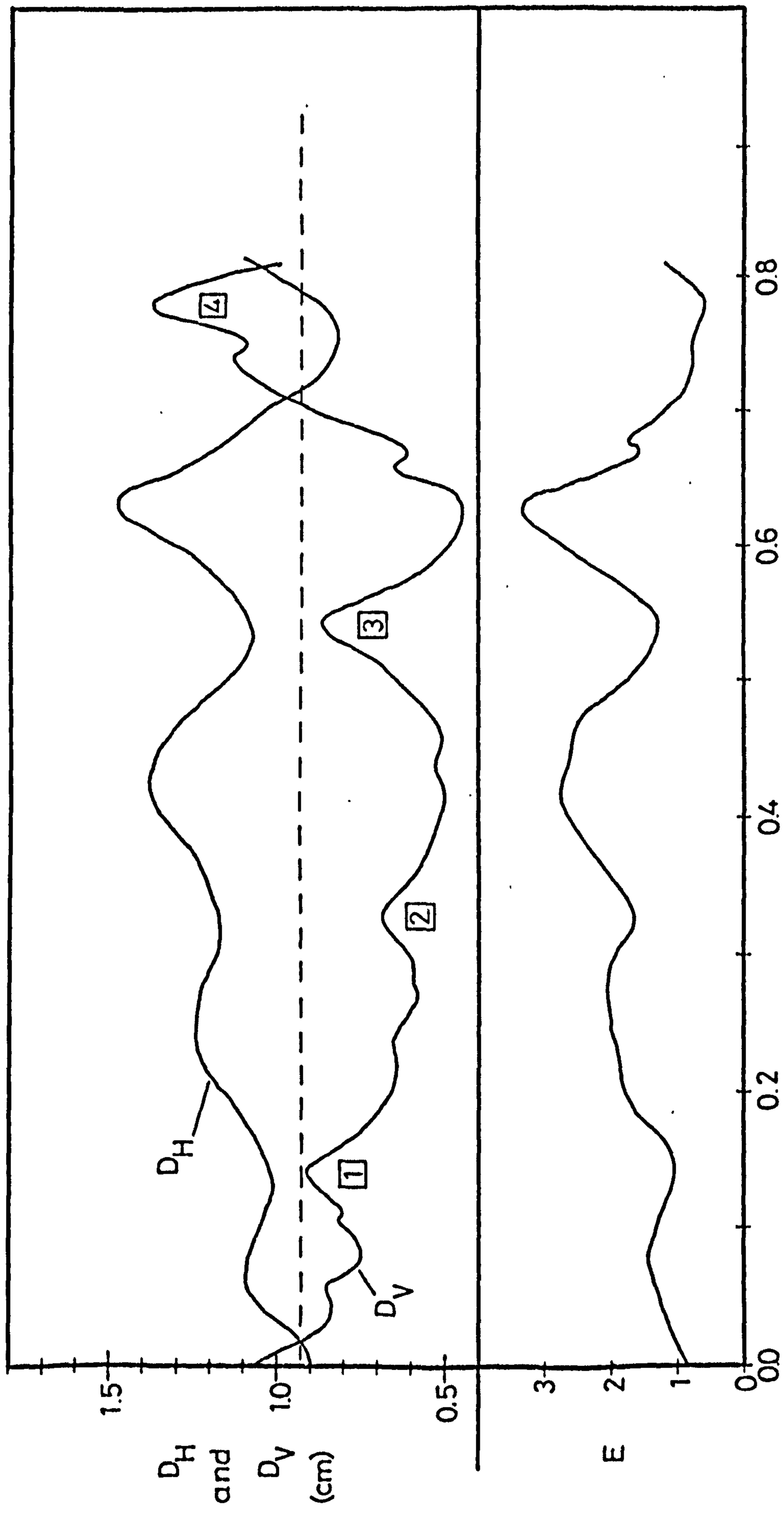

Fig.12 Variation of D_H, D_V, and E with time for bursting chlorobenzene drops falling from rest in water. ——D_{EJ}=0.932 cm, □ D_V-oscillation number

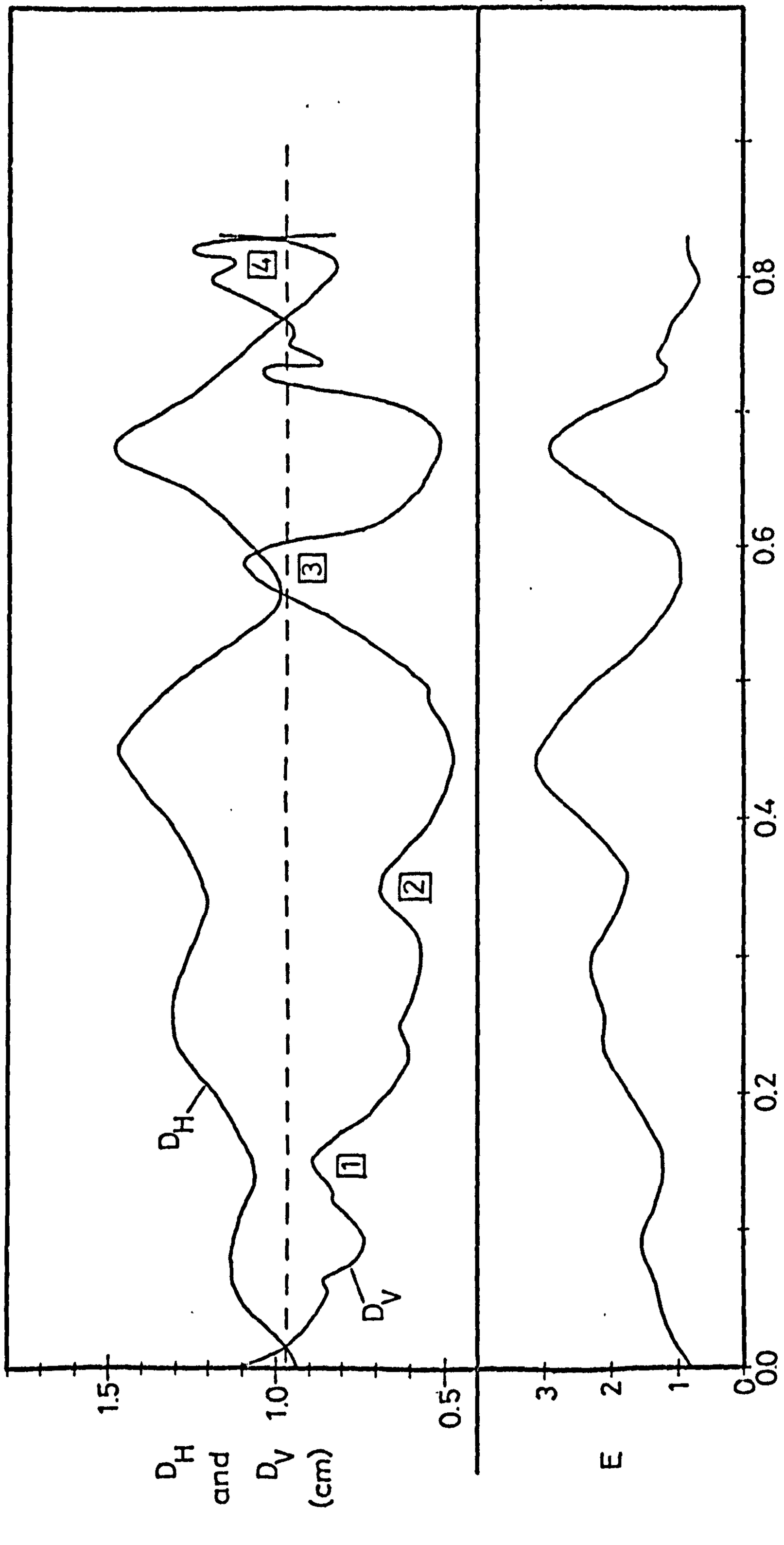

Fig.13 Variation of D_H, D_V, and E with time for breaking chlorobenzene drops in water. — — — D_{Eq}= 0.969 cm, □ D_V-oscillation number

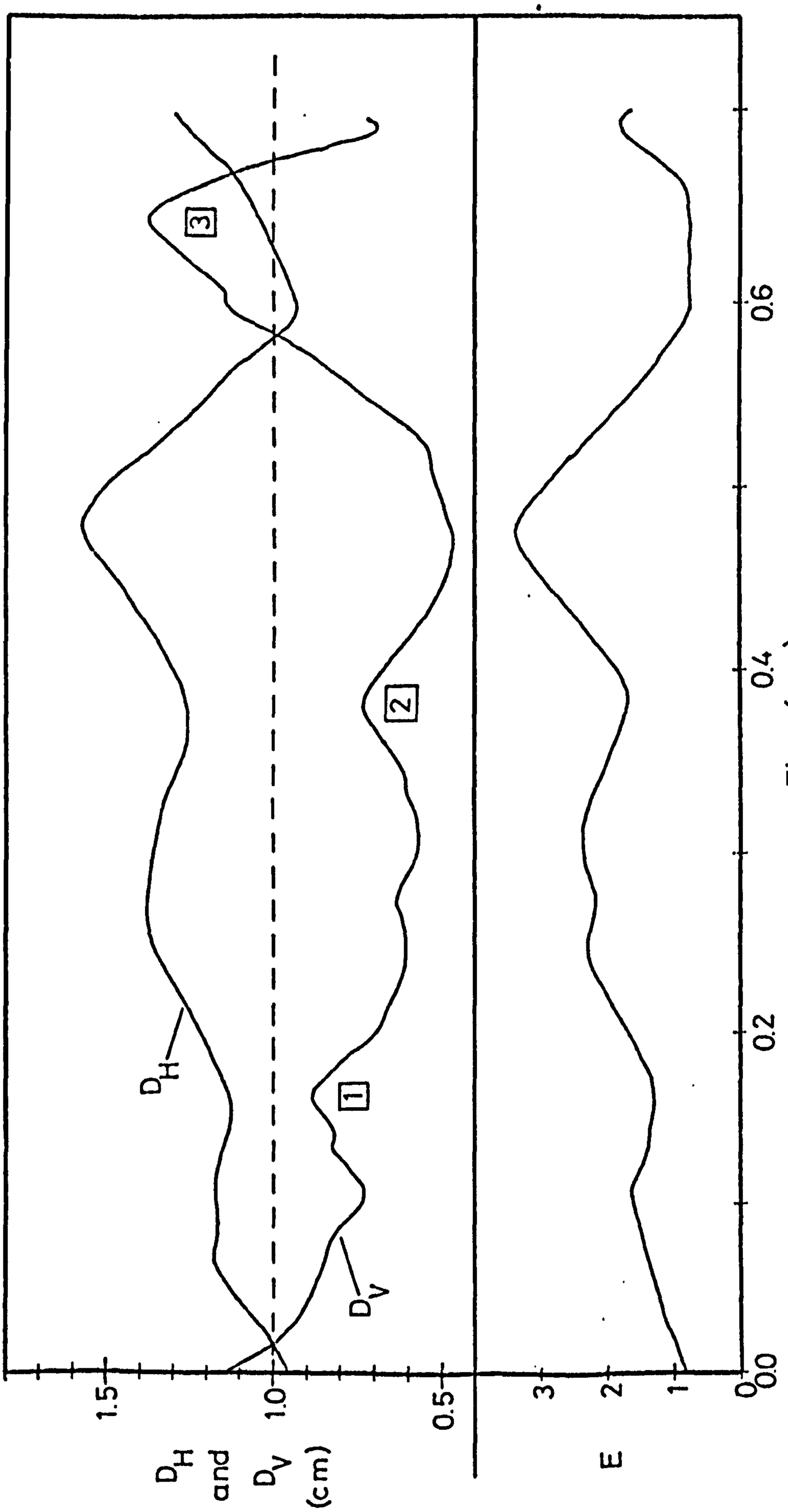

Fig.14 Variation of D_H, D_V, and E with time for breaking chlorobenzene drops falling from rest in water. — — D_{Ej}=0.998 cm. □ D_V-oscillation number

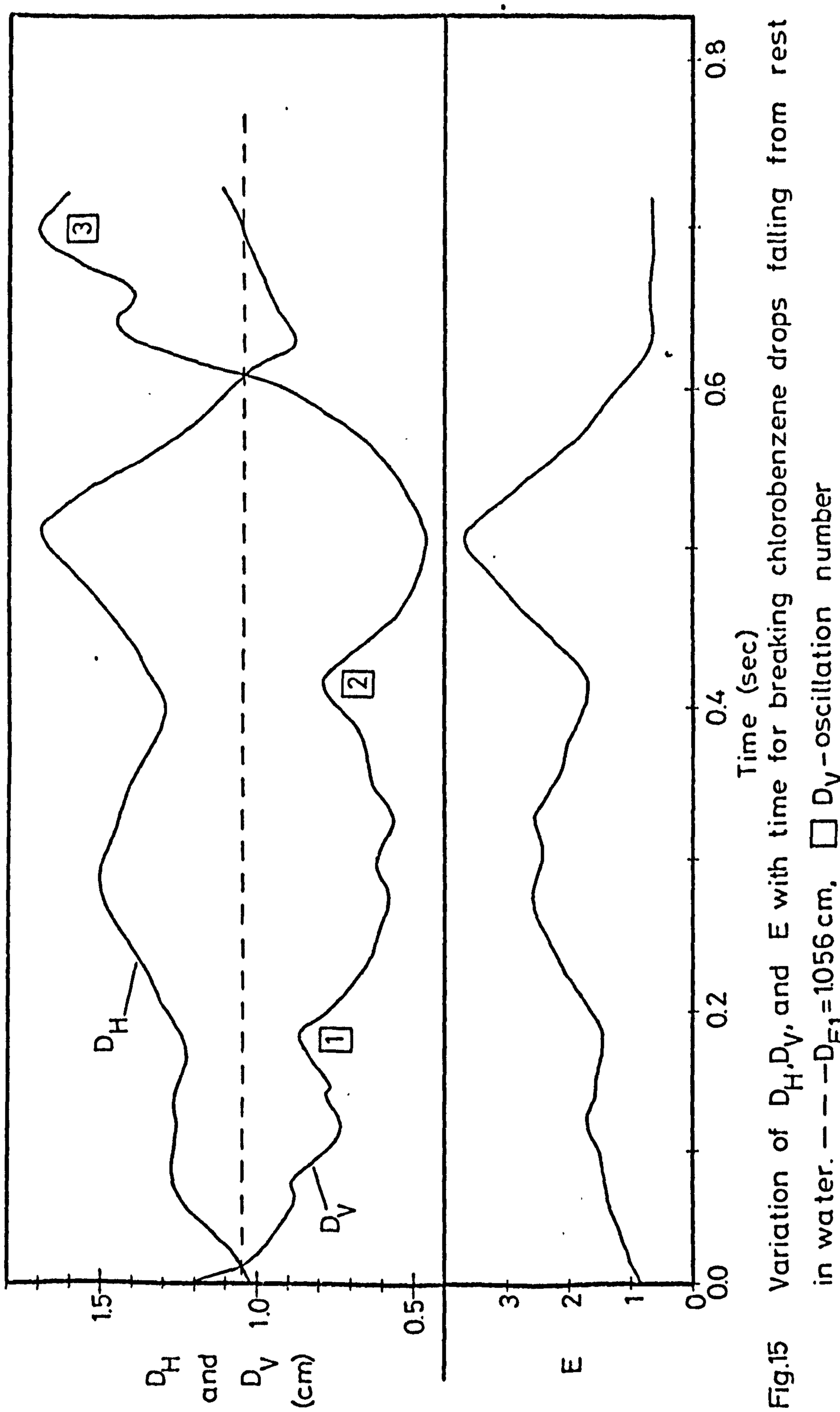

Fig.15 Variation of D_H, D_V, and E with time for breaking chlorobenzene drops in water. — — — D_{EJ} = 1.056 cm, □ D_V-oscillation number

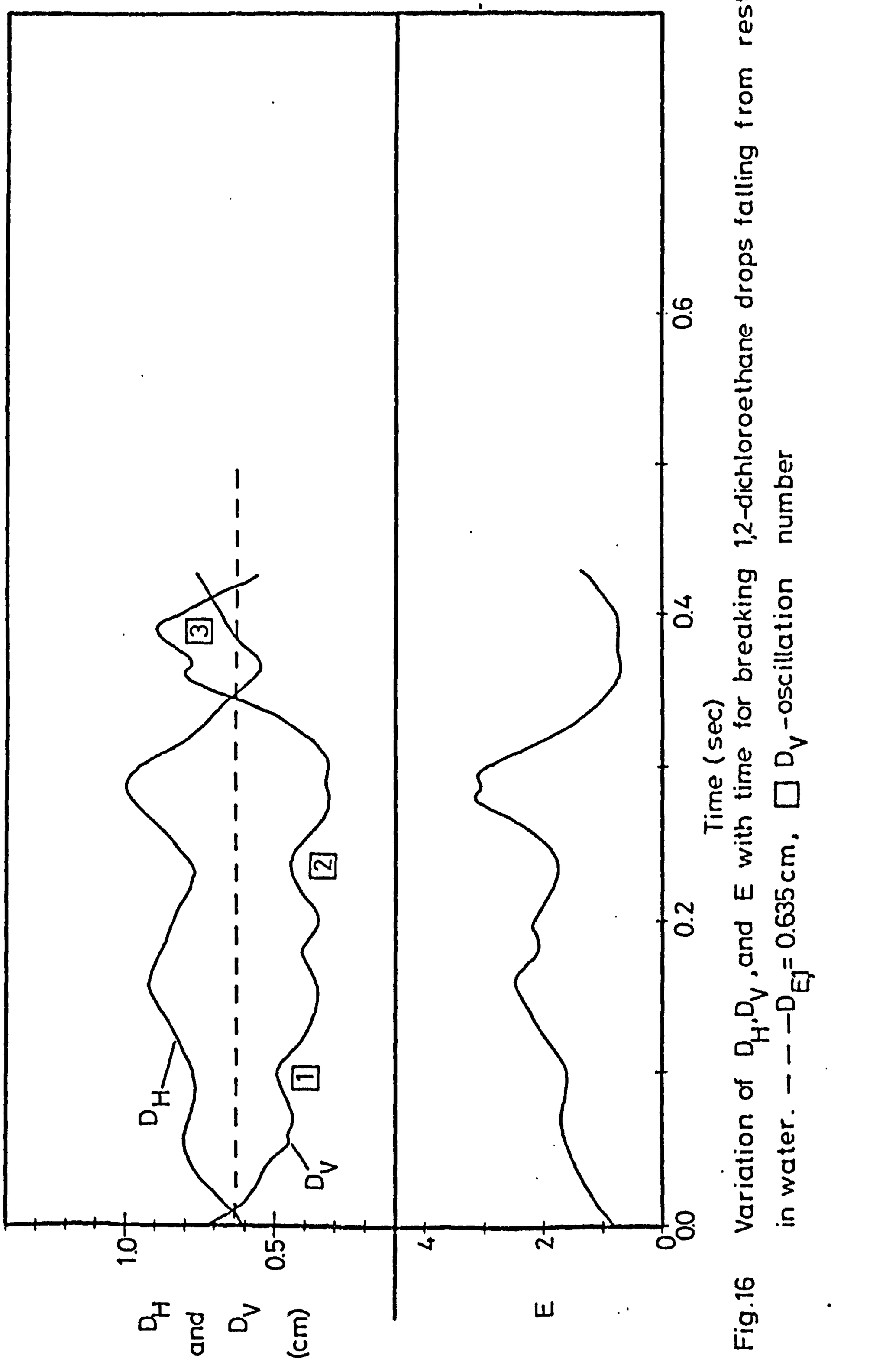

Fig.16 Variation of D_H, D_V, and E with time for breaking 1,2-dichloroethane drops falling from rest in water. ——D_{Ej}= 0.635 cm, □ D_V-oscillation number

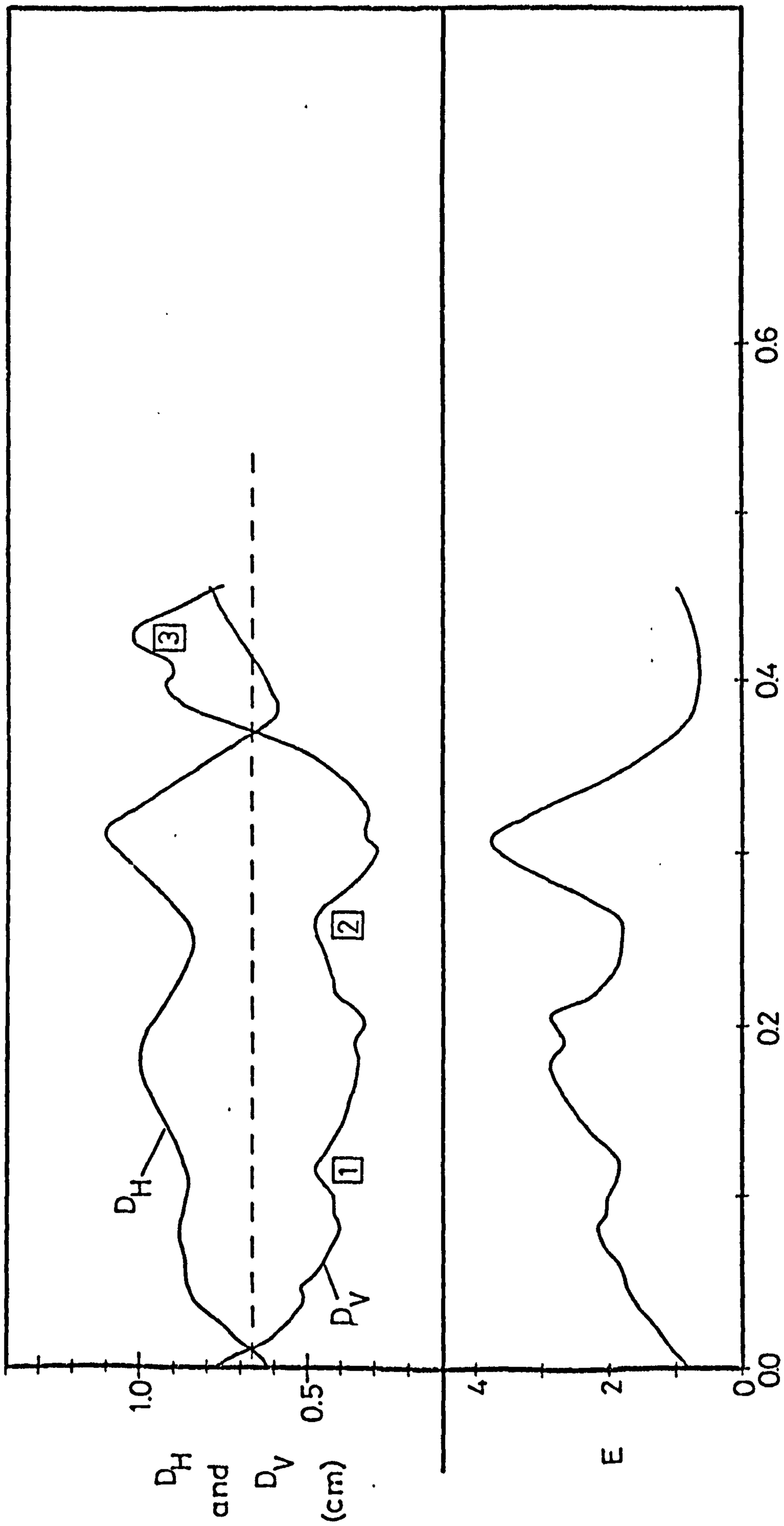

Fig.17 Variation of D_H, D_V, and E with time for breaking 1,2-dichloroethane drops falling from rest in water. — — — D_{Eq} = 0.666 cm, □ D_V - oscillation number

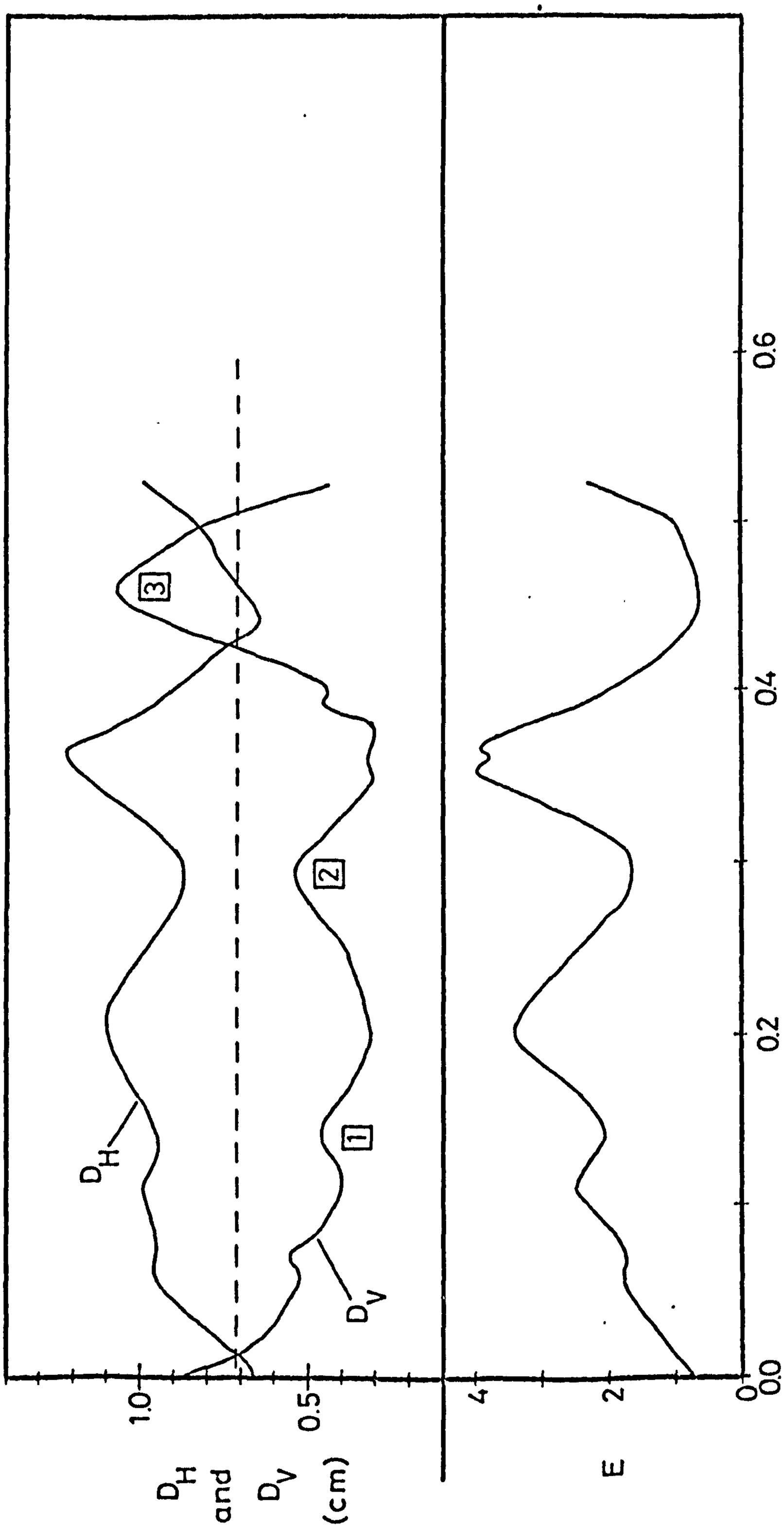

Fig.18 Variation of D_H, D_V, and E with time for breaking 1,2-dichloroethane drops falling from rest in water.— D_{EI}= 0.712 cm, □ D_V -oscillation number

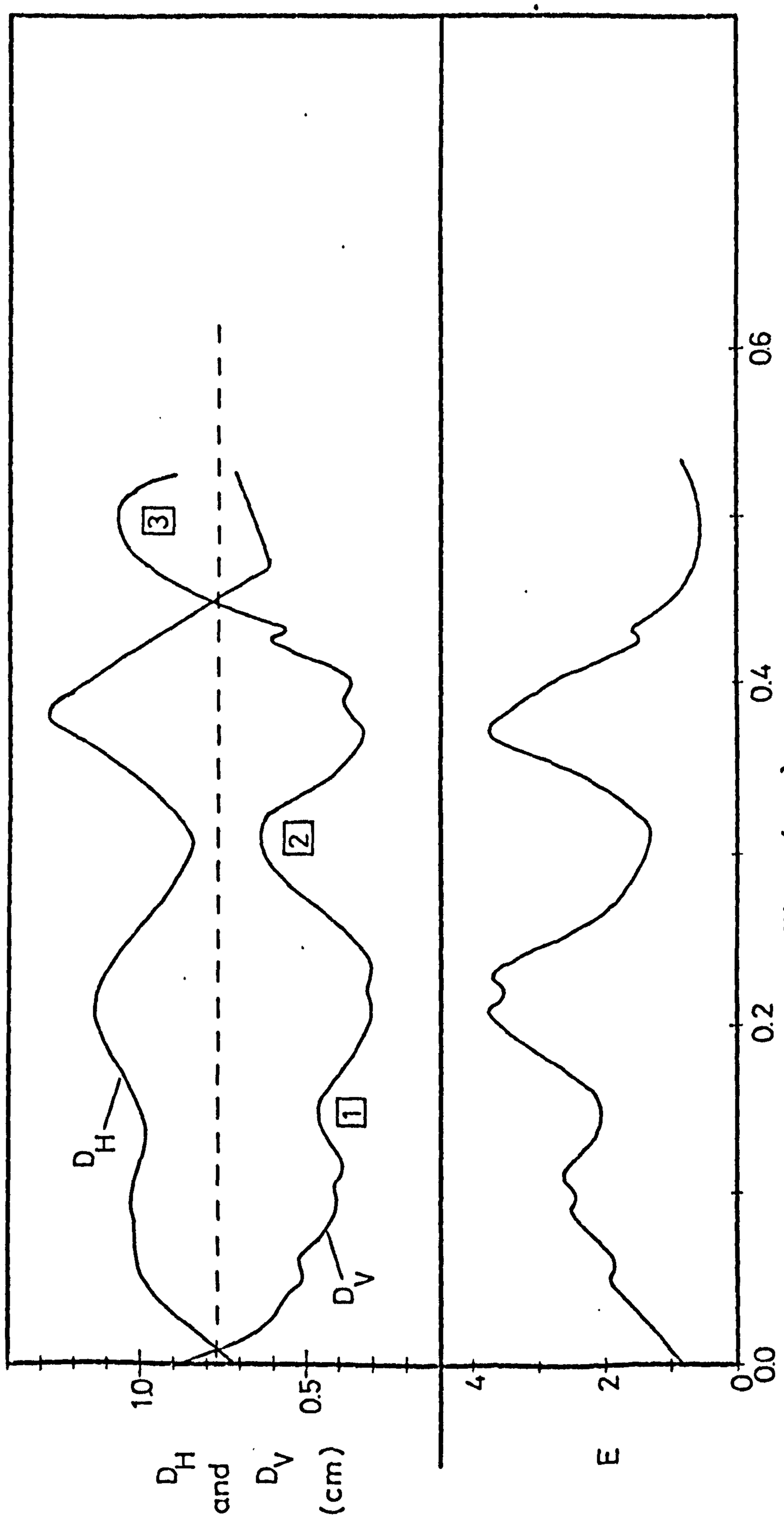

Fig.19 Variation of D_H, D_V, and E with time for breaking 1,2-dichloroethane drops falling from rest in water. — — — D_{Ej} = 0.768 cm, □ D_V-oscillation number

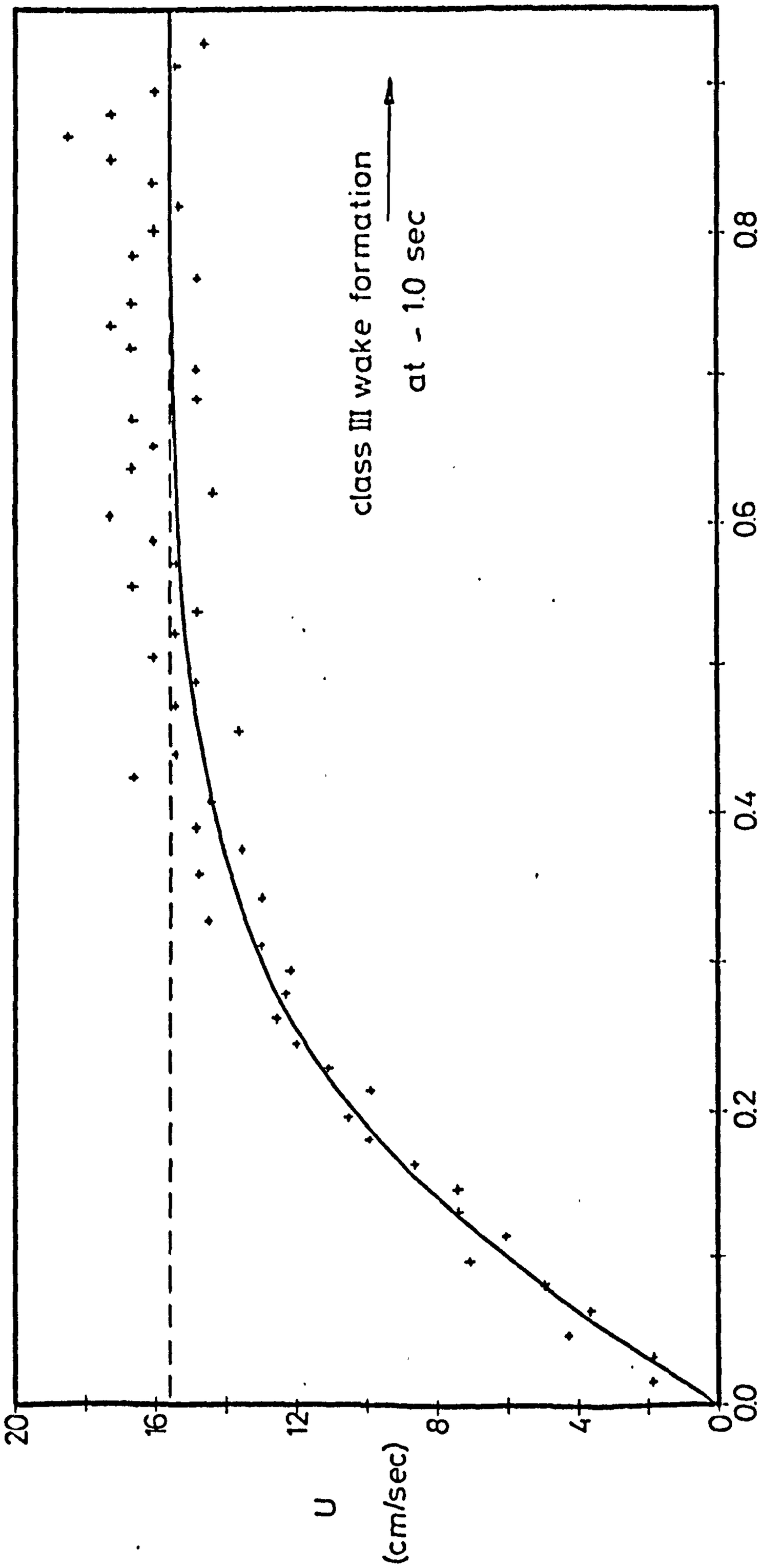

Fig.20 Variation of the velocity of fall with time for chlorobenzene drops falling from rest in water. $D_{E,1}$=0.560 cm, — — — gross terminal velocity, ——— Equation 6.2

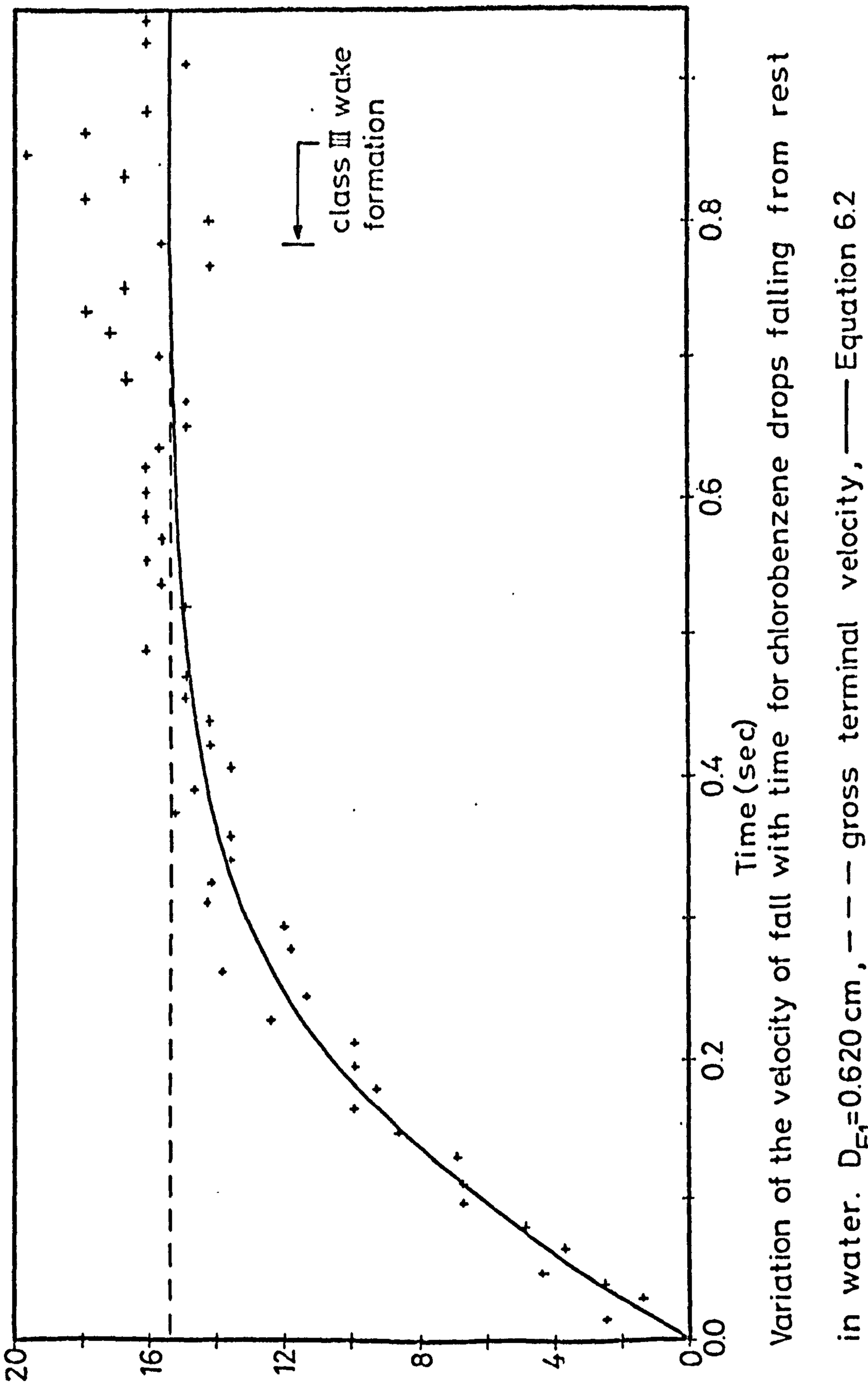

Fig.21 Variation of the velocity of fall with time for chlorobenzene drops falling from rest in water. D_{Ej}=0.620 cm, — — — gross terminal velocity, —— Equation 6.2

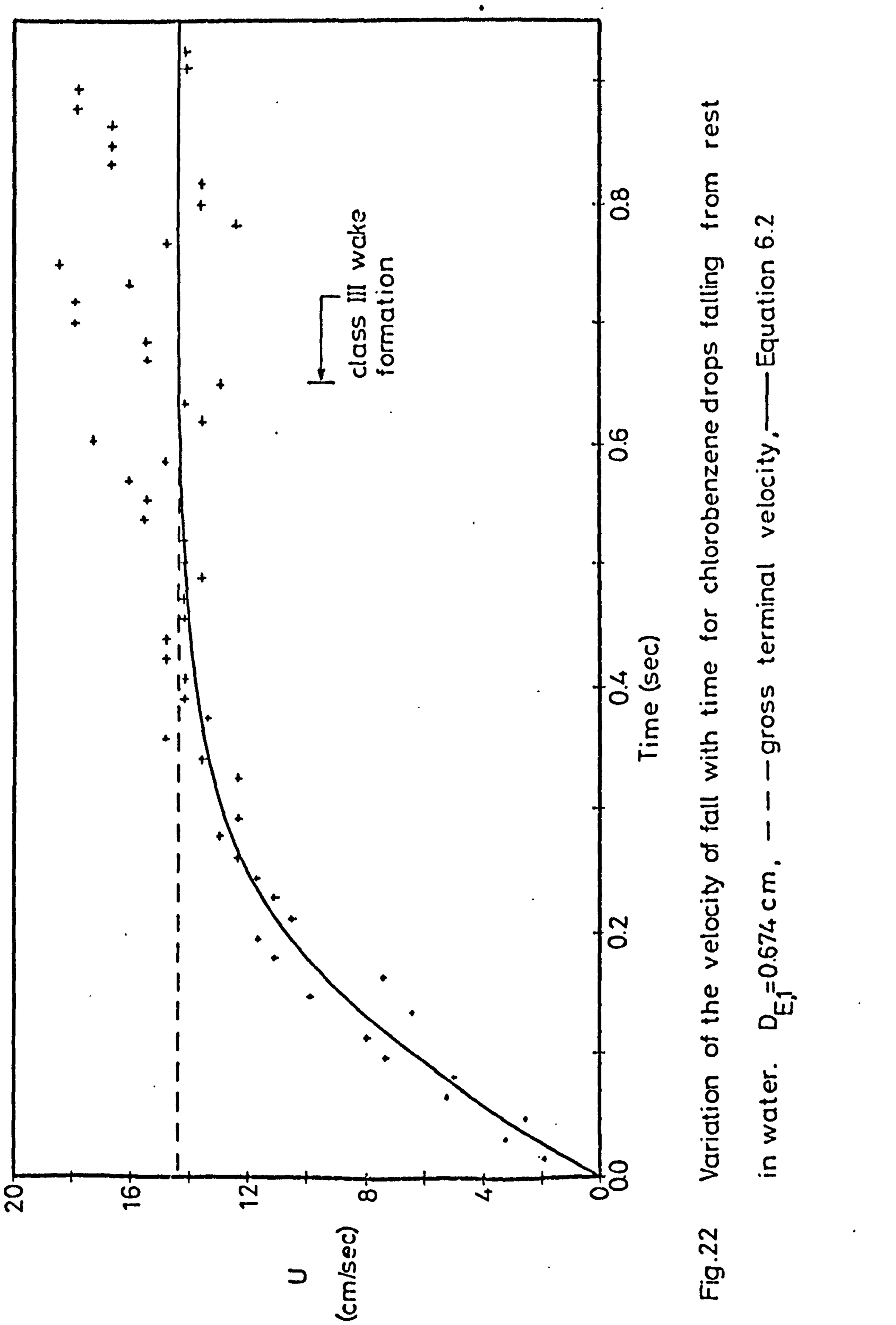

Fig.22 Variation of the velocity of fall with time for chlorobenzene drops falling in water. $D_{E,1}$=0.674 cm, — — — gross terminal velocity, —— Equation 6.2

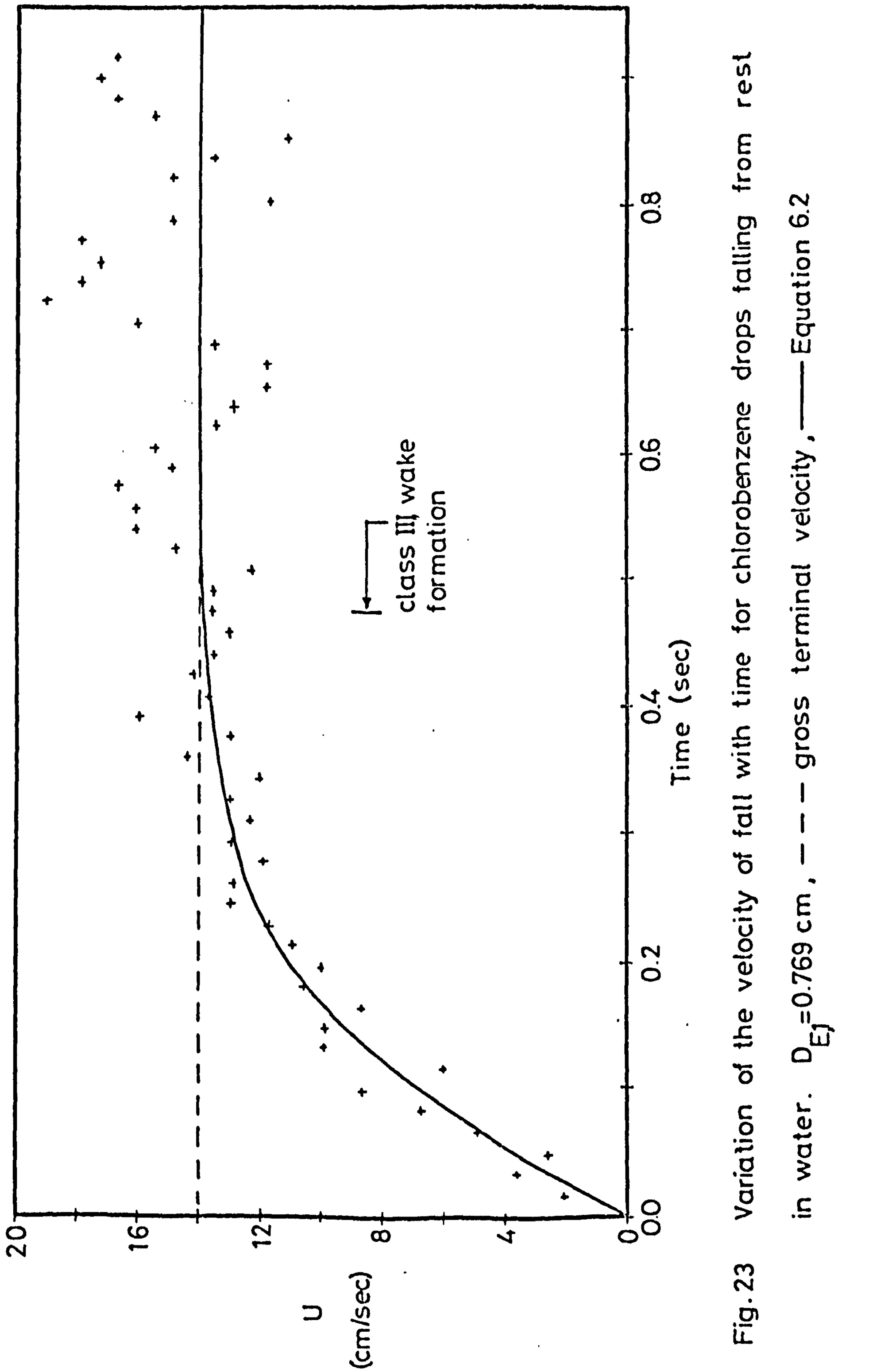

Fig. 23 Variation of the velocity of fall with time for chlorobenzene drops falling from rest in water. D_{Ej}=0.769 cm, — — — gross terminal velocity, ——— Equation 6.2

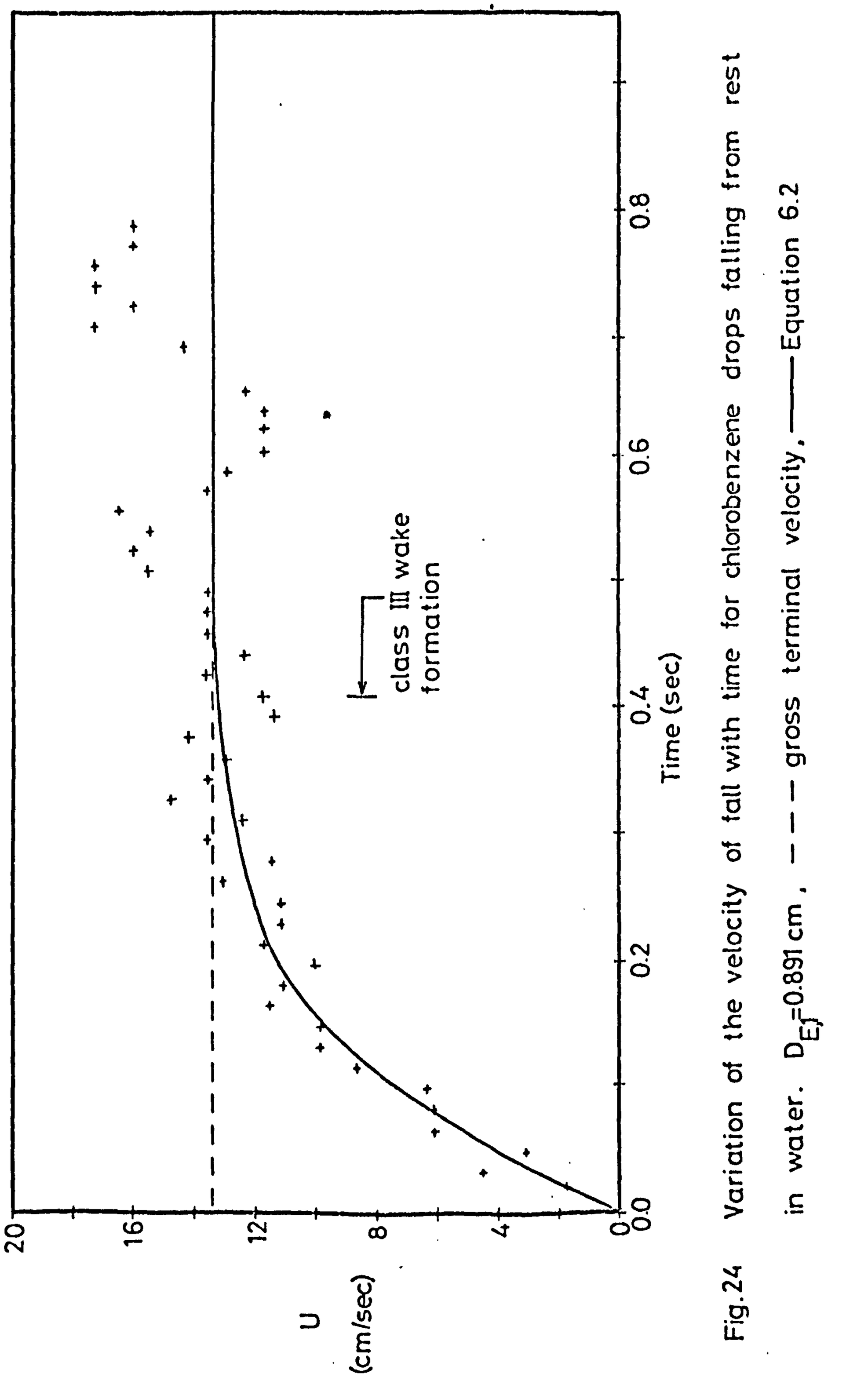

Fig.24 Variation of the velocity of fall with time for chlorobenzene drops falling from rest in water. D_{EJ}=0.891 cm, — — — gross terminal velocity, ——— Equation 6.2

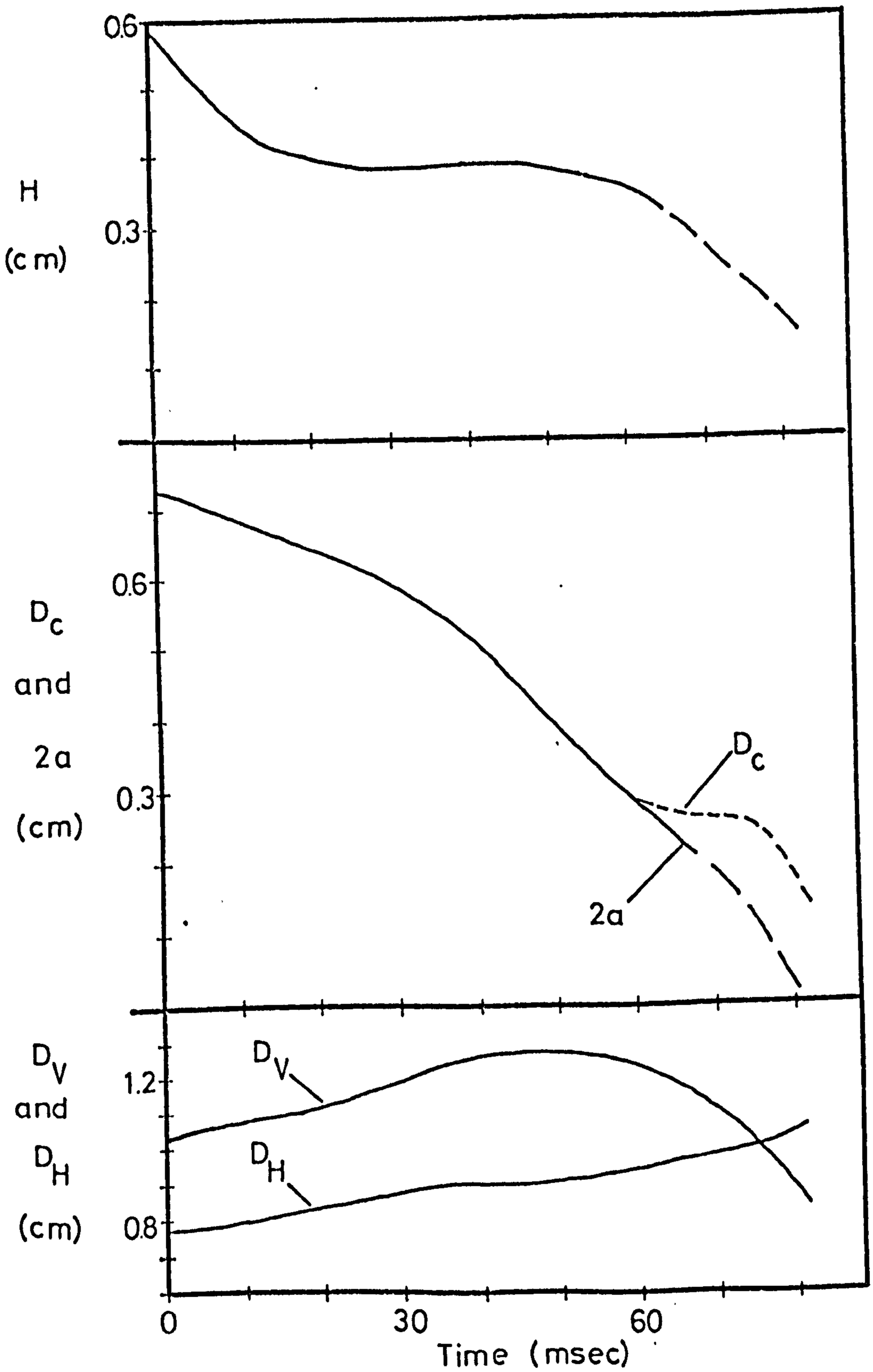

Fig.25 The dimensions of the drop during breakup

System: chlorobenzene/water, $D_{E,1}$=0.896 cm

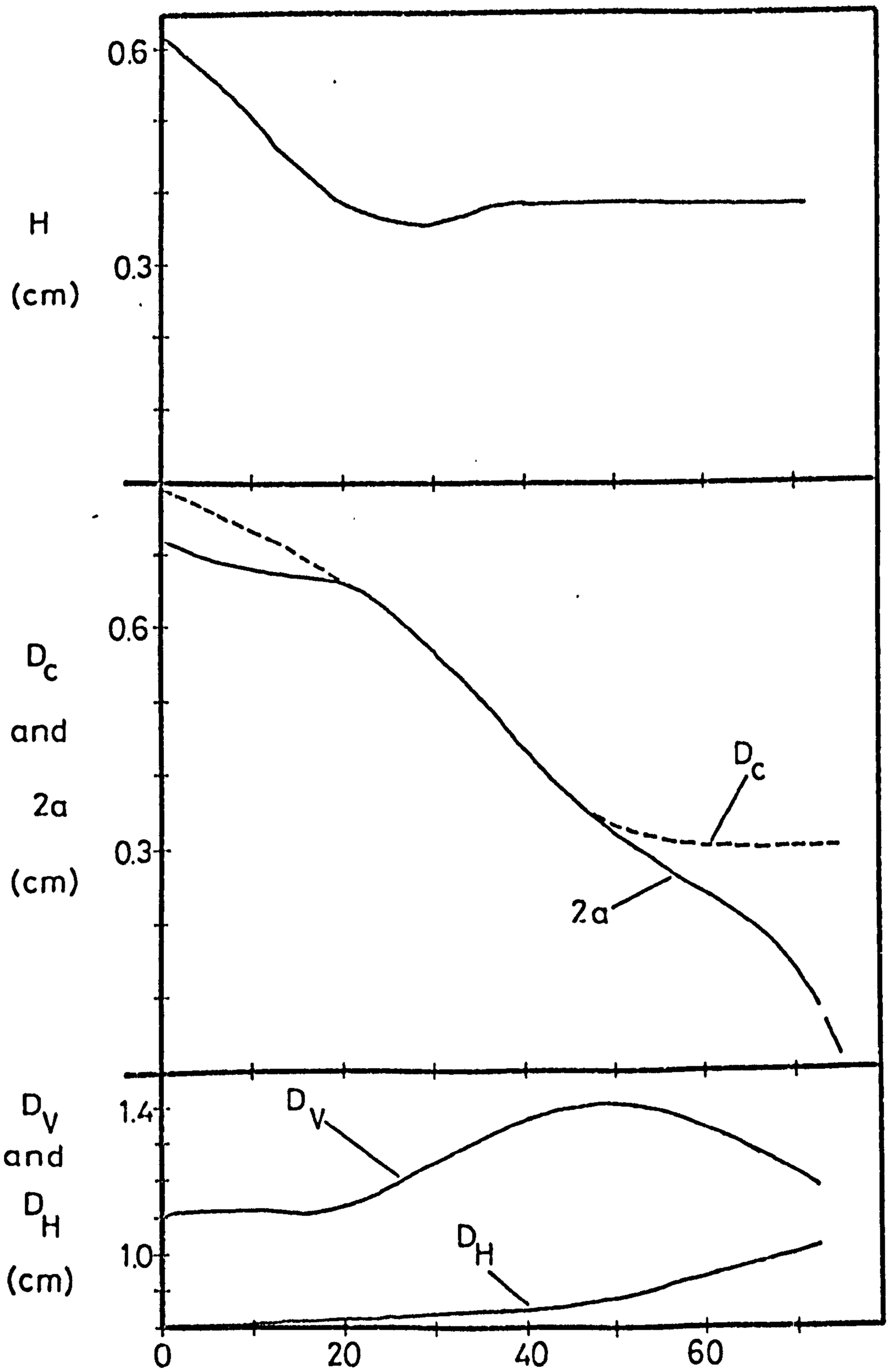

Fig. 26 The dimensions of the drop during breakup

System: chlorobenzene/water, $D_{E,1}$ = 0.906 cm

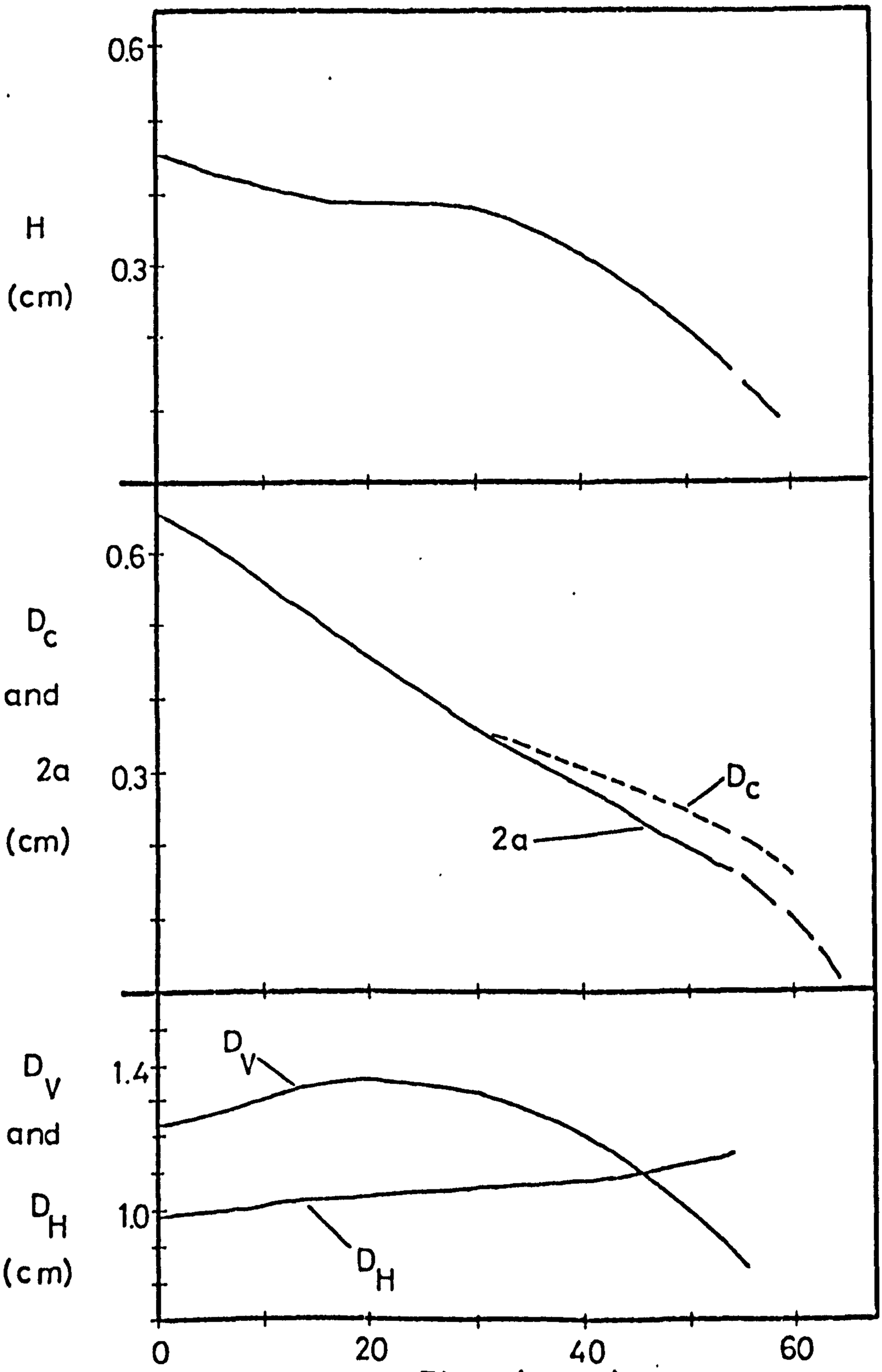

Fig.27 The dimensions of the drop during breakup

System: chlorobenzene/water, $D_{E,1}$ =0.998 cm

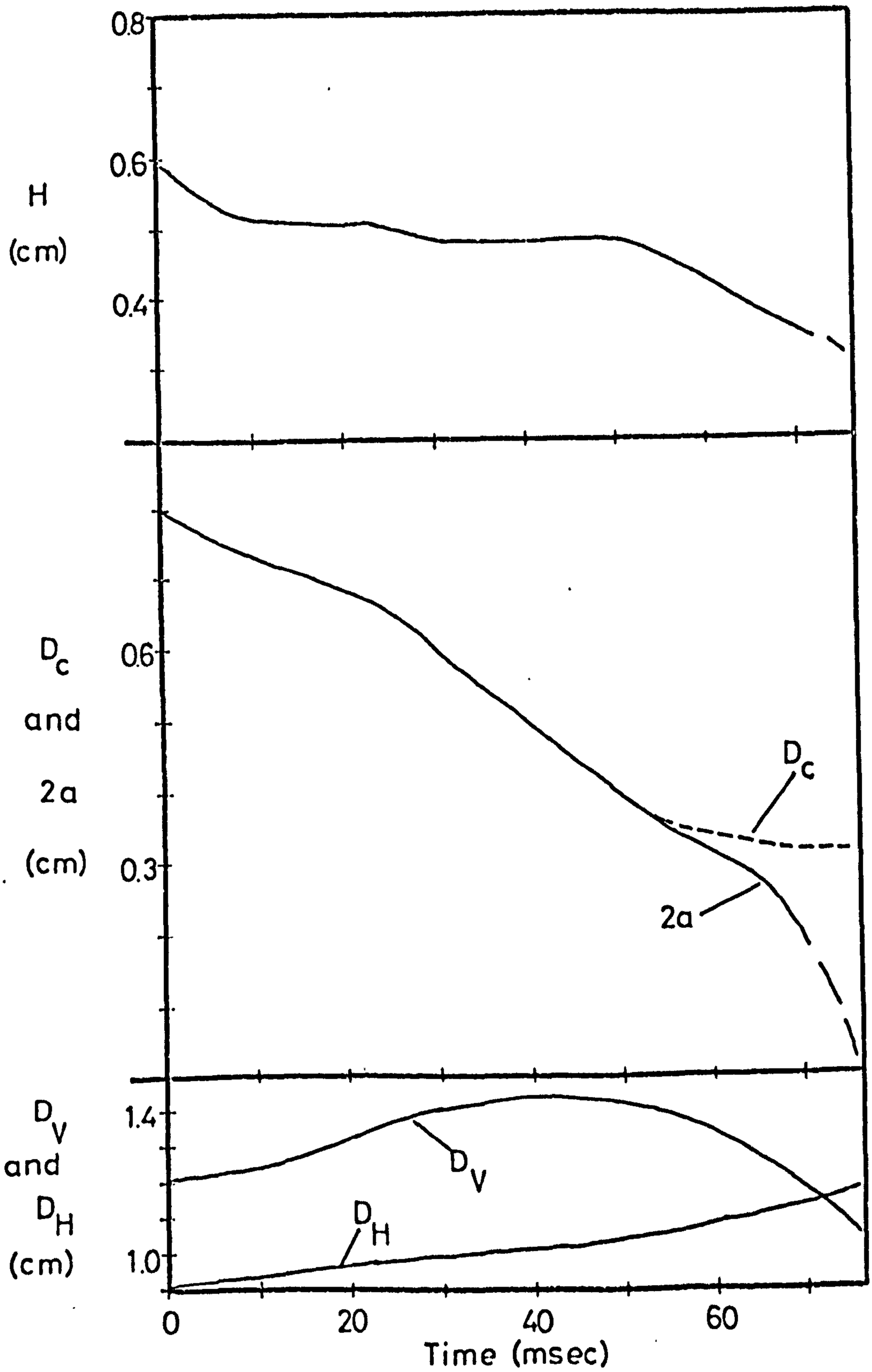

Fig.28 The dimensions of the drop during breakup

System: chlorobenzene/water, $D_{E,1}$ =1.013 cm

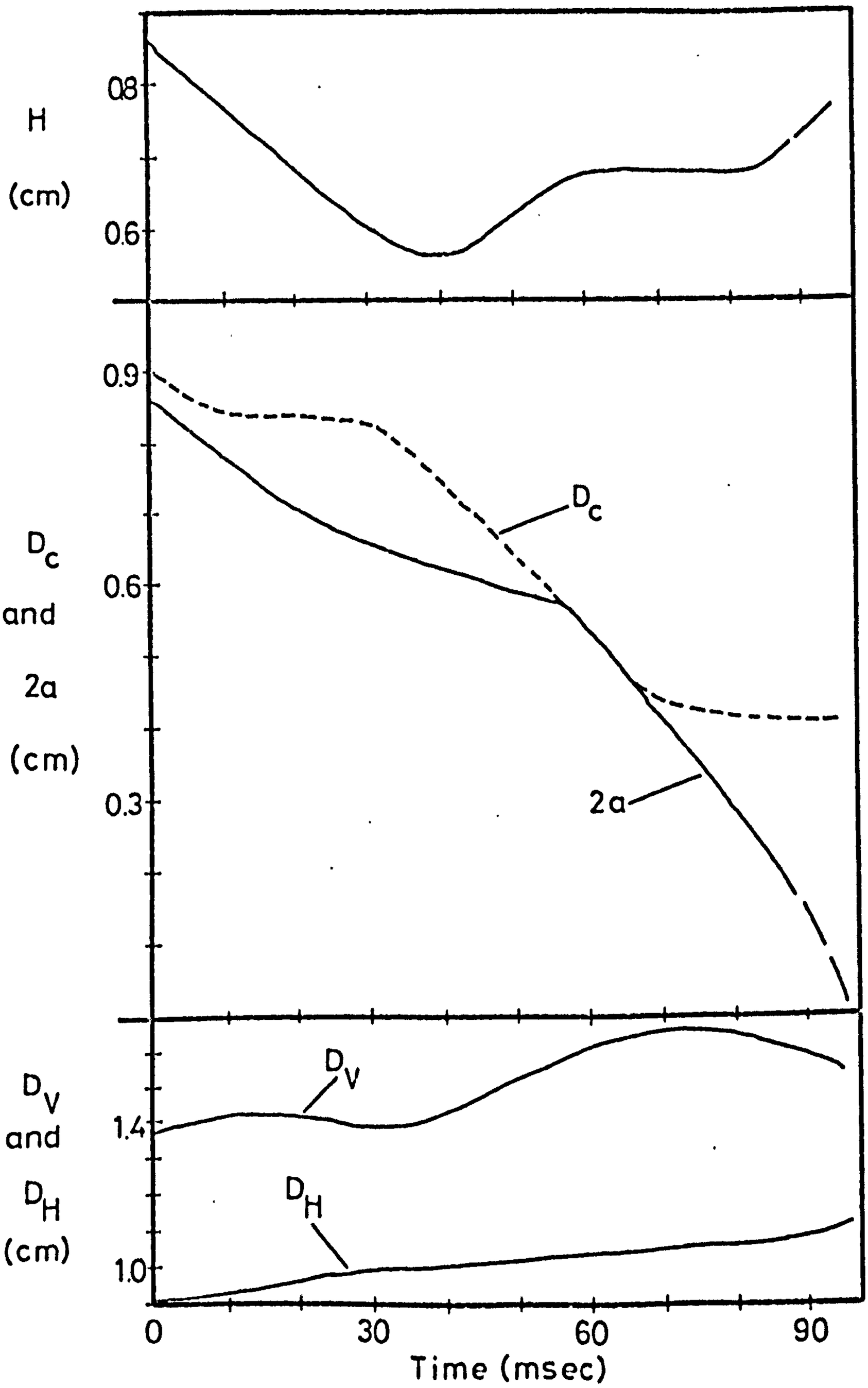

Fig.29 The dimensions of the drop during breakup

System: chlorobenzene/water, $D_{E,1}$ =1.056 cm

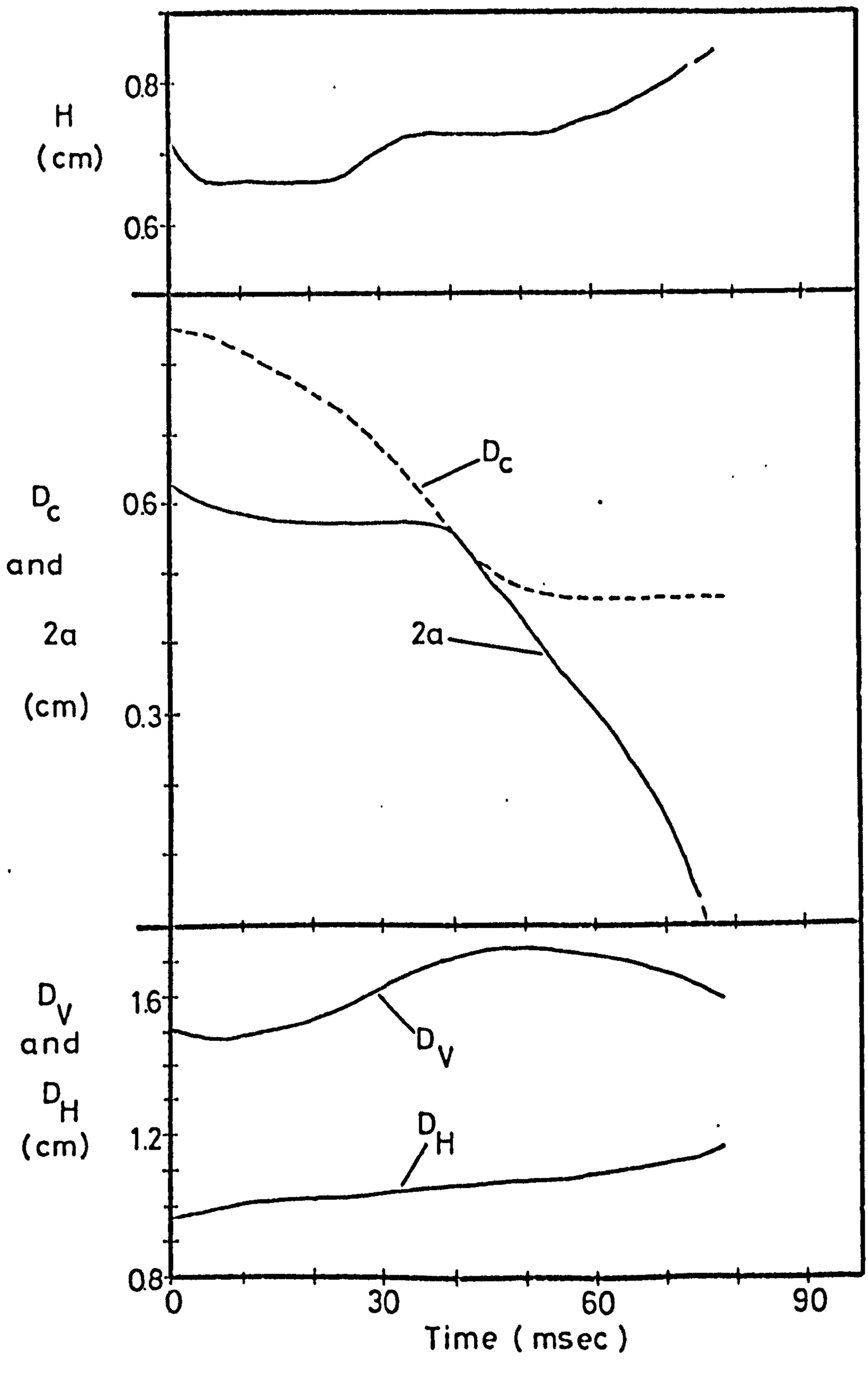

Fig.30 The dimensions of the drop during breakup

System: chlorobenzene/water, $D_{E,1}$ =1.088 cm

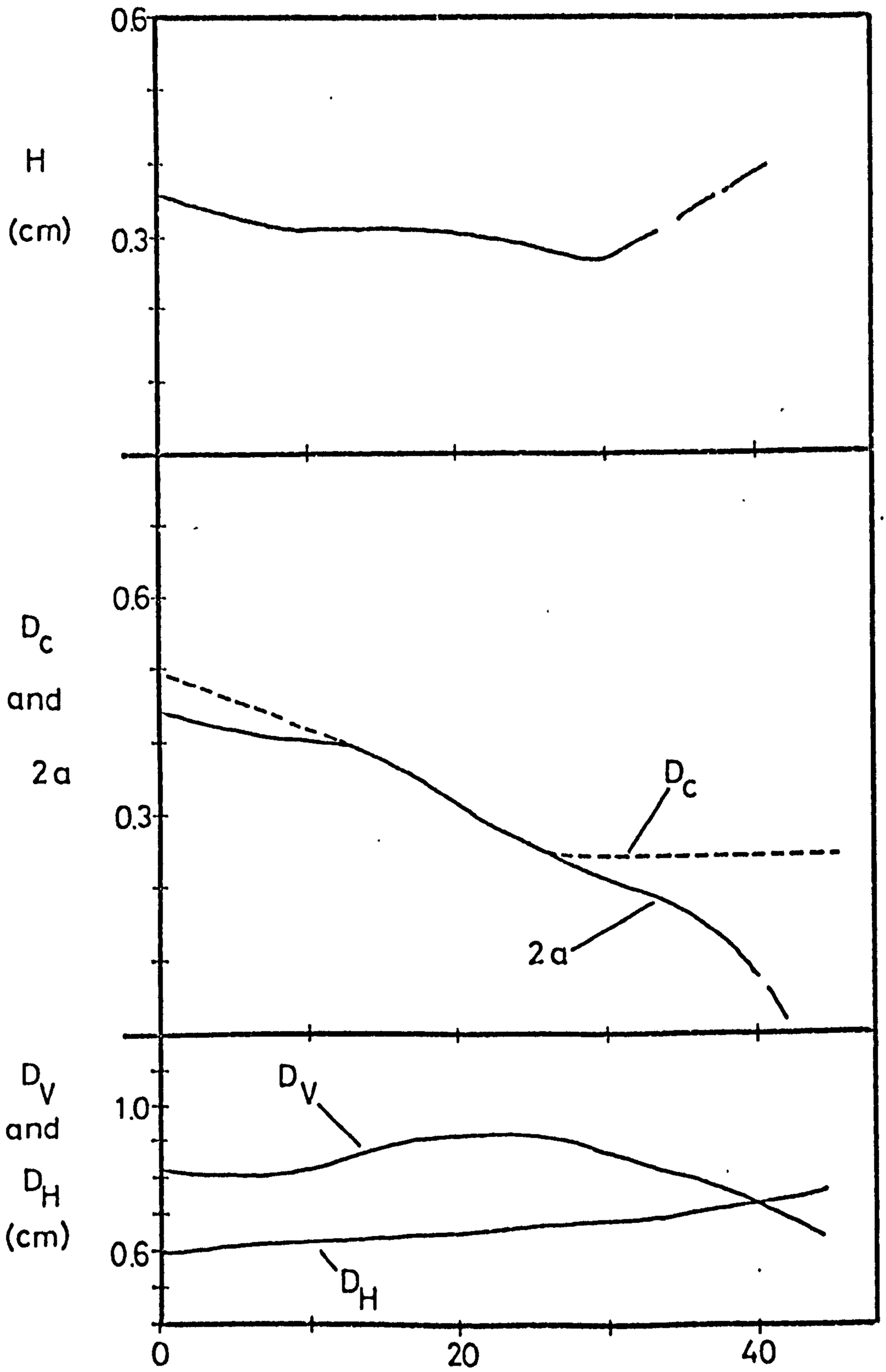

Fig.31 The dimensions of the drop during breakup

System: 1,2-dichloroethane/water, $D_{E,1}$ =0.635 cm

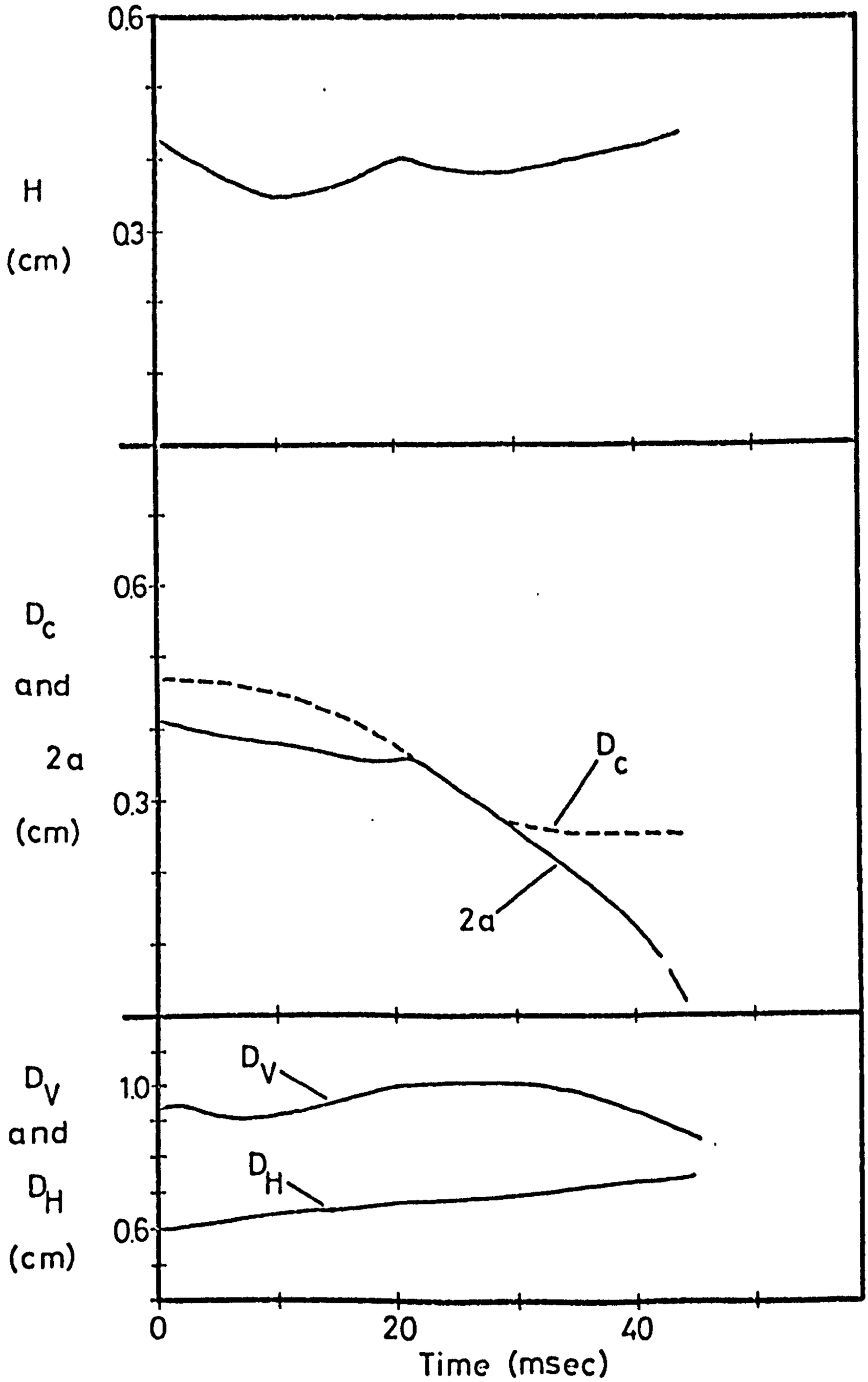

Fig.32 The dimensions of the drop during breakup

System: 1,2-dichloroethane/water, $D_{E,1}$=0.657 cm

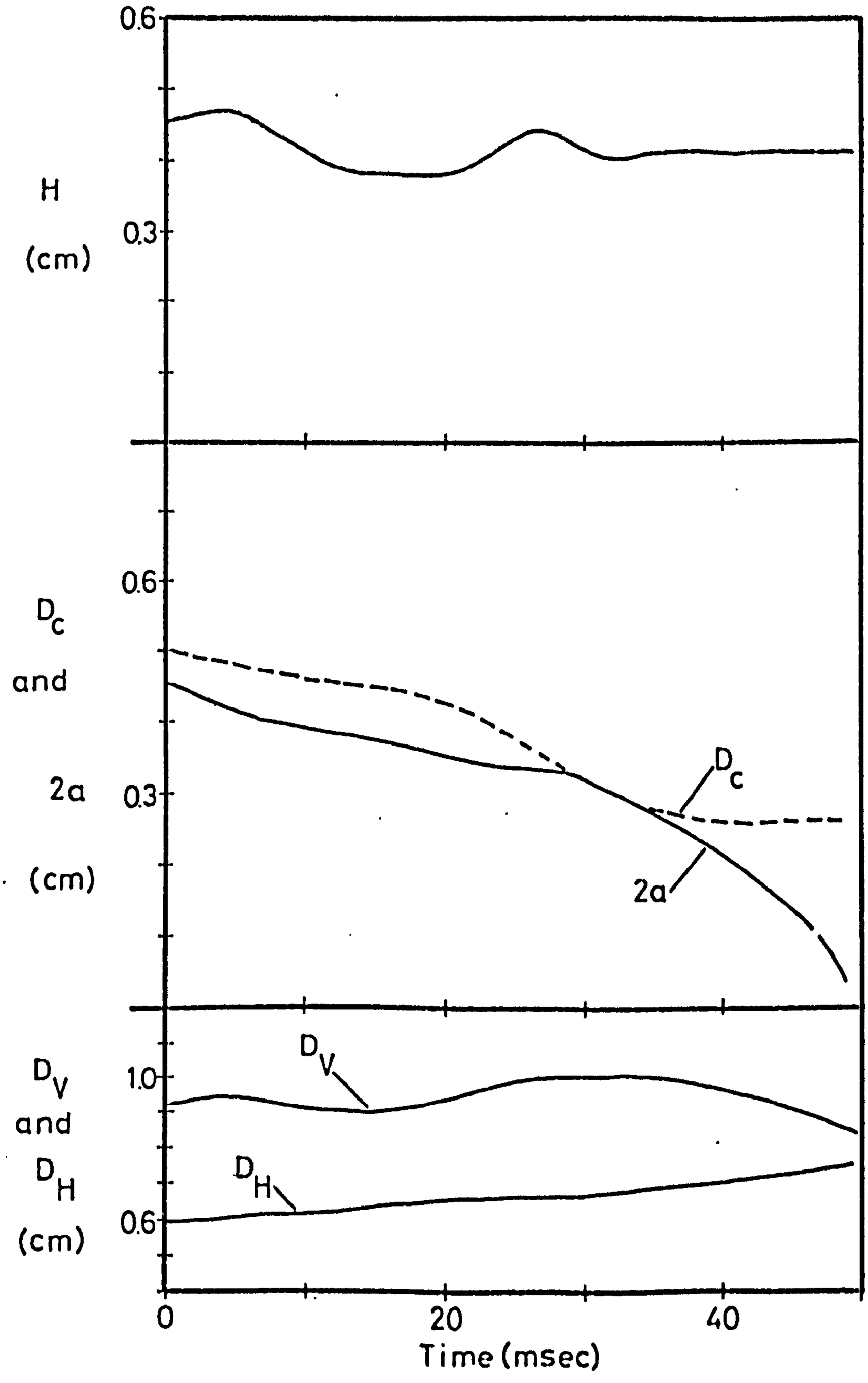

Fig.33 The dimensions of the drop during breakup

System: 1,2-dichloroethane/water, $D_{E,1}$ =0.666 cm

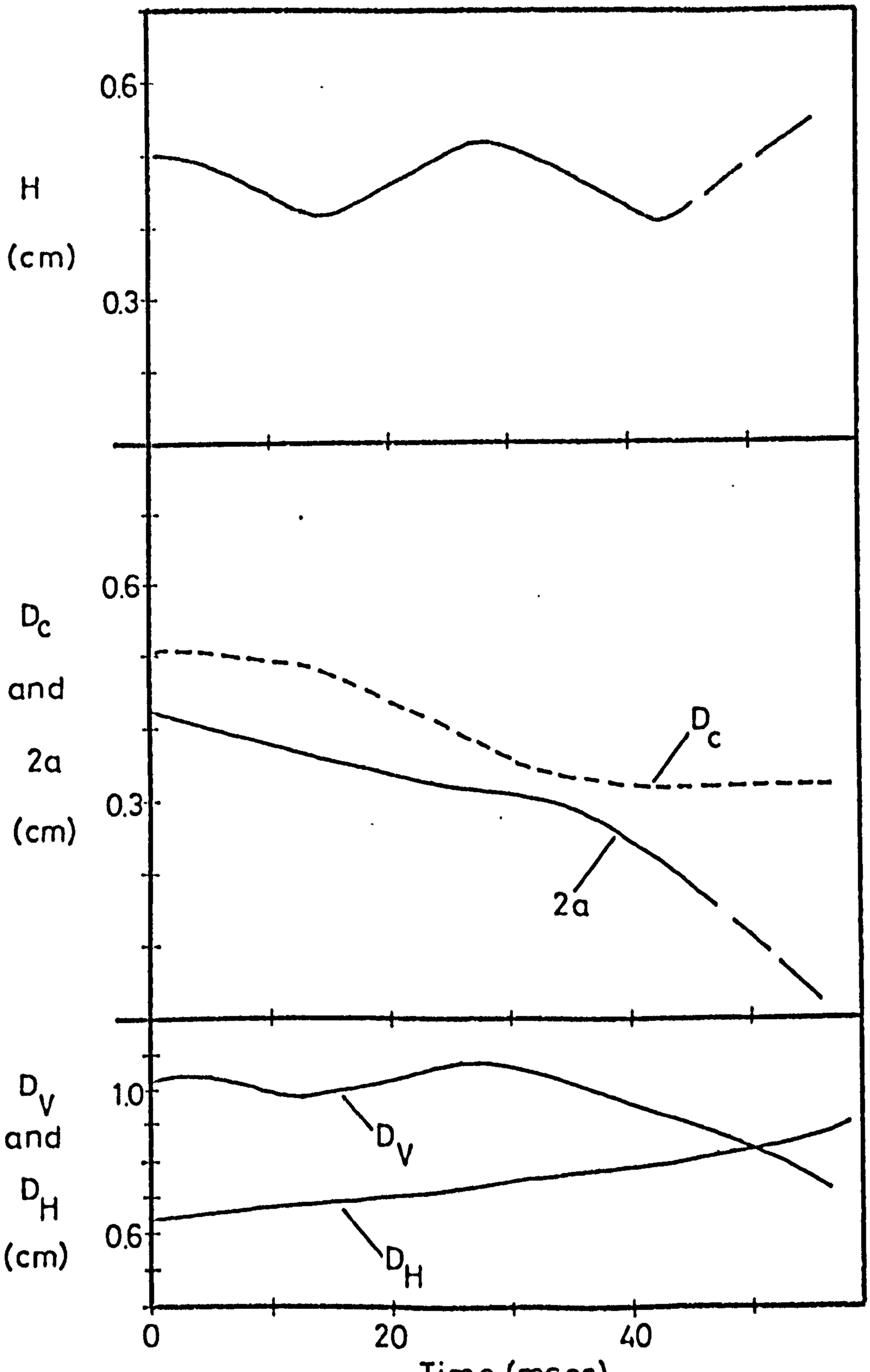

Fig.34 The dimensions of the drop during breakup

System: 1,2-dichloroethane/water, $D_{E,1}$ =0.694 cm

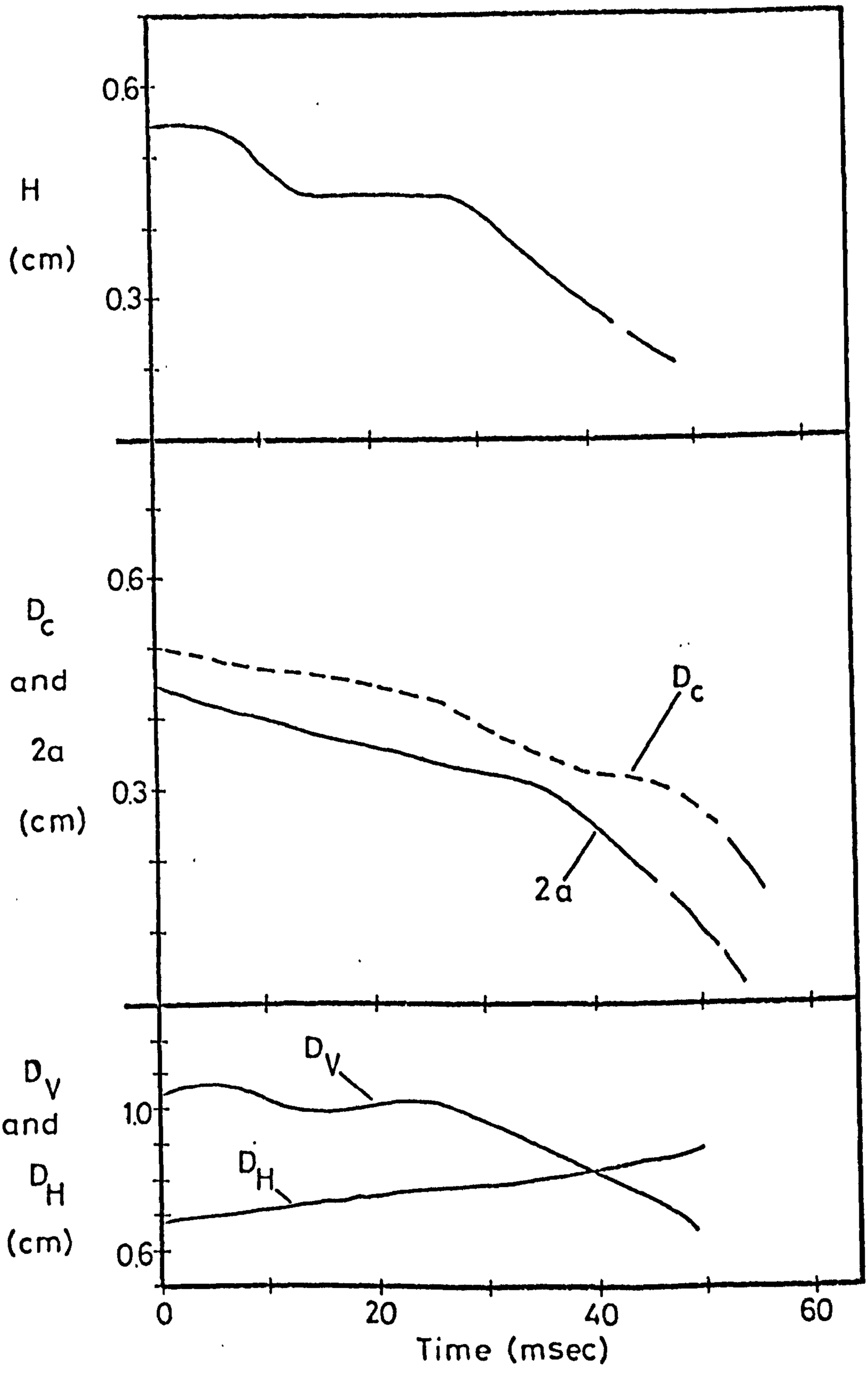

Fig. 35 The dimensions of the drop during breakup

System: 1,2-dichloroethane/water, $D_{E,1}$ =0.712 cm

APPENDIX III

TABLES OF RESULTS

TABLE Internal diameters of the drop forming tips

TIP	internal diameter (cm)
05	0.119
04	0.158
03	0.170
02	0.250
01	0.404
00	0.454
0	0.390
1	0.411
2	0.453
2'	0.457
3	0.485
4	0.543
5	0.613
6	0.642
7	0.742
8	0.806
9	0.919
10	0.989

TABLE 1 Sizes of nonbreaking drops formed from the tips at various rates of formation

System : Chlorobenzene/Water

TIP	number of drops in sample	time of formation (sec)	$D_{E,1}$ + (cm)	% S.D.
05	20	7.0	0.560	0.13
04	15	8.0	0.620	0.11
03	15	8.0	0.674	0.10
02	10	10.0	0.769	0.13
01	10	10.0	0.891	0.19

System : 1,2-Dichloroethane/Water

TIP	number of drops in sample	time of formation (sec)	$D_{E,1}$ + (cm)	% S.D.
05	40	6.5	0.360	0.59
03	30	8.0	0.410	0.71
02	30	9.0	0.512	0.31
01	30	10.0	0.578	0.30
00	20	10.0	0.600	1.20

+ mean of three separate measurements

TABLE 2 Sizes of breaking chlorobenzene drops formed from the tips at 10 sec intervals

TIP	number of drops in sample	$D_{E,1}$ (cm)$^{+}$	% S.D.
1	20	0.896	0.08
2	20	0.906	0.00
3	20	0.932	0.13
4	20	0.969	0.07
5	15	0.998	0.23
6	15	1.013	0.07
7	15	1.056	0.16
8	15	1.088	0.00
9	15	1.124	0.06
10	15	1.146	0.06

$^{+}$mean of three separate measurements

TABLE 3 Sizes of breaking chlorobenzene drops formed from the tips at various rates of formation

TIP	number of drops in sample	time of formation (sec)	$D_{E,1}$ (cm)$^{+}$	% S.D.
1	20	5.0	0.898	0.08
2'	20	7.0	0.922	0.08
	20	14.0	0.918	0.08
3	20	5.0	0.945	0.11
	20	24.0	0.923	0.16
4	15	5.0	0.980	0.07
	15	25.0	0.958	0.07
5	15	5.0	1.008	0.10
	15	20.0	0.990	0.07
6	15	7.0	1.020	0.07
	15	22.5	1.000	0.07

$^{+}$mean of three separate measurements

TABLE 4 Sizes of breaking 1,2-dichloroethane drops formed from the tips at 10 sec intervals

TIP	number of drops in sample	$D_{E,1}^{+}$ (cm)	% S.D.
3	20	0.612	0.16
4	20	0.635	0.09
5	20	0.657	0.00
6	20	0.666	0.19
7	20	0.694	0.08
8	20	0.712	0.18
9	20	0.744	0.00
10	20	0.768	0.11

+mean of three separate measurements

TABLE 5 Sizes of breaking ethylbromide drops formed from the tips at 10 sec intervals

TIP	number of drops in sample	$D_{E,1}$ (cm)	% S.D.
0	60	0.481	0.12
1	30	0.493	0.17
2'	30	0.505	0.00
3	30	0.514	0.11
4	30	0.531	0.15
5	25	0.552	0.10
6	25	0.555	0.10
7	25	0.587	0.10
8	25	0.602	0.21
9	25	0.631	0.13
10	25	0.639	0.27

+mean of three separate measurements

TABLE 6 Sizes of the secondary drops

System : Chlorobenzene/Water

Primary drops were formed at 10 sec intervals

TIP	$D_{E,1}$ (cm)	rear formation		front formation	
		$D_{E,2}^{+}$ (cm)	% S.D.	$D_{E,2}^{+}$ (cm)	% S.D.
1	0.896	0.058	5.7	-	-
2	0.906	0.312	5.0	-	-
3	0.932	-	-	-	-
4	0.969	-	-	0.146	5.0
5	0.998	0.075	3.3	0.202	0.6
6	1.013	0.299	0.7	0.257	1.4
7	1.056	0.478	1.4	0.080	8.1
8	1.088	0.543	2.2	0.146	8.7
9	1.124	0.622	11.4	-	-
10	1.146	0.595	8.3	0.237	2.9

$^{+}$mean of three separate measurements

TABLE 7 Sizes of the secondary drops

System : Chlorobenzene/Water

Primary drops were formed at various rates

TIP	time of formation (sec)	$D_{E,1}$ (cm)	rear formation		front formation	
			$D_{E,2}^{+}$ (cm)	% S.D.	$D_{E,2}^{+}$ (cm)	% S.D.
1	5.0	0.898	0.243	5.5	-	-
2'	7.0	0.922	0.048	7.1	-	-
	14.0	0.918	0.293	4.3	-	-
3	5.0	0.945	-	-	0.071	6.4
	24.0	0.923	0.084	7.7	-	-
4	5.0	0.980	-	-	0.156	5.6
	25.0	0.958	-	-	0.104	8.6
5	5.0	1.008	0.159	2.7	0.213	7.8
	20.0	0.990	-	-	0.175	3.7
6	7.0	1.020	0.335	2.1	0.260	3.9
	22.5	1.000	0.105	6.6	0.201	3.3

+ mean of three separate measurements

TABLE 8 Sizes of the secondary drops

System : 1,2-Dichloroethane/Water

Primary drops were formed at 10 sec intervals

TIP	$D_{E,1}$ (cm)	rear formation		front formation	
		$D_{E,2}^{+}$ (cm)	% S.D.	$D_{E,2}^{+}$ (cm)	% S.D.
3	0.612	-	-	-	-
4	0.635	0.244	3.2	-	-
5	0.657	0.293	1.9	-	-
6	0.666	0.305	2.0	-	-
7	0.694	0.358	1.4	-	-
8	0.712	0.081	9.6	-	-
9	0.744	-	-	0.111	3.2
10	0.768	-	-	0.110	4.5

$^{+}$mean of three separate measurements

TABLE 9 Sizes of the secondary drops

System : Ethylbromide/Water

Primary drops were formed at 10 sec intervals

TIP	$D_{E,1}$ (cm)	rear formation		front formation	
		$D_{E,2}^{+}$ (cm)	% S.D.	$D_{E,2}^{+}$ (cm)	% S.D.
0	0.481	0.163	4.8	-	-
1	0.493	0.207	4.9	-	-
2'	0.505	0.247	5.7	-	-
3	0.514	0.267	2.5	-	-
4	0.531	0.134	5.6	-	-
5	0.552	-	-	-	-
6	0.555	-	-	-	-
7	0.587	-	-	0.107	4.1
8	0.602	-	-	0.117	5.0
9	0.631	0.331	3.0	0.092	6.1
10	0.639	0.422	3.5	0.098	6.6

$^{+}$mean of three separate measurements

TABLE 10 The velocity of fall, the frequency of oscillation and the wake class in the terminal region for nonbreaking drops, as reported by EDGE and GRANT[36][37]

System : Chlorobenzene/Water

$D_{E,1}$ (cm)	U_∞ (cm/sec)	w (1/sec)	wake class
0.560	15.6	9.76	III
0.620	15.4	8.80	III
0.674	14.4	8.04	III
0.769	14.0	6.54	IV
0.891	13.4	5.35	V

System : 1,2-Dichloroethane/Water

$D_{E,1}$ (cm)	U_∞ (cm/sec)	w (1/sec)	wake class
0.360	16.9	15.1	III
0.410	16.8	13.0	III
0.512	15.4	9.5	IV
0.578	14.7	8.8	IV
0.600	14.6	7.8	IV

TABLE 11 Mean eccentricity and the amplitude of eccentricity oscillations for nonbreaking drops in the terminal region

System : Chlorobenzene/Water

$D_{E,1}$	mean E^{+}_{max}	% S.D.	mean E^{+}_{min}	% S.D.	mean E^{+}	% S.D.	mean ΔE^{+}	% S.D.
0.560	2.11	1.1	1.47	1.5	1.79	1.2	0.64	0.0
0.620	2.12	3.7	1.24	9.1	1.68	0.8	0.88	21.7
0.674	2.07	1.4	1.25	1.8	1.66	0.0	0.83	6.0
0.769	2.46	6.6	0.97	14.6	1.72	0.6	1.49	0.6
0.891	2.56	7.2	1.01	2.2	1.79	4.4	1.56	13.1
Overall mean eccentricity					1.73			
% S.D.					3.50			

System : 1,2-Dichloroethane/Water

$D_{E,1}$	mean E^{+}_{max}	% S.D.	mean E^{+}_{min}	% S.D.	mean E^{+}	% S.D.	mean ΔE^{+}	% S.D.
0.360	2.30	2.5	1.59	2.7	1.95	0.5	0.71	13.9
0.410	2.72	2.9	1.27	2.8	2.00	1.1	1.45	7.8
0.512	2.61	1.6	1.13	8.2	1.87	1.5	1.49	9.0
0.578	2.60	1.1	1.16	1.9	1.88	1.5	1.45	0.7
0.600	2.74	0.0	1.13	7.5	1.94	2.2	1.61	5.3
Overall mean eccentricity					1.93			
% S.D.					2.78			

$^{+}$ mean of two separate measurements

TABLE 12 Drop eccentricity when $\omega = \omega^*$ for nonbreaking drops

<u>System : Chlorobenzene/Water</u>

$D_{E,1}$ (cm)	E
0.560	1.10
0.620	1.12
0.674	1.08
0.769	1.14
0.891	1.00

<u>System : 1,2-Dichloroethane/Water</u>

$D_{E,1}$ (cm)	E
0.410	1.13
0.512	1.12
0.578	1.20
0.600	1.10

TABLE 13 Constants of equation (6.3) and the time required to reach 90% of the terminal velocity for nonbreaking drops

System : Chlorobenzene/Water

$D_{E,1}$ (cm)	mean^{+} τ (1/sec)	% S.D.	k	$t_{0.9}$ (sec)
0.560	4.09	1.7	0.75	0.36
0.620	4.18	1.9	0.63	0.35
0.674	4.82	6.8	0.46	0.31
0.769	5.38	1.7	0.28	0.27
0.891	6.18	2.9	0.14	0.24

$^{+}$mean of two measurements

TABLE 14 The D_V peak at which the critical oscillation occurs and the mode of drop breakup

System : Chlorobenzene/Water

$D_{E,1}$ (cm)	number of D_V peak after detachment	mode of breakup
0.620	8	no breakup
0.674	7	no breakup
0.769	5	no breakup
0.891	4	no breakup
0.896	4	rear breakup
0.906	4	rear breakup
0.932	4	no breakup
0.969	3 - 4	front breakup
0.998	3	rear and front breakup
1.013	3	rear and front breakup
1.056	3	rear and front breakup
1.088	3	rear and front breakup
1.124	3	rear breakup
1.146	3	rear and front breakup

TABLE 15 The D_V peak at which the critical oscillation occurs and the mode of drop breakup

System : 1,2-Dichloroethane/Water

$D_{E,1}$ (cm)	number of D_V peak after detachment	mode of breakup
0.410	6	no breakup
0.512	3	no breakup
0.578	3	no breakup
0.600	3	no breakup
0.612	3	no breakup
0.635	3	rear breakup
0.657	3	rear breakup
0.666	3	rear breakup
0.694	3	rear breakup
0.712	3	rear breakup
0.744	2 - 3	front breakup
0.768	2 - 3	front breakup

TABLE 16 The D_V peak at which the critical oscillation occurs and the mode of drop breakup

System : Ethylbromide/Water

$D_{E,1}$ (cm)	number of D_V peak after detachment	mode of breakup
0.481	3	rear breakup
0.493	3	rear breakup
0.505	3	rear breakup
0.514	3	rear breakup
0.531	3	rear breakup
0.552	3	no breakup
0.555	3	no breakup
0.587	2 - 3	front breakup
0.602	2 - 3	front breakup
0.631	2	rear and front breakup
0.639	2	rear and front breakup

TABLE 17 Constants of the equation (8.1) for the various systems

System	breakup at the D_V peak number	V_o (cm^3)	$D^*_{E,1}$ (cm)
chlorobenzene	4	1.580	0.8959
	3	0.985	0.9978
1,2-dichloroethane	3	0.204	0.6120
ethylbromide	3	0.237	0.4721
	2	2.545	0.6236

TABLE 18 Dimensions of the drops prior to necking

System : Chlorobenzene/Water

$D_{E,1}$ (cm)	H^+ (cm)	% S.D.	R_c^+ (cm)	% S.D.	$\frac{H^+}{2\pi R_c}$	% S.D.	D_V^+ (cm)	% S.D.
0.896	0.358	3.1	0.147	3.9	0.39	6.8	1.239	1.5
0.906	0.406	6.6	0.181	8.3	0.36	9.5	1.410	2.4
0.998	0.347	7.7	0.164	6.3	0.34	2.4	1.274	2.8
1.013	0.445	3.4	0.178	3.1	0.40	2.0	1.397	2.1
1.056	0.667	1.5	0.237	2.3	0.45	2.2	1.662	0.6
1.088	0.744	4.0	0.272	2.5	0.44	5.6	1.746	1.5

System : 1,2-Dichloroethane/Water

$D_{E,1}$ (cm)	H (cm)	% S.D.	R_c (cm)	% S.D.	$\frac{H}{2\pi R_c}$	% S.D.	D_V (cm)	% S.D.
0.635	0.287	2.0	0.139	3.7	0.33	3.5	0.920	1.3
0.657	0.379	1.1	0.143	4.0	0.42	5.3	1.009	1.3
0.666	0.405	2.1	0.144	1.1	0.45	2.6	1.027	1.6

+mean of three separate measurements

TABLE 19 Values of R_c for drainage of the rear column to occur by Models C_1, C_2, and C_3

System : Chlorobenzene/water

$D_{E,1}$ (cm)	experiment R_c^+ (cm)	% S.D.	Model C_1 R_c^+ (cm)	% S.D.	Model C_2 R_c^+ (cm)	% S.D.	Model C_3 R_c^+ (cm)	% S.D.
0.896	0.147	3.9	0.160	1.0	0.071	2.4	0.096	2.1
0.906	0.181	8.3	0.168	2.0	0.078	5.1	0.104	4.2
0.998	0.164	6.3	0.169	3.1	0.071	6.0	0.097	5.4
1.013	0.178	3.1	0.186	1.0	0.086	2.4	0.115	2.1
1.056	0.237	2.3	0.214	0.3	0.114	1.0	0.147	0.7
1.088	0.272	2.5	0.224	0.8	0.124	2.4	0.158	2.2

System : 1,2-Dichloroethane/Water

$D_{E,1}$ (cm)	experiment R_c^+ (cm)	% S.D.	Model C_1 R_c^+ (cm)	% S.D.	Model C_2 R_c^+ (cm)	% S.D.	Model C_3 R_c^+ (cm)	% S.D.
0.635	0.134	3.7	0.118	0.8	0.055	1.8	0.073	1.4
0.657	0.143	4.0	0.130	0.4	0.067	0.9	0.087	0.7
0.666	0.143	0.9	0.133	0.6	0.070	1.2	0.091	1.6

$^+$ mean of three separate measurements

TABLE 20 Experimental and theoretical values of the rate of necking at the onset of necking

System : Chlorobenzene/Water

$D_{E,1}$ (cm)	experimental $-\frac{da}{dt}^{+}$ (cm/sec)	equation (8.10) $-\frac{da}{dt}^{+}$ (cm/sec)
0.896	5.8	8.0
0.906	5.7	8.7
1.013	5.0	7.2
1.056	6.05	5.5
1.088	6.05	5.2

System : 1,2-dichloroethane/Water

$D_{E,1}$ (cm)	experimental $-\frac{da}{dt}^{+}$ (cm/sec)	equation (8.10) $-\frac{da}{dt}^{+}$ (cm/sec)
0.635	7.2	10.3
0.657	5.4	8.2
0.666	5.5	7.7

+ mean of three separate measurements

APPENDIX IV

PREPARATION OF THE CHROMIC ACID SOLUTION

Chromic acid solution was prepared as follows : Sodiumdichromate was added to water until no more would dissolve. Then concentrated sulphuric acid was added to the saturated dichromate solution. The chromium trioxide which precipitated was redissolved by further addition of concentrated sulphuric acid. This solution was kept in bottles or in glass tanks tightly covered with glass plates.

NOMENCLATURE

Commonly used symbols are given below. Other symbols are defined in the text.

a	radius of the rear column at the point of necking	(cm)
A	area	(cm^2)
A_V	($=D_{V,max}-D_{V,min}$) amplitude of D_V oscillation	(cm)
b	"carried mass" in equation (2.58) and (I-A.2)	(g)
b_A	amplitude factor, equation (2.40)	
b^*	property parameter, equation (2.17)	
C_A, C_B	radii of curvature, equation (8.10)	(cm)
C_D	drag coefficient	
D	Diameter of the sphere	
D_H	diameter of the major (horizontal) axis of the drop	(cm)
D_V	diameter of the minor (vertical) axis of the drop	(cm)
$D_{E,1}$	equivalent spherical diameter of the primary drop	(cm)
$D^*_{E,1}$	constant in equation (8.1)	(cm)
$D_{E,2}$	equivalent spherical diameter of the secondary drop	(cm)
E	($=D_H/D_V$) eccentricity of the drop	

ΔE	$(=E_{max}- E_{min})$ amplitude of eccentricity oscillation	
F_D	drag force	(dyne)
h	height of the cylindrical part of the rear column	(cm)
H	total height of the rear column	(cm)
k	constant in equation (6.3)	
K_1, K_2	constants in equation (2.29)	
n	positive integer (including zero)	
q	growth rate of the disturbance	(1/sec)
r, r'	cylindrical coordinate, spherical coordinate	(cm)
R_c	radius of the column	(cm)
R_o	radius of the drop excluding the column	(cm)
t	time	(sec)
$t_{0.9}$	time required by the drop to reach 90 % of the gross terminal velocity	(sec)
U	velocity	(cm/sec)
V_1	volume of the primary drop	(cm^3)
V_2	volume of the secondary drop	(cm^3)
V_o	constant in equation (8.1)	(cm^3)
z	cylindrical coordinate	(cm)
α	amplitude of disturbance	(cm)
β	quantity in equation (I-B.3)	(cm)
Δ	difference	
δ_o	amplitude of disturbance at t=0	(cm)
ε	surface free energy per length of the column	(dyne)

θ	cylindrical coordinate	
λ	wavelength of the disturbance	(cm)
μ	viscosity	(poise)
ρ	density	(g/cm^3)
σ	interfacial tension	(dyne/cm)
τ	constant in equation (6.2)	(1/sec)
ω	frequency of oscillation	(1/sec)
ω^*	frequency of oscillation predicted by Lamb, equation (2.37)	(1/sec)

Subscripts

a	continuous fluid
c	column
crit	critical value
d	drop fluid
max	maximum value
min	minimum value
opt	optimum value
St	value given by Stokes
trans	transition value
w	water phase
∞	value in the terminal period

Dimensionless Groups

Eö	Eötvös number	$\frac{g \Delta\rho D_{E,1}^2}{\sigma}$
Re	Reynolds number	$\frac{\rho_a U_\infty D_{E,1}}{\mu_a}$

Sr	Strouhal number	$\frac{\omega D_{E,1}}{V_\infty}$
We	Weber number	$\frac{\rho_d V_\infty^2 D_{E,1}}{\sigma}$
Z	Ohnesorge number	$\frac{\mu_d}{(\rho_d \sigma D_{E,1})^{1/2}}$

REFERENCES

(1) ALLEN, H.S.
Phil.Mag., 1900, 50, 323

(2) ALLEN, H.S.
Phil.Mag., 1900, 50, 519

(3) ALLEN, D.N. de G. - SOUTHWELL, R.V.
Quart.J.Mech., 1955, 8, 129

(4) BARTOK, W. - MASON, S.J.
J.Coll.Sci., 1957, 12, 243

(5) BARTOK, W. - MASON, S.J.
J.Coll.Sci., 1959, 14, 13

(6) BASSET, A.B.
'Hydrodynamics', Vol II, 1888, Cambridge

(7) BASSET, A.B.
Trans.Roy.Soc., 1888, A 179, 43

(8) BASSET, A.B.
Quart.J.Math., 1910, 41, 369

(9) BIDONE, G.
1829, (Imprimerie Royale : Turin)

(10) BLASIUS, H.
Z.Math.u.Phys., 1908, 56, 1

(11) BOGGIO, T.
Rend.d.R.Acad. dei Lincei, 1907, 16, November

(12) BOLTZE, E.
Ph.D. Thesis, 1908, Göttingen

(13) BOND, W.N.
'Introduction to Fluid Motion', 1925, London

(14) BOND, W.N.
Phil.Mag., 1927, 4, 889

(15) BOND, W.N. - NEWTON, D.A.
Phil.Mag., 1928, 5, 794

(16) BOUSSINESQ, J.
Compt.Rend.Acad.Sci., 1913, 156, 983

(17) BOUSSINESQ, J.
Compt.Rend.Acad.Sci., 1913, 156, 1035

(18) BOUSSINESQ, J.
Compt.Rend.Acad.Sci., 1913, 156, 1124

(19) BOUSSINESQ, J.
Ann.Chim.et Phys., 1913, 29, 349

(20) BOUSSINESQ, J.
Ann.Chim.et Phys., 1913, 29, 357

(21) BOUSSINESQ, J.
Ann.Chim.et Phys., 1913, 29, 364

(22) BROWN, A.H. - HANSON, C.
'Solvent Extraction Chemistry', 1967,
(Amsterdam : North-Holland)

(23) BURKHOLDER, H.C. - BERG, J.C.
A.I.Ch.E.J., 1974, 20, 863

(24) BURKHOLDER, H.C. - BERG, J.C.
A.I.Ch.E.J., 1974, 20, 872

(25) CALDERBANK, P.H. - KORCHINSKI, I.J.O.
Chem.Engng Sci., 1956, 6, 65

(26) CERF, R.
J.Clin.Phys., 1951, 48, 59

(27) CHAO, B.T.
Phys.Fluids, 1962, 5, 69

(28) CHARLES, G.E. - MASON, S.G.
J.Coll.Sci., 1960, 15, 105

(29) CHARLES, G.E. - MASON, S.G.
J.Coll.Sci., 1960, 15, 263

(30) COOK, G.
Phil.Mag., 1920, 39, 350

(31) DAVIES, C.N.
Proc.Phys.Soc.(London), 1945, 57, 259

(32) DAVIES, C.N.
'Symp.on Part.Size Analysis', Suppl. Trans.
Instn Chem.Engrs., 1947

(33) DAVIES, J.T.
'Turbulence Phenomena', 1972, (London:Acad.Press)

(34) DAVIES, J.T. - RIDEAL, E.K.
'Interfacial Phenomena',1963, (N.Y.:Acad.Press)

(35) DIMIAN, Al. - RUCKENSTEIN, E.
Chem.Engng Sci., 1970, 25, 1821

(36) EDGE, R.M. - GRANT, C.D.
Chem.Engng Sci, 1971, 26, 1001

(37) EDGE, R.M. - GRANT, C.D.
Proc.Int.Solvent Extr.Conf., 1971, 1, 82

(38) EDGE, R.M. - GRANT, C.D.
Chem.Engng Sci., 1972, 27, 1709

(39) ELZINGA, E.R. - BANCHERO, J.T.
A.I.Ch.E.J., 1961, 7, 394

(40) FINLAY, B.A.
Ph.D. Thesis, 1957, (Birmingham)

(41) GARNER, F.H.
Trans.Instn Chem.Engrs, 1950, 28, 88

(42) GARNER, F.H. - GRAFTON, R.W.
Proc.Roy.Soc.(London), 1954, A 224, 64

(43) GARNER, F.H. - HAYCOCK, P.J.
Proc.Roy.Soc.(London), 1959, A 252, 457

(44) GARNER, F.H. - JENSON, V.G. - KEEY, R.B.
Trans.Instn Chem.Engrs, 1959, 37, 191

(45) GARNER, F.H. - LANE, J.J.
Trans.Instn Chem.Engrs, 1959, 37, 154

(46) GARNER, F.H. - SKELLAND, A.H.P.
Trans.Instn Chem.Engrs, 1951, 29, 315

(47) GARNER, F.H. - SKELLAND, A.H.P.
Ind.Engng Chem., 1954, 46, 1255

(48) GARNER, F.H. - SKELLAND, A.H.P.
Chem.Engng Sci., 1955, 4, 149

(49) GARNER, F.H. - TAYEBAN, M.
An.R.Soc.esp.Fis.Quim., 1960, B 56, 479

(50) GOLDBURG, A. - FLORSHEIM, B.H.
Phys.Fluids, 1966, 9, 45

(51) GOLDSTEIN, S.
Proc.Roy.Soc.(London), 1929, A 123, 225

(52) GOLDSTEIN, S.
'Modern Developments in Fluid Dynamics', 1938,
(Oxford)

(53) GÖRTLER, H.
Arch.d.Math., 1948, 1, 138

(54) GUNN, R.
J.Geophys.Res., 1949, 54, 383

(55) HABERMAN, W.L. - MORTON, R.K.
The David W. Taylor Model Basin Report 802,1953

(56) HADAMARD, J.
Compt.Rend.Acad.Sci., 1911, 152, 1735

(57) HADAMARD, J.
Compt.Rend.Acad.Sci., 1912, 154, 109

(58) HAMIELEC, A.E. - HOFFMAN, T.W. - ROSS, L.L.
A.I.Che.E.J., 1967, 13, 212

(59) HANSON, C. - BROWN, A.H.
I.Chem.E.Sympos.Series No.26, 1967, 57

(60) HARKINS, W.D. - BROWN, F.E.
J.Am.Chem.Soc., 1919, 41, 499

(61) HARMATHY, T.Z.
A.I.Ch.E.J., 1960, 6, 281

(62) HARPER, J.F. - MOORE, D.W.
J.Fluid Mech., 1968, 32, 367

(63) HAYWORTH, C.B. - TREYBAL, R.E.
Ind.Engng Chem., 1950, 42, 1174

(64) HEERTJES, P.M. - de NIE, L.H.
Chem.Engng Sci., 1966, 21, 755

(65) HILL, M.J.M.
Phil.Trans., 1894, A 185, 213

(66) HINZE, J.O.
Appl.Sci.Res., 1948, A 2, 263

(67) HINZE, J.O.
Appl.Sci.Res., 1948, A 2, 273

(68) HINZE, J.O.
A.I.Ch.E.J., 1955, 1, 289

(69) HOCHSCHWENDER, E.
Ph.D. Thesis, 1919, (Heidelberg)

(70) HOLDER, D.W. - NORTH, R.J.
'Schlieren Methods', 1963, (London:H.M.S.O.)

(71) HORTON, J.J. - FRITSCH, T.R. - KINTNER, R.C.
Can.J.Chem.Engng, 1965, 43, 143

(72) HU, S. - KINTNER, R.C.
A.I.Ch.E.J., 1955, 1, 42

(73) HUGHES, R.R. - GILLILAND, E.R.
Chem.Engng Prog., 1952, 48, 497

(74) JEFFREYS, G.V.
Chem.Process Engng, 1968, 49, 111

(75) JENSON, V.G.
Proc.Roy.Soc.(London), 1959, A 249, 346

(76) JENSON, V.G. - HORTON, T.R. - WEARING, J.R.
Trans.Instn Chem.Engrs., 1968, 46, 177

(77) JOHNSON, A.I. - BRAIDA, L.
Can.J.Chem.Engng, 1957, 35, 165

(78) JOHNSTONE, H.F. - WILLIAMS, G.C.
Ind.Engng Chem., 1939, 31, 996

(79) KARAM, H.J. - BELLINGER, J.C.
Ind.Eng.Chem.Fund., 1968, 7, 576

(80) KAWAGUTI, M.
Rep.Inst.Sci.(Tokyo), 1948, 2, 66

(81) KAWAGUTI, M.
Rep.Inst.Sci.(Tokyo), 1950, 4, 154

(82) KAWAGUTI, M.
J.Phys.Soc.Japan, 1953, 8, 747

(83) KEITH, F.W. - HIXSON, A.N.
Ind.Engng Chem., 1955, 47, 258

(84) KINTNER, R.C.
'Advances in Chemical Engineering',1963,4, 51

(85) KINTNER, R.C. - HORTON, T.J. - GRAUMANN, R.E. - AMBEKAR, S. Can.J.Chem.Engng, 1961, 39, 235

(86) KLEE, A.J. - TREYBAL, R.E.
A.I.Ch.E.J., 1956, 2, 444

(87) KLÜSENER, O.
V.D.I.Zeitschrift, 1933, 77, 171

(88) KRISHNA,P.M.-VENKATESVARLU,D.-NARASIMHAMURTY,G.
J.Chem.Engng Data, 1959, 4, 340

(89) LAMB, H.
'Hydrodynamics', 1945, 6th edn (Dover)

(90) LANE, W.R.
Ind.Engng Chem., 1951, 43, 1312

(91) LAPPLE, C.E. - SHEPHERD, C.E.
Ind.Engng Chem., 1940, 32, 605

(92) LAWS, J.O.
Agric.Eng., 1940, 21, 431

(93) LAWS, J.O.
Trans.Am.Geophys.Union, 1941, 22, 709

(94) LENARD, P.
Met.Z., 1904, 21, 249

(95) LENARD, P.
Ann.Phys., 1921, 65, 629

(96) LETAN, R. - KEHAT, E.
A.I.Ch.E.J., 1968, 14, 398

(97) LEVICH, V.G.
Zhur.Ekspty.i Teoret.Fiz., 1949, 19, 18

(98) LEVICH, V.G.
'Physicochemical Hydrodynamics',1962,(PrenticeH.)

(99) LICHT, W. - NARASIMHAMURTY, G.S.R.
A.I.Ch.E.J., 1955, 1, 366

(100) LINDLAND, K.P. - TERJESEN, S.G.
Chem.Engng Sci., 1956, 6, 265

(101) LISTER, M.
Ph.D. Thesis, 1953, (London)

(102) LITTAYE, G.
C.R.Acad.Sci., 1943, 217, 99

(103) LUNNON, R.G.
Proc.Roy.Soc.(London), 1926, A 110, 302

(104) LUNNON, R.G.
Proc.Roy.Soc.(London), 1928, A 118, 680

(105) MAGARVEY, R.H. - BISHOP, R.L.
Nature, 1960, 188, 735

(106) MAGARVEY, R.H. - BISHOP, R.L.
Can.J.Phys., 1961, 39, 1418

(107) MAGARVEY, R.H. - BISHOP, R.L.
Phys.Fluids, 1961, 4, 800

(108) MAGARVEY, R.H. - BLACKFORD, B.L.
Can.J.Phys., 1962, 40, 1036

(109) MAGARVEY, R.H. - MACLATCHY, C.S.
A.I.Ch.E.J., 1968, 14, 260

(110) MAGARVEY, R.H. - TAYLOR, B.W.
J.Appl.Phys., 1956, 27, 1129

(111) MAGNUS, P.
Pogg.Ann., 1855, 95

(112) MAHAJAN, L.D.
Phil.Mag., 1929, 7, 247

(113) MAHAJAN, L.D.
Phil.Mag., 1930, 10, 383

(114) MARKOWITZ, A. - BERGLES, A.E.
Chem.Engng Prog.Symp.Ser. No.102, 1970

(115) MEISTER, B.J. - SCHEELE, G.F.
A.I.Ch.E.J., 1969, 15, 689

(116) MELHUS, B.J. - TERJESEN, S.G.
Chem.Engng Sci., 1957, 7, 83

(117) MILLER, C.A. - SCRIVEN, L.E.
J.Fluid Mech., 1968, 32, 417

(118) MÖLLER, W.
Phys.Z., 1938, 39, 57

(119) MUNTEAN, O - DIMIAN, A. - HRISTESCU, E.
Chem.Engng Sci., 1971, 26, 1953

(120) NEMENYI, P.
Trans.Am.Geophys.Union, 1940, 21, 633

(121) NISI, H. - PORTER, A.W.
Phil.Mag., 1923, 46, 754

(122) O'BRIEN, V.
J.Met., 1961, 18, 549

(123) OSEEN, C.W.
Ark.matematik Astr.Fys.Bd., 1910, 6

(124) PEARCEY, T. - HILL, G.W.
Austral.J.Phys., 1956, 9, 19

(125) PEARCEY, T. - McHUGH, B.
Phil.Mag., 1955, 46, 783

(126) PICCIATI, C.
Rend.del.R.Acad.d.Lincei, 1907, 16, July

(127) PLATEAU, M.T.
Phil.Mag., 1856, 12, 286

(128) PLATEAU, M.T.
'Statique Experimentale et Theorique des Liquides soumis aux seules Forces Moleculaires, 1873, Paris

(129) RAYLEIGH, J.S.W.
Proc.Lond.Math.Soc., 1878, 10, 4

(130) RAYLEIGH, J.S.W.
Proc.Roy.Soc.(London), 1879, 29, 71

(131) RAYLEIGH, J.S.W.
Phil.Mag., 1892, 34, 145

(132) REINHART, A.
Chem.Ing.Tech., 1964, 36, 740

(133) RIMON, Y. - CHENG, S.I.
Phys.Fluids, 1969, 12, 949

(134) ROSE, P.M. - KINTNER, R.C.
A.I.Ch.E.J., 1966, 12, 530

(135) RUMSCHEIDT, F.D. - MASON, S.G.
J.Coll.Sci., 1961, 16, 210

(136) RUMSCHEIDT, F.D. - MASON, S.G.
J.Coll.Sci., 1961, 16, 238

(137) RYBCZINSKI, W.
Bull.Acad.Sci.Cracovie, 1911, 40

(138) SAITO, S.
Sci.Rept.Tohoku Univ., 1913, 2, 179

(139) SATAPATHY, R. - SMITH, W.
Fluid Mech., 1961, 10, 561

(140) SAVART, F.
Ann.Chim., 1833, 53, 337

(141) SAVIC, P.
Natl.Council Can.Mech.Eng.Rept., 1953, MT 22

(142) SCHARDIN, H.
Ergebnisse der exakten Naturwissen., 1941, 10

(143) SCHLICHTING, H.
'Boundary Layer Theory', 1960, (N.Y.:McGrawHill)

(144) SCHMIEDEL, J.
Phys.Z., 1928, 29, 593

(145) SCMIDT, F.S.
Ann.Phys., 1920, 61, 633

(146) SCHROEDER, R.R. - KINTNER, R.C.
A.I.ChE.J., 1965, 11, 5

(147) SCHWABE, M.
Ingr-Archiv, 1935, 6, 34

(148) SCHWABE, M.
NACA Tech.Memo.No.1039, 1943

(149) SPALDING, D.B. - PATANKAR, S.V.
'Heat and Mass Transfer in Boundary Layers',
1967, (London:Morgan-Grampian)

(150) SPELLS, K.E.
Proc.Phys.Soc.(London), 1952, B 65, 541

(151) STOKES, G.G.
Trans.Camb.Phil.Soc., 1843, 8, 105

(152) STOKES, G.G.
Trans.Camb.Phil.Soc., 1850, 9, 8

(153) STOKES, G.G.
Mathematical and Physical Papers, 1880, 1, 17

(154) STOKES, G.G.
Mathematical and Physical Papers, 1901, 3, 55

(155) STUKE, B.
Z.f.Phys., 1954, 137, 376

(156) TANEDA, S.
J.Phys.Soc.Japan, 1956, 302, 11

(157) TANEDA, S.
J.Phys.Soc.Japan, 1956, 11, 1104

(158) TANEDA, S.
Rep.Res.Inst.App.Mech., 1956, 4, 99

(159) TAYLOR, G.I.
Proc.Roy.Soc.(London), 1932, A 138, 41

(160) TAYLOR, G.I.
Proc.Roy.Soc.(London), 1934, A 146, 501

(161) TAYLOR, G.I.
Proc.Roy.Soc.(London), 1954, A 226, 34

(162) TAYLOR, T.D. - ACRIVOS, A.
J.Fluid Mech., 1964, 18, 466

(163) THOM, A.
Aero.Res.Coun.Rep.Memor., 1927, No.1194

(164) THORSEN, G. - STORDALEN, R.M. - TERJESEN, S.G.
Chem.Engng Sci., 1968, 23, 413

(165) THORSEN, G. - TERJESEN, S.G.
Chem.Engng Sci., 1962, 17, 137

(166) TOEPLER, A.
Poggendorff's Ann.d.Phys.u.Chum., 1880, 9, 502

(167) TOLLMIEN, W.
Handb.d.Exper.-Phys., 1931, IV(I), 277

(168) TOMOTIKA, S.
Proc.Roy.Soc.(London), 1935, A 150, 322

(169) TOMOTIKA, S.
Proc.Roy.Soc.(London), A 153, 1936, 302

(170) TOMOTIKA, S. - AOI, T.
Quart.J.Mech., 1950, 3, 140

(171) TRAVELYAN, B.J. - MASON, S.G.
J.Coll.Sci., 1951, 6, 354

(172) TRIEBNIGG, H.
Der Einzelblase und Einspritzvorgang bei Dieselmashinen, 1925, Vienna

(173) WARSHAY,M.-BOGUSZ,E.-JOHNSON,M.-KINTNER, R.C.
Can.J.Chem.Engng, 1959, 37, 29

(174) WEBER, C.
Z.f.angew.Math.und Mech., 1931, 11, 136

(175) WELLEK, R.M. - AGRAWAL, A.K. - SKELLAND, A.H.P.
A.I.Ch.E.J., 1966, 12, 854

(176) WESTWATER, S.W.
Chem.Engng Prog., 1959, 55, 49

(177) WILLIAMS, D.H.
Phil.Mag., 1915, 29, 526

(178) WINNIKOW, S. - CHAO, B.T.
Phys.Fluids, 1966, 9, 50

(179) WINNY, H.F.
Aero.Res.Coun.Rep.and Mem., 1932, No.1531

(180) YEHESKEL, J. - KEHAT, E.
Chem.Engng Sci., 1971, 26, 1223